Novel optical fibers for high power lasers

A THESIS SUBMITTED FOR THE DEGREE OF

DOCTOR OF PHILOSOPHY

by

Deepak Jain

to

OPTOELECTRONICS RESEARCH CENTRE

FACULTY OF PHYSICAL SCIENCES AND ENGINEERING

UNIVERSITY OF SOUTHAMPTON

SOUTHAMPTON, UK

JUNE 2015

To my mother

Declaration of Authorship

I, **Deepak Jain** declare that the thesis entitled "**Novel optical fibers for high power lasers**" and the work presented in it are my own. I confirm that:

1. This work was done wholly or mainly while in candidature for a research degree at this University;

2. Where any part of this thesis has previously been submitted for a degree or any other qualification at this University or any other institution, this has been clearly stated;

3. Where I have consulted the published work of others, this is always clearly attributed;

4. Where I have quoted from the work of others, the source is always given. With the exception of such quotations, this thesis is entirely my own work;

5. I have acknowledged all main sources of help;

6. Where the thesis is based on work done by myself jointly with others, I have made clear exactly what was done by others and what I have contributed myself;

7. Parts of this work have been published as: [please see list of publications]

Signed: Deepak Jain

Date: 15-09-2015

Publications:-

Journals

1. **D. Jain,** C. Baskiotis, and J. K. Sahu, **"**Mode-area scaling with multi-trench rod type fiber," Optics Express, **21**, 1448 (2013).
2. **D. Jain,** C. Baskiotis, and J. K. Sahu, "Bending performance of large mode area multi-trench fibers," Optics Express, **21**, 26663 (2013).
3. **D. Jain,** C. Baskiotis, T. C. May-Smith, J. Kim, and J. K. Sahu, "Large mode area multi-trench fiber with delocalization of higher order modes," IEEE Journal of Selected Topics in Quantum Electronics, Special issue on high power fiber lasers (**INVITED**), **20**, 0902909 (2014).
4. **D. Jain**, Y. Jung, J. Kim, J. K. Sahu, "Robust single-mode all-solid multi trench fiber with large effective mode area," Optics Letter, **39,** 5200 (2014).
5. **D. Jain**, Y. Jung, M. N. Velazquez, and J. K. Sahu, "Extending single mode performance of all-solid large-mode-area single trench fiber," Optics Express, **22**, 31078 (2014).
6. **D. Jain**, Y. Jung, P. Barua, S. Alam, and J. K. Sahu, "Demonstration of ultra-low step index fiber for high power fiber laser applications," **23**, 7407, Optics Express, (2015).
7. **D. Jain**, C. Codemard, Y. Jung, S. Alam, M. N. Zervas, and J. K. Sahu, "High power, compact, picosecond MOPA based on single trench fiber with single polarized diffraction-limited output," Optics Letter, **40**, 4150, (2015).
8. **D. Jain** S. Alam, Y. Jung, P. Barua, M. N. Velazquez,and J. K. Sahu**,** "Highly efficient Yb-free Er-La-Al doped ultra-low NA large mode area single-trench fiber laser," **Submitted to Optics Express.**
9. **D. Jain**, Y. Jung, P. Barua, C. Sones, and J K Sahu, "Large mode area multi trench fiber for UV and visible transmission," **Submitted to Optics Letters.**
10. Y. Jung, P. C. Shardlow, M. Belal, Z. Li, A. M. Heidt, J. M. O. Daniel, **D. Jain**, J. K. Sahu, W. A. Clarkson, B. Corbett, J. O' Callaghan, S. U. Alam, D. J. Richardson, "First demonstration of a 2μm few-mode TDFA for mode division multiplexing," Optics Express, **22**, 10544 (2014).
11. N. Li, S. Yoo, X. Yu, **D. Jain,** and J. K. Sahu **"**Pump power depreciation by photodarkening in ytterbium-doped fibers and amplifiers," IEEE Photonics Technology Letters, **26**, 115 (2014).

Conferences

12. **D. Jain**, P. Gorman, C. Codemard, Y. Jung, M. N. Zervas, and J. K. Sahu, "Picosecond Yb-doped single-trench-fiber amplifier with diffraction-limited output," Photonic West, San Francisco, USA, 9344-27, Feb. 2015.

13. **D. Jain**, Y. Jung, P. Barua, S. Alam, and J. K. Sahu, "Scaling the mode area of Rare-Earth doped step index fiber under current state of the art MCVD technology," CLEO-2015, San Jose, USA, SM2L.2, May 2015.
14. **D. Jain**, Y. Jung, P. Barua, S. Alam, and J. K. Sahu, "Experimental demonstration of single-mode large mode area multi-trench fiber for UV-VIS light transmission," CLEO-Europe, Munich, Germany, CJ 3.2, June 2015.
15. **D. Jain**, C. Baskiotis, and J. K. Sahu, "Large mode area Pixelated trench fiber," Specialty optical fiber, Advance Photonics Congress, Barcelona, Spain, SoW4B.3, Aug. 2014.
16. **D. Jain**, C. Baskiotis, and J. K. Sahu, "Large mode area hybrid multi-trench fiber for anomalous dispersion Large mode area hybrid multi-trench fiber for anomalous dispersion," OFC, San Francisco, USA, Th2A.40, March 2014.
17. **D. Jain** and J. K. Sahu, "Ring fiber with flat-top profile for extremely large mode area single mode operation," ASSL, Shanghai, China, AM5A.29, Nov. 2014.
18. **D. Jain,** C. Baskiotis, and J. K. Sahu, "Large mode area hybrid multi-trench fiber for spectral filtering," FIO, Orlando, USA, FW2A.3, Oct 2013.
19. **D. Jain** and J. K. Sahu, "Trench-assisted large mode area fiber for high power fiber lasers," IONS-KOALA, Adelaide, Australia, Nov. 2014.
20. **D. Jain**, T.C. May-Smith, J. K. Sahu, "Multi-trench Fiber for high power laser applications," Photon, London, UK, 14677, Sep. 2014.
21. **D. Jain**, Y. Jung, and J. K. Sahu, "Multi trench fiber: an industrial solution for high power fiber laser manufacturing," 3rd Annual EPSRC Manufacturing the Future Conference, Glasgow, UK, Sep. 2014.
22. **D. Jain,** C. Baskiotis, J. K. Sahu, "Multi Trench Fiber: an ultra large mode area solution for industrial manufacturing," 2nd Annual EPSRC Manufacturing the Future Conference, Cranfield, UK, Sep. 2013.
23. P. Shardlow, **D. Jain**, R. Parker, J. Sahu, and W.A. Clarkson, "Optimising Tm-Doped Silica Fibres for High Lasing Efficiency," Accepted, CLEO-Europe, Munich, Germany, CJ 14.3, June 2015.
24. P. C. Shardlow, **D. Jain**, J. K. Sahu, and A. Clarkson, "Design and fabrication of next generation optical fibers for 2μm laser," 3rd Annual EPSRC Manufacturing the Future Conference, Glasgow, UK, Sep. 2014.
25. A. Billaud, P. Shardlow, A. Butler, **D. Jain**, J. Sahu, and W.A. Clarkson, "High Power Spectrally-Tailorable Thulium-Doped Fibre Amplified Spontaneous Emission Source," CLEO-Europe, Munich, Germany, CJ 14.3, June 2015.
26. Y. Jung, P. Shardlow, M. Belal, Z. Li, A. Heidt, J. Daniel, **D. Jain**, J. K. Sahu, W. A. Clarkson, B. Corbett, J. O' Callaghan, S-U. Alam, D. J. Richardson, "Few mode TDFA for mode division multiplexing at 2μm," IEEE Summer Topical Meeting, Montréal, Canada, ME2.4, July 2014.
27. Z. Li, S. U. Alam, J. M. O. Daniel, P. C. Shardlow, **D. Jain**, N. Simakov, A. M. Heidt, Y. Jung, J. K. Sahu, W. A. Clarkson, and D. J. Richardson, " 90 nm Gain Extension Towards 1.7 μm for Diode-Pumped Silica-Based Thulium-Doped Fiber Amplifiers," ECOC, Cannes, France, Tu.3.4.2, Sep. 2014.
28. N. Simakov, Z. Li, S. U. Alam, P. C. Shardlow, J. M. O. Daniel, **D. Jain**, J. K. Sahu, A. Hemming, W. A. Clarkson, and D. J. Richardson, "Holmium-Doped Fiber Amplifier for

Optical Communications at 2.05–2.13 μm," OFC, Los Angeles, USA, Accepted, Tu2C.6, March 2015.

Invited talks/Seminar

29. **D. Jain,** C. Baskiotis, J. Kim, and J. K. Sahu, "First demonstration of single-trench fiber laser," CLEO, San Jose, USA, (**Invited**), SF1N.1, June 2014.
30. **D. Jain,** Y. Jung, and J. K. Sahu "Trench fiber for high power fiber lasers," Seminar at Max Planck Institute of science for the light, Erlangen, Germany, **(Invited)**, 17th Feb. 2014.
31. **D. Jain,** Y. Jung, and J. K. Sahu "Trench fiber for high power fiber lasers," Seminar at OFS Labs, Somerset, NJ, USA, **(Invited)**, 20th March 2014.
32. **D. Jain**, Y. Jung, and J. K. Sahu "Next generation optical fiber designs for power scaling," Seminar at Centre for optical fiber technology, Nanyang Technological University, Singapore, **(Invited)** 20th Jan. 2014.
33. J. K. Sahu, **D. Jain,** and Y. Jung**,** "Multi Trench Fiber: a novel solution for high power fiber laser" ASSL, Shanghai, China, (**Invited)**, AW3A.5, Nov. 2014.
34. J. K. Sahu, **D. Jain**, Y. Jung, "Trench-assisted all-solid large mode area fiber for robust single mode operation," Photonics, Kharagpur, India, **(Invited)**, T2A.1, Dec. 2014.
35. J. K. Sahu, **D. Jain**, S. Jain, T. C. May-Smith, C. Baskiotis, "Novel optical fibers for telecommunications and high-power laser applications," International Conference on Optics and Optoelectronics, Dehradun, India, (**Invited**), IT-LAA-04, Mar. 2014.
36. J. K. Sahu, S. Jain, **D. Jain**, N. K. Thipparapu, T. C. May-Smith, **"**Novel geometry fibers for use in optical communications and high power lasers," International Conference on Optics and Optoelectronics, Leeds, UK (**Invited**), Jul. 2014.
37. J. K. Sahu, **D. Jain,** A. S. Webb, S. Yoo, and T. C. May-Smith, "Speciality doped fibers in high power lasers Workshop on Specialty Optical Fiber and their Applications," Workshop on specialty optical fiber, Sigtuna, Sweden, (**Invited**), T2.2, Aug 2013.
38. J. K. Sahu and **D. Jain**, "Specialty fibers for high power lasers and amplifiers," Optics and Optoelectronics SPIE Conference, Prague, Czech Republic, (Invited), 9507, April 2015.
39. **D. Jain**, "Power of Light: making life better," Talk at Bilkent University, Ankara, Turkey, Sep. 2015.

ABSTRACT

High power fiber lasers have several applications thanks to their outstanding features such as good beam quality, all fiberized compact device size, robustness, wavelength tuning, high wall-plug efficiency, and low cost. Due to these features high power fiber lasers are replacing other solid-state lasers for several applications. Fiber lasers are being used commercially for several applications such as surgery, material processing (cutting, drilling, polishing etc.), oil and gas sensing, pumping several other lasers, and space communication etc. However, non-linear effects restrict the output power level of fiber lasers. Although reducing power density by using large core diameter fibers can increase the threshold of non-linear effects, however large core diameter leads to multi-mode behavior and is prone to bend-induced effective area reduction. Several novel large mode area fibers have been proposed to scale the output power level. However, the advantages of all-fiberized device and low cost disappear as most of these fibers involve complex fabrication and cannot be spliced to optical components such as conventional pump fibers. This thesis deals with novel large mode area fibers which are suitable for mass scale production and can offer low cost production compared to other competitive fiber designs thanks to their simple design. These novel fibers are all-solid and can be easily spliced to other fibers, thus can lead to an all-fiberized device. Moreover, some of the novel fibers proposed in this thesis offer the delocalization of powers of the higher order modes outside the core. This delocalization of the higher order modes can be useful to ensure an effective single mode operation in a double clad configuration. The proposed novel fibers offer better or competitive mode area scaling performance compared to other competitive fibers.

In this thesis, firstly conventional step-index fibers have been exploited for mode area scaling by reducing the refractive index of the actively doped core with respect to the cladding. Prior to this thesis, the lowest reported NA of a Yb-Al doped fiber was 0.048 corresponding to 0.0008 refractive index of core with respect to cladding. In this thesis, optimized solution doping process leads to a NA of 0.038 for a Yb and Al doped core corresponding to 0.0005 refractive index of core with respect to cladding. This reduction in NA of core leads to an effective area increase from ~450μm^2 to ~700μm^2 at 32cm bend diameter ensuring effective single mode operation. This is the lowest NA ever reported using cost-effective solution doping process to the best of author's knowledge, which is widely used in manufacturing of rare-earth doped fiber. Further, in a 4%-4% laser configuration, a 35μm core diameter 0.038 NA fiber shows high laser efficiency (~81%) with good M^2 (~1.1) value of output beam at 1040nm. Thesis also reports a novel fiber design known as single trench fiber, where a passive Ge-doped ring has been added around the core. This ring known as resonant ring facilitates the suppression of the higher order modes thanks to resonant coupling between modes of core and ring. The combination of ultra-low NA (~0.038) and a surrounding ring can lead to an effective single mode operation of fiber having a core diameter as large as of 50μm offering an effective area of ~1,500μm^2 at ~40cm bend diameter. A 40μm core diameter single trench fiber has been successfully fabricated in house and shows robust effective single mode behavior. Further, a 30μm single trench fiber has been tested in a master oscillator power amplifier configuration delivering ~23.5ps pulses at 13.5MHz repetition rate carrying up to ~3.8μJ pulse energy corresponding to >160kW peak power and ~52.3W of average power, while maintaining ~76% slope efficiency. Numerical Performance of STF has also been reported at other wavelengths such as 1550nm and 2000nm. A detailed comparative analysis has been performed with other competitive fiber designs showing the advantages of single trench fiber over other fiber designs. Further, another fiber design known as multi trench fiber has also been proposed. Multi trench fiber can scale effective area as large as of 12,000μm^2 in a rod-type configuration. Multi-trench fibers offer several advantages such as easy cleaving and splicing thanks to the all-solid structure; however refractive index of active core has to be same as of passive cladding. Nevertheless, this fiber has shown a strong potential for applications in ultrafast rod-type fiber lasers. A 90μm core diameter passive fiber has been fabricated in house using rod-in-tube technique in conjunction with modified chemical vapour process. Experiments ensure an effective single mode operation. Furthermore, this fiber also shows the potential to be used for beam delivery applications with a small core diameter thanks to effective single mode operation over a wide range of bend radii. MTFs of 30μm and 20μm core diameter have been successfully fabricated and both ensure robust single mode operation over a wide range of bend radii at 1060nm and 632nm respectively. Numerical simulations show the possibility of a 10μm fiber to be effectively single moded at a wavelength of 300nm.

ACRONYMS

A-PCF: Asymmetrical photonic crystal fiber

ARROW-Anti-resonant reflecting optical waveguide

ASE-Amplified spontaneous emission

ASPBGF- All solid photonic bandgap fiber

BR- Bend radius range

CR-Criterion

CVD-Chemical vapour deposition

ESM- Effective single mode

FWM-Four wave mixing

FUT-Fiber under test

H-MTF-Hybrid multi trench fiber

LCF- Leakage channel fiber

LMA- Large mode area

LPF- Large pitch fiber

MCVD-Modified chemical vapour deposition

MOPA-Master oscillator power amplifier

MPI-Multiple path interference

MTF- Multi trench fiber

MTIR-Modified total internal reflection

NA-Numerical aperture

P-CCC: Polygonal chirally coupled core

PCF- Photonic crystal fiber

PECVD-Plasma enhanced chemical vapour deposition

PML- Perfectly matched layer

RE-Rare-earth

SAPs-Stress applying parts

SBS-Stimulated Brillouin scattering

SHARC-Semi-guiding high aspect ratio core

SIF-Step index fiber

SPM-Self phase modulation

SRS-Stimulated Raman scattering

STF- Single trench fiber

TIR: Total internal reflection

TLS : Tunable laser source

VAD- Vapour-phase axial deposition

Contents

Chapter 2 Ultra-low NA fibers

Chapter 3 Fabrication of Ultra-low NA fibers

Chapter 4 Multi trench fibers

List of Figures

Chapter 1

Chapter 2

Chapter 3

Figure 3.13 shows (a) experimental set-up (b) slope efficiency and (c) output Beam Quality. All of these measurements were done at Tokai University by Prof. Kazuyoku Tei and his team.

Figure 3.14 shows the splicing of STF (on right side) with dissimilar fiber using a conventional splicer demonstrating clear advantages of all solid design of doped fiber.

Figure 3.15 (a) refractive index profile of Yb and co-dopants doped preform. Inset shows the microscope image of fiber end (b) white light absorption spectrum of a 1.55m long fiber.

Figure 3.16 shows (a) experiment set-up used for single-mode characterization of STF (b) output with respect to optimum launching of single mode in loosely coiled and bent at 20cm conditions (c) output power with respect to offset launching of single mode input (d) output beam profile with respect to offset launching of single mode input.

Figure 3.17 (a) profile of input multimode beam (b) output beam with respect to input beam (c) and (d) binary phase plate to generate pure LP_{11} and LP_{21} mode (c) and (f) shows the output profile with respect to pure LP_{11} mode (g) shows the output profile with respect to pure LP_{21} mode.

Figure 3.18 (a) experimental set-up used for calculating LP_{11} bend loss (b) output power of 57cm long fiber with respect to LP_{11} mode launch.

Figure 3.19 shows (a) experimental set-up used for fiber laser efficiency (b) slope efficiency of 3.3m long fiber. Inset shows the profile of output beam (c) measured spectrum of output beam at different power levels.

Figure 3.20 shows the refractive index profile at different positions along the length of the preform. Blue and Red colour corresponds to profiles at 0 degree and 90 degree angular positions respectively.

Figure 3.21 shows (a) output image of the fiber at 1064nm captured with a CCD camera (b) white light transmission spectra of 1.26m long fiber in bend and unbent configurations.

Figure 3.22 (a) experimental set-up for modal verification of the fiber, (b) input mixed modes (LP_{01} and LP_{11}) using phase plate, (c) output beam profiles for LP_{01} mode launch, and (d) output beam profiles for a mixed mode launch.

Figure 3.23 shows (a) experimental set-up for single mode verification, (b) profile of the output beam with respect to LP_{01} mode launch, and (c) profile of output beam with respect to mixed mode launch. A 3m long fiber coiled at ~32cm (+/- 0.5cm) bend diameter was used in this experiment.

Figure 3.24 shows (a) experimental set-up for single mode verification, (b) profile of the output beam with respect to LP_{01} mode launch, and (c) profile of output beam with respect to mixed mode launch. A 3m long fiber coiled at ~32cm (+/- 0.5cm) bend diameter was used in this experiment.

Chapter 4

Refractive index profile of H-MTF along the X and Y axis (c) Computed bending loss of the MTF and H-MTF with two orthogonal bend orientations.

Figure 4.20(a), 4.20(b), and 4.20(c) shows calculated leakage loss, dispersion, and power fraction of the fundamental mode of MTF and H-MTF respectively in the case of an unbent configuration. Inset also shows normalized electric field of the fundamental core mode of H-MTF at certain wavelengths.

Figure 4.21 Bend loss spectrum (a), power fraction spectrum (b), dispersion (c) of the fundamental core mode of the H-MTF of the figure 4.19(c) at a 15cm bend radius, for two orthogonal bending orientations.

Chapter 5

Figure 5.1 shows refractive index profile of fabricated MTF using recipe B249 shown in table 5.2.

Figure 5.2 shows refractive index profile of fabricated MTF using recipe C256 shown in table 5.3.

Figure 5.3 shows refractive index profile of fabricated MTF using recipe D266 shown in table 5.4.

Figure 5.4 shows refractive index profile of fabricated MTF using recipe E269 shown in table 5.5.

Figure 5.5 shows refractive index profile of fabricated MTF using recipe F320 shown in table 5.5.

Figure 5.6 shows refractive index profile of fabricated MTF using recipe G324 shown in table 5.7.

Figure 5.7 shows refractive index profile of fabricated MTF using recipe H330 shown in table 5.8.

Figure 5.8 shows refractive index profile of fabricated MTF using recipe I349 shown in table 5.9 and rod-in-tube technique.

Figure 5.9 shows refractive index profile of fabricated MTF preform using recipe J342 shown in table 5.10.

Figure 5.10 shows refractive index profile of fabricated MTF using recipe J376 shown in table 5.10 and rod-in tube technique. Inset shows the microscope image of fiber.

Figure 5.11(a) the measurement set-up used for verification of single mode behaviour, (b) output beam profile with optimum launching, (c), (d), (e) output beam profile under various launching conditions, (f) multimode input beam profile, and (g) profile of output beam for different multimode input beam launch.

Figure 5.12(a) the measurement setup used for transmission spectrum measurement, (b) transmission spectra for two different length of fiber.

List of Tables

Chapter 1

Chapter 2

Chapter 3

Chapter 4

Chapter 5

Chapter 6

Chapter 1 Review of fiber designs

1.1 Introduction

High power fiber lasers have established themselves in laser market as an attractive source of laser [1-7]. Fiber lasers have several advantages over solid-state lasers thanks to the outstanding features of the optical fiber [1-6]. Optical fibers ensure an excellent beam quality (i.e. a Gaussian beam thanks to the single mode behaviour of mono-mode fiber). The thermal distortion of the output beam is negligible as compared to the solid state lasers thanks to the large surface area to volume ratio offered by fiber. Fiber lasers can offer fully fiberized cavities, which mitigate the need of alignment of free space components thanks to the fiber based components. This brings outstanding robustness and reliability to the fiber lasers. Fiber lasers offer excellent flexibility to deliver output beam thanks to bendable low-loss optical fiber. On the top of these advantages, low intrinsic loss of rare-earth-doped fibers and small quantum defects ensure high wall-plug efficiencies of fiber lasers. Figure 1.1(a) shows the comparative analysis of different lasers over several desired features of lasers such as power scaling, beam quality, wavelength tuning, maintenance, footprint, and ownership costs. Figure 1.1(b) shows the increasing power level of different high power lasers namely CO_2, Nd: YAG, and fiber laser in last few decades.

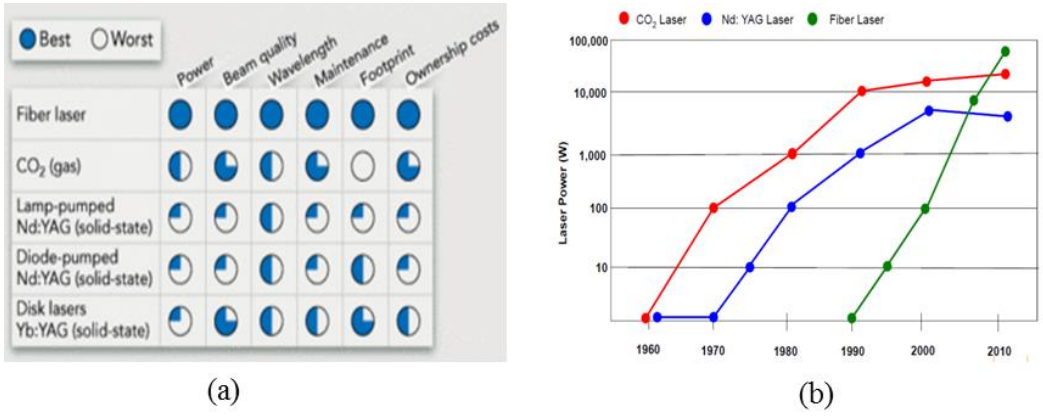

Figure 1.1(a) advantages of fiber laser over other lasers (b) increasing power level of different lasers in last few decades. (Figure source [8]; © 2006 Industrial Laser Solutions.)

In nut shell, fiber lasers offer the advantages of good beam quality, better thermal management, all-fiberized operation, compact device size, small foot print, versatility, low maintenance, and high wall-plug efficiency [1-6]. This has drawn enormous research interest in fiber lasers in the last decade. Currently, fiber lasers have crossed the output power level of 10kW in continuous wave regime with diffraction-limited beam quality [7] and more than 6GW output peak power in pulsed regime [9] at ~1μm, and as a consequence fiber lasers have become the backbone for high power laser applications. Fiber lasers have enormous applications in different areas such as material processing, oil and gas sensing, surgery, defence, and space communication etc as shown in figure 1.2. Now, fiber lasers are being seen as a potential candidate for next-generation particle

accelerators, nuclear transmutation, nuclear waste treatment, astrophysics, and other industrial applications [10].

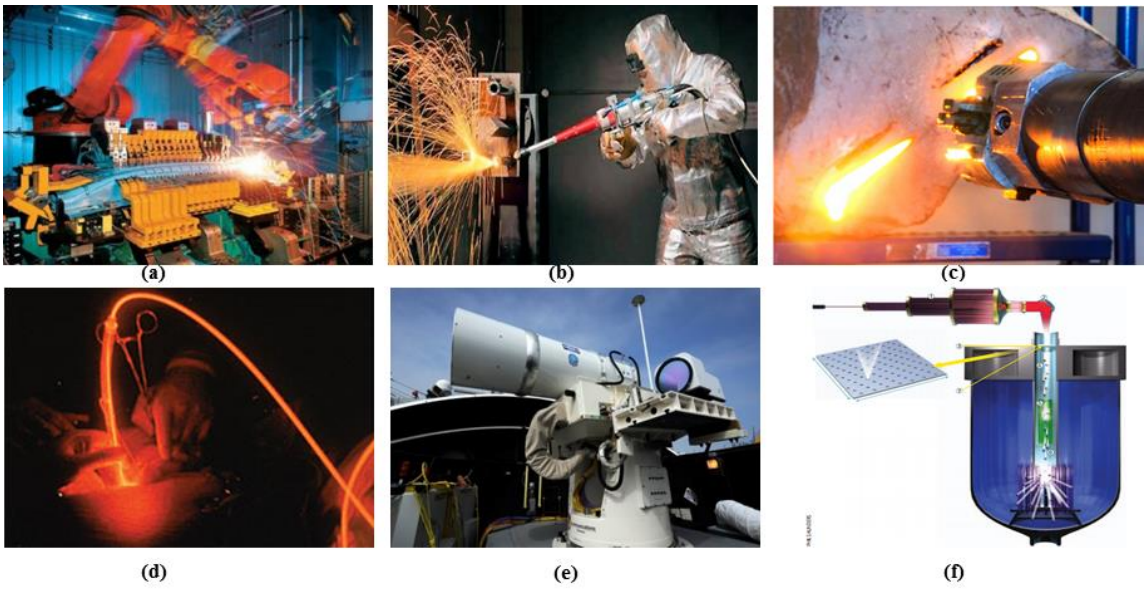

Figure 1.2 various applications of fiber lasers. (a) & (b) material processing (drilling, marking, welding etc.) (c) rock drilling (for oil and gas sensing) (d) surgery (e) defense (for high power laser weapons) (f) next generation particle accelerators. (Figure sources (a) [11] (b) [12] (c) [13] (d) [14] (e) [15] (f) [10].)

1.2 Fiber laser

Most of the high power fiber laser consists of a rare-earth doped optical fiber coated with a low-index polymer coating as shown in figure 1.3. However it is possible to have a fiber laser without rare-earth ions such as lasers based on non-linear effect. Fibre laser can be thought as a device which converts low brightness of laser diodes to high brightness. Multi-moded laser diodes (known as pump) is launched at the one end of active fiber, which is guided by cladding and absorbed by rare-earth ions doped in core. The emission of rare-earth ions, spatial distribution of light in core, and gratings ensure a stable Gaussian lasing output beam. Figure 1.4(a) and 1.4(b) shows the schematic of cross-section of a typical optical fiber and refractive index profile of the optical fiber respectively for fiber lasers. Core of the optical fiber is typically doped with rare-earth oxide such as Yb_2O_3, Er_2O_3, Tm_2O_3 etc. with additional dopants such as Al_2O_3 or P_2O_5 in silica matrix to avoid quenching of rare earth ions and photo-darkening. All of these oxides are refractive index increasing components; hence they constitute high refractive index core of fiber. On the other hand, cladding is normally pure silica and the outermost cladding is a polymer coating. Also, an air-clad jacket is used in high power fiber lasers as outermost pump cladding in place of low-index polymer coating to avoid thermal degradation of polymer.

Typically, circular double clad pumping scheme leads to reduced cladding pump efficiency because circular symmetry give birth to helical modes in cladding and which have minimal interactions with the core. In order to break this circular symmetry, various models have been proposed having different fibre core and cladding geometries for enhanced pump absorption

like D shaped fibre, offset core fibre, octagonal fibre, square or rectangular fibre, and flower shaped fibre etc as shown in figure 1.5.

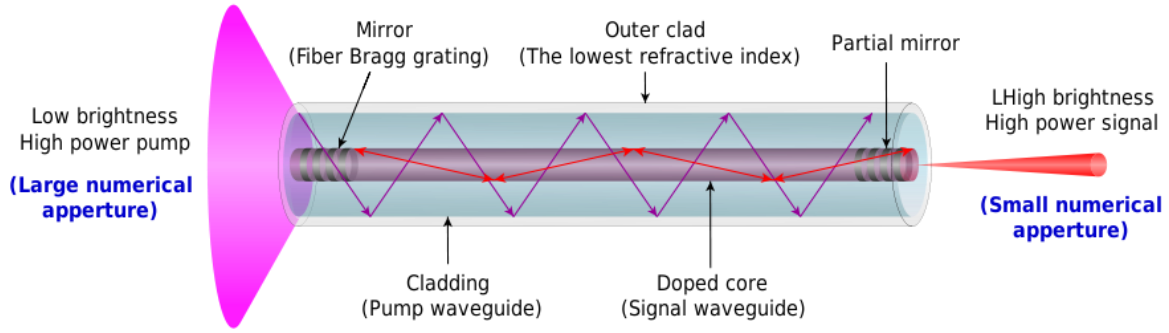

Figure 1.3 schematic of a fiber laser showing rare-earth doped core, pump guiding cladding, outer cladding, and Bragg gratings. (Figure source [16])

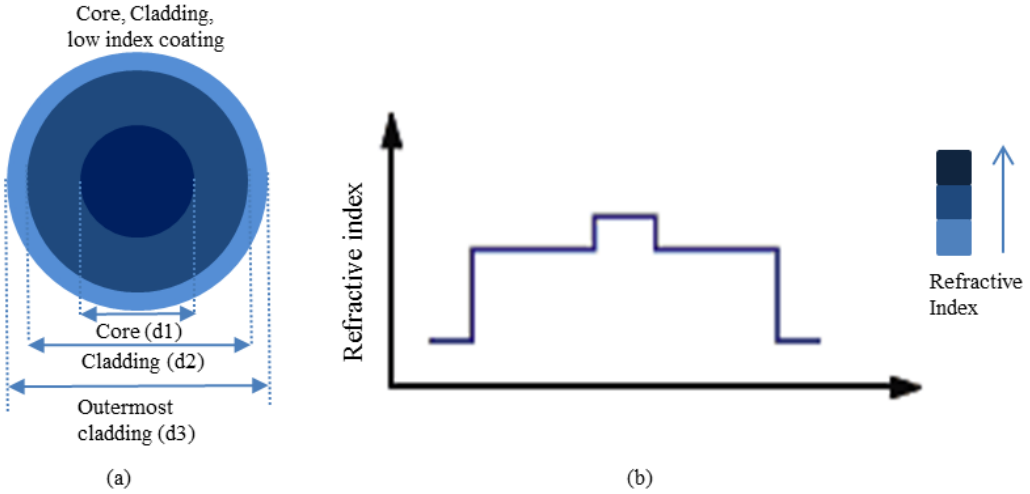

Figure 1.4(a) schematic of cross-section of optical fiber used for fiber laser application (b) schematic of refractive index profile of the optical fiber.

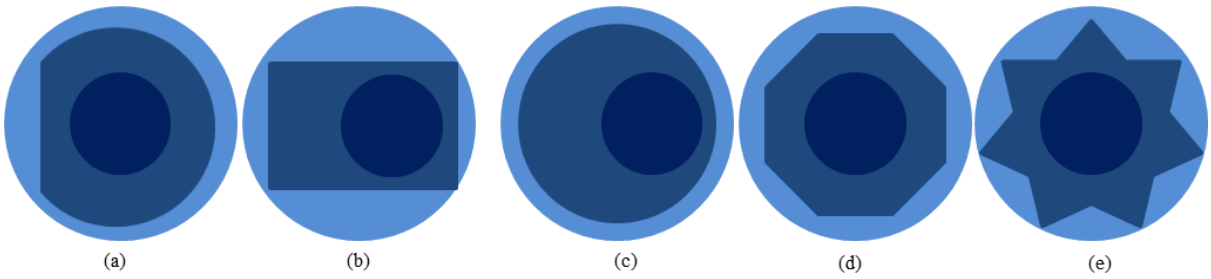

Figure 1.5 various fiber geometries for enhanced pump absorption. (a) D-shaped (b) off-set core (c) octagonal (d) square or rectangle (e) star shaped.

The output power of fiber laser is limited by the non-linear effects. There are various non-linear effects such as Stimulated Brillouin Scattering (SBS), Stimulated Raman Scattering (SRS), Self Phase Modulation (SPM), Four Wave Mixing (FWM), and Self-Focusing effect

etc that are encountered in optical fiber. Table 1.1 shows the dominating non-linear effect in different conditions. On the top of these, self-focusing effect decides the ultimate power limit.

Table 1.1 non-linear effects and their dominance.

Non-linear effect	**Dominance**
SBS	Narrow band signals
SRS	Broadband signals
SPM	Short and ultra-short pulses

Figure 1.6 shows the typical example of onset of SRS effect in a kW class Yb-doped fiber laser output spectrum [17]. Figure 1.6(a) shows the experimental set-up for fiber laser and figure 1.6(b) shows the output power of the laser with respect to pump power, which is limited upto 3kW before the onset of SRS effect. Figure 1.6(c) shows the SRS near around 1150nm, which is highly undesired. Further scaling of output power was mitigated by temporal instabilities related to SRS.

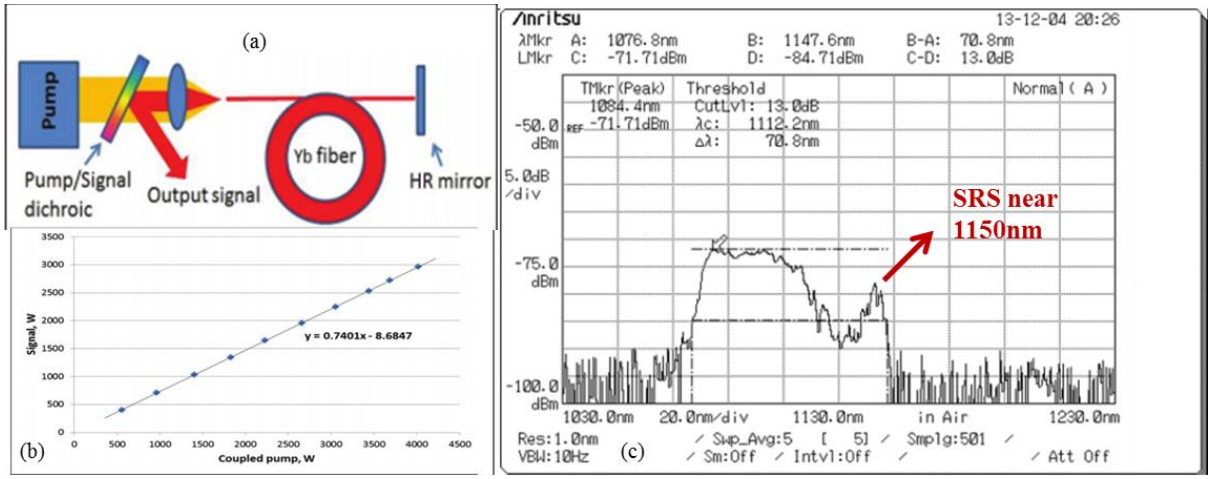

Figure 1.6 (a) fiber laser set-up (b) output power with respect to pump power (c) output spectrum around 1090nm and SRS around 1150nm. (Figure source [17]; © 2014 SPIE.)

The threshold of non-linear effect is generally dominated by following equation 1.1, where P is the peak power, λ is the central wavelength of output beam, EA is the effective area of the fundamental mode of fiber, n_2 is the non-linear response of the optical fiber (based on material), and L is the effective interaction length of fiber [18].

$$P_{th} = \lambda . \frac{EA}{2\pi . n_2 . L} \tag{1.1}$$

According to this equation the threshold level of non-linear effects increases with increasing effective area of the fundamental mode of the optical fiber. Increasing the effective area of the fundamental mode, decreases the power density in core hence more power can propagate through fiber before reaching the threshold of non-linear effects. It is pertinent to note that all the non-linear effects cannot be succinctly suppressed by scaling the mode area of optical fiber, however large mode area is a useful parameter for optical fiber designers to avoid non-linear effects to a larger extent.

1.3 Optical fiber for fiber lasers

Conventional step-index fiber used for optical communication having 8μm core diameter, ~0.005 core refractive index difference with respect to cladding, and 125μm outer diameter offers very low loss 0.2dB/km and are well suitable for long haul communication. However, fiber laser needs fiber which can offer large effective area of the fundamental mode to avoid non-linear effects. One way to increase the effective area of the fundamental mode is to increase the core diameter in a step index fiber. However increase in core diameter limits single-mode operation of fiber, which is another important requirement for fiber laser applications. Therefore, a trade-off exists between the large effective area and single mode operation. The normalized frequency of a step-index fiber should be less than 2.405 for single mode operation as shown by following equation 1.2:

$$V = \frac{2.\pi.a.\sqrt{n_2^2 - n_1^2}}{\lambda} < 2.405 \qquad (1.2)$$

Where a is the core radius, n_2 is the refractive index of core and n_1 is the refractive index of cladding, and λ is the wavelength of operation. It is clear that, there is a trade-off between core radius and numerical aperture (NA) which is defined as $\sqrt{n_2^2 - n_1^2}$. Hence, in order to achieve large core diameter while maintaining single-mode operation, fiber NA can be reduced so that V remains lower than 2.405. However, conventional fiber fabrication technologies are not mature enough to fabricate rare-earth doped fibers having NA lower than 0.05 (prior to the current thesis), which restricts the maximum core diameter to be around 16μm at 1μm for single mode operation. It is pertinent to note that, with decreasing core NA, fundamental mode is susceptible to high bend losses, although losses in the order of 10s of dB/km are acceptable for fiber lasers unlike 0.2dB/km loss for long haul communication fibers. Figure 1.7 shows the calculated modes of a 40μm core diameter step index fiber (SIF) with a low NA of 0.038 in unbent and bent (20cm bend radius) case. It is clear that fiber is multi-moded in both cases. In order to address these issues, researchers over the last two decades are working over novel optical fiber designs which can provide effective single mode (ESM) operation by supressing higher order modes while offering large effective area of the fundamental mode. There are also several techniques in addition to novel optical fibers to suppress higher order modes such as bend-induced losses in a low NA, modal filtering, and tapering of fiber etc. (These will be discussed in details in this chapter later on.) Moreover, this trade-off between large effective area and effective single mode operation poses severe challenges to several merits of fiber laser such as flexibility, compact device size, reliability, and stable output power etc.

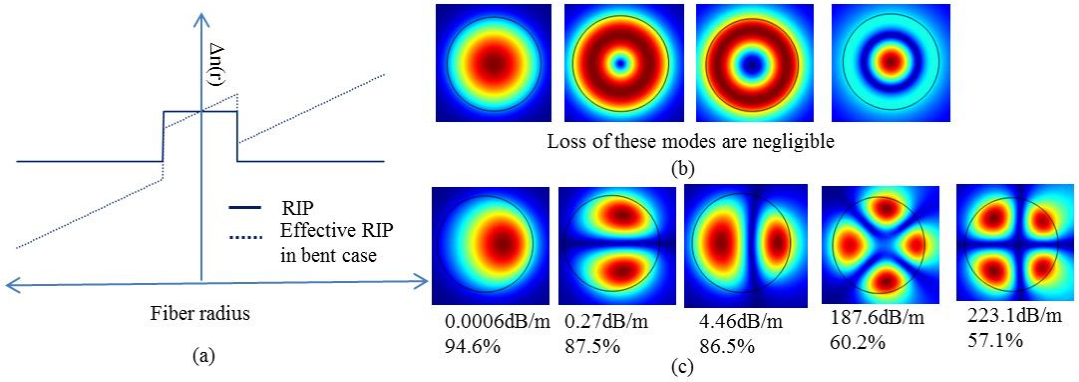

Figure 1.7 (a) fiber in unbent and bent condition (b) normalized electric field of different core modes in unbent and bent condition of optical fiber.

1.3.1 ESM for large mode area fiber

There is lack of standards while designing the large mode area (LMA) fiber design offering ESM for fiber laser applications. Therefore, in this PhD work a standard definition for ESM is being defined. ESM is a relative term and depends on the chosen criterion, for example a criterion of loss of the fundamental mode lower than 0.1dB/m and higher order mode larger than 10dB/m was proposed by M. -Ji. Li et. al. for ESM [2]. There can be different criterion for ESM for different applications, however high loss for all the higher order modes and low loss for the fundamental mode is highly preferred. Another interesting fact is that a bend radius range over which criterion is fulfilled normally depends on chosen criterion as shown in figure 1.8(a). Figure 1.8(a) shows that a criterion CR_1 is being fulfilled over a bend radius range of BR_1, on the other hand a criterion CR_2 is being fulfilled over a bend radius of BR_2. Furthermore, effective area decreases rapidly with decreasing bend radius for LMA fiber as shown in figure 1.8(b) [3-4]. ESM is defined for LMA at a particular wavelength as Criterion of the suppression of higher order modes while keeping the loss of the fundamental mode to be lower than a level fulfilled over a range of Bend radius with a range of Effective area achieved at that wavelength, known as "CBE" {Criterion, Bend radius, Effective area}. It is pertinent to note that a standard such as "CBE" is indispensable to compare the performance of various LMA fiber designs and provides useful definition to fiber designers while designing new LMA fiber.

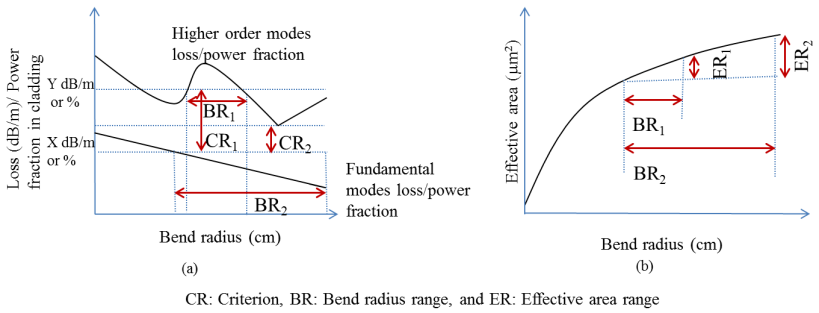

Figure 1.8 (a) loss or power fraction in cladding for fundamental mode and higher order mode as a function of bend radius in a LMA (b) effective area achieved as a function of bend radius for fundamental mode.

1.3.2 Desired characteristics for LMA fiber

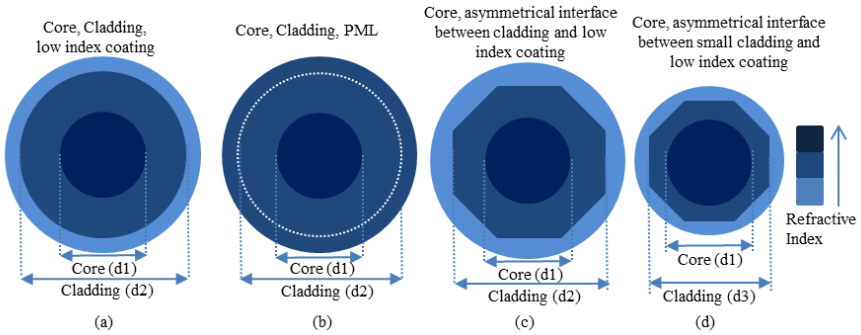

Figure 1.9 schematic of 2-D cross section of the fiber showing core and cladding with (a) low index coating (b) PML having same index as of cladding (dotted line distinguish cladding and PML) (c) asymmetrical interface of cladding and low index coating (d) asymmetrical interface of small thickness of inner cladding and low index coating.

In order to have a good beam quality, it is better to have the losses of the higher order modes as high as possible. However, more desired criterion of ESM operation is power delocalization of the higher order modes as the fiber lasers are used in double clad configuration (where losses of core modes can be much lower in reality). In case of high power fiber lasers, the second cladding is generally either a low index polymer coating or an air-holes layer as shown in figure 1.9(a) and this is really different from when fiber is generally simulated in computer's world for calculating loss of the higher order modes as shown in figure 1.9(b). In simulations, an additional layer known as perfectly matched layer (PML) having same refractive index as of cladding is used in place of low index coating that is why loss calculated by simulations may not be true in reality. However, recent experiments show that asymmetrical interface between first and second cladding in double cladd case can lead to real calculated loss of core modes (as shown in figure 1.9(c)) [4]. It is worth noting that in this study, the effect of cladding thickness and cladding refractive index profile were not considered. A cladding diameter eight times larger than core diameter was used in this experiment. On the other hand, Y. A. Uspenskii et. al. have proved the significant role of cladding layer thickness in determining the experimental loss of the fundamental mode [4]. This study reveals that a larger cladding thickness of cladding can lead close to calculated loss. Recently, researchers have stressed on the use of criterion of power delocalization of the higher order modes esp. in case of rod-type fiber lasers, where a small thickness of inner cladding is used. For example, a fiber having 100µm core diameter and 170µm inner cladding diameter [5]. A small cladding diameter is an indispensable option to increase the cladding pump absorption in rod-type fiber lasers where fiber length is merely 1m to 2m. Moreover, the refractive index of the doped core is same as of the cladding and it becomes difficult to incorporate high amount of index raising rare earth ions and co-dopants while compensating their index with index decreasing components. Furthermore, higher suppression of the higher order modes using power delocalization can be one factor to mitigate detrimental modal instability phenomenon. It is important to note here that a small cladding diameter is not an indispensable choice in flexible fiber laser configuration inspite of the fact that most of the LMA fiber designs need same refractive index as of cladding, as a

longer length of fiber can be used in bendable fiber laser unlike rod-type fiber lasers. However, using a longer length of fiber laser can reduce the threshold of non-linear effects. Nevertheless, it is important to understand that power delocalization of the higher order modes in flexible fiber laser configuration might not be an indispensable criterion but definitely fiber design employing this feature can dramatically enhance the performance of fiber lasers.

On the other hand, a small bend radius is preferred for small foot print of device and obviously effective area of the fundamental mode as high as possible is desired. Moreover, it is not just the trade-off between large effective area and ESM that requires research but fiber designers also need to focus on several other aspects of the optical fiber to keep the advantages of fiber laser alive. For example, fiber should be suitable for low cost fabrication process such as modified chemical vapor deposition (MCVD) so that fibers are suitable for mass production. In order to have an all fiberized laser device, we need optical fibers which can be spliced to fiber based components. This would prefer all-solid fiber design so that they can be easy cleaved and spliced. Figure 1.10 shows the desired characteristics for a LMA fiber.

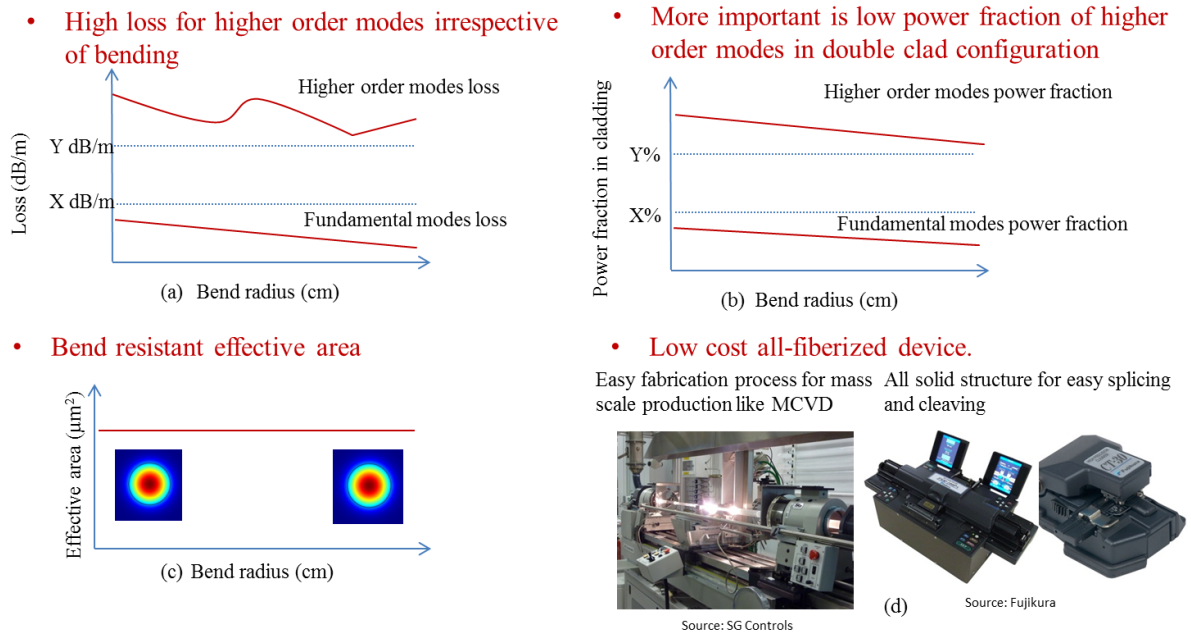

Figure 1.10 (a) loss and (b) power fraction in cladding for fundamental mode and higher order mode as a function of bend radius in a LMA (c) ideal effective area achieved as a function of bend radius for fundamental mode (d) low cost fabrication and all fiberized device.

1.3.3 Real world is really different

Unfortunately, real word of LMA fibers is really different from above mentioned desired conditions. Figure 1.11 provides a brief introduction to challenges faced by fiber designers for fiber lasers applications.

(a) *Difficult to fulfil the criterion of ESM over a wide range of bend radius*

It is really difficult to fulfil the criterion of ESM (higher order mode loss or power fraction in cladding larger than a particular set level and fundamental mode loss and power fraction in cladding lower than a particular set level) over a large range of bend radius. Figure 1.11(a) shows the calculated losses of a graded-index fiber over a wide range of bend radius, as it is clear that both loss curves are steep and different from flat desired curve as shown in figure 1.10. Due to these steep curves, the criterion (here it is 1dB/m for higher order mode and 0.1 dB/m for fundamental mode) cannot be fulfilled over a very short range of bend radius (15cm+/- 0.2cm). Therefore, these fibers are not good candidates for high power beam delivery, hence reduces the flexibility of fiber lasers.

(b) bend induced effective area reduction and high black fraction

Effective area of the fundamental mode reduces dramatically under bent condition as shown in figure 1.11(b). Moreover, this bend-induced effective area reduction is more dominating with increasing core size [3-4]. This bend-induced effect has severally challenged the power scaling level of fiber lasers [5]. To avoid this problem, researchers have demonstrated a rod-type fiber (which cannot be bent as they are few mm thick). However, rod-type fiber laser dramatically reduce the flexibility of fiber laser and more importantly loses the advantage of small footprint offered by fiber lasers.

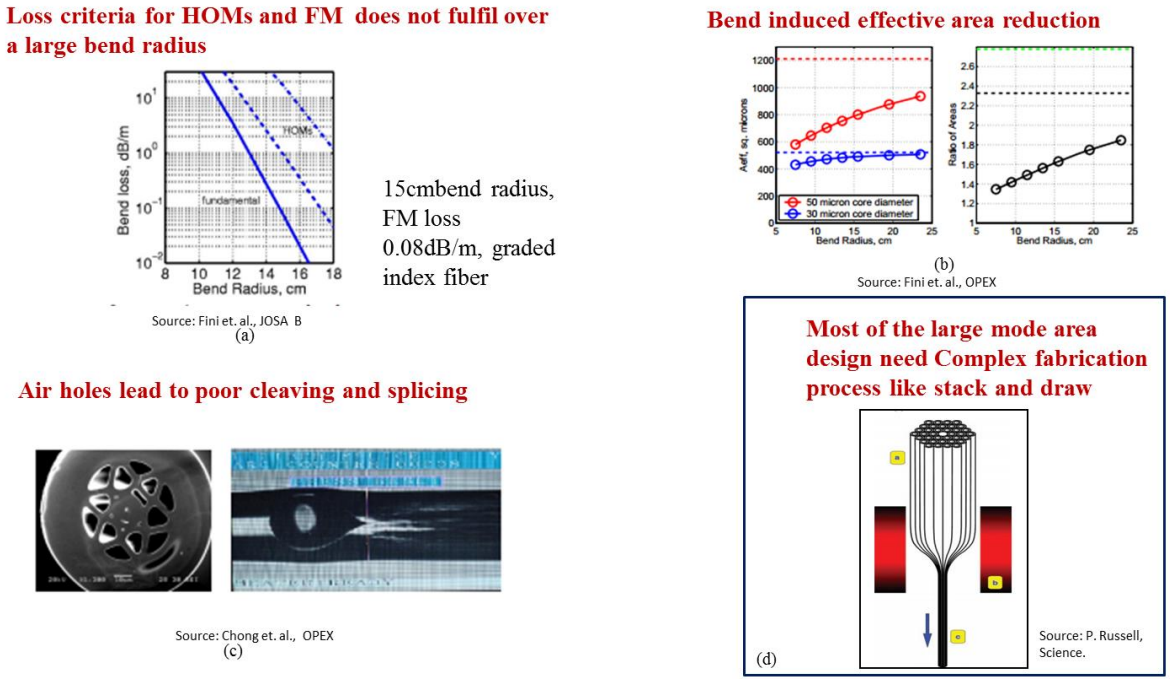

Figure 1.11 (a) steep loss curve of fundamental mode (FM) and higher order mode (HOM) (b) bend-induced effective area reduction (c) poor splicing due to presence of air-holes (d) stack and draw process for Photonic crystal fibers. (Figure source (a) [4]; © 2007 OSA (b) [3]; ©2006 JOSA B (c) [10]; © 2003 OSA (d) [9]; © 2003 AAAS.)

(c) Air holes lead to poor cleaving and splicing

Most of the upcoming fiber designs, which offer ESM for large effective area of the fundamental mode, are based on photonic crystal fibers (these designs will be discussed later in details in this chapter). Photonic crystal fibers are also known as holey fiber, where air-holes constitute the cladding of fiber, which run along the length of fiber [9]. However, large mode area fibers based on photonic crystal fiber are difficult to cleave and splice due to presence of air-holes as shown in figure 1.11(c) [10]. This threatens the possibility of all-fiberized fiber laser operation.

(d) Fiber fabrication

Fiber fabricator face severe challenges while fabricating large mode area fibers as they require very low NA rare earth doped fibers. Conventional rare-earth doped fibers are mostly fabricated by MCVD process in conjunction with solution doping process. However, the solution doping process is unable to control the NA below 0.05 (prior to this current thesis). Moreover, fiber design based on photonic crystal fiber and photonic bandgap fiber requires same refractive index of core as of cladding. Unfortunately, refractive index of rare-earth ions is index raising. Hence, to match the refractive index of rare-earth doped silica core and undoped silica cladding, core requires micro-structuring of high and low index filaments. It is a cumbersome process to do in fiber fabrication. Moreover, most of the recent LMA fibers are based on photonic crystal fiber and they require stack and draw process for fabrication. Stack and draw is a complex fabrication and increase the fiber fabrication cost.

1.4 Optical fiber fabrication for fiber lasers

Optical fibers for fiber lasers are most commonly made up of silica glass because silica has a good mechanical strength and thermal stability. Moreover, fiber fabrication technology for silica has developed to high standards in past decades. Although, there is a significant difference between fibers for use in communication and fiber lasers but fabrication is similar else than there are few additional steps in fabrication of optical fiber for fiber laser, which involves rare earth doping. However, increasing demand of output power level has changed the optical fiber design, therefore there have been dramatic changes in fiber fabrication process as well.

In 1966 Kao and Hockman [1] suggested that low loss silica-based fibers could be used as a transmission medium in the near infrared frequency region. After that there has been tremendous progress in fibre fabrication technologies. Several preform fabrication techniques such as outside vapour deposition (OVD) [2], modified chemical vapour deposition (MCVD) [3], vapour-phase axial deposition (VAD) [4], the double crucible technique [5], and plasma enhanced chemical vapour deposition (PECVD) [6] have been demonstrated. OVD, VAD, and PECVD are commercially used across the world for single mode telecommunication fibers. On the other hand, MCVD process is used for specialty optical fiber such as rare-earth doped optical fiber for fiber lasers and amplifiers. MCVD was first demonstrated by MacChesney et. al. at Bell laboratories [7-9].

1.4.1 MCVD Process

In this process, a carrier gas such as O_2, N_2 or He is used to carry vapours of various precursors. Precursors can be either in liquid or gas from. Typical precursors such as $SiCl_4$, $POCl_3$, $GeCl_4$, and BBr_3 are liquid at room temperature and have very high vapour pressure. Carrier gas passes through the precursors and absorbs them to carry them to the final tube, where deposition takes place. The high vapour pressure of these dopants compared to metal impurity (present in dopants sources) mitigates their entry into deposition tube. A schematic of MCVD process is shown in figure 1.12. The amount of dopant is controlled by mass flow controller, which controls the flow of carrier gas. It is pertinent to note that, the temperature of bubbler and vapour pressure of precursor plays an important role in the dopant amount. Carrier gas having dopant vapours and dopants in gas form (such as SF_6, SiF_4 etc) enters to the final deposition tube through delivery tube. An ultra-pure silica tube is used as a deposition tube mounted in a lathe, where deposition takes place inside the tube. An oxy-hydrogen burner traverses along the length of deposition tube to provide high temperature for reaction to take place. The temperature of burner can be easily controlled by flow of H_2 and O_2.

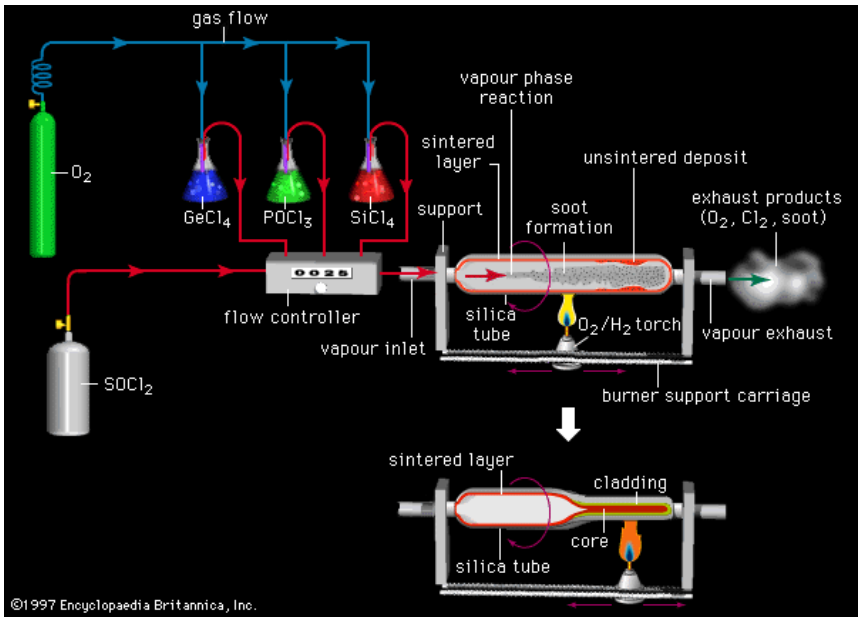

Figure 1.12 MCVD fabrication process. (Figure Source: http://global.britannica.com/technology/modified-chemical-vapour-deposition; © 1997 Encyclopaedia Britannica.)

The reaction takes place inside the silica tube and forms soot particles which deposit on the inner walls of soot tube following the principle of thermophoresis. The following equation 1.3 shows the silica formation:-

$$SiCl_4\ (g) + O_2(g) \rightarrow SiO_2(s) + 2Cl_2(s) \qquad (1.3)$$

Thermophoresis is generated by thermal gradient due to moving torch [10]. The soot particles produced by vapour phase reaction have diameters in the range of 20-100nm and are, thus, entrained in the gas flow. The basic mechanism of thermophoresis is that a suspended particle in a temperature gradient experiences a net force in the direction of decreasing temperature,

resulting from the fact that molecules impacting the particle on opposite sides have different average velocities due to the temperature gradient. As the soot particle moves to cooler region they start deposit on cooler wall, they are still of porous nature and when burner pass through cooler region it becomes consolidated. This process can be repeated a number of times to get the desired profile. After that, collapsing of tube into a rod can be performed as shown in figure 1.12.

1.4.2 Fiber drawing process

Optical fiber drawing process is based on conservation of mass and momentum [11-12]. Preforms prepared by CVD process are drawn into fiber by holding the preform vertically and heating the end of the preform above the glass softening temperature until a glob of glass falls from the end. This forms a neck-down region, which provides transition to a small-diameter filament. The essential components of a draw tower, shown schematically in figure 1.13, are a preform feed mechanism, a furnace capable of 2500^0C, a diameter monitor, a polymer coating applicator, coating curing system, capstan and winding mechanism. The uniformity of the fiber diameter depends on the control of the preform feed rate, the preform temperature, and the pulling tension.

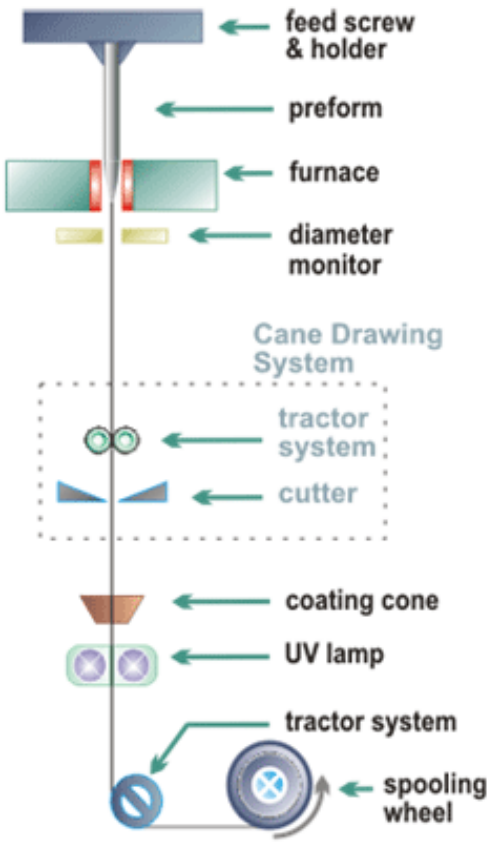

Figure 1.13 fiber drawing tower.
(Figure source: https://www.mpl.mpg.de/en/russell/research/topics/fabrication.html © Max Planck institute for the Science of Light.)

1.4.3 Rare-earth ion incorporation

The highly polymerized structure of pure silica glass does not allow easy accommodation of rare-earth (RE) ions (such as Yb^{3+}, Er^{3+}, Tm^{3+}, and Ho^{3+}) even at low concentrations. Trivalent RE ions do not substitute for silicon in the glass network easily [13] and at the same time they need six to eight oxygen ions for their coordination. Silica has very few non-bridging oxygen ions that can provide such coordination and RE ions are forced to cluster together to share those few oxygen ions that are present in the network. Such clustering can lead to enhanced energy transfers between f^{N-1} energy levels of neighbouring RE ions, concentration self-quenching of luminescence even at low doping level, and rapid phase separation at higher doping levels. The signature of concentration quenching is the decrease of luminescence lifetime with increasing RE concentration [14]. This reduction in lifetime can be represented as following equation 1.4 [15]:-

$$t = \frac{t_o}{(1+(\frac{\rho}{Q})\text{^}p)} \qquad (1.4)$$

Where t_o is the lifetime in the limit of zero concentration
Q is the quenching concentration, ρ is concentration of RE ion, and $p \sim 2$.

Another deleterious process involves energy transfer to the OH^- complex, which serves as a trap and is extremely effective at quenching excited rare earth ions [16]. At high OH^- concentrations, this can occur through direct transfer from the excited ion; at the low OH^- levels present in optical fibres, however, a more likely process is fast energy transfer between interacting donor ions until the excitation reaches one near an OH^- impurity [16]. The latter mechanism is a type of concentration quenching, because of the energy transfer process, hence the rare earth concentration will control the quenching rate. Although donor-donor transfer to OH^-, has been observed for rare earth doped bulk glass samples, it is not consistent with pump-power-dependent behaviour reported for Er^{3+}-doped silica fibers [17].

Co-doping is the most dominant technique to compensate the effects of clustering. Other than reducing clustering they can improve refractive index, shift excited state absorption, increasing emission bandwidth. Co-dopants cluster together with optically active ions shielding them from one another and therefore decreasing energy transfer [18-19]. The most popular solubilizer is Aluminium. Aluminium can be incorporated into the silica network either in tetrahedral coordination as a network former or in octahedral coordination as a network modifier. The four coordinated aluminium shares non-bridging oxygen ions with RE ions, therefore reducing RE ion clustering [20].

Phosphorus is another co-dopant, when co-doped into silica, phosphorus plays a role similar to aluminium and incorporates in two tetrahedral configurations P_2O_5 and P_2O_4. Similar to use of Al, addition of P can be used to solubilize the RE or alter the spectral properties. Phosphorus is essential for efficient operation of Er/Yb-co-doped systems.

1.4.4 Rare-earth doping

There are no inorganic rare-earth compounds that have high enough vapour pressure to be deposited in the same way as P_2O_5, SiO_2 etc. There are two different approaches that can be used to dope the core with RE.

(1) Solution doping technique
(2) Vapour-phase method

1.4.4.1 Solution doping technique

Solution doping is a common method to be used to dope rare earth ions in silica core [21-22]. During soot deposition temperature is reduced so that soot remains porous. Later on, soot is soaked with solution (methanol containing RE ions and other dopants) for some time. Afterwards, soot is dried for some time to remove the methanol, soot is sintered to glass and finally preform is collapsed to a solid rod. The solution doping process can be performed in two ways.

1. Vertical solution doping [21-22].
2. In-situ solution doping technique [23]

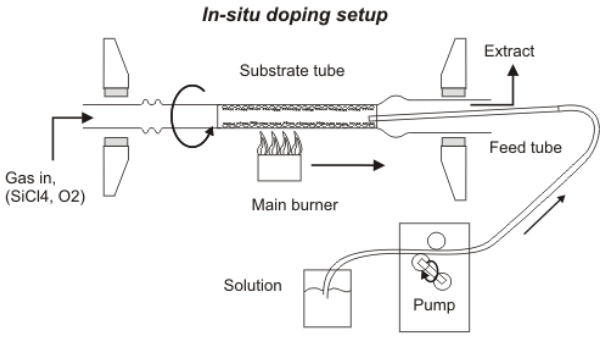

(a)

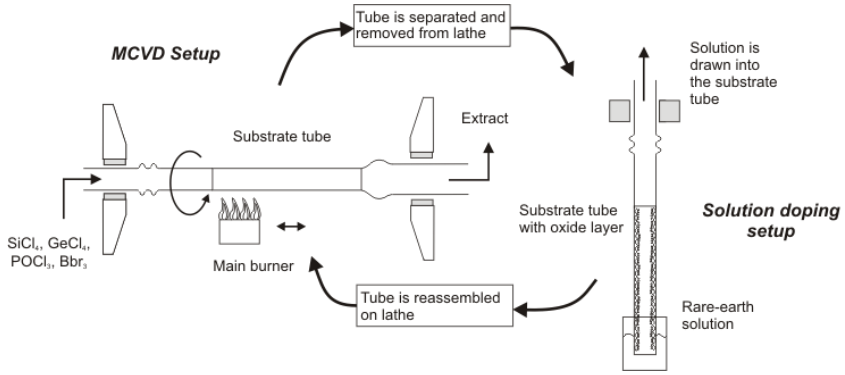

(b)

Figure 1.14 demonstration of (a) vertical solution doping and (b) in-situ solution doping technique. (Figure source: 2014 Silica group, ORC, University of Southampton, UK.)

In-situ solution doping technique is shown in figure 1.14(a). In this technique silica tube remains over the lathe for all the time. A feed tube is inserted through soot tube to feed the solution to silica tube and other end of feed tube is connected to solution bottle via a pump. After doping, soot is dried for some time and then sintered. On the other hand, in vertical solution doping technique after soot deposition, silica tube with delivery tube is removed from lathe and kept in vertical position and then filled with solution using a pump. After the soaking, solution is removed and kept in the same position for drying for some time. After that it is mounted back on lathe and joined with other soot tube.

Advantages of in-situ solution doping technique over vertical solution doping technique:-

1. In-situ doping allows fabrication of more number of doped layers.
2. In-situ solution doping is economical since vertical solution doping leads to wastage of some part of preform while cutting and joining to soot tube. Moreover, in-situ solution doping process lead to less chances of contamination.
3. In-situ solution doping process is time saving compared to vertical solution doping.

1.4.4.2 Vapour phase method

Rare-earth solution doping is a reliable process for rare-earth doped fiber fabrication. However, there are limitations of solution doping techniques such as limited rare-earth element incorporation which restricts higher amount of rare-earth dopants. Researchers have proposed an alternative way of incorporating rare-earth ions using vapour phase delivery [24]. In this RE-chelate can be heated over 150^{o}C to generate sufficient vapours [25-27].

The advantage of this method is that it can incorporate several layers of high amount of rare-earth dopants, which can results into high NA and large diameter core rare-earth doped fiber. This process also takes less time as there is no drying process involved like solution-doping process, so a large number of rare-earth doping steps can be implemented in a relatively short period of time. This technique does not require solution so OH incorporation is relatively low.

However, this process is quite difficult to control since vapour pressure of RE precursors exponentially increase with temperature. That is why, vapour-phase method is difficult to implement in case complex refractive-index profile is required. Moreover, there are several problems associated with vapour delivery system as they need to have a high temperature throughout the delivery system to avoid any condensation of vapours. Moreover, lack of availability of high purity RE-chelate compounds lead to high background loss compared to solution doping process.

1.4.5 Fiber fabrication process for non-cylindrical fiber

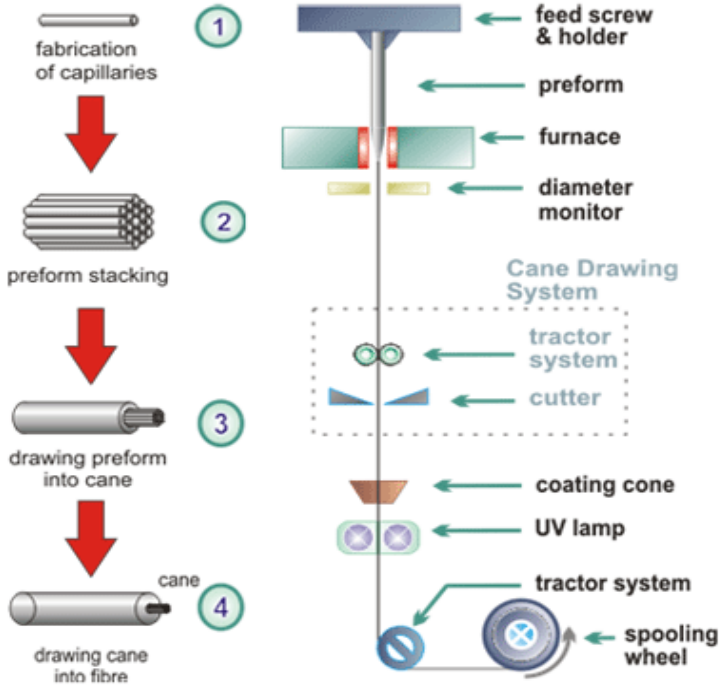

Figure 1.15 stack and draw process for photonic crystal fiber fabrication.
(Figure source: https://www.mpl.mpg.de/en/russell/research/topics/fabrication.html © Max Planck institute for the Science of Light.)

Non-cylindrical fibers such as photonic crystal fiber are typically fabricated by the "stack-and-draw" procedure [28-30]. In this procedure, glass capillaries are stacked into perform carefully in a cleanroom environment (into the desired fiber pattern) as shown in step 1 to 2 in figure 1.15. Preform is inserted into a glass tube to provide mechanical strength. Afterwards this preform is drawn into canes on fiber drawing tower with optimized temperature conditions to fuse the capillaries. However, optimized pressure conditions are used to avoid the collapse of capillaries.

In second step, canes are drawn into final desired fiber. Furnace temperature, feed speed of preform, drawing speed of fiber, and pressure conditions are optimized during fiber drawing process to achieve the desired parameters of final fiber such as core diameter, diameters of air-holes, pitch of air holes etc. Fiber is subsequently coated with a polymer coating to increase mechanical strength of fiber.

1.5 Journey of large mode area optical fiber

Fiber laser were first demonstrated in 1960s by “Father of glass lasers” Snitzer and his colleagues at American Optical Company. Snitzer first demonstrated a Nd doped fiber laser in his seminal paper entitled “Amplification in a Fiber Laser” [1-4]. In this experiment,

Snitzer used flash lamp for pumping a helically coiled Nd doped fiber of 10μm core diameter as shown in figure 1.16. The fiber laser technology was further improved by Stone et. al. in 1973 [5] and Payne et. al. in 1985 [6-9]. A major breakthrough came in 1998, when again Snitzer proposed a double clad fiber for laser diode pumping [10]. This invention made possible to launch multi-moded high pump power into double-clad fiber and opened the door for high power fiber laser.

Afterwards researchers have been working over power scaling and very soon it was realized that telecommunication fibers are not enough for power scaling. In the last decade of 20th century, researchers start working over LMA fibers and different strategies to improve the mode area of the fundamental mode to address non-linear effects.

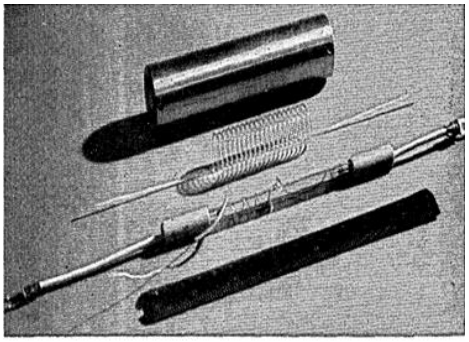

Fig. 1. Coiled fiber laser. From the top the components are: cavity, fiber laser, flashtube, and 18 cm scale

Figure 1.16 first demonstration of fiber laser. (Figure source [3]; © 1964 OSA.)

1.5.1 Effective single approach

The instant approach which came to researchers' mind in order to increase the core diameter was to reduce the NA of core. Early demonstration of low NA Er-doped fibers were limited to 0.066 and were used for pulse amplification in a MOPA configuration [1-2]. Pulse energy upto 180mJ were obtained using these low NA fibers. However, NA was limited around 0.05 even in further developments due to constraint of uniformity and yield of low NA rare-earth doped fiber fabrication technology [1-2]. Afterwards, a term effective single mode operation (ESM) came into picture, where researchers realized that it is not necessary for fiber to be intrinsically single moded to obtain a good output beam quality from a fiber laser. It was found that if it is possible to induce high loss (or small gain) for higher order modes, while achieving low loss (or high gain) in comparison to fundamental mode, then output beam will mainly dominated by amplified fundamental mode even in multi-moded optical fiber [3-5]. However, it is important to note here that, early low NA fibers mostly had central dip in their refractive index profile; central dips are detrimental to mode area of the fundamental mode and beam quality. It is also one of the objectives of this thesis is to develop a low NA (~0.038 with flat refractive index profile. The below-mentioned approaches become popular in the past years for ESM operation.

1.5.1.1 Bend induced loss

In order to achieve high loss for higher order modes, researchers proposed the idea to utilize bend induced loss in a weakly guiding fiber [1-4]. This is a successful approach and is being used for most of the fibers even today. Fiber can be designed in such a way that at a practical bend radius (around 10-20cm for a compact device size) the losses of the higher order modes are larger than a particular level, while the fundamental mode loss remains lower than a particular level. This idea was first exploited in 2000 by Koplow et. al. for a step index fiber of 25μm core diameter and ~0.1NA, in which fiber was coiled to offer high loss to higher order modes without any considerable loss laser efficiency [1].

Later on, similar concept was used by Jeong et. al. for breaking the kilowatt barrier of output power level from a SIF. A Yb-Al doped 40μm core diameter SIF with NA around 0.05 coiled at around 24cm bend diameter was used to achieve a M^2=1.4 [5]. A criterion of just 1dB/m was used to filter out higher order mode with a total length of around 12m. However, M. J. Li et. al. later on claimed that a higher M^2 =1.4 in this experiment is perhaps due to lower criterion of the higher order modes loss [6]. They suggested a criterion of 10dB/m for higher order modes while keeping fundamental mode loss to be lower than 0.1dB/m. Following this criterion, a maximum achievable effective area of 300μm^2 (including bend-induced effective area reduction) can be achieved for a 0.06 NA as shown in figure 1.17(a). It is pertinent to note that, it is difficult to standardize a particular criterion of loss level of higher order modes to ensure a good beam quality as a good M^2 does not always ensure a single-mode operation [7]. It depends on several factors such as length of fiber used, modal excitation, gain for fundamental mode and higher order modes etc. In 2013, V. Khitrov et. al. has also demonstrated a Yb doped SIF with NA as low as 0.048, although fiber laser shows significant Raman generation at 3kW output [8]. Figure 1.17 shows the numerically computed maximum achievable effective areas of different NA (0.06, 0.038) of step-index fiber for different criterion of higher order modes loss such as 1dB/m and 10dB/m while keeping fundamental mode loss to be lower than 0.1dB/m. Table 1.2 summarizes the result shown in figure 1.17. The maximum achievable effective area for 10dB/m loss criterion of higher order mode loss is ~302μm^2 and ~700μm^2 for two different NAs 0.06 and 0.038 respectively. The core diameter is approximately ~24μm and ~35μm for 0.006 and 0.038 NAs respectively. It is interesting to note that bend diameter required here is ~8.25cm and ~32cm for 0.06 and 0.038 NAs respectively. Similarly, the maximum achievable effective area for 1dB/m loss criterion of higher order mode loss is ~374μm^2 and ~866μm^2 for two different NAs 0.06 and 0.038 respectively. The core diameter is approximately ~32μm and ~46μm for 0.06 and 0.038 NAs respectively. It is interesting to note that bend diameters required here are ~8cm and ~30cm for 0.06 and 0.038 NAs respectively. It is interesting to note here that the bend diameter (30cm to 32cm) achieved in case of 0.038NA is quite large as compared to ~8cm for NA of 0.06, which is lower than 10cm. Infact, it is another advantage offered here by low NA SIF which addresses the issue of mechanical reliability of large diameter optical fiber under tight bending condition.

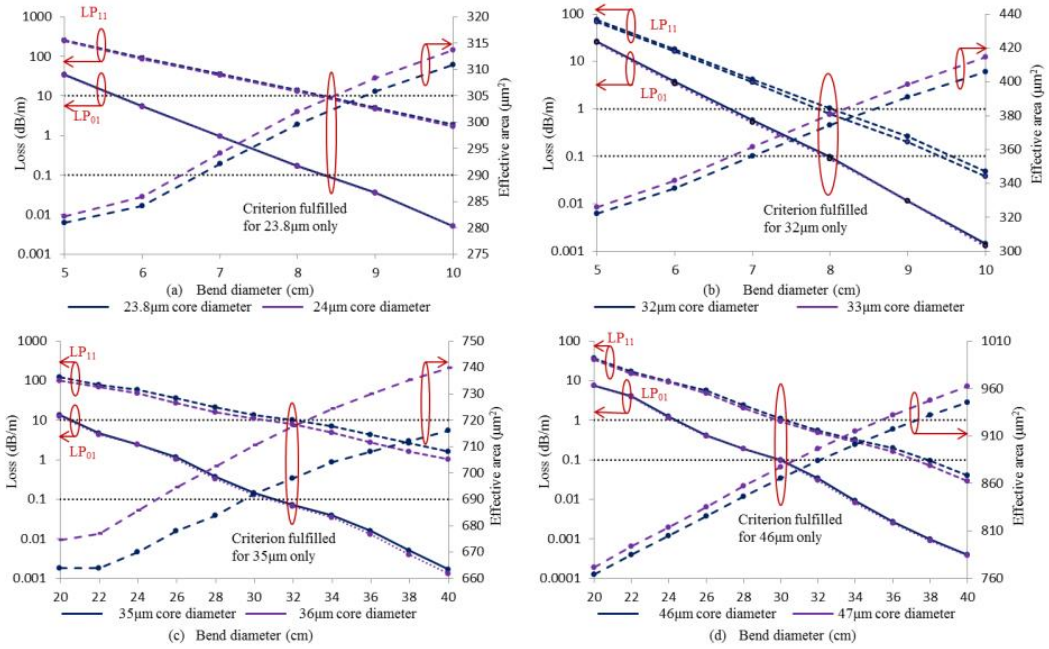

Figure 1.17 (a) and (b) the loss of LP_{01} and LP_{11} modes and effective area of LP_{01} of SIF w.r.t. bending diameter for different core diameter with fixed core Δn of 0.00124 at 1060nm to fulfill the different criterion of 10dB/m and 1dB/m respectively (c) and (d) the loss of LP_{01} and LP_{11} modes and effective area of LP_{01} of SIF w.r.t. bending diameter for different core diameter with fixed core Δn of 0.0005 at 1060nm to fulfil the different criterion of 10dB/m and 1dB/m respectively.

Fini et. al proposed that a parabolic fiber has natural immunity to bend-induced effective area reduction compared to SIF [9-10]. However, parabolic fiber offers less effective area compared to same core diameter SIF. Recently Fini et. al. demonstrated a bend-compensated parabolic fiber, which can achieve an effective area of 1,000μm^2 at 15cm bend radius [11]. The ESM operation is ensured by keeping fundamental mode to be lower than 0.01dB/m and higher order modes to be larger than 100dB/m. This is an extraordinary achievement in terms of mode are scaling of a fiber in bent configuration as the loss ratio exceeds 10^4. However, the requirement in controlling refractive index is on the scale of 10^{-4}, which is very difficult to achieve in the current limit of fabrication technology. Therefore, no experimental realization of fiber has been achieved successfully so far.

Table 1.2 maximum achievable effective area for different criterion.

Core Δn (NA)	Maximum Effective area for Criterion 10dB/m	Core Diameter	Bend Diameter	Maximum Effective area for Criterion 1dB/m	Core Diameter	Bend Diameter
0.00124 (0.06)	~302μm^2	23.8μm	8.25cm	~374μm^2	32μm	8cm
0.0005 (0.038)	~700μm^2	35μm	32cm	~866μm^2	46μm	30cm

1.5.1.2 Single mode excitation

Single mode excitation is another approach to achieve a Gaussian output beam in a multi-moded fiber, where excitation of light can be done in such a way that only single-mode is excited even in a multi-moded fiber [1]. In 1977, Fermann et. al. at IMRA demonstrated an effective single-mode output from a 45μm core diameter multi-moded fiber (NA=0.13) with outer diameter of 250μm at 1.56μm wavelength [2]. A 20m long fiber bend at ~32cm bend diameter was used in this experiment. Fermann found that a large cladding diameter is helpful to mitigate modal coupling, which disturbs the single mode operation [2]. This technique was further exploited by Stacey et. al. that a 300μm core diameter passive fiber (NA=0.389) can also provide a single-mode operation using this technique [3]. However, in this experiment a very small length of fiber (up to 20cm) was used. Moreover, fiber was kept straight and input beam was carefully aligned to launch light in fiber. Hurand et. al. also implemented single mode excitation technique in a 100μm to 400μm fiber with varying outer cladding diameter [4]. Studies reveal a good agreement with Fermann observation that increase in outer diameter leads to improvement in beam quality due to less mode coupling. Researchers at University of Michigan successfully implemented this technique to an 80μm core diameter low NA coiled SIF (0.06) to achieve a good beam-quality (M^2~1.3) [4-5]. Table 1.3 shows the M^2 output from different core diameter SIF (NA=0.06) using coiling and single-mode excitation [5-7]. It is important to note that single-mode excitation in a multi-moded fiber using a careful excitation of input beam is an effective technique to control output beam. However, it reduces the reliability and flexibility of fiber laser and limited to laboratory experiments.

Table 1.3 M^2 output from different core diameter SIF (NA=0.06) using coiling and single-mode excitation.

Core diameter	Obtained M^2 value
65μm	1.1
80μm	1.3
115μm	5
200μm	6.5

1.5.1.3 Fiber tapering

The need of tapering of single mode optical fiber was felt in developing phase of optical fiber for communication as early as in 1980s [1]. One of the initial purposes of tapering single mode fiber was to overcome the difficult launching into single mode fiber due to its small core size. Fiber was tapered up to increase the core dimension to make launching process easier. This technique was later on exploited for fiber laser by Alvarez-Chavez et. al. in 1999 [2]. In a multi-moded fiber laser cavity, a small length of fiber was tapered down to strip off the higher order modes. However, any improvement in beam quality was achieved on the cost of reduced slope efficiency, for example in order to improve M^2 from 2.6 to 1.4, a 18% reduction from 85% to 67% in slope efficiency was observed. Researchers at Tampere University of Technology have explored this technique in details from 2008 onwards. They

tapered the fiber over a long length to uniformly strip off the higher order modes to avoid reduction in laser efficiency. In 2008, a 84W output power ytterbium doped fiber laser was demonstrated with M^2 =1.07 using a 10.5m long tapered fiber with good slope efficiency of 92% [3-4]. In 2009, power was scaled to 600W with M^2=1.08 using tapered fiber but slope efficiency was reduced to 63% [5]. This efficiency was further improved to 80% with output power of 750W [6]. Further, an actively Q-switched tapered double clad fiber laser capable of single-shot generation of 1.6mJ, 64ns pulses at ~1060nm was demonstrated using tapered fiber. However, reported beam quality was 2.7 and 1.8 at wide and narrow end of fiber [7]. In 2012, a tapered fiber of 7m long length with 5m tapered length was demonstrated [8]. The core diameter was 117μm and 6.5μm at wide and narrow bend respectively. Cut-back measurement shows single to multi-mode operation, while going from narrow to wide end. These experiments show that tapering of large mode area fiber can be used for improving beam quality of fiber. However, it is important to understand that the offered large mode area is only for very small length of fiber. After travelling through large mode area region, light has to travel narrow region, which might cause non-linear effects when power level is exceeding threshold level of non-linear effects.

1.5.1.4 Helical core fiber

In order to induce high loss to higher order modes, a radical approach of helical core has been used [1-4]. In this case, core offer high loss to higher order modes due to its intrinsic bend configuration in fiber [1]. Figure 1.18 shows the schematic of a helical core fiber. Fiber has a core with offset of Q from centre of fiber and core has a helical nature with respect to axis of fibre's centre with a pitch of P. Preforms having offset core were fabricated using conventional MCVD in conjunction with rod-in-tube process [3-4]. A helical core was obtained by spinning the preform during fiber drawing [3-4]. Helical core fibers have their roots in 1980s, when these were investigated for polarization maintaining fiber for passive transmission and sensor application [5-6]. In 2003, Moore et. al. demonstrated the idea of using a helical core fiber for high power fiber laser [2]. In 2004 and 2006, researchers at ORC, University of Southampton first experimentally demonstrated a helical core fiber for high power fiber laser [3-4]. A 26μm core diameter and 0.14 NA Yb-doped fiber was used for core pumped laser configuration [3-4]. In 2006, a 30μm helical-core fiber with 0.087NA was reported yielding 84% laser efficiency in a cladding pump configuration with maximum output power of 60.4W and 1.4M^2 [3-4].

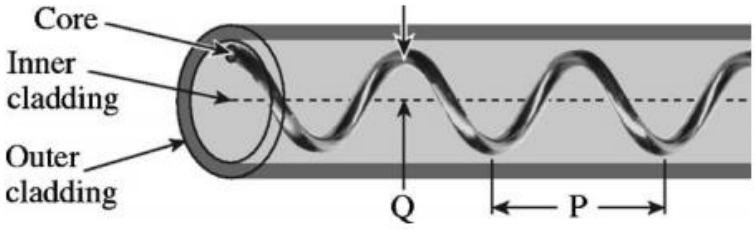

Figure 1.18 schematic of helical core fiber. Q is the offset distance of core from center of fiber. P is the pitch of helical core. (Figure source [7]; © 2006 OSA)

Advantages of helical core fiber can be briefly summarized as follow:-

1. Polarization maintaining: - As explored in early 80s, helical core fiber maintains circular birefringence thanks to their geometry [3-4]. It can be made large enough for maintaining linear or circular polarization in a fiber laser configuration by carefully choosing the fiber parameters. This polarization maintaining property was also observed in above mentioned experiments.

2. Enhanced pump absorption: - Helical trajectory of core helps to absorb skew rays of pump light and this can lead to enhanced pump absorption.

3. Mode area scaling: - The main purpose of using helical-core fiber in fiber laser is to gain in terms of LMA. Figure 1.19 shows the calculated propagation loss of LP_{01} and LP_{11} modes in unbent case reported by Wang et. al. in 2006 [3-4]. The loss of the fundamental mode is lower than 0.6dB/m and LP_{11} is larger than 9dB/m. It is important to note that 0.6dB/m is quite large for fundamental mode in unbent case, normally a fundamental mode loss lower than 0.1dB/m and higher order modes larger than 10dB/m in bent case is acceptable. Moreover, Wang et. al. did not report any numerically calculated losses for helical-core fiber in bent case. However, they observed significant loss during laser efficiency measurement, which may be due to bend losses of helical-core fiber. Wang et. al also drew a step index fiber from same preform and obviously step index fiber in unbent case shows multimode operation. It is important to note that, a 30μm core SIF with core NA 0.087 is heavily multi-moded and does not offer significant discrimination between fundamental mode and higher order modes, even though helical-core fiber does not fulfil criterion of effective single mode operation for fiber laser case but it seems to offer better performance than step-index fiber. However, a detailed investigation is required to find out whether helical-core fiber performs better than step-index fiber while fulfilling criterion for effective single mode operation. In 2006, Jiang et. al. proposed that an effective single mode operation can be scaled up to 100μm core diameter using helical core fiber [7]. However, loss discrimination between fundamental mode and higher order modes is low and bending behaviour of fiber is not reported [7].

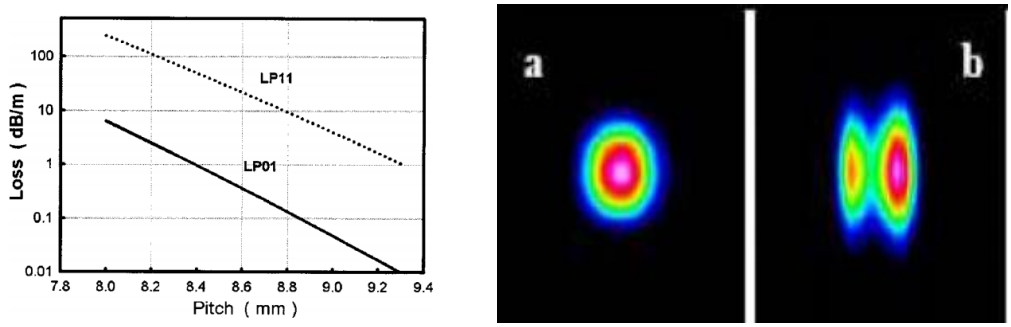

Figure 1.19 propagation loss of LP_{01} and LP_{11} in an unbent 30μm helical-core fiber with NA0.087 and pitch to be ~8.5mm to ~8.8mm. Inset shows the fiber laser output from helical core fiber and step index fiber drawn from same fiber. (Figure source [4]; © 2006 OSA)

Disadvantages: - This fiber suffers from severe problem of splicing with other conventional fibers due to helical trajectory of its core. It is also very difficult to launch light in core owing to lateral offset and angular tilt of its core. Above experiments were done using free space optics and a considerable difficulties were reported in launching light in fiber core. Recently, Kim et. al. demonstrated a new launch scheme for a helical-core fiber using an adiabatically tapered splice technique [8]. Adiabatically tapered splice have been used in past to splice different modal field diameters fiber for efficient coupling. However, this technique provides merely a 26% coupling efficiency in case of helical core fiber [8].

1.5.1.5 Flat field fiber

A fiber providing flat-field or top-hat profile can be very useful to dramatically enhance the effective-area of the fundamental mode of optical fiber. This idea was first adopted by Ghatak et. al. in 1999 [1]. Figure 1.20 shows the electric field profile of a step index fiber of core radius 15µm, dn=0.00124 and a flat-field fiber with r_{in}=12.6µm, r_{out}=15µm, and dn_{in}=0.001 and dn_{out}=0.002. It is easy to observe from the profile of the normalized electric field of fundamental mode of both fibers that field of flat field fiber is actually flat and this leads to a large effective area of ~782µm^2 of the fundamental mode compared to ~467µm^2 achieved by fundamental mode of step-index fiber with same fiber parameters. This dramatic increase in effective area can be extremely useful for mitigating non-linear effects. Later on in 2003 and 2004, researchers at Lawrence Livermore National Laboratory experimentally demonstrated flat-field fiber and compared the results with step index fiber [2-3].

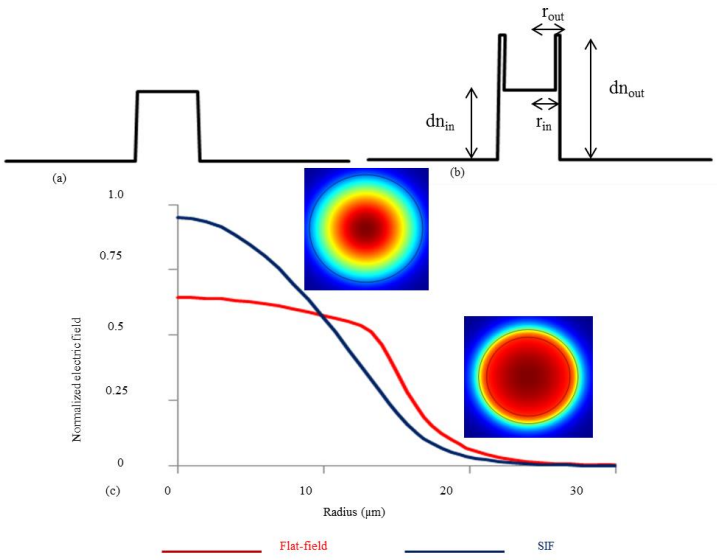

Figure 1.20 (a) schematic of step index fiber (b) flat-field or top-hat fiber (c) normalized electric field of fundamental mode of both fibers.

In order to understand the advantages of flat field fiber in bent configuration, numerical simulations were performed on flat-field fiber parameters (r_{in}, r_{out}, dn_{in}, and dn_{out}) proposed by Dawson et. al. at Lawrence Livermore National Laboratory [2-3]. Figure 1.21 (a) and (b) shows the normalized electric field of the fundamental mode for both fibers at different bend radii. Figure 1.21(c) shows the computed effective area of fundamental mode for both fibers.

It is interesting to see that, the dramatic increase in effective area achieved for the fundamental mode in unbent case disappear very quickly with decreasing bend radius. Dawson et. al. did not consider this important fact in their study. It is pertinent to note here that achievement of large effective area of the fundamental mode achieved by flat fiber is not quite effective in bend case. The effective area of the fundamental mode in flat fiber case reduces from ~782 μm^2 to ~431μm^2 at 10cm bend radius, on the other hand the effective area of the fundamental mode in step-index fiber case reduces from ~487 μm^2 to ~450μm^2 at 10cm bend radius for same fiber parameters. At 10cm bend radius, the effective area of the fundamental mode of SIF is larger than flat field fiber.

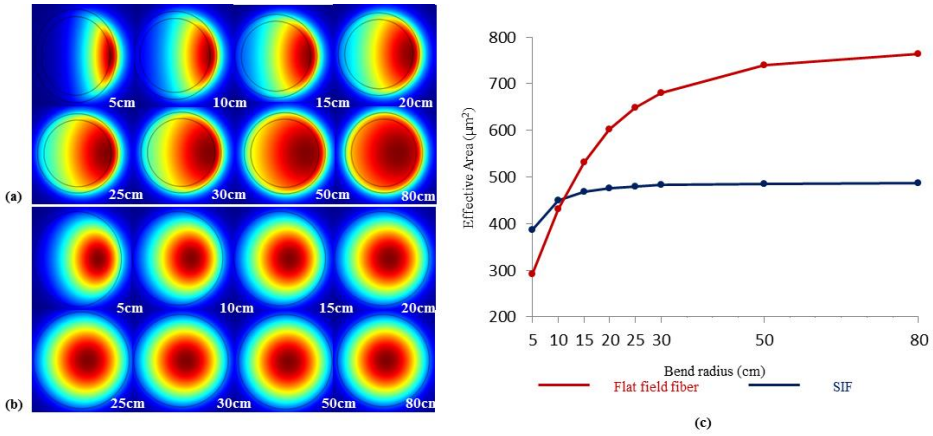

Figure 1.21 (a) 2-D normalized electric field of the fundamental mode of flat field or top-hat fiber at different bend radii (b) 2-D normalized electric field of fundamental mode of step index fiber at different bend radii (c) effective area of fundamental mode of both fibers with respect to different bend radii.

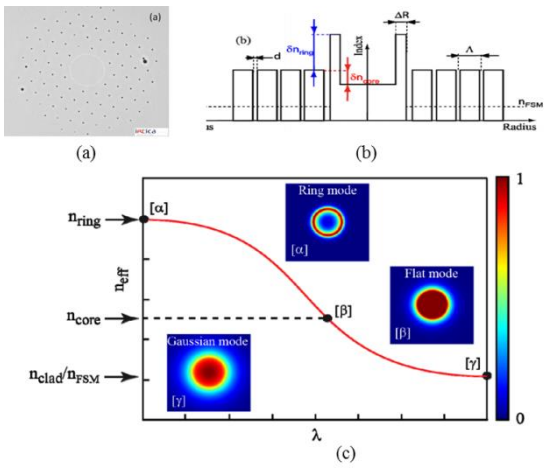

Figure 1.22 (a) 2-D normalized electric field of flat field or top-hat fiber at different bend radius (b) 2-D normalized electric field of step index fiber at different bend radius (c) effective area of both fibers with respect to different bend radius. (Figure source [4]; © 2013 OSA)

Researchers have applied similar technique to photonic crystal fiber to achieve flat field [4]. It is also important to understand that while achieving flat field of the fundamental mode, a challenge of achieving ESM operation still remains there. In 2013, Valentin et. al. experimentally demonstrated first flat-field photonic crystal fiber [4]. A PCF with index depressed core surrounding by a high-index ring was used to achieve a flat field as shown in

figure 1.22(a) and (b). Figure 1.22(c) shows the schematic of fundamental mode of core with respect to wavelength. At shorter wavelengths, mode is very well guided in the ring and appears like a ring mode. At intermediate wavelengths, n_{eff} of the fundamental mode is equal of refractive index of core and mode appears as a flat mode. At higher wavelengths, n_{eff} of the fundamental mode is lower than the refractive index of core and appears as a typical Gaussian mode.

However, the above mentioned effective single-mode flat mode is achieved at the cost of higher loss of the fundamental mode. The loss of fundamental mode is ~0.23dB/m in unbent case. Moreover, the bending loss exceeds 5dB/m for a ~10cm bend radius for merely a ~13.5μm core fiber. Fiber has an effective area of ~320μm^2 in unbent case for fundamental mode.

Researchers at Clemenson University also adopted an index depressed core technique in a leakage channel fiber to achieve a flat field and large effective area of the fundamental mode as shown in figure 1.23(a) [5]. However, as discussed above the area is extremely bend sensitive, to achieve any advantaged of flat field over conventional fiber a bend diameter of ~1m is required as shown in figure 1.23(b). Moreover, the achieved effective area is just 1,000μm^2 and the losses of the higher order mode are very low at this bend diameter of 1m as shown in figure 1.23(c) [5]. In lieu of above analysis, it can be concluded that in case of flat field, it is difficult to achieve any advantage in term of large effective area in a compact device size. Moreover, if one use the flat-fiber in unbent case then it is difficult to induce high losses for the fundamental mode to achieve single mode operation.

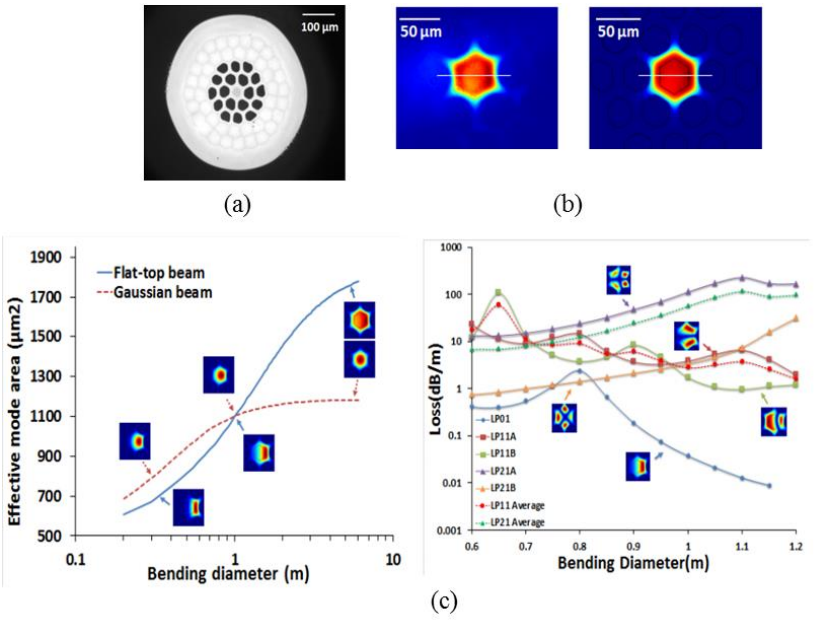

Figure 1.23 (a) 2-D normalized electric field of flat field or top-hat fiber at different bend radius (b) 2-D normalized electric field of step index fiber at different bend radius (c) effective area of both fibers with respect to different bend radius. (Figure source [5]; © 2013 OSA)

1.5.1.6 SHARC fiber

A novel fiber having high-aspect-ratio rectangular core instead of a circular core for mode area scaling has been proposed by Rockwell et. al. in 2011 [1-2] as shown in figure 1.24. Fiber can be intrinsically single moded along fast-axis and leaky multi-moded along slow-axis. That is why, these fibers are known as semi-guiding high aspect ratio rectangular core fiber (SHARC fiber). Along slow-axis, higher order modes can be filtered out owing to high leakage losses and an ESM operation can be obtained.

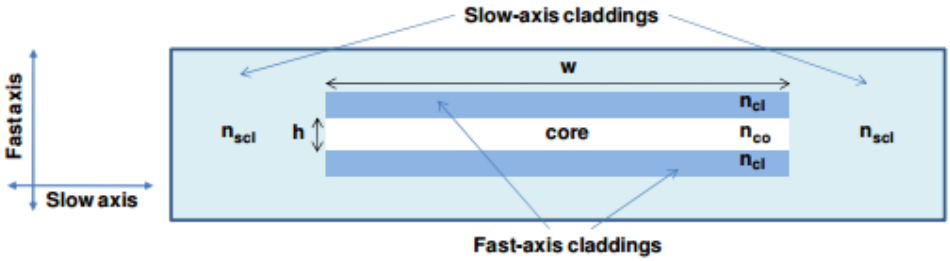

Figure 1.24 (a) Schematic cross section of a semi-guiding high-aspect-ratio core (SHARC) fiber. (Figure source [1]; © 2011 OSA)

The fiber shows several advantages such as resistant to mode area shrinking under bend configuration, all-solid design, and higher refractive index than cladding. SHARC fiber can offer large mode area under tight configuration compared to their counterparts. However, authors have not clearly mentioned the loss ratio between fundamental mode and higher order modes to maintain effective single-mode operation. Moreover, SHARC fiber does not have compatibility with fiber laser components to have an all-fiberized fiber laser. It would be difficult to splice them with circular core fibers due to their high-aspect-ratio rectangular fiber. Moreover, no successful demonstration of a laser device based on SHARC fiber has been demonstrated.

1.5.1.7 Higher order mode approach

Ramachandran et. al. at proposed a radical approach for mode area scaling by using higher order modes instead of using fundamental mode in a conventional fiber [1]. Higher order modes have several advantages of such as larger mode area compared to fundamental mode [2] and natural bend induced immunity to mode area shrinking under bend condition [3].

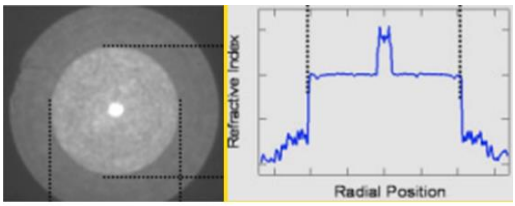

Figure 1.25 (a) 2d-cross-section of double-clad step index fiber (b) refractive index profile of double clad step-index fiber. (Figure source [1]; © 2008 WILEY-VCH Verlag GmbH & Co. KGaA, Weinheim.)

To exploit the advantages of higher order modes, Ramachandran et. al. used a conventional double clad step-index fiber shown in figure 1.25. Figure 1.25(a) shows the cross-section of double clad step-index fiber and 1.25(b) shows the refractive index profile of double-clad step-index fiber. An UV-induced in-fiber long period grating is used to convert LP_{01} core mode to other higher order modes (such as LP_{08}) residing in first cladding. After the amplification in cladding, higher order mode can be converted back to the fundamental mode using long period gratings.

Higher order modes have the following advantages over fundamental mode;-

(1) Large mode area
(2) Bend resistant effective area reduction

It is possible to have a higher order mode having large effective area compared to LP_{01} mode thanks to the spatial distribution of their field [2]. Moreover, higher order modes have better bend resistance than fundamental mode as shown in figure 1.26 due to lower effective refractive index than the fundamental mode as shown in figure 1.27 [3]. Figure 1.26 shows the ratio of bent area to area under unbent condition. Higher order modes (such as LP_{07} and LP_{03}) shows better ratio than the fundamental mode. Due to this property higher order modes can be a viable solution to address the effective area reduction of the fundamental mode in bent configuration. To avoid the reduction of the effective area of the fundamental mode under bend configuration, a large coil diameter is used. This problem leads to an increased large device size. To a certain extent, higher order modes are able to address the challenge of effective area reduction. However, there are few speculations about this approach. First is that waveguide is still multi-moded, just launching one mode cannot ensure always single-mode operation. Fiber is heavily multi-moded and can lead to excitation of other higher modes under external perturbations. Second concern is about LPG capability to withstand high temperature while scaling power level of fiber lasers.

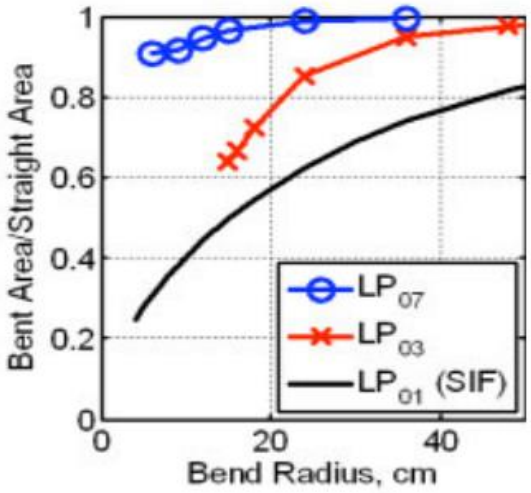

Figure 1.26 (a) ratio of bent area to straight area of different modes for different bend radii of a SIF. (Figure source [1]; © 2008 WILEY-VCH Verlag GmbH & Co. KGaA, Weinheim.)

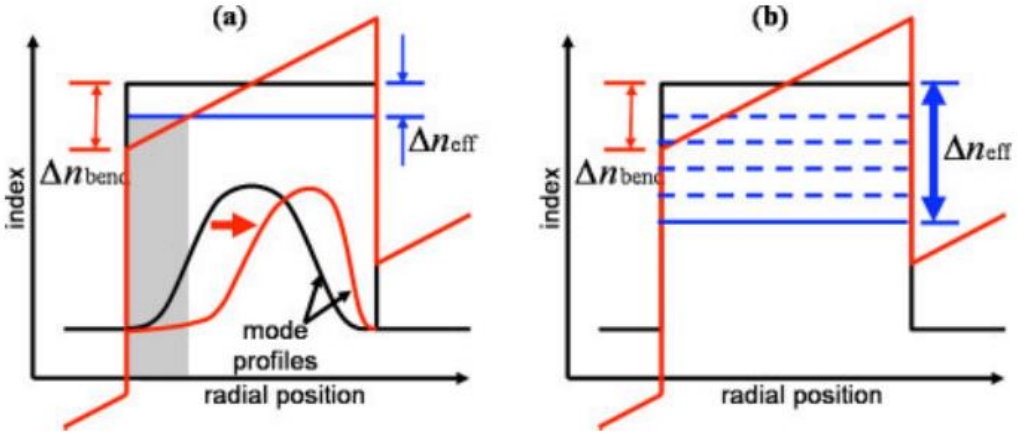

Figure 1.27 (a) bend induced mode shrinking of LP_{01} mode of core (b) natural immunity of the higher order modes due to higher Δn_{eff} compared to Δn_{bend}. (Figure source [1]; © 2008 WILEY-VCH Verlag GmbH & Co. KGaA, Weinheim.)

1.5.1.8 Tailoring Dopant profile

Tailoring of gain of different modes can be achieved by confined doping as shown in figure 1.28 [1-3]. Figure 1.28 shows that the inner section of the core is doped with rare-earth ions. Otherwise, both undoped and doped regions of the core have same refractive index. Due to confined doping, fundamental mode receives higher gain compared to other higher order modes due to larger spatial overlap with doped region. Therefore, it is possible to have an ESM operation thanks to the gain discrimination.

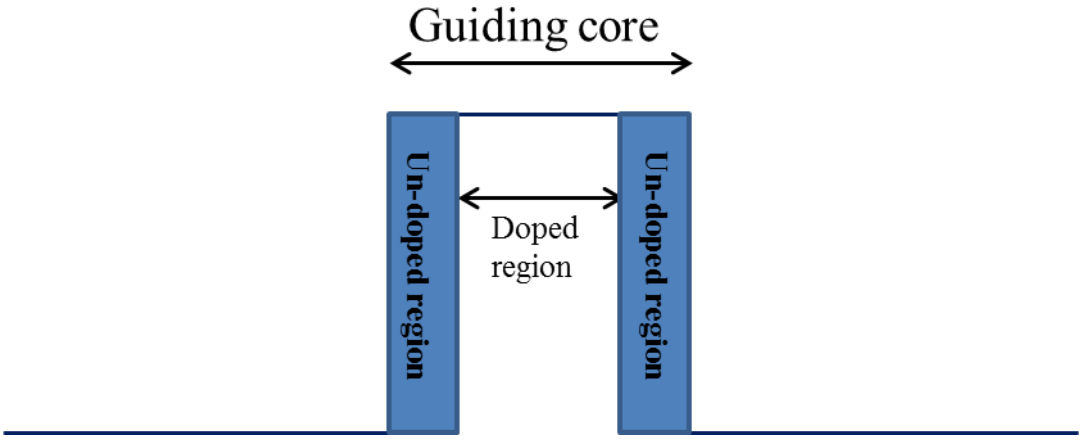

Figure 1.28 a step-index fiber having confined doping, only central part is doped and surrounding region is un-doped.

Marciante et. al. demonstrated a 28μm core diameter fiber, in which the doped region is 17μm, can show a diffraction limited output (M^2 value ~1.3) in a fiber laser cavity [1-2]. On the other hand, a 28μm core diameter fiber with fully doped core shows a higher M^2 value. Yb-doped fibers of 0.06NA were used at a bend diameter of 6cm in these experiments. Table 1.4 shows the overlap of LP_{01} and LP_{11} (both polarizations) modes with doped section of core and complete core for above mentioned

parameters. It is interesting to note that modal overlap discrimination between fundamental mode and LP_{11} modes differ significantly for confined doped core, which ensures a minimum overlap discrimination of 18%. On the other hand, in case of a fully doped core difference in overlap is merely ~5%. In this case, fiber is bent at 6cm and other higher order modes of the core such as LP_{21}, LP_{02} etc. are heavily leaky.

In unbent case, the discrimination between LP_{01} and LP_{11} in case of confined doping is ~28%, which is larger than bent case. It is due to mode shrinking effect as shown in Figure 1.29. However, fiber in unbent case is heavily multimoded and there are other higher order mode such as LP_{02} has high power fraction in core.

Table 1.4 overlap of power with doped section of core and complete core for bent and unbent cases.

Mode	**Overlap with doped section of core (overlap with complete core) in bent case**	**Bend induced loss at 6cm radius**	**Overlap with doped section of core (overlap with complete core) in unbent case**
LP_{01}	58.40% (95.74%)	0.00007dB/m	64% (97.10%)
LP_{11}(a)	32.29% (90.56%)	0.02dB/m	36% (91.85%)
LP_{11}(b)	40.47% (90.60%)	0.54dB/m	36% (91.85%)

Confined doping can certainly provide some discrimination in gain between fundamental and higher order modes. This technique has been successfully implemented in rod-type fiber lasers as an additional mechanism of ensuring effective single mode operation [4]. However, this technique cannot be used solely for ensuring single mode operation due to following reasons:

1. The tendency of modes to shrink (esp. fundamental mode) towards outer region of core under bent configuration significantly reduces the discrimination of modal overlap with confined doping region between fundamental and other modes as shown in figure 1.29.

2. Discrimination achieved even in unbent case is not high enough to ensure robust ESM operation. Researchers have pointed out that a minimum of ~30% discrimination is required [5].

3. In the demonstration by Marciante et. al., a M^2 of ~1.3 has been obtained for merely a ~28μm core diameter [2], which is not good compared to same core diameter fiber laser demonstration using other technique (such as low NA SIF). Moreover, due to reduced cladding absorption (because of less doping area) longer length of fiber is required for lasing and this is detrimental for non-linear effects. Furthermore, mode shrinkage increases with increasing core diameter under bent configuration.

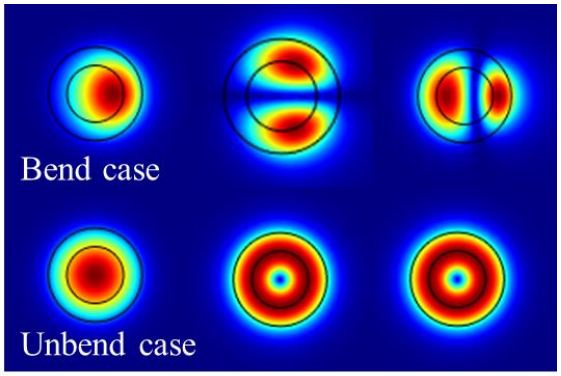

Figure 1.29 normalized electric field of first three modes for both bent and unbent case. Inner circle in bend case shows the doped region.

1.5.1.9 Gain-Guiding Index Anti-guiding approach

A radical approach known as "Gain-guiding Index anti-guiding" approach was proposed by Siegman in 2003 [1]. As it is clear from the name, core has lower refractive index than cladding hence it cannot guide due to total internal reflection, that is why all the modes are heavily lossy. However, core is doped with rare-earth ion, where it can see the gain, so there can be guidance due to gain only. The loss due to anti-guidance can be overcome by gain. It is obvious that higher order modes have larger loss and lower gain than fundamental mode. In this way, it is possible to achieve an effective single mode lasing operation. Detailed theoretical investigations have been reported by Siegman in his two papers [2-3].

A 100μm core diameter and further extended to 200-400μm core diameter also been demonstrated experimentally using this approach by researchers at University of Central Florida [4-5]. However, this approach did not attract further interest as there are several issues with this approach. For example, high lasing threshold level and poor cladding pump efficiency leads to poor laser efficiency and limited power scaling.

1.5.1.10 Photonic crystal fiber

Photonic crystal fibers (PCFs) also known as micro-structured fibers are one of the most important landmarks achieved in the last century in the field of optical fibers [1-8]. PCFs are made up of a single material (typically of un-doped silica), basically a two dimensional photonic crystal in which air-holes are periodically arranged along the cross section of fiber. Few missing air-holes constitute the core of fiber, where the guidance of light takes place. Figure 1.30 shows the schematic of a PCF. The distance between adjacent air-holes is known as pitch (Λ). This arrangement of air-holes in undoped silica provides outstanding properties such as endlessly single mode guidance, anomalous dispersion, and achievement of ultra-low numerical aperture of core etc. [1-8].

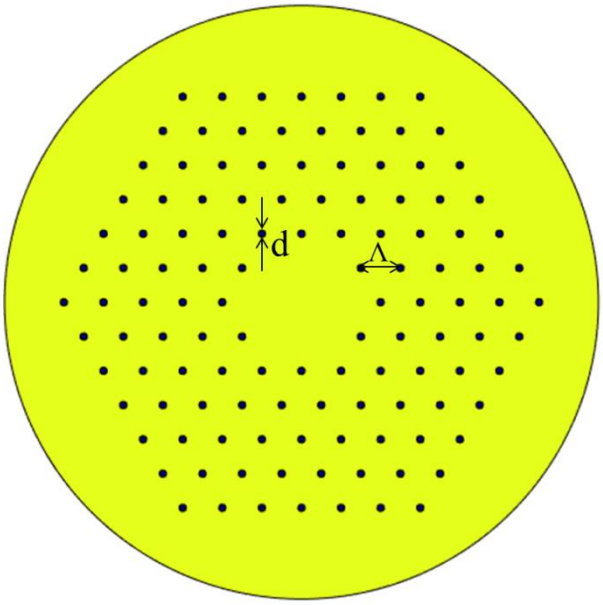

Figure 1.30 schematic of a typical photonic crystal fiber. Blue and yellow colour presents air-hole and silica region respectively, where Λ is distance between two air-holes and d is the diameter of air hole.

(a) Endlessly single mode operation

In a conventional fiber, a single mode is ensured by keeping normalized frequency lower than 2.405.

$$V = \frac{2*\pi*a*\sqrt[2]{\left(n_{core}^2 - n_{cladding}^2\right)}}{\lambda} \quad (1.5)$$

It is evident from this equation 1.5 that, a single mode behaviour (V<2.405) is difficult to ensure over a wide range of wavelength esp. at lower wavelength due to inverse proportionality to wavelength of operation. The guidance principle of PCFs is still based on modified form of well-known total internal reflection, which is known here as modified total internal reflection (MTIR). In case of PCF the normalized frequency can be modified as shown by equation 1.6:-

$$V = \frac{2*\pi*a*\sqrt[2]{\left(n_{core}^2 - n_{cladding}^2(\lambda)\right)}}{\lambda} \quad (1.6)$$

In this case, cladding can be made a function of operating wavelength, which can counteract the effect of inverse dependence of normalized frequency to wavelength of operation. At lower wavelengths (lower than dimensions of air-holes), air-holes does not guide light and have evanescent light only, hence light resides only in silica region between air holes. This leads to higher refractive index of cladding. On other hand, at longer wavelength (larger than dimensions of air holes) light in cladding see refractive index as average effective refractive index of silica and air region, which leads to lower cladding effective index compared to lower wavelengths. A single mode operation from 337nm to 1550nm has been demonstrated

for a PCF [2]. This outstanding feature of PCF can be understood from the highly dispersive nature of cladding.

(b) Modal Sieving

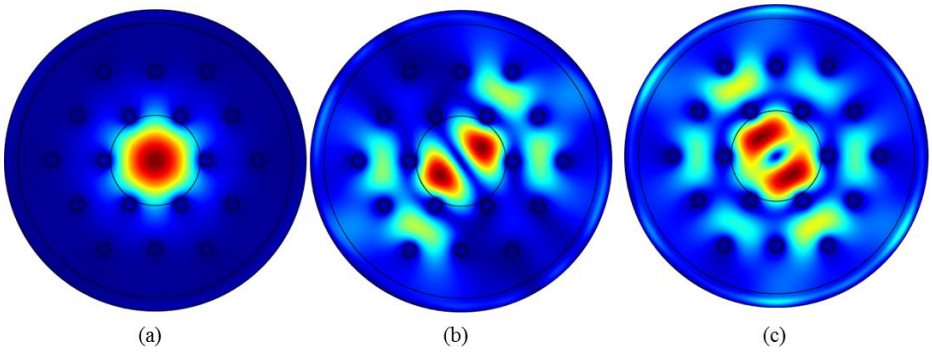

Figure 1.31 normalized electric field of three modes (LP_{01} and two different orientations of LP_{11}) showing modal sieving nature of PCF.

Due to non-continuous interface between solid-core and air-holes, cladding acts a modal siever [6]. The region between two air-holes allows light to leak away, therefore modes having smaller lobes have higher leakage loss. Fundamental mode having single lobe suffer from least leakage loss compared to other higher order modes. Figure 1.31 shows the normalized electric field pattern of fundamental and LP_{11} like modes of a PCF having only two rings of air-holes with relatively large pitch. Here two rings and large pitch have been used intentionally to emphasize the modal sieving property. This property has been successfully used by researchers for mode area scaling of effective single mode operation [8-9].

(c)Ultra-low NA for mode area scaling

The refractive index of cladding can be controlled by controlling the diameter of air holes and pitch of air holes. This is helpful in achieving low numerical aperture of core, which is difficult to achieve in case of a conventional step index fiber. Prior to this thesis work, only possible achievable NA for rare-earth doped SIF was ~0.05 to 0.06 with good reproducibility. Based on capability of low NA of PCF and modal sieving, PCF has been exploited for mode area scaling of ESM operation in coiled configuration for a compact device [8]. In order to further scale the mode area, some modification has been made to PCF, by reducing number of rings of holes and optimizing the pitch thickness for rod-type configuration [9]. Rod-type photonic crystal fiber will be discussed in detail in other chapters of this thesis.

1.5.1.11Leakage channel fiber (LCF)

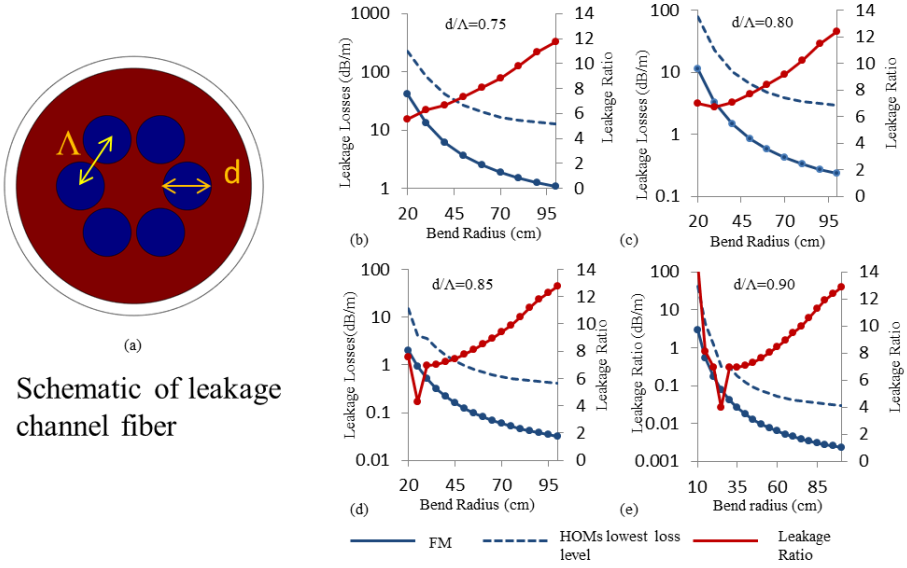

Figure 1.32 (a) schematic of leakage channel fiber (LCF). (b-e) calculated loss of the fundamental and lowest lossy higher order modes for different d/Λ ratios for a fixed 2*Λ-d=60μm.

Leakage channel fiber is a modified form of photonic crystal fiber, which has one ring of air-holes (or F-doped rods) [1]. Figure 1.32 (a) shows the schematic of a typical LCF. A ring of six air-holes (or F-doped rods) has been used as a cladding. LCF are based on modal sieving property for ESM operation, as core and air-holes (F-doped rods) interface is non-continuous. Due to this, modes having smaller size lobes suffer from high loss. In order to avoid problems caused by air-holes during post-processing (such as cleaving and splicing), F-doped rods have been used in LCF design as well. Figure 1.32(a) also shows the notation used here: D is the diameter of F-doped rod, Λ is the pitch, Δn is the refractive index between core and F-doped region, and ~2*Λ-d is the effective core diameter. Figure 1.32(b-e) show the calculated loss of the fundamental mode, lowest lossy higher order mode, and the loss ratio of higher order mode to fundamental mode for different d/Λ and bend radii for a fixed 60μm core diameter (2*Λ-d=60μm). The effective area of the fundamental mode varies from 1140μm^2 to 1,500μm^2. It is interesting to note that, achieved results are not very interesting as discrimination between higher order mode and fundamental mode is poor (lower than 15 for all the cases).

In order to further improve the discrimination between fundamental mode and higher order modes, two rings of air-holes (F-doped rods) have been used [2-3]. An effective area of ~900μm^2 (taking bend-induced distortion into account) at ~20cm bend radius has been obtained experimentally, following the criterion of fundamental mode loss lower than ~0.1dB/m and higher order mode loss larger than 10dB/m using two rings of F-doped rods (Δn=~-0.0155) with slight different features of rods [2-3]. There are several reports from University of Clemenson which suggest that core diameter can be scaled even large than 100μm [4-5]. However, fibers having larger core diameter are very sensitive to bend perturbations. Moreover for a practical bend radius (10cm-20cm), the gain in effective area

due to large core is subsided by bend–induced effective area reduction effect. However, LCF can be suitable for applications in rod-type fiber lasers. Although, Researchers have shown that large pitch fibers have better performance than leakage channel fiber for mode area scaling [6].

1.5.1.12 2D-All-Solid Photonic Bandgap fiber (2D-ASPBGF)

2D-all solid photonic bandgap fiber (2D-ASPBGF) is another form of photonic crystal fiber, where guidance is not based on total internal reflection like PCFs [1-3]. In 2D-ASPBGF, there is a periodic arrangement of high-index solid rods in cladding similar to air-holes as in case of holey fibers. Figure 1.33 shows the schematic of a conventional 2D-all solid photonic bandgap fiber. Light is guided in core for bandgap spectrum formed by high index rods in cladding. Photonic bandgap guidance can be explained in a simplified way by Anti-resonant reflecting optical waveguide "ARROW" model [3]. In this model, for certain wavelengths, light is not in resonance with high index rods in cladding, hence light faces reflection and come back to core (similar to total reflection at core and cladding boundary in case of SIF) [3]. This region of wavelengths is known as bandgap, where guidance of light takes places into core. On the other hand, where light is in resonance with high-index rods, they do not see any reflection and there is no guidance is core. The critical frequencies at which resonance is achieved can be obtained by following equation 1.7 [3]:

$$\lambda = \frac{2*d*\sqrt{n_{high}^2 - n_{core}^2}}{m+1/2} \tag{1.7}$$

Where, d is the diameter and n_{high} is the refractive index of Ge-doped rods in cladding, n_{core} is the refractive index of core, and m ={1, 2,3,……}. The above mentioned equation is a simplified version of equation for cut-off conditions of high-index cylindrical inclusions.

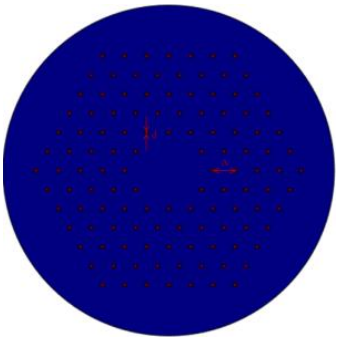

Figure 1.33 schematic of an all-solid 2D-photonic bandgap fiber. Blue and red colour presents silica and Ge-doped silica region respectively.

It is important to understand here that resonance wavelength can be easily obtained from parameters of high-index inclusion. However, it is difficult to obtain the value of leakage loss of core modes between resonant wavelengths by just having parameters of high index inclusions. The leakage losses of core mode depends on several parameters such as total no. of rings of high index rods, pitch of rods for fixed diameter, and refractive index of high index inclusions. Researchers have exploited photonic bandgap fiber for mode area scaling

purpose in a coiled configuration [4-9]. Photonic bandgap fibers similar to PCF have non-continuous interface between core and high index inclusion, which provides natural discrimination between loss of fundamental mode and other higher modes having small lobes. On the top of this, an effective single-mode operation has been ensured in photonic bandgap fiber by exploiting bending losses, optimizing the parameters of high index inclusions, and optimizing number of rings of high index inclusions.

Recently, S. Saitoh et. al. numerically investigated the optimized parameters for photonic bandgap fiber for mode area scaling [8]. Investigations show that the feasibility of achieving effective area between 1,000-1,400μm^2 at 20cm bend radius, while ensuring fundamental mode loss to be lower than 0.1dB/m and higher order modes loss to be higher than 10dB/m. This performance of photonic bandgap fiber is better than leakage channel fiber. A photonic bandgap fiber has also been demonstrated experimentally with effective area larger than 9,00μm^2 [7].

1.5.1.13 Hybrid Photonic crystal fiber (H-PCF)

A novel type of fiber has been introduced to exploit the properties of PCF and PBGF simultaneously, where guidance of light take place based on both principles: total internal reflection (TIR) and PBG, known as hybrid PCF (H-PCF) [1]. Figure 1.34 shows the schematic of H-PCF. Here, one line of air-holes has been replaced with Ge-doped rods to achieve anti-resonant properties of PBG fiber. Researchers have explored this design to further scale the mode area. High index rods are used to filter out higher order modes residing in core. Moreover, wavelength spectrum tailoring due to photonic bandgap actions with large mode area provides an important tool for gain shaping [2]. However fiber shows high sensitivity to bend induced losses, therefore this technique does not pose serious candidature for mode area scaling capability [2-3].

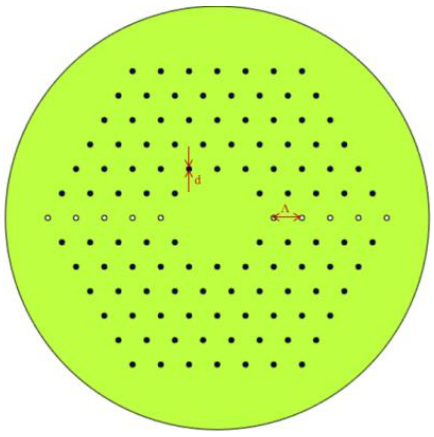

Figure 1.34 schematic of all-solid 2D-photonic bandgap fiber. Green, blue, and white colors present silica, air, and Ge-doped silica regions respectively.

1.5.1.14 Asymmetric Photonic crystal fiber (A-PCF)

Asymmetrical photonic crystal fiber has been proposed to compensate the bend-induced perturbation [1]. Here, pitch of air-holes along one side of fiber is different from other side of

fiber cross-section as shown in figure 1.35(a) [1]. Figure 1.35 shows the image of asymmetrical photonic crystal fiber. It is evident from figure that pitch of air-holes is different on one side from other side. Fiber can be bent in such a way that side of the fiber having smaller pitch of air-holes is away from the center of curvature, so that the effect of bending induced perturbation can be minimized. It is easy to understand intuitively that fiber can address bend-induced perturbations thanks to the additional degree of freedom available during fiber design. However, this comes on the cost of reduced fiber flexibility, as fiber need to be bend along specific direction only. Figure 1.35(b) shows the comparative analysis of this fiber with competitive fibers [1]. Chen et. al., implemented this technique to further scale the mode area [2]. In spite of advantages, there is a very little scope for these fibers to be implemented for practical applications, because of limitations of fiber handling.

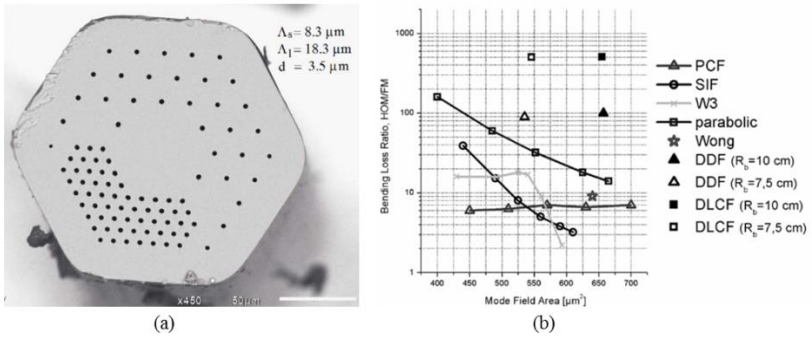

Figure 1.35 (a) cross-sectional image of a symmetrical photonic crystal fiber. Pitch of air-holes is different on one side of fiber to other side (b) comparing the performance of fiber with other fibers. [Figure source [1]; © 2011 OSA]

1.5.1.15 Resonant coupling based designs

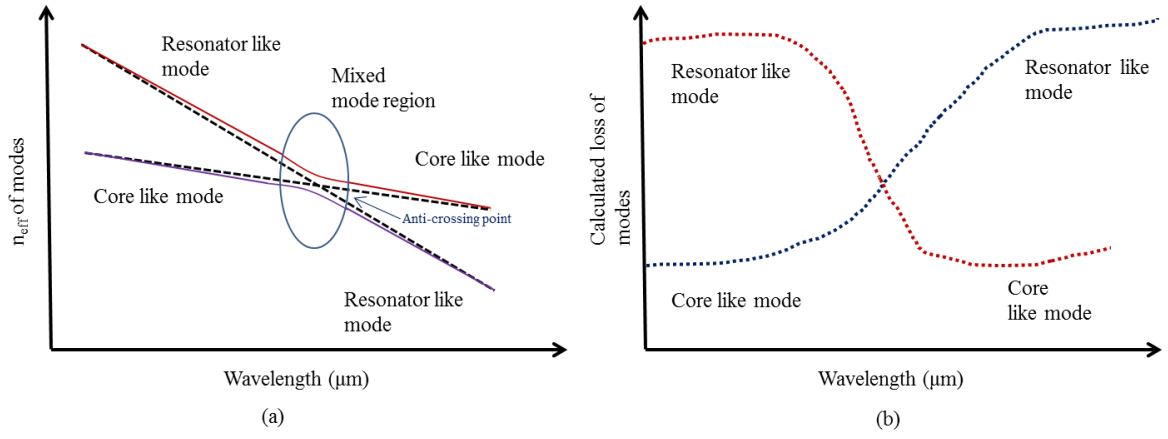

Figure 1.36 schematic of a complete coupling between two leaky modes (a) phase matching: n_{eff} of the core and resonator modes with respect to wavelength. Dashed line shows n_{eff} of core and resonator modes as a different waveguide (b) calculated loss of resonator and core modes.

There has been another approach to achieve ESM operation by filtering out higher order modes using resonance between higher order modes of cores and modes of resonator present in the cladding [1-6]. In order to have a complete coupling between two modes, there are two

important conditions to meet: first is the phase matching of modes and second is the loss matching of modes as shown in figure 1.36 [3]. However, to induce enough losses to the higher order modes of core, it is not necessary to have a complete coupling of higher order modes of core to modes of resonator. Even a partial coupling can be enough to induce enough loss required for ESM operation.

Similarly, resonant coupling can be used for filtering out particular wavelengths as shown in figure 1.37. Resonators in cladding can be tuned in such a way that only at a particular wavelength resonance between core and resonator will take place. This is the same concept used in ARROW waveguides. This is a really useful technique for filtering unwanted wavelengths. For example, wavelength around SRS (~1120nm) can be supressed for ~1060nm operation of Yb-doped fiber laser.

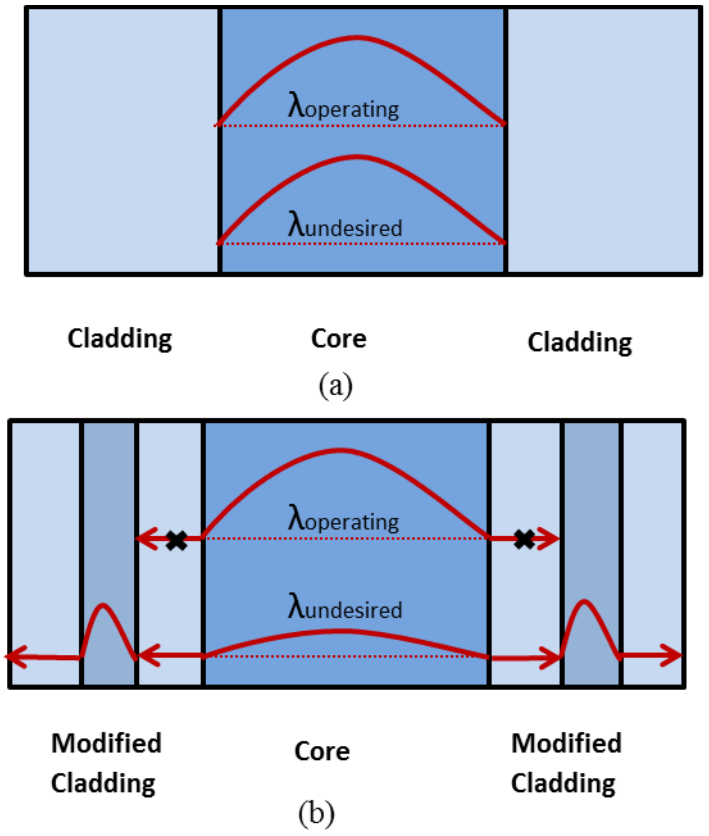

Figure 1.37 schematic of spectral filtering to filter unwanted wavelength using resonant coupling with resonator present in cladding.

There can be several fiber designs for mode area scaling of ESM operation based on resonant coupling. In these designs, normally there is an additional waveguide other than central core of fiber to filter out higher order modes from the core. It can be a ring, few rods, and additional defects other than defects for central core in periodic arrangement of air-holes/F-doped rods/high index inclusion. Few of these fiber designs are shown in figure 1.38 [2, 4-6].

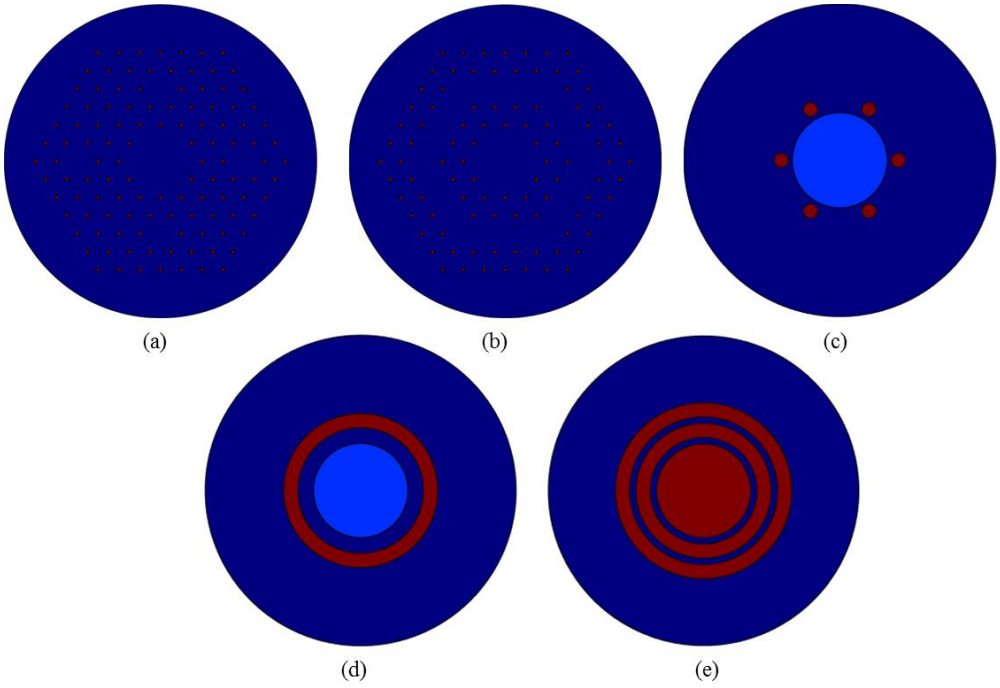

Figure 1.38 schematic of various fiber designs employing resonant coupling mechanism for effective single mode operation. Dark blue, light blue, and red colour represents the refractive index in increasing order.

1.5.1.16 Bragg fiber

Bragg fiber is constituted of a core surrounded by a periodic cladding which consists of high and low-index rings as shown in figure 1.39 [1]. Here, low-index rings have same refractive index as of the core. The light is confined in the core thanks to reflections from the micro-structured high index rings in cladding similar to 2D-all solid photonic bandgap fiber. Here the resonant frequency can be obtained by following equation 1.8 [2]:

$$\lambda = \frac{2*d*\sqrt[2]{n_{high}^2 - n_{core}^2}}{m} \tag{1.8}$$

Where d is the thickness of high index ring, n_{high} is the refractive index of Ge-doped rings in cladding, and n_{core} is the refractive index of core which is equal to refractive index of cladding , and m ={1, 2,3,……}.

An ESM operation can be ensured for a fixed diameter core by optimizing the low-index ring thickness such that the effective-indices of the higher-order-modes of the core are either matched or near to low-index ring modes' effective-indices. Here, low-index rings decide the resonance of higher order modes; therefore we call them as resonant-rings. An optimized thickness of low index resonant ring to filter out higher order modes can be obtained using following equation 1.9 [3-5]:

$$t = \frac{p\pi/2}{u_{lm}}, \tag{1.9}$$

Where, p is an integer, even value of p gives antiresonance and odd values give resonance point, u_{lm} presents the transverse propagation constant of a core mode, t is the thickness of low-index layer.

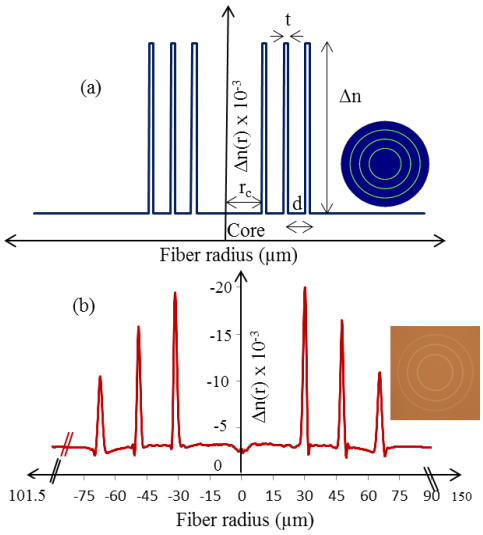

Figure 1.39 (a) schematic of a conventional Bragg fiber. Inset shows the schematic of 2D-cross-section of fiber. (b) refractive index profile of Bragg fiber fabricated by MCVD process. Inset shows the microscope image of fiber end.

Baskiotis et. al. have demonstrated that a 60μm core Bragg fiber with optimized thicknesses and refractive indices of low index ring, high index rings, and core can achieve an ESM operation with ~1020μm^2 at 1.06μm and ~20cm bend radius [5]. An ESM operation can be ensured by achieving higher order modes loss to be larger than 10dB/m and fundamental mode to be lower than 0.1dB/m.

Bragg fiber offers the advantages of easy fabrication thanks to the cylindrical symmetry of fiber. However, the presence of the high-index rings in the Bragg fiber can cause unwanted couplings between the core and the high-index ring modes due to slight imperfections in the realized fibers [6]. Moreover, these high-index rings do not allow the Stress Applying Parts (SAPs) to be put outside of the core region, which makes the realization of a polarization maintaining Bragg fiber difficult. On the other hand, by placing the SAPs inside the core of the Bragg fiber, a single-polarization Bragg fiber has been demonstrated. However, this dramatically reduces the effective area of the fundamental mode [6].

1.5.1.17 Polygonal-Chirally Coupled Core (P-CCC)

Chirally coupled core fiber works on angular momentum assisted quasi-phase matching between modes of core and helically twisted side core [1-2]. The modes of helically twisted side core are leaky in nature thanks to the bend loss. Chirally coupled core fibers are limited in mode area scaling due to reduced coupling between core and one side core with increasing core size. In order to further enhance the mode area scaling, researchers have proposed Polygonal chirally coupled core (P-CCC) as shown in figure 1.40(a) [3]. In this new proposal, a polygonal core which is helically twisted along its axis has eight equally spaced helically

twisted side cores. In this new fiber design, there is an additional filtering mechanism, where higher order modes of central core couple to the leaky modes of central core itself [3]. A 55µm to 60µm core passive and active fibers have been demonstrated [3]. Figure 1.40(b) shows the calculated loss of the LP_{01} and LP_{11} modes in case of polygonal chirally coupled core fiber and chirally coupled core fiber with circular core [3]. In case of 55µm core fiber, a fundamental mode loss lower than 0.2dB/m and higher order modes higher than 10dB/m can be achieved in case of unbent fiber [3]. Authors did not report the effect of bending on loss of LP_{01} and LP_{11} [3]. It is important to report the performance of such a fiber in bent case as well to understand their advantages for real applications.

P-CCC fibers offer the advantages of all-solid fiber design and higher refractive index of core compared to cladding. However, requirement of additional eight side cores and spinning during fiber drawing to achieve helical twisting are considerable restrictions to make it a commercial success.

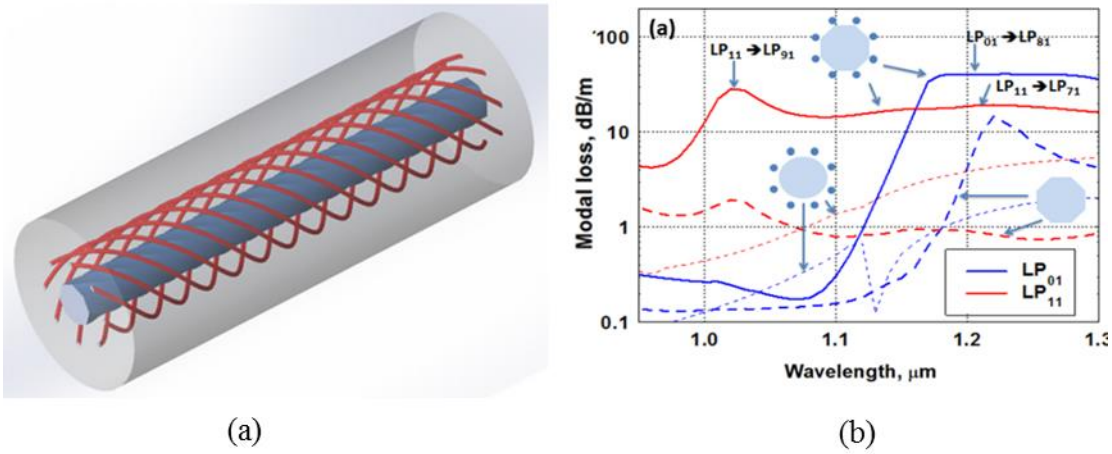

Figure 1.40 (a) schematic of Polygonal-chirally coupled core fiber (b) numerically computed loss of different modes of different type chirally coupled core fiber. (Figure source [3]; © 2014 OSA.)

1.6 CONCLUSION

Performance of different LMA fiber designs at a particular wavelength can be compared based on the following parameters:-

1. **Effective area** achieved for a fixed Criterion of fundamental mode loss lower than 0.1dB/m and loss of the higher order modes larger than 10dB/m at a Bend radius of maximum 20cm.

2. **All-solid design** is an important aspect, as all-solid fiber can be easily cleaved and spliced compared to fiber having large number of air-holes.

3. **Cylindrical symmetrical design** is also an essential aspect to ensure mass scale production, as cylindrical symmetrical fiber can be produced using conventional fiber fabrication techniques.

4. **Core index higher than cladding** can allow fabrication of rare-earth doped fiber using solution doping/vapour phase method otherwise a cumbersome expensive pixelation and micro-structuration process is needed.

Table 1.5 comparison of different fiber designs.

Fiber Design	**Maximum effective area** (Fundamental mode loss < 0.1dB/m & higher order mode loss >10dB/m) Bend radius equal to lower than 20cm	**All-solid**	**Cylindrical symmetrical**	**Core index higher than cladding**
Low NA-SIF [1]	~370µm^2	Yes	Yes	Yes
LCF [2,3]	~900µm^2	Yes	No	No
2D-ASPBGF [4,5]	~1,000-1,400µm^2	Yes	No	No
Bragg Fiber [6]	~1,020µm^2	Yes	Yes	No
P-CCC [7]	Not provided	Yes	No	Yes
Bend compensated Parabolic fiber [8]	~1,000µm^2	Yes	Yes	Yes
Objective of this Thesis	**Large effective area**	**Yes**	**Yes**	**Yes**

Table 1.5 shows the comparative analysis of different LMA fiber designs. Comparative analysis includes the effective area achieved for different fiber design, their structure such as all-solid structure or not, cylindrical symmetry or not, and core refractive index higher than cladding or not. It is necessary to mention few points here about different designs listed in table; which have not been possible to mention in table. 2D-ASPBGF can provide effective area in range of 1000-1400µm^2, however as effective area increases from 1,000µm^2 to 1,400µm^2 the mode suffers from rapid distortion. Distortion (or illuminated fraction) of a mode can be defined as ratio of effective area of the fundamental mode in bent condition (here it is 20cm bend radius) to effective area of the fundamental mode in straight condition. In case of 2D-ASPBGF, the black fraction of the fundamental mode drops from 0.67 to 0.30 for 1100µm^2 to 1400µm^2 effective area. On the other hand, P-CCC fiber has been reported with ~55µm to ~60µm core. However, the bending performances of fundamental mode and higher order modes loss and the effective area of the fundamental mode in bend configuration have not been reported, which is extremely important to show a substantial candidature for fiber laser applications. That is why, it is not possible to report effective area here for P-CCC, and hence only structural aspect is mentioned here. In case of bend compensated parabolic fiber, the effective area ~1000µm^2 is numerically reported at 15cm bend radius, which is a spectacular performance. However, this design requires a high precision in controlling the doped refractive index profile of fiber on ~10^{-4} level, which might be challenging to achieve. **One of the objectives of this thesis is to fill in one row of table 1.5 with a novel fiber design, which is suitable for low cost fabrication (such as MCVD in conjunction with**

solution doping process) compared to other competitive fibers, all fiberized (all solid fiber), compact (small coil diameter), and an effective single mode with large effective area fiber laser device.

It is also important to note from the analysis presented in previous section, that mode area scaling in coiled configuration is limited by physics of fiber optics. In order to achieve few thousands of effective area, fiber need to keep straight (known as rod-type fibers) to avoid bend induced effective area reduction. **The other objective of thesis is to develop all-solid novel fiber design which is suitable for applications in rod-type fiber laser.**

1.7 References:

[1.1 Introduction and 1.2 Fiber laser]

1. C. Jauregui, J. Limpert, and A. Tunnermann, "High-power fiber lasers," [Invited], Nature Photonics **7**, 861-867 (2013).
2. M. N. Zervas and C. A. Codemard, "High Power Fiber Lasers: A Review," [Invited], IEEE JSTQE **20,** 0904123 (2014).
3. D. J. Richardson, J. Nilsson, and W. A. Clarkson, "High power fiber lasers: current status and future perspectives [Invited]," *JOSA B*, vol. 27, no. 11, pp. B63-B92, Nov. 2010.
4. J. Limpert, F. Stutzki, F. Jansen, H. J. Otto, T. Eidam, C. Jauregui, and A. Tunnermann, "Yb-doped large-pitch fibers: effective single-mode operation based on higher-order mode delocalization", *Light: Sci. & App.*, vol. 1, pp. 1-5, March 2012.
5. J. W. Dawson, M. J. Messerly, R. J. Beach, M. Y. Shverdin, E. A. Stappaerts, A. K. Sridharan, P. H. Pax, J. E. Heebner, C. W. Siders and C.P.J. Barty, "Analysis of the scalability of diffraction-limited fiber lasers and amplifiers to high average power," *Opt. Exp.*, vol. 16, no. 17, pp. 13240-13266, Aug. 2008.
6. J. Cao, S. Guo, X. Xu, J. Chen, and Q. Lu, "Investigation on Power scalability of Diffraction-Limited Yb-doped Fiber Lasers, IEEE J. Sel. Top. Quant. Elec., 0903211, Sep. 2014.
7. M. O'Connor, V. Gapontsev, V. Fomin, M. Abramov, and A. Ferin, "Power Scaling of SM Fiber Lasers toward 10kW," in Conference on Lasers and Electro-Optics/International Quantum Electronics Conference, OSA Technical Digest (CD) (Optical Society of America, 2009), paper CThA3.
8. B. Shiner, "High-power fiber lasers gain market share," Industrial Laser Solutions for Manufacturing 21(2), (2006).
9. A. Klenke, S. Hädrich, T. Eidam, J. Rothhardt, M. Kienel, S. Demmler, T. Gottschall, J. Limpert, and A. Tünnermann," 22 GW peak-power fiber chirped-pulse-amplification system," Opt. Lett. 39(24), 6875-6878 (2014).
10. G. Mourou, B. Brocklesby, T. Tajima, and J. Limpert, Commentary, Nature Photonics 7**,** 258 (2013).
11. http://www.lia.org/blog/2011/03/laser-applications-in-the-automotive-industry/
12. http://www.twi-global.com
13. M. Zediker, "High-power fiber lasers for geothermal, oil, and gas industries," Newsroom, SPIE (2014).
14. https://visualsonline.cancer.gov/details.cfm?imageid=2267
15. US Navy laser weapon system, Luis Martinez "Navy's New Laser Weapon Blasts Bad Guys From Air, Sea". ABC. Retrieved April 9, 2013.
16. http://en.wikipedia.org/wiki/Double-clad_fiber
17. V. Khitrov, J. D. Minelly, R. Tumminelli, V. Petit, and E. S. Pooler, "3kW single-mode direct diode-pumped fiber laser," in Fiber Lasers XI, Photonic West conference, San Francisco, Cali., 2014 Paper 8961.
18. G. P. Agrawal, Nonlinear Fiber Optics, 4th ed. (Academic, 2007).

[1.3 Optical fiber for fiber lasers]

1. A. W. Snyder and J. D. Love, Optical Waveguide Theory (Kluwer Academic Publishers, 1983).
2. M.-J. Li, X. Chen, A. Liu, S. Gray, J. Wang, D. T. Walton, and L. A. Zenteno, "Limit of effective area for single-mode operation in step-index large mode area laser fibers," J. Lightwave Technol. **27**, 3010-3016 (2009).
3. J. M. Fini, "Bend-resistant design of conventional and microstructure fibers with very large mode area," Opt. Exp. **14**, 69-81 (2006).
4. J. M. Fini, "Design of large-mode-area amplifier fibers resistant to bend-induced distortion," JOSA B **24**, 1669-1676 (2007).
5. J. W. Nicholson, J. M. Fini, A. D. Yablon, P. S. Westbrook, K. Feder, and C. Headley, "Demonstration of bend-induced nonlinearities in large-mode-area fibers," Opt. Lett. 32(17) 2562-2564 (2007).
6. G. Gu, F. Kong, T. W. Hawkins, P. Foy, K. Wei, B. Samson, and L. Dong, "Impact of fiber outer boundaries on leaky mode losses in leakage channel fibers," Opt. Exp. **21**, 24039-24048 (2013).
7. Yu. A. Uspenskii, E. E. Uzorin, A. V. Vinogradov, M. E. Likhachev, S. L. Semjonov, M. M. Bubnov, E. M. Dianov, R. Jamier and S. Février, "Effect of polymer coating on leakage losses in Bragg fibers," Opt. Lett. **32**, 1202-1204 (2007).
8. J. Limpert, F. Stutzki, F. Jansen, H. J. Otto, T. Eidam, C. Jauregui, and A. Tunnermann, "Yb-doped large-pitch fibers: effective single-mode operation based on higher-order mode delocalization", *Light: Sci. & App.*, vol. 1, pp. 1-5, March 2012.
9. P. St. J. Russell, "Photonic Crystal Fibers," Review article, Science 299, 358-362 (2003).
10. J. H. Chong and M. K. Rao, "Development of a system for laser splicing photonic crystal fiber," Opt. Exp., 11(12) 1365-1370 (2003).

[1.4 Optical fiber fabrication for fiber lasers]

1. K. C. Kao and G. A. Hockman, “Dielectric-fiber surface waveguides for optical frequencies”, Proc. IEE, vol. 113, no. 7, p.1151, 1966.
2. D. B. Keck, P. C. Schultz, and F. Zirnar, U.S. Patent 3373292.
3. J. B. MacChesney and P. B. O’Connor, U.S. Patent 4217027.
4. T. Izawa, S. Kobayashi, S. Sudo, and F. Hanawa, in Tech. Dig.2nd Int. Cof Int. Opt., Opt. Fiber Commun., Tokyo, Japan,1977.
5. G. R. Newns, K. J. Beales, and C. R. Day, in Dig. 2nd Znt. Conf,Int. Opt., Opt. Fiber Commun., Tokyo, Japan, 1977.
6. J. Koenings, D. Kuppers, H. Lydtin, and H. Wilson, in Proc. 5thConf Vap. Dep., 1975, p. 270.
7. J. B. MacChesney, P. B. O’Connor, F. V. DiMarcello, J. R. Simpson,and P. D. Lazay, “Preparational low loss opticaJ fibers using simultaneous vapor phase deposition and fusion,” in Proc. 1WInt. Congr. Glass, 1974, pp. 6-40-6-44.
8. J. B. MacChesney, P. B. O’Connor, and H. M. Presby, “A new technique for preparation of low-loss and graded index optical fibers:’ Proc. IEEE, vol. 62, pp. 1278-1279, Sept. 1974.
9. S. R. Nagel, J. B. Macchesney, and K. L. Walker,” An overview of the modified chemical vapor deposition (MCVD) process and performance”, IEEE Trans. On microwave thoery and techniques, MTT-30, No. 4,1982
10. P G Simplins, “ Thermophoresis: The mass transfer mechanism in modified chemical vapour deposition”, J. Appl. Phys, 50, 5676-5681, 1979.
11. U. C. Paek and R. B. Runk , “Physical behavior of the neck-down region during furnace drawing of silica fibers,” J. Appl. Phys, 49, 4417 (1978).
12. A. Mawardi and R. Pitchumani, “Optical Fiber Drawing Process Model Using an Analytical Neck-Down Profile,” IEEE Photonics Journal, 2(4), 620-629 (2010).
13. B. T. Stone and K. L. Bray, “Fluorescence properties of Er^{3+}-doped sol-gel glasses”, J. Noncrystalline Solids, 197, 136-144.
14. S. Sen, “Atomic environment of high-field strength Nd and Al cations as dopants and major components in silicate glass: A Nd L-$_{III}$-edge and Al K-edge X-ray absorption spectroscopic study”, J. Noncrystalline Solids, 261, 226-236, 2000.
15. R. Reisfeld, M. Eyal, E. Greenberg, C. K. Jorgensen, “Luminescence of six J-levels of holmium(III) in barium zirconium fluoride glass at room temperature”, Chem. Phys. Lett. 118, 25-28, 1985.
16. V. P. Gapontsev, S. M. Matitsin, A. A. Isineev, V. B. Kravchenko, “Erbium glass lasers and their applications”, Opt. Laser technol, 14, 189-196, 1982.
17. R. Wyatt, “Spectroscopy of rare-earth doped fibers”, Proc. SPIE 1171, 54-64, 1989.
18. M. Nakazawa and Y. Kimura , “Lanthanum codoped erbium fiber amplifier”, Electron. Lett., 27, 1065-1067, 1991.
19. P Myslinski, “Performance of high-concentration erbium-doped fiber amplifiers”, IEEE Photonics Technol. Lett., 11, 973-975, 1999.
20. L. L. Lee and D. S. Tsai, “Ion clustering and crystallization of sol gel derived erbium silicate glass”, J. Materials Sci. Lett, 13, 615-617, 1994.
21. J. Stone and C A Burrus, “Nd^{3+} doped SiO_2 lasers in end pumped fiber geometry, Appl. Phys. Lett., 23, 388-389, 1973.
22. S. Poole, “Fabrication and characterization of low-loss optical fibers containing rare earth ions”, J. Lightwave Technol., LT-4, 870-876, 1986.
23. A. S. Webb, A. J. Boyland, R. J. Standish, S. Yoo, J. K. Sahu, D. N. Payne, “MCVD in-situsolutiondoping process for the fabrication of complex design large core rare-earth doped fibers”, J. Noncrystalline solids, 356, 848-851, 2010.
24. R. P. Tumminelli, B. C. Mccollum, and E. Snitzer, “Fabrication of High-Concentration Rare-Earth Doped Optical Fibers Using Chelates,” J. of Lightwav. Technol., 8(11) 1680-1683 (1990).
25. M. Saha, A. Pal, and R. Sen, “Vapor Phase Doping of Rare-Earth in Optical Fibers for High Power Laser,” IEEE Photonics Technol. Letter., 26(1) 58-61 (2014).
26. S. Unger, F. Lindner, C. Aichele, M. Leich, A. Schwuchow, J. Kobelke, J. Dellith, K. Schuster, and H. Bartelt, “A highly efficient Yb-doped silica laser fiber prepared by gas phase doping technology,” Laser Physics Letter 24, 035103 (2014).
27. R. Sen, M. Saha, A. Pal, M. Pal, M. Leich, and J. Kobelke, “High power laser fiber fabricated through vapor phase doping of Ytterbium,” Laser Physics Letter 11, 085105 (2014).
28. J. C. Knight, T. A. Birks, P. S. J. Russell, and D. M. Atkin, “All-silica single-mode optical fiber with photonic crystal cladding,” Opt. Lett. 21, 1547 – 1549 (1996).
29. S. C. Xue, R. I. Tanner, G. W. Barton, R. Lwin, M. C. J. Large, and L. Poladian, “Fabrication of microstructured optical fibers – Part 1 & 2,” J. Lightwave Technol. 23, 2245 – 2266 (2005).
30. R. Kostecki, H. Ebendorff-Heidepriem, S. C. Warren-Smith, and T. M. Monro, “Predicting the drawing conditions for Microstructured Optical Fiber fabrication,” Opt. Mat. Exp. 4(1), 29-40 (2013).

[1.5 Journey of large mode area optical fiber]

1. E. Snitzer, “Proposed fiber cavities for optical lasers,” Journal of Appl. Phys. **32**, 36-39 (1961).
2. E. Snitzer, “Optical maser action of Nd^{3+} in a barium crown glass,” Phys. Rev. Lett. **7**, 444-446 (1961).
3. C. J. Koester and E. Snitzer, “Amplification in a fiber laser,” Appl. Opt. **3**, 1182-1186 (1964).
4. E. Snitzer, “Glass Lasers,” Appl. Opt. **5**, 1487-1499 (1966).
5. J. Stone and C. A. Burrus, “Neodymium-doped silica lasers in end-pumped fiber geometry,” Appl. Phys. Lett. **23**, 388-389 (1973).
6. S. B. Poole, D. N. Payne, and M. E. Fermann, “Fabrication of low loss optical fibers containing rare-earth ions,” Electron. Lett. **21**, 737-738 (1985).
7. R. J. Mears, L. Reekie, S. B. Poole, and D. N. Payne, “Neodymium-doped silica single-mode fibre laser,” Electron Letter 21, 737-738 (1985).
8. J. E. Townsend, S. B. Poole, and D. N. Payne, “Solution-doping technique for fabrication of rare-earth-doped optical fibres,” Electron. Lett. **23** (7), 329-331 (1987).
9. R. J. Mears, L. Reekie, I. M. Jauncey, and D. N. Payne, “Low-noise erbium-doped fiber amplifier operating at 1.54μm,” Electron. Lett. **23**, 1026-1028 (1987).
10. E. Snitzer, H. Po., F. Hakimi, R. Tumminelli, and B. C. McCollum, “Double-clad, offset core Nd fiber laser,” Optical fiber sensors, 1998, PD5.

[1.5.1 Effective single mode approach]

1. D. Taverner, D. J. Richardson, L. Dong, and J. E.Caplen, “158-mJ pulses from a single-transverse-mode, large-mode-area erbium-doped fiber amplifier,” Opt. Lett. 22, 378 (1997). {low NA}
2. D. J. Richardson, P. Britton, and D. Taverner, “Diode-pumped, High Energy, Single Transverse Mode Q-Switch Fiber Laser,” Electron. Lett. **33**, 1955-1956 (1997). {low NA}

3. H. L. Offerhaus, N. G. R. Broderick, R. S. Sammut, L. Dong, J. E. Caplen, and D. J. Richardson, " High-Energy Single-Transvers-Mode Q-switched Fiber Laser on a Multimode Large-Mode-Area Erbium-Doped Fiber," Opt. Lett. 23, 1683 (1998).
4. J. A. Alvarez-Chavez, H. L. Offerhaus, J. Nilsson, P. W. Turner, W. A. Clarkson, and D. J. Richardson, "High-energy, high-power ytterbium-doped Q-switched fiber laser," Opt. Lett. **25**, 37-39 (2000).
5. N. G. R. Broderick, H. L. Offerhaus, D. J. Richardson, R. A. Sammut, J. Caplen, and L. Dong, "Large Mode Area Fibers for high Power Applications," Opt. Fiber Technol. **5**, 185-196 (1999).

[1.5.1.1 Bend induced loss]

1. J. P. Koplow, D. A. V. Kliner, and L. Goldberg, "Single-mode operation of a coiled multimode fiber amplifier," Opt. Lett. **25**, 442-444 (2000).
2. R. T. Schermer, "Mode scalability in bent optical fibers," Opt. Exp. **15**, 15674-15701 (2007).
3. Z. Li, J. Zhou, W. Wang, B. He, Y. Xue, abnd Q. Lou, "Limitations of coiling technique for mode controlling of multimode fiber lasers," CLEO/Pacific Rim 2009, Shangai China.
4. B. Sevigny, X. Zhang, M. Garneau, M. faucher, Y. K. lize, and N. Holehouse, "Modal sesitivity analysis for single-mode operation in large mode area fiber," Proc. of SPIE 6873, 68730A (2008).
5. Y. Jeong, J. K. Sahu, D. N. Payne, and J. Nilsson, "Ytterbium-doped large-core fiber laser with 1.36 kW continuous-wave output power," Opt. Express 12(25), 6088–6092 (2004).
6. M.-J. Li, X. Chen, A. Liu, S. Gray, J. Wang, D. T. Walton, and L. A. Zenteno, "Limit of effective area for single-mode operation in step-index large mode area laser fibers," J. Lightw. Technol. **27**, 3010 (2009).
7. V. Khitrov, J. D. Minelly, R. Tumminelli, V. Petti, and E. S. Pooler, "3kW single-mode direct diode-pumped fiber laser," Photonic West, Fiber Lasers XI, **8961** (2014).
8. S. Wielandy, "Implications of higher order mode content in large mode area fibers with good beam quality," Opt. Exp. **15**, 15402-15409 (2007).
9. J. M. Fini, "Bend-resistant design of conventional and microstructure fibers with very large mode area," Opt. Exp. **14**, 69-81 (2006).
10. J. M. Fini, "Design of large-mode-area amplifier fibers resistant to bend-induced distortion," JOSA B **24**, 1669-1676 (2007).
11. J. M. Fini and J. W. Nicholson, "Bend compensated large-mode-area fibers: achieving robust single-modedness with transformation optics," Opt. Exp. **21**, 19173-19179 (2013).

[1.5.1.2 Single mode excitation]

1. P. Facq, F. de Fornel, and F. Jean, "Tunable Single-Mode Excitation in Multimode Fibres," Electron. Lett. **20**, 613-614 (1984).
2. M.E. Fermann, "Single-Mode Excitation of Multimode Fibers with Ultrashort Pulses," Opt. Lett. **23**, 52-54 (1998).
3. C. D. Stacey, R. M. Jenkins, J. Banerji, and A.R. Davies, "Demonstration of fundamental mode only propagation in Highly Multimode Fiber for High Power EDFAs," Opt. Commun. **269**, 310-314 (2007).
4. S. Hurand, L.-A Chauny, H. El-Rabii, S. Joshi, and A. P. Yalin, "Mode coupling and output beam quality of 100–400μm core silica fibers," Appl. Opt. 50, 492-499 (2011).
5. K. C. Hou, M. Y. Cheng, D. Engin, R. Changkakoti, P. Mamidipudi, and A. Galvanauskas, "Multi-MW Peak Power Scaling of Single Transverse Mode Pulses Using 80μm Core Yb-doped LMA Fibers," Advance Solid State Photonics, 2006.
6. A. Galvanauskas, Ming-Yuan Cheng, Kai-Chung Hou, and Kai-Hsiu Liao, "High Peak Power Pulse Amplification in Large-Core Yb-Doped Fiber Amplifiers," IEEE JSTQE (INVITED) **13**, 559-566 (2007).
7. K. –C. Hou, S. George, A. G. Mordovanakis, K. Takenoshita, J. Nees, B. Lafontaine, M. Richardson, and A. Gavanauskas, "High power Fiber Laser Driver for Efficient EUV Lithography Source with Tin-Doped water Dropelet Targets," Opt. Exp. **16**, 956-974 (2008).

[1.5.1.3 Fiber tapering]

1. N. Amitay, H. Presby, F. DiMarcello, and K. Nelson, "Optical fiber tapers--A novel approach to self-aligned beam expansion and single-mode hardware," J. Lightwave Technol. 5, 70- 76 (1987).
2. J. A. Alvarez-Chavez, A. B. Grudinin, J. Nilsson, P. W. Turner, amd W. A. Clarkson, "Mode selection in high power cladding pumped fiber lasers with tapered section," CLEO 1999.
3. V. Filippov, Y. Chamorovskii, J. Kerttula, K. Golant, M. Pessa, and O. G. Okhotnikov, "Double clad tapered fiber for high power applications," Opt. Exp. 16, 1929-1944 (2008).
4. V. Filippov, Y. Chamorovskii, J. Kerttula, A. Kholodkov, and O. G. Okhotnikov, "Single-mode 212 W tapered fiber laser pumped by a low-brightness source," Opt. Lett. 33, 1416-1418 (2008)
5. V. Filippov V., Y. Chamorovskii, J. Kerttula, A. Kholodkov, and O. G. Okhotnikov, "600 W power scalable single transverse mode tapered double-clad fiber laser," Opt. Express 17, 1203-1214 (2009).
6. V. Filippov, J. Kerttula,Y. Chamorovskii, K. Golant, and O. G. Okhotnikov, "Highly efficient 750 W tapered double-clad ytterbium fiber laser," Op. Exp. **18**(12), 12499-12512 (2010).
7. J. Kerttula, V. Filippov, Y. Chamorovskii, K. Golant, and O. Okhotnikov, "Actively Q-switched 1.6-mJ tapered double-clad ytterbium-doped fiber laser," Opt. Express 18, 18543-18549 (2010).
8. J. Kerttula, V. Filippov, V. Ustimchik, Y. Chamorovskiy and O. G. Okhotnikov, "Mode evolution in long tapered fibers with high tapering ratio," Opt. Exp. **20** (23), 25461-25470, Oct. 2012

[1.5.1.4 Helical core optical fiber]

1. D. Marcuse, "Radiation loss of a helically deformed optical fiber," J. Opt. Soc. Am. **66**, 1025–1031 (1976).
2. G. T. Moore and J. R. Marciante, "Cladding-pumped fiber with helical rare-earth-doped core for fiber lasers and amplifiers," U.S. patent 6,650,664 (November 18, 2003).
3. P. Wang, L. J. Cooper, R. B. Williams, J. K. Sahu, and W. A. Clarkson, "Helical-core ytterbium-doped fibre laser," Electron. Lett. 40(21), 1325–1326 (2004).

4. P. Wang, L. J. Cooper, J. K. Sahu, and W. A. Clarkson, "Efficient single-mode operation of a cladding-pumped ytterbium-doped helical-core fiber laser," Opt. Lett. **31**, 226–228 (2006).
5. Qian, J., and Hussey, C.D.: 'Circular birefringence in helical-core fibre', Electron. Lett., 1986, 22, pp. 515–517
6. R. D. Birch, "Fabrication and characterisation of circularly birefringent helical fibers," Electron. Lett. **23**, 50–52 (1987).
7. Z. Jiang and J. R. Marciante, "Mode-area scaling of helical-core, dual-clad fiber lasers and amplifiers using an improved bend-loss model," JOSA B, 23, 10, 2051-2058, Oct. 2006
8. H. Kim, J. Kim,Y. Jung, L. A. Vazquez-Zuniga, S. J. Lee, G. Choi, K. Oh, P. Wang, W. A. Clarkson, and Y. Jeong, "Simple and reliable light launch from a conventional single-mode fiber into a helical-core fiber through an adiabatically tapered splice," Opt. Exp., 20(23), 25562-25571 (2012).

[1.5.1.5 Flat field fiber]

1. A. K. Ghatak, I. C. Goyal, and R. Jindal, "Design of waveguide refractive index profile to obtain flat modal field," Proc. SPIE 3666, 40–44 (1999).
2. J. W. Dawson, Z. M. Liao, I. Jovanovic, B. Wattellier, R. Beach, S. A. Payne, and C. P. J. Barty, "Large flattened mode optical fiber for high output energy pulsed fiber lasers," in Proceedings of CLEO 2003, paper CWD5,
(2003).
3. J. W. Dawson, R. Beach, I. Jovanovic, B. Wattellier, Z. M. Liao, S. A. Payne, and C. P. J. Barty, "Large flattened mode optical fiber for reduction of non-linear effects in optical fiber lasers," Proc. SPIE 5335, 132–139 (2004).
4. C. Valentin, P. Calvet, Y. Quiquempois, G. Bouwmans, L. Bigot, Q. Coulombier, M. Douay, K. Delplace, A. Mussot, and E. Hugonnot, "Top-hat beam output of a single-mode microstructured optical fiber: Impact of core index depression," Opt. Express 21, 23250-23260 (2013).
5. F. Kong, G. Gu, T. W. Hawkins, J. Parsons, M. Jones, C. Dunn, M. T. Kalichevsky-Dong, K. Wei, B. Samson, and L. Dong, "Flat-top mode from a 50 μm-core Yb-doped leakage channel fiber," Opt. Express 21(26), 32371–32376 (2013).

[1.5.1.6 SHARC fiber]

1. D. A. Rockwell, V. V. Shkunov, and J. R. Marciante, "Semi-guiding high-aspect-ratio core (SHARC) fiber providing single-mode operation and an ultra-large core area in a compact coilable package," Opt. Express, 19(15), 14746-14762 (2011).
2. J. R. Marciante, V. V. Shkunov, and D. A. Rockwell, "Semi-guiding high-aspect-ratio core (SHARC) fiber amplifiers with ultra-large core area for single-mode kW operation in a compact coilable package," Opt. Express, 20(18), 20238-20254 (2012).

[1.5.1.7 Higher order mode approach]

1. S. Ramachandran, J. M. Fini, M. Mermelstein, J. W. Nicholson, S. Ghalmi, and M. F. Yan, "Ultra-large effective-area, higher-order mode fibers: a new strategy for high-power lasers," Lasers & Photon Rev., 2(6), 429-448 (2008).
2. S. Ramachandran, J. W. Nicholson, S. Ghalmi, M. F. Yan, P. Wisk, E. Monberg, and F. V. Dimarcello, "Light propagation with ultra large modal areas in optical fibers," Opt. Lett. **31**(12), 1797–1799 (2006).
3. J. M. Fini and S. Ramachandran, "Natural bend-distortion immunity of higher-order-mode large-mode-area fibers," Op. Lett. **32**(7), 748-750 (2007).

[1.5.1.8 Tailoring dopant profile]

1. J. R. Marciante, "Gain Filtering for Single-Spatial-Mode Operation of Large-Mode-Area Fiber Amplifiers," IEEE JSTQE, 15(1), 30-36, (2009).
2. J. R. Marciante, R. G. Roides, V. V. Shkunov, and D. A. Rockwell, "Near-diffraction-limited operation of step index large-mode-area fiber lasers via gain filtering," Opt. Lett. **35**(11), 1828–1830 (2010).
3. J. M. Sousa and O. G. Okhotnikov, "Multimode Er-doped for single-transverse-mode amplification," Applied Physics Letter 74 1528-1530 (1999).
4. J. Limpert, F. Stutzki, F. Jansen, H. J. Otto, T. Eidam, C. Jauregui, and A. Tunnermann, "Yb-doped large-pitch fibers: effective single-mode operation based on higher-order mode delocalization", *Light: Sci. & App.*, vol. 1, pp. 1-5, March 2012.
5. M. M. Jorgensen, S. R. Petersan, M. Laurila, J. Laegsgaard, and T. T. Alkeskjold, "Optiminizing single mode robustness of the distributed modal filtering rod fiber amplifier," *Opt. Exp.*, vol. 20, no. 7, pp. 7263-7273, March 2012.

[1.5.1.9 Gain-Guiding Index Antiguiding approach]

1. A. E. Siegman, "Propagating modes in Gain-Guided Optical Fibers," JOSA. A, 20 1617-1628 (2003).
2. A. E. Siegman, "Gain-Guided, Index-Antiguided Fiber Lasers," JOSA B 24, 1677-1682 (2007).
3. A. E. Siegman, Y. Chen, V. Sudesh, M. C. Richardson, M. Bass, P. Foy, W. Hawkins, and J. Ballato, Appl. Phys. Lett. 89, 251101 (2006).
4. Y. Chen, T. Mccomb, V. Sudesh, M. Richardson, and M. Bass, "Lasing in a gain-guided index antiguided fiber," JOSA B 24, 1683-1688 (2007).
5. Y. Chen, T. Mccomb, V. Sudesh, M. Richardson, and M. Bass, "Very large-core, single-mode, gain-guided, index anti-guided fiber lasers," Opt. Lett. 32, 2505-2507 (2007).

[1.5.1.10 Photonic crystal fiber]

1. J. C. Knight, T. A. Birks, P. St. J. Russell, and D. M. Atkin, "All-silica single-mode optical fiber with photonic crystal cladding," Opt. Lett., 21(19), 1547-1549 (1996).
2. T. A. Birks, J. C. Knight, and P. St. J. Russell, "Endlessly single-mode photonic crystal fiber," Opt. Lett., 22(13), 961-963 (1997).

3. J. C. Knight, T. A. Birks, and P. St. J. Russell, "Properties of photonic crystal fiber and the effective index model," JOSA A 15(3), 748-752 (1998).
4. J. C. Knight, J. Arriaga, T. A. Birks, A. Ortigosa-Blanch, W. J. Wadsworth, and P. St. J. Russell, "Anomalous Dispersion in Photonic Crystal Fiber," IEEE Photonics Techno., 12(7), 807-809 (2000).
5. J. C. Knight, "Photonic crystal fibers," Review article, Nature 24, 847-851 9 (2003).
6. P. St. J. Russell, "Photonic Crystal Fibers," Review article, Science 299, 358-362 (2003).
7. P. St. J. Russell, "Photonic Crystal Fibers," Invited article, J. Lightwav. Techno. 24(12), 4729-4749 (2006).
8. J. Limpert, A. Liem, M. Reich, T. Schreiber, S. Nolte, H. Zellmer, and A. Tunnermann, "Low-nonlinearity single-transverse-mode ytterbium-doped photonic crystal fiber amplifier," Opt. Exp. **12**, 1313-1319 (2004).
9. J. Limpert, F. Stutzki, F. Jansen, H. J. Otto, T. Eidam, C. Jauregui, and A. Tunnermann, "Yb-doped large-pitch fibers: effective single-mode operation based on higher-order mode delocalization", *Light: Sci. & App.*, vol. 1, pp. 1-5, March 2012.

[1.5.1.11 Leakage channel fiber]

1. L. Dong, T. W. Wu, H. A. Mckay, L. Fu, J. Li, and H. G. Winful, "All glass leakage channel fibers with highly fluorine-doped silica pump cladding," IEEE J. Sel. Top. Quant. Electron. **15**, 47-53 (2009).
2. G. Gu, F. Kong, T. W. Hawkins, P. Foy, K. Wei, B. Samson, and L. Dong, "Impact of fiber outer boundaries on leaky mode losses in leakage channel fibers," Opt. Exp. **21**, 24039-24048 (2013).
3. R. A. Barankov, K. Wei, B. Samson, and S. Ramachandran, "Resonant bend loss in leakage channel fibers," Opt. Lett. **37**, 3147-3149 (2012).
4. L. Dong, J. Li, H. A. McKay, A. Marcinkevicius, B. K. Thomas, M. Moore, L. Fu, and M. E. Fermann, "Robust and practical optical fibers for single mode operation with core diameters up to 170 μm," CLEO post-deadline paper CPDB6 (2008).
5. F. Kong, G. Gu, T. W. Hawkins, J. Parsons, M. Jones, C. Dunn, M. T. Kalichevsky-Dong, S. P. Palese, E. Cheung, and L. Dong, "Quantitative mode quality characterization of fibers with extremely large mode areas by matched white-light interferometry," Opt. Exp. **22**(12) 14657-14665 (2014).
6. F. Jansen, F. Stutzki, H. J. Otto, M. Baumgartl, C. Jauregui, J. Limpert, and A. Tünnermann, "The influence of index-depressions in core-pumped Yb-doped large pitch fibers," Opt. Express 18(26), 26834–26842 (2010).

[1.5.1.12 All solid 2D-photonic bandgap fiber]

1. A. Argyros, T. A. Birks, S. G. Leon-Saval, C. M. B. Cordeiro, and P. St. J. Russell, "Guidance properties of low-contrast photonic bandgap fibres," Opt. Express 13, 2503-2511 (2005).
2. A. Wang, A. K. George, and J. C. Knight, "Three-level neodymium fiber laser incorporating photonic bandgap fiber," Optics Letters 31, 1388-1390 (2006).
3. N. M. Litchinitser, S. C. Dunn, B. Usner, B. J. Eggleton, T. P. White, R. C. McPhedran, C. Martijn de Sterke, "Resonance and modal cut off in microstructured optical waveguides," Opt. Express, vol 11, no. 10, pp. 1243-1251, May 2003.
4. O. N. Egorova, S. L. Semjonov, A. F. Kosolapov, A. N. Denisov, A. D. Pryamikov, D. A. Gaponov, A. S. Biriukov, E. M. Dianov, M. Y. Salganskii, V. F. Khopin, M. V. Yashkov, A. N. Gurianov, and D. V. Kuksenkov, "Single-mode all-silica photonic bandgap fiber with 20-microm mode-field diameter," Opt. Express 16(16), 11735–11740 (2008).
5. A. Shirakawa, H. Maruyama, K. Ueda, C. B. Olausson, J. K. Lyngsø, and J. Broeng, "High-power Yb-doped photonic bandgap fiber amplifier at 1150-1200 nm," Opt. Express 17(2), 447–454 (2009).
6. S. Saitoh, K. Saitoh, M. Kashiwagi, S. Matsuo, and Liang Dong, "Design optimization of large-mode-area all-solid photonic bandgap fibers for high-power laser applications," J. Lightwave Technol. **32,** 440-449 (2014).
7. F. Kong, K. Saitoh, D. Mcclane, T. Hawkins, P. Foy, G. Gu, and L. Dong, "Mode area scaling with all-solid photonic bandgap fibers," Opt. Exp. 20(24), 26363-26372 (2012).
8. M. Kashiwagi, K. Saitoh, K. Takenaga, S. Tanigawa, S. Matsuo, and M. Fujimaki, "Effectively single-mode all solid photonic bandgap fiber with large effective area and low bending loss for compact high-power all-fiber lasers," Opt. Express 20(14), 15061–15070 (2012).

[1.5.1.13 H-PCF]

1. S. Arismar Cerqueira, Jr., F. Luan, C. M. B. Cordeiro, A. K. George, and J. C. Knight, "Hybrid photonic crystal fiber," Opt. Exp. 14(2) 926-931 (2006).
2. S. R. Petersen, T. T. Alkeskjold, F. Poli, E. Coscelli, M. M. Jørgensen, M. Laurila, J. Lægsgaard, and J. Broeng, "Hybrid Ytterbium-doped large-mode-area photonic crystal fiber amplifier for long wavelengths," Opt. Exp. 20(6), 6010-6020 (2012).
3. T. T. Alkeskjold, "Large-mode-area ytterbium-doped fiber amplifier with distributed narrow spectral filtering and reduced bend sensitivity," Opt. Exp. **17**, 16394-16405 (2009).

[1.5.1.14 Asymmetric PCF]

1. M. Napierała, T. Nasilowski, E. Bereś-Pawlik, P. Mergo, F. Berghmans, and H. Thienpont, "Large-mode-area photonic crystal fiber with double lattice constant structure and low bending loss," Opt. Exp., 19(23) 22628-22636 (2011).
2. M.-Y. Chen, Yu-R. Li, J. Zhou, and Y.-K. Zhang, "Design of Asymmetric Large-mode Area Optical Fiber With Low-bending Loss," J. of Lightwav. Technol., 31(3), 476-481 (2013).

[1.5.1.15 Resonant coupling based fiber design]

1. A. W. Snyder and J. D. Love, Optical Waveguide Theory (Kluwer Academic Publishers, 1983).
2. J. M. Fini, R. T. Bise, M. F. Yan, A. D. Yablon, and P. W. Wisk, "Distributed fiber filter based on index-matched coupling between core and cladding," Opt. Exp. **13**, 10022-10033 (2005).
3. Z. Zhang, Y. Shi, B. Bian, and J. Lu, "Dependence of leaky mode coupling on loss in photonic crystal fiber with hybrid cladding," Opt. Exp. **16**, 1915-1922 (2008).
4. K. S. Chiang and V. Rastogi, "Optical fiber," US Patent, 7711227 B2, (2010).

5. A. Kumar and V. Rastogi, “Design and analysis of a multilayer cladding large-mode-area optical fiber,” J. Opt. A, Pure Appl. Opt. 10(1), 015303 (2008).
6. M. Devautour, P. Roy, and S. Fevrier, “3D Modeling of modal competition in fiber laser: application to HOM suppression in multi-layered fiber,” Joint CLEO Poster Session II (JWA) (2009).

[1.5.1.16 Bragg fiber]

1. P. Yeh, A. Yariv, and E. Marom, “Theory of Bragg fiber”, JOSA B, vol. 68, no. 9, pp. 1196-1201, May 1978.
2. N. M. Litchinitser, S. C. Dunn, B. Usner, B. J. Eggleton, T. P. White, R. C. McPhedran, C. Martijn de Sterke, “Resonance and modal cut off in microstructured optical waveguides,” Opt. Express, vol 11, no. 10, pp. 1243-1251, May 2003.
3. J. –L. Archambault, R J Black, S. Lacroix, and J. Bures, “Loss calculations for antiresonant waveguides”, vol. 11, no. 3, JLT March 1993.
4. C. Baskiotis, Y. Quiquempois, M. Douay, and P. Sillard, “Extending the effective area of coiled all-solid silica single-mode Bragg fibers,” in ECOC, Geneva, Switzerland, 2011, paper **We.10.P1.02**.
5. E. M. Dianov, M. E. Likhachev, and S. Fevrier, “Solid-Core photonic bandgap fibers for high-power fiber lasers,” IEEE J. Sel. Top. Quantum Electronics, vol. 15, no. 1, pp. 20-29, Feb. 2009.
6. S. S. Aleshkina, M. E. Likhachev, A. D. Pryamikov, D. A. Gaponov, A. N. Denisov, M. M. Bubnov, M. Y. Salganskii, A. Y. Laptev, A. N. Guryanov, Y. A. Uspenskii, N. L. Popov, and S. Février, “Very-large-mode-area photonic bandgap Bragg fiber polarizing in a wide spectral range,” Opt. Lett. **36**, 3566-3568 (2011).

[1.5.1.17 P-CCC]

1. X. Ma, C.-H. Liu, G. Chang, and A. Galvanauskas, “Angular-momentum coupled optical waves in chirally coupled-core fibers,” Opt. Express 19(27), 26515–26528 (2011).
2. X. Ma, “Understanding and controlling angular momentum coupled optical waves in chirally-coupled-core (CCC) fibers,” PhD Thesis, University of Michigan at Ann Arbor.
3. X. Ma, C. Zhu, I-Ning Hu, A. Kaplan, and A. Galvanauskas, “Single-mode chirally-coupled-core fibers with larger than 50μm diameter cores,” Opt. Exp. **22**, 9206-9219 (2014).

[1.6 Conclusion]

1. M.-J. Li, X. Chen, A. Liu, S. Gray, J. Wang, D. T. Walton, and L. A. Zenteno, “Limit of effective area for single-mode operation in step-index large mode area laser fibers,” J. Lightwave Technol. **27**, 3010-3016 (2009).
2. G. Gu, F. Kong, T. W. Hawkins, P. Foy, K. Wei, B. Samson, and L. Dong, “Impact of fiber outer boundaries on leaky mode losses in leakage channel fibers,” Opt. Exp. **21**, 24039-24048 (2013).
3. R. A. Barankov, K. Wei, B. Samson, and S. Ramachandran, “Resonant bend loss in leakage channel fibers,” Opt. Lett. **37**, 3147-3149 (2012).
4. G. Gu, F. Kong, T. Hawkins, J. Parsons, M. Jones, C. Dunn, M. T. Kalichevsky-Dong, K. Saitoh, and L. Dong, “Ytterbium-doped large-mode-area all-solid photonic bandgap fiber lasers” Opt. Exp. **22**, 13962-13968 (2014).
5. S. Saitoh, K. Saitoh, M. Kashiwagi, S. Matsuo, and Liang Dong, “Design optimization of large-mode-area all-solid photonic bandgap fibers for high-power laser applications,” J. Lightwave Technol. **32,** 440-449 (2014).
6. C. Baskiotis, Y. Quiquempois, M. Douay, and P. Sillard, “Extending the effective area of coiled all-solid silica single-mode Bragg fibers,” in ECOC, Geneva, Switzerland, 2011, paper **We.10.P1.02**.
7. X. Ma, C. Zhu, I-Ning Hu, A. Kaplan, and A. Galvanauskas, “Single-mode chirally-coupled-core fibers with larger than 50μm diameter cores,” Opt. Exp. **22**, 9206-9219 (2014).
8. J. M. Fini and J. W. Nicholson, “Bend compensated large-mode-area fibers: achieving robust single-modedness with transformation optics,” Opt. Exp. **21**, 19173-19179 (2013).

Chapter 2 Ultra-low NA fibers

In this chapter, mode area scaling of optical fiber has been investigated numerically by exploring the possibility of ultra-low refractive index (~0.0005) of rare-earth doped core with respect to cladding. Based on ultra-low refractive index of core with respect to cladding, conventional SIF shows significant increment in mode area scaling. A new fiber design known as single-trench fiber employing ultra-low refractive index of core with respect to cladding (~0.0005) offers the possibility of an all-fiberized, low cost, and compact fiber laser device with larger mode area scaling capability than other competitive fiber designs.

2.1 Introduction

Rare-earth doped SIF is known to be the simplest fiber design for fiber lasers thanks to the outstanding features such as cylindrical symmetry, all-solid design, and higher refractive index of core than cladding [1-2]. However, performance of mode area scaling of rare-earth doped SIF is limited by achievable NA. The lowest reported NA for rare-earth doped SIF is ~0.048 in 2013 [3].

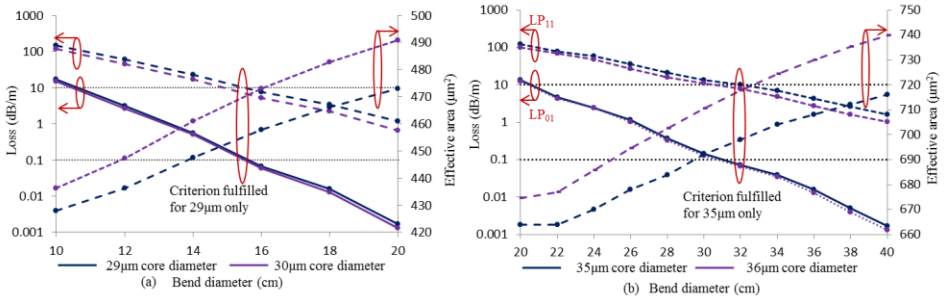

Figure 2.1 (a) and (b) the loss of LP_{01} and LP_{11} modes and effective area of the LP_{01} mode of a SIF w.r.t. bending diameters at 1060nm for two different core diameters and with a fixed core Δn of 0.0008 (corresponding to an NA of 0.048) and 0.0005 (corresponding to an NA of 0.038) respectively.

Figure 2.1(a) shows the mode area scaling capability of SIF with NA of ~0.048 (corresponding to a refractive index difference of ~0.0008 between core and cladding) at 1060nm. The effective single mode operation is ensured by keeping fundamental mode loss to be lower than or equal to 0.1dB/m and the loss of the higher order modes to be higher 10dB/m. Figure 2.1(a) ensures the maximum achievable effective area of ~455μm^2 at ~7.5cm bend radius from a ~29μm core diameter fiber with ~0.048 NA. On the other hand, figure 2.1(b) shows the maximum achievable mode area from a SIF with an even lower NA of ~0.038 (corresponds to a refractive index of ~0.0005 between core and cladding). Figure 2.1(b) ensures an effective area of ~700μm^2 at ~32cm bend diameter from a 35μm core diameter fiber. The loss ratio of fundamental mode to higher order mode remains above 130. However, core diameter larger than 35μm is unable to fulfil the above criterion as shown in figure 2.1(b). It is interesting to note that the bend diameter (~32cm) required here is large as compared to the case of ~29μm core diameter SIF with NA of

0.048, where it is lower than 16cm [2]. Here a lower bend diameter is a necessary requirement to ensure single mode operation; this also leads to reduction of the effective area of the fundamental mode. An additional advantage offered by ultra-low NA SIF (~0.038) is that the issue of mechanical reliability of large diameter optical fiber under tight bending condition can be addressed too. A bend diameter of 32cm is deemed to be large enough to avoid mechanical failure of the optical fiber, while it is small enough to maintain a compact device size. It is important to note that, the effective area achieved here is a significant improvement over the effective area (~455μm^2) offered by SIF with NA 0.048. However, there are lot of challenges associated with fabrication of ultra-low NA (such as 0.038) rare-earth doped SIF. Table 2.1 shows the comparative analysis of mode area scaling for both cases at 1060nm.

Table 2.1 comparative analysis of mode area scaling for different NA of core in case of SIF at 1060nm.

NA (corresponding to Δn)	**Core diameter (μm)**	**Required bend diameter in cm (for minimum 10dB/m loss for the higher order modes and less than 0.1dB/m for fundamental mode)**	**Achieved effective area in μm^2 (taking bend induced distortion into account)**
0.048 (0.0008)	~29	~15.5	~455
0.038 (0.0005)	~35	~32	~700

2.2 Importance of ultra-low NA

It is important to note that PCFs were seen as a potential candidate for fiber lasers for large effective area because of their capability to achieve lower NA than SIF due to presence of air holes in their cladding. However, numerical simulations of ultra-low NA presented in previous section bring SIF in a closer competition to PCF for mode area scaling. In the last decade, there have been several demonstrations of LMA fibers of various kinds such as PCF based designs like LCF and Re-LCF, photonic band gap based designs like 2D-ASPBF and Bragg fiber, different versions of SIF like parabolic fiber and W-type fiber, and resonant coupling based designs like P-CCC claiming better mode area scaling capability than SIF. However, it is important to compare the achievable effective area of the fundamental mode not the core size offering similar level of suppression of the higher order modes (e.g. 10dB/m) and low loss for the fundamental mode (e.g. 0.1dB/m) in a reasonable device size (for which the bend diameter is considered to be lower than 40cm) to find out any additional advantages offered by these designs.

Analysis presented in previous chapter concludes that some of these designs have the capability of achieving effective area as large as 1,000μm^2 at wavelength around 1060nm following above mentioned criterion of ESM operation (fundamental mode loss lower than 0.1dB/m and higher

order mode loss higher than 10dB/m) for a compact size device (bend radius with in 40cm) thanks to the pertinent efforts of the researchers across the globe. However in many of the LMA designs, this increment in effective area comes at the cost of associated difficulties in fabrication process. There are also additional drawbacks like cleaving and splicing in the case of PCF due to presence of air hole and reduced pump cladding efficiency in case of 2D-ASPBGF due to the presence of high index elements in the cladding. Beyond any doubt, SIF is the simplest design to implement and not known to suffer from any additional difficulties such as of cleaving and splicing. If ultra-low NA of ~0.038 can be fabricated with good yield and uniformity, then SIF can pose a serious candidature for compact fiber laser device suitable for mass scale production without any problems encountered in case of other competitive fiber designs.

2.3 Who is stopping mode area scaling of ultra-low NA SIF?

Figure 2.1(b) shows that a core diameter larger than 35µm having NA of 0.038 is unable to fulfil the criterion of ESM. In order to understand the reason of this behavior, it is important to understand the reason of low loss level of LP_{11} mode. Figure 2.2(a) shows the calculated loss of LP_{01}, $LP_{11}(x)$, and $LP_{11}(y)$ for a 50µm core diameter fiber with 0.038NA for different bend diameters. At a bend diameter of 30cm, loss of the fundamental mode is lower than 0.1dB/m and the loss of $LP_{11}(x)$ is higher than 10dB/m. Other higher order modes such as LP_{21}, LP_{02}, and LP_{31} etc. are also having loss higher than 10dB/m. However, $LP_{11}(y)$ has low loss, even lower than 1dB/m. The effective area is ~911µm^2 of the fundamental mode at 30cm bend diameter.

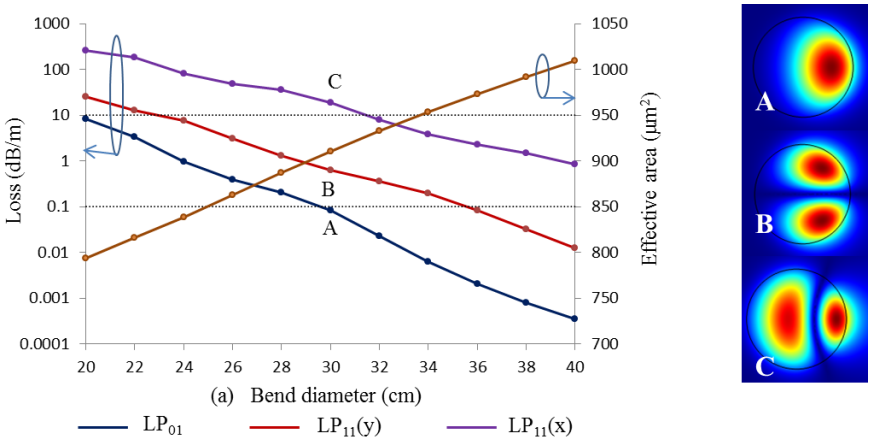

Figure 2.2 (a) the loss of LP_{01} and both LP_{11} modes and effective area of the LP_{01} mode for a SIF w.r.t. bending diameters at 1060nm of 50µm core diameter SIF and with a fixed core Δn of 0.0005 (corresponding to an NA of 0.038) (b) shows the normalized electric field of LP_{01}, LP_{11} (x), and $LP_{11}(y)$ modes corresponding to X,Y, and Z points in figure 2.2(a).

Figure 2.3 shows the equivalent refractive index profile of a 50µm core diameter SIF with ~0.038NA under a bend diameter of ~30cm using following equation 2.1 [4].

$$n^2_{eq}(x) = n^2(x) * \left(1 + \frac{2x}{\rho R}\right), \qquad (2.1)$$

Where, n(x) is the refractive index at a point of the unbent fiber, R is the bend radius, x is the value of x coordinate at a point, and ρ (fixed to 1.25) has been included to take into account of the stress factor [5]. It is evident from equation 2.1 and which is further explored in figure 2.3 that $LP_{11}(x)$ will see cladding modes along x-direction having effective refractive index comparable to core modes. Therefore, it is easy for $LP_{11}(x)$ to filter out by resonant coupling with cladding modes. On the other hand, it would be difficult for $LP_{11}(y)$ to see any such cladding modes along y-directions. Therefore, $LP_{11}(y)$ is unable to see such resonant coupling with the cladding modes and that is why low loss level of $LP_{11}(y)$ is limiting effective single mode operation.

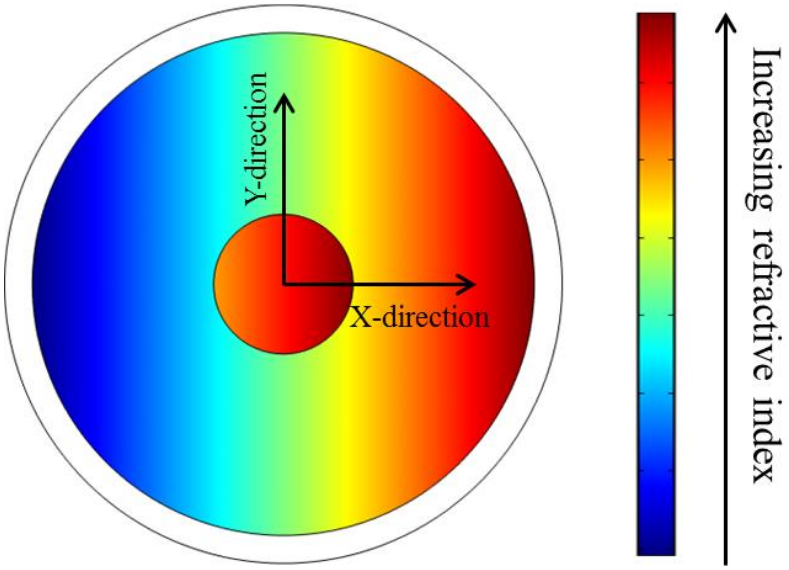

Figure 2.3 equivalent refractive index profile of a bend perturbed 50μm core diameter SIF having ~0.038NA at a bend diameter of 30cm.

2.3.1 Solution

In order to induce high loss to $LP_{11}(y)$ and scale the mode area of ultra-low NA SIF, there can be following solutions.

(a) High-index resonators in cladding

Figure 2.4 shows the additional two high index rods along y-direction for filtering out $LP_{11}(y)$ modes. The diameter and refractive index of these rods can be figured out in such a way that there is a resonant mode coupling between $LP_{11}(y)$ and modes of rod. In order to make this technique work, fiber is required to be kept in such a way that the plane having rods should be perpendicular to the bending plane. This arrangement poses a severe problem of fiber handling in a device. In order to resolve this issue, fiber can be designed in such a way that fiber can be bend only along one-axis, for example, a rectangular core fiber. These fibers were reported as "SHARC" fiber in a modified form by Rockwell et. al. [6]. However, being rectangular in shape (to avoid bending along another direction) poses sever challenges of post–processing of fiber such as cleaving and splicing etc.

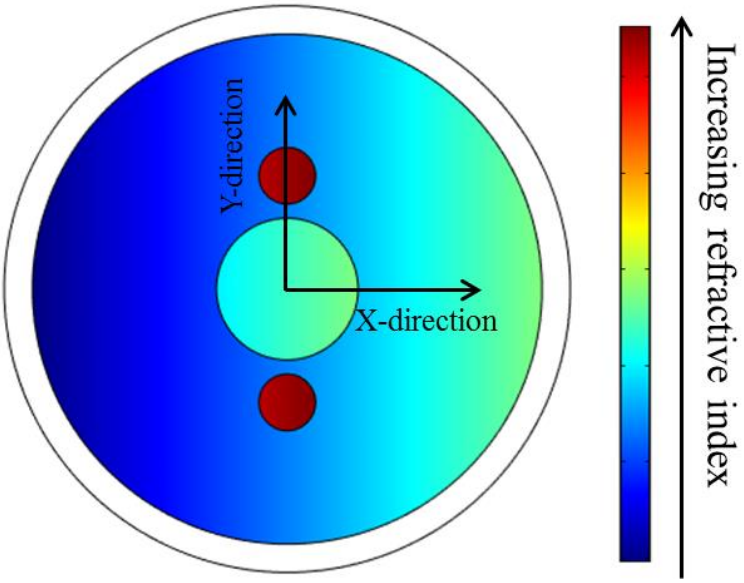

Figure 2.4 equivalent refractive index profile of a bend perturbed 50μm core diameter SIF having ~0.038NA having two high-index rods along y-direction at a bend diameter of 30cm.

(b) Twisting fiber to induce similar loss to both modes

One way to induce high loss to $LP_{11}(y)$ is to change the plane of bending of fiber in such a way that $LP_{11}(x)$ becomes $LP_{11}(y)$ and $LP_{11}(y)$ becomes $LP_{11}(x)$ to achieve similar level of loss. One example can be a quasi-helical coiling of fiber as shown in figure 2.5. However, this technique cannot induce high loss to both modes, as a compromise is involved to induce high loss to both the modes, as each LP_{11} is having loss only for half of the total length of fiber. This similar technique has been implemented in hollow core photonic band gap fiber to achieve effective single mode operation [7-8].

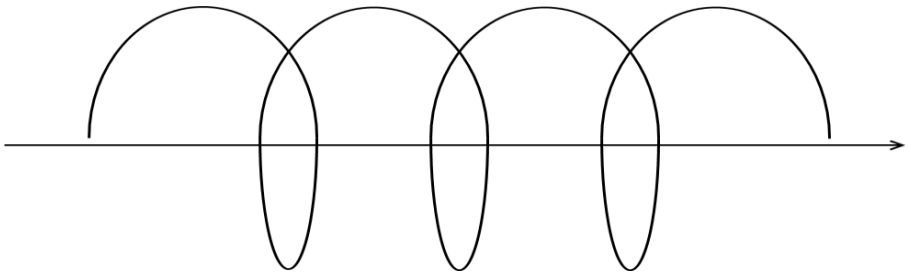

Figure 2.5 Quasi-helically coiled fiber to the change the bending plane at regular interval.

Another approach can be to use multiple rods [9] or a single rod which is helically coiled as in the case of CCC fibers discussed in previous chapter [10]. Using multiple rods can induce enough losses to both the higher order modes. However, rods would require stack and draw process or drilling holes with rod-in-tube process, which would increase the cost of fiber fabrication. However, objective of this thesis to develop fiber designs which can offer robust effective single mode and can be used for industrial scale fiber laser device production. In order to meet these needs, a modification in ultra-low NA SIF is needed which is easy to fabricate. In next section, one successful fiber design achieved during this thesis is mentioned in details.

2.4 Solution: *single trench fiber*

In order to address this issue, an optical fiber design with a core surrounded by a high-index ring (as shown in figure 2.6) known as single trench fiber (STF) can be a potential solution. An ESM operation can be ensured thanks to the resonant coupling between modes of core and surrounding ring. In this case, fiber can be bend along any direction which ensures the flexibility of fiber thanks to the cylindrical symmetry of fiber. Figure 2.6 shows the schematic ofrefractive index profile of the STF. STF has a high index ring surrounding the core of fiber, there is a low index ring between core and high index ring. The low index ring has same refractive index as of the cladding and high index ring has same refractive index as of the core.

Figure 2.6(a) also presents the notations used in this work: r_c is the core radius, t is the thickness of low-index ring (trench), d is the thickness of high-index ring (resonant ring), and Δn is the refractive index difference between the core (or resonant ring) and trench (or outer cladding). Figure 2.6(b) shows the 2D-cross section of the fiber.

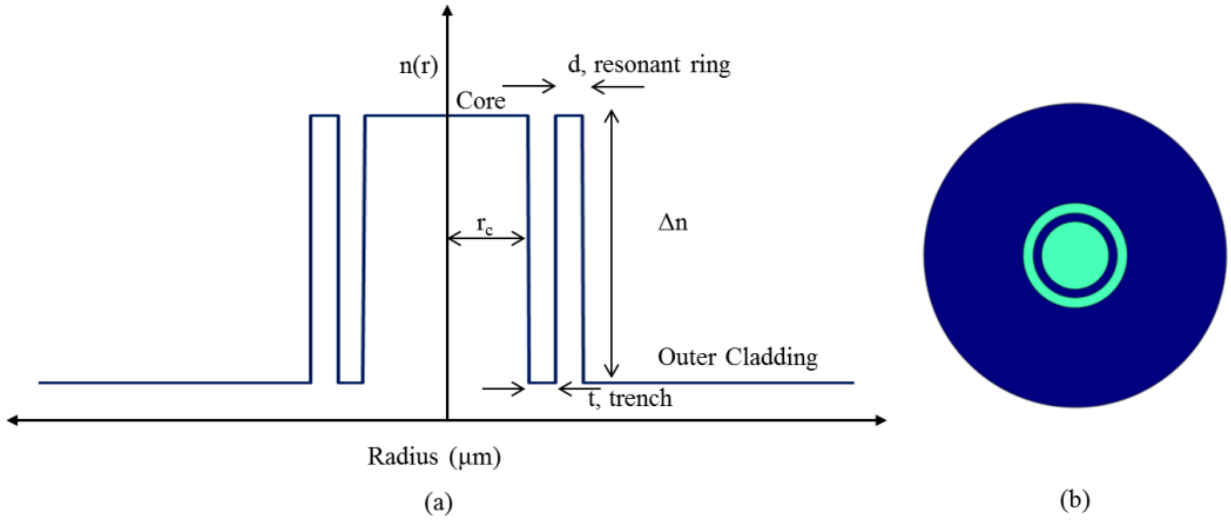

Figure 2.6(a) Schematic of refractive index profile of the STF. (b) Schematic cross-section of the STF. Green and blue colours represent high and low-refractive index regions respectively.

Initially the wavelength of operation is chosen as 1.06μm which falls within the emission band of Yb. After achieving ESM operation at 1.06μm, simulations at longer wavelengths of interest such as 1.55μm and 2μm were also performed. Numerical simulations presented in this thesis have been done using COMSOL MULTIPHYSICS software based on finite element method [11]. The domain truncation has been ensured by using the user defined circular anisotropic perfectly matched layer (PML) [12].

Bending loss of STF has been analyzed using standard conformal mapping as in case of SIF with additional stress perturbations by following the standard equation 2.1. During simulations, great care was taken to optimize the mesh size and PML parameters to achieve accurate results. A fine mesh was used irrespective of computational demand. Figure 2.7 shows the one of the fine mesh used for numerical simulations of STF. A mesh size of 1μm resulted in a complete mesh consists

of 93,138 domain elements and 1,728 boundary elements. Accuracy of parameters was verified by obtaining results in good agreement with already reported fiber deigns in the literature.

Figure 2.7 A complete mesh consists of 93,138 domain elements and 1,728 boundary elements.

The effective area of the fundamental mode is calculated using following equation 2.2:

$$effective\ area = \frac{2\pi(\int_0^\infty (E(r))^2 rdr)^2}{\int_0^\infty (E(r))^4 rdr} \quad (2.2)$$

The power fraction in core with respect to cladding is calculated using following equation 2.3:

$$Power\ fraction\ in\ core = \frac{\int_0^{2\pi}\int_0^a Re\{E_x H_Y - E_y H_x\} r dr d\varphi}{\int_0^{2\pi}\int_a^\infty Re\{E_x H_Y - E_y H_x\} r dr d\varphi} \quad (2.3)$$

Where E_x, H_x, E_y, and H_y is the amplitude of the components of electric and magnetic field as a function of radius of fiber.

It is important to mention here that, STF design is novel and was not known prior to this thesis. However, the principle involved here known as "resonant coupling" of modes is well known and have been used for several other designs.

2.4.1 Illustration of design principle of STF

Figure 2.8(a) shows the schematic of refractive index profile of a low NA-SIF in unbent condition and effective refractive index profile in bent condition. Figure 2.8(b) and 2.8(c) shows the normalized electric field of several modes in unbent and bent case respectively for core diameter=40μm, Δn=0.0005, and bent at 20cm bend radius. The leakage loss of the individual modes is negligible in case of unbent condition and fiber is multi-moded. On the other hand, in bent case each mode (mainly higher order modes) has significant loss due to bend induced coupling to cladding. However, the induced loss is still lower than 1dB/m for LP_{11} (whereas the desired loss is ~10db/m) and the higher order modes have significant power fraction in the core.

To improve the performance of low NA-SIF, a resonant ring around the core has been added which makes it STF, as shown in figure 2.8(d). The refractive index of resonant ring is same as that of the core and the region between core and resonant ring has lower refractive index that is same as that of the outer cladding. Figure 2.8(e) and 2.8(f) shows the normalized electric field of several modes in unbent and bent case respectively for STF core diameter=40μm, Δn=0.0005, t=8μm, d=6μm, and bent at 20cm bend radius. The modes of STF have negligible loss in unbent case similar to low NA-SIF case as shown in figure 2.8(b). However, the normalized electric field of modes is different from low NA-SIF case due to interaction between core and ring modes. In case of low NA-SIF we have only four guiding modes (V~4.51), on the other hand in case of STF there are nine guiding modes (first seven modes are shown here in figure 2.8(e)) including both core and resonant ring modes [13]. On the other hand, in bent case higher order modes of STF have high loss compared to low NA-SIF case thanks to the bend induced resonant coupling between core and resonant ring modes [14-15]. It is well known that for a complete resonant coupling to take place between two leaky modes, there are two basic conditions to satisfy. First one is the phase matching and second one is the loss matching of two leaky modes under coupling [15] as shown in figure 2.9.

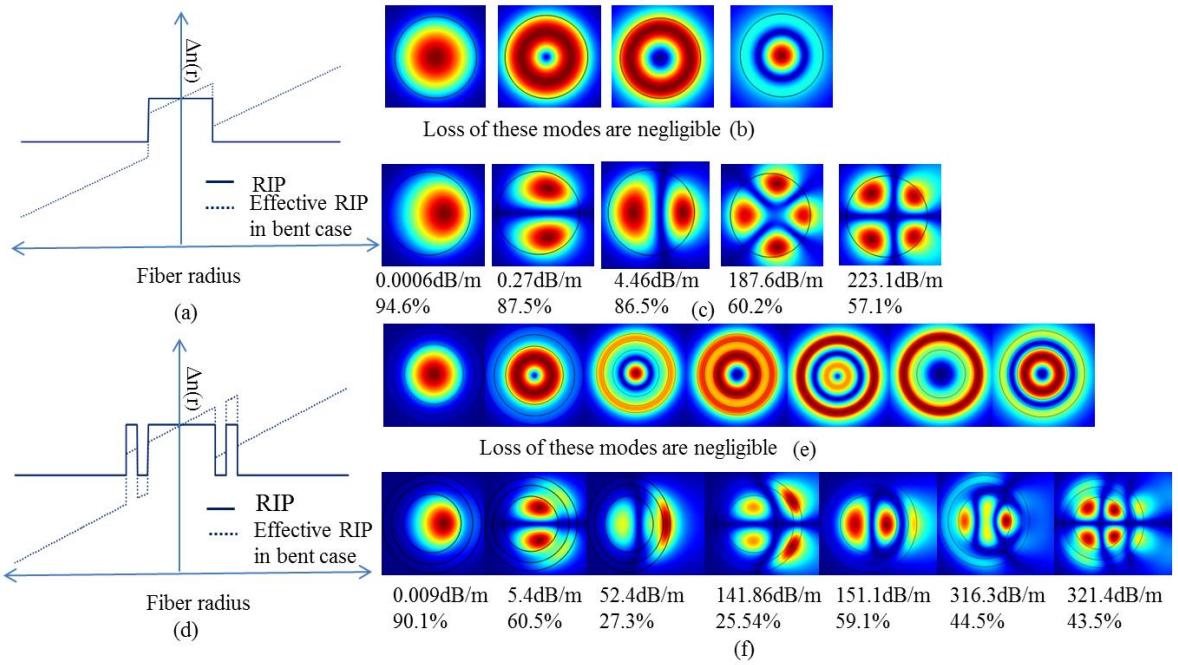

Figure 2.8(a) schematic of refractive index profile of low NA-SIF in unbent and bent case (b) and (c) normalized electric field of different modes in bent and unbent case with their losses and power fractions in core for 40µm core diameter SIF with Δn=0.0005 and 20cm bend radius (d) schematic of refractive index profile of STF in unbent and bent case (e) and (f) normalized electric field of various modes in bent and unbent case with their losses and power fractions in core for 40µm core diameter SIF with Δn=0.0005, t=8µm, d=6µm, and 20cm bend radius. The wavelength of operation is ~1.06µm.

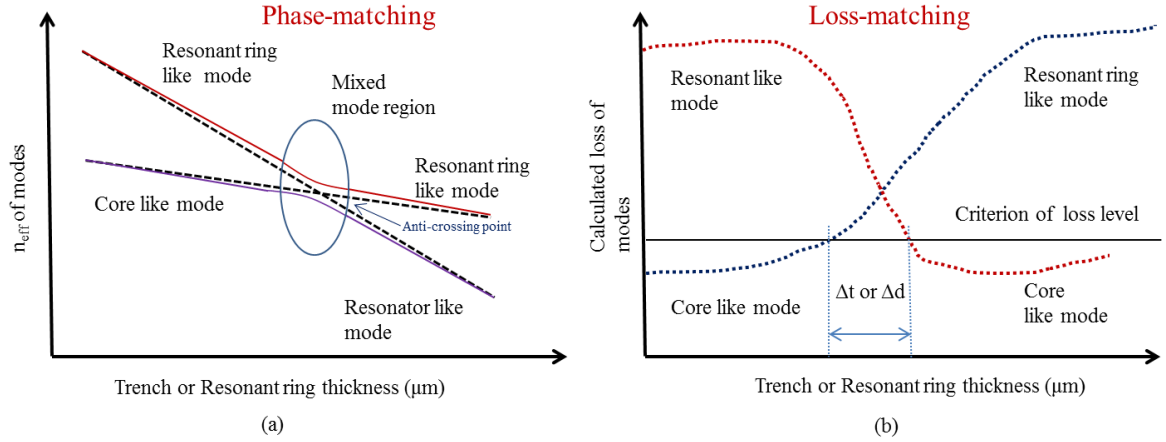

Figure 2.9 schematic of a complete coupling between two leaky modes (a) Phase matching: n_{eff} of the core and resonator modes with respect to trench or resonator ring thickness. Dashed line shows n_{eff} of core and resonator modes as a different waveguide (b) calculated loss of resonator and core modes. A black straight line shows the loss level of higher order mode, which is required to filter out them. Δt or Δd shows the range of trench thickness and resonant ring over which the loss level is met.

Due to low refractive index of core and resonant ring with respect to cladding, the modes of both core and resonant ring are leaky in bend condition. In this fiber design, idea is to have high losses for higher order modes of core irrespective of focusing on complete resonant coupling between

core and resonant ring modes. Therefore, it is possible to find out an optimized range of trench thickness (t) and resonant ring thickness (d) for fixed parameters of fiber design (such as fixed core diameter, refractive index between core and cladding, and bend radius) and a wavelength of operation so that the higher order modes have enough loss to ensure ESM operation as shown in figure 2.9(b). In the next sections, optimization of trench and resonant ring thickness has been presented for ensuring ESM operation for different core diameters.

2.4.2 Mode area scaling of STF for different core diameter STF

(a) 20μm core diameter STF

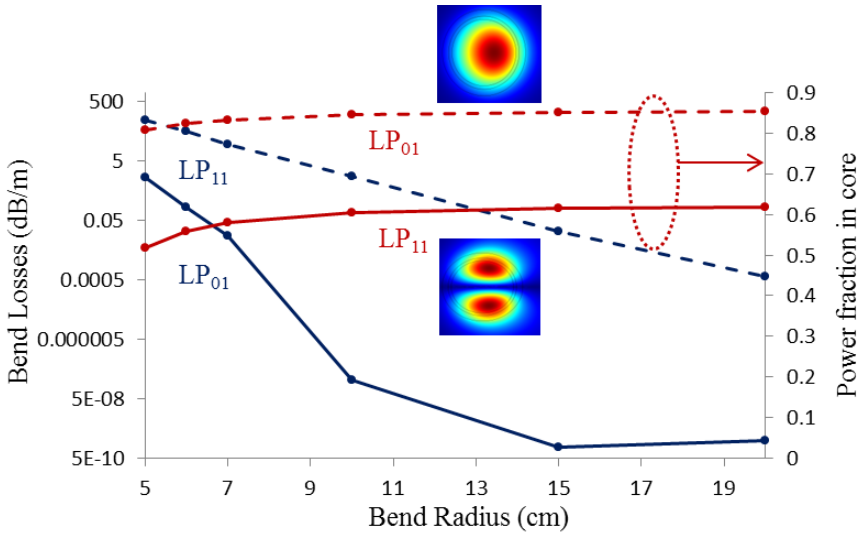

Figure 2.10 computed bend losses and power fraction of the LP_{01} and LP_{11} mode for different bend radii. Inset shows the images of the fundamental mode and LP_{11} mode at 7cm bend radius.

Figure 2.10 shows the numerically computed loss of the fundamental mode and LP_{11}(y) mode (here LP_{11}(y) has lowest losses and highest power fraction among all other higher order modes). The fiber parameters considered in this simulation study are r_c=10μm, t=1μm, Δn=0.001, and d=2μm. The bending loss of the LP_{11}(y) mode is larger than 18dB/m and for the fundamental mode it is lower than 0.016dB/m at 7cm bend radius, ensuring a loss ratio of the higher order modes to fundamental mode larger than 10^3 and the effective area is ~340μm^2. Moreover, power fraction ratio of the higher order modes to the fundamental mode in core maintains a good ratio of ~0.7 irrespective of bend radius. It is important to note that, in a double clad fiber laser, where all the real losses may be lower than calculated losses, low power fraction of the higher order modes in core compared to the fundamental mode is an important factor to ensure ESM operation. Due to this low power fraction of the higher order modes compared to the fundamental mode in core, an ESM output can be ensured irrespective of the bend radius thanks to the delocalization of the LP_{11} mode. The delocalization of the LP_{11} mode is due to presence of the resonant ring surrounding the core. This simulation study shows a significant improvement over the mode area scaling capability of STF. Figure 2.17(a) presented in chapter 1 shows the maximum mode area scaling of SIF is merely ~302μm^2, where higher order mode loss are limited by 10dB/m. On the top of this, SIF does not offer any considerable discrimination in power fraction in core for the fundamental and higher order modes as achieved in case of STF

here. Moreover, in case of SIF a bend diameter of ~8.25cm is a mandatory to induce enough bending loss to the higher order modes as bend-induced loss is the only mechanism to filter out higher order modes. From a perspective of fabrication of this fiber, it is necessary to investigate the tolerances of thickness of trench and resonant ring to ensure ESM. Figure 2.11 shows the loss of the higher order mode among all the possible modes of core and the fundamental mode at 7cm bend radius for different thicknesses of trench (t) and resonant ring (d). The core refractive index with respect to cladding is 0.001 and core diameter is fixed to 20μm. It is interesting to note that for t={1-3μm} and d={1-3μm} the loss of the higher order modes remain larger than 8dB/m and power fraction in core is lower than 0.62, on the other hand, loss of fundamental mode is lower than 0.1dB/m and power fraction in core is larger than 0.77. The effective area of the fundamental mode varies from ~290μm^2 and ~374μm^2.

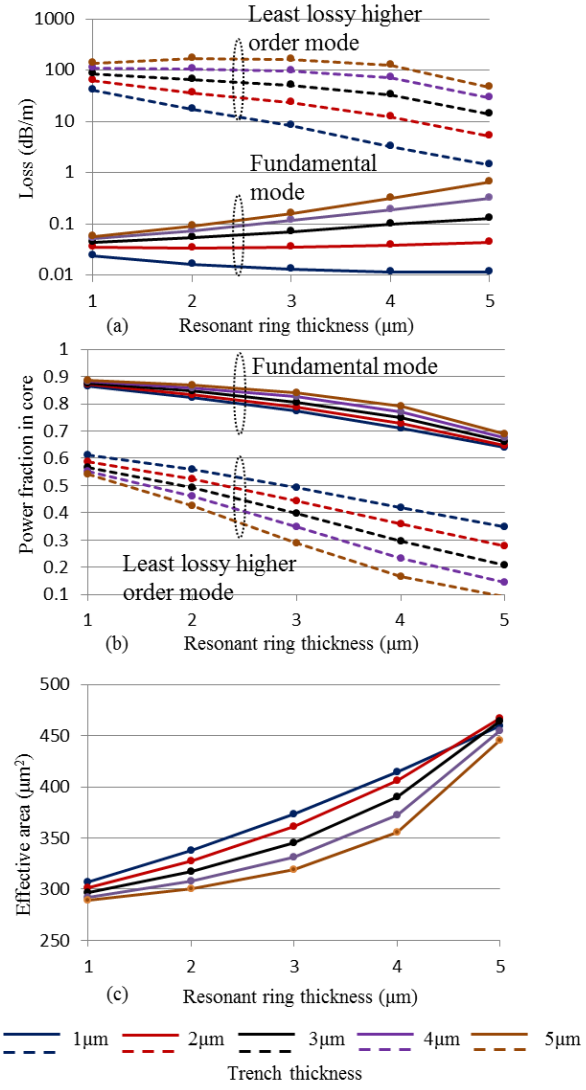

Figure 2.11 (a) computed loss (b) power fraction (c) effective area of the fundamental mode and least lossy mode for different thickness of resonant ring and trench at 7cm bend radius for 20μm core diameter SIF with core refractive index with respect to cladding to be equal to 0.001.

Intuitive understanding of impact of thickness of trench and resonant ring

When the wavelength of operation and bend radius are kept constant, the modes of resonant ring and their effective refractive indices depend on three parameters: thickness of ring, its distance from centre, and refractive index of ring with respect to cladding. On the other hand, the modes of core and their effective refractive indices depend on two parameters: core diameter and refractive index of core with respect to cladding. Here core diameter, refractive index of core, and resonant ring are also kept constant. So, the only varying parameters are ring thickness and trench thickness. However, study shown in figure 2.11 exhibits that varying thickness and distance from core of ring affect the loss and power fraction of the fundamental and other higher order modes of core dramatically. Intuitively there are following reasons behind this dramatic impact:

(1) Increasing trench thickness (distance between core and ring) decrease the interaction between modes of core and ring.

(2) Increasing trench thickness increase the interaction between modes of core and trench region (cladding between core and ring)

(3) Increasing trench thickness increase the number of modes in ring, it also changes the position of ring. It is important to understand here a bent fiber is being considered, so placing ring far from centre would significantly impact guided modes in ring and their loss due to bent induced perturbations.

(4) Increasing ring thickness would increase the number of guided modes in ring.

All of these parameters would impact core properties due to change in phase matching, loss matching, and interaction between core and ring modes. The following trends can be obtained from figure 2.11.

Increasing ring thickness while trench thickness is constant

Loss of the fundamental mode is increasing with increasing thickness of resonant ring for a constant trench thickness (as shown in figure 2.11(a)) because of the increased coupling between core and ring. With increasing thickness of ring, the effective index of the fundamental mode of resonant ring is increasing and phase matching between the fundamental mode of core and ring is increasing. This increased phase matching is bringing both modes in anti-crossing region as shown in figure 2.9(a). This increased coupling is also leading to extended field of the fundamental mode, which leads to increased effective area and decreased power fraction in core for the fundamental mode as shown in figure 2.11(c).

For higher order modes, the loss decreases with increasing thickness of resonant ring, as the core modes observe phase-mismatching with effective indices of ring (due to increasing thickness of ring). This mismatching leads them out of anti-crossing region.

Increasing trench thickness while ring thickness is constant

On the contrary, with increasing trench thickness, the effective area decreases and the power fraction in core increases due to decreasing interaction between core and ring with increasing distance between them. However, the loss of the fundamental mode increases due to increased interaction between core and trench region. For higher order modes, the loss increases with increasing thickness of trench region due to increased interaction with trench region.

(b) 30µm core diameter STF

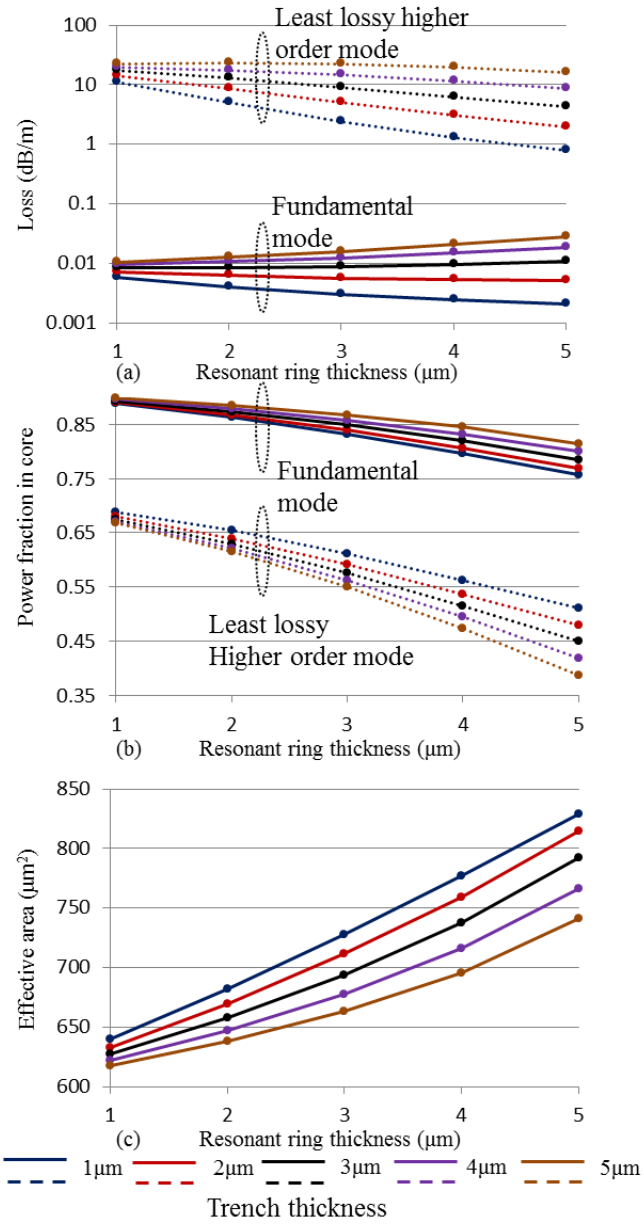

Figure 2.12 (a) computed loss (b) power fraction (c) effective area of the fundamental mode and least lossy higher order mode for different thickness of resonant ring and trench at 20cm bend radius for 30µm core diameter SIF with core refractive index with respect to cladding to be equal to 0.0005.

In order to achieve an ESM for 30μm core diameter STF, the core refractive index contrast was reduced to 0.0005 from 0.001, leading to a NA of 0.038. Figure 2.12(a) shows the loss of least lossy higher order mode and the fundamental mode at 20cm bend radius for different thicknesses of trench and resonant ring. Figure 2.12(b) shows the power fraction of least lossy higher order mode and the fundamental mode in core at 20cm bend radius for different thicknesses of trench and resonant ring. The other higher order modes have loss higher than 10dB/m and poor power fraction in core. The effective area of the fundamental mode varies from 620μm^2 to 830μm^2 for different thickness shown here. It is interesting to observe that, the trends of loss, power fraction, and the effective area of the fundamental mode with respect to thickness of trench and ring are similar to trends observed in case of 20μm core fiber. It is also interesting to note that for a wide range of resonant ring and trench thicknesses a robust ESM can be achieved. For an example, for t={4-5μm} and d={1-5μm}, the loss of the higher order modes remain larger than 8dB/m and power fraction in core is lower than ~0.70, on the other hand, loss of fundamental mode is lower than 0.03dB/m and power fraction in core is larger than ~0.80. The effective area of the fundamental mode varies from ~618μm^2 to ~767μm^2. The corresponding MFD is ~28μm to ~31.2μm. The power fraction for the fundamental mode and higher order modes were also calculated for low index layer in place of PML layer. The power fraction remains same even in case of low index layer as of PML case. It is worth noting that, delocalization of the power fraction is very important as fiber is used in double clad configuration for fiber laser configuration. The loss of the higher order modes might not be very effective in case of low index polymer coating.

(c) 40μm core diameter STF

In the same series, a 40μm core diameter with 0.0005 refractive index of core with respect to cladding was investigated for different thickness of trench and resonant ring. Figure 2.13(a) shows the calculated loss of the fundamental mode and higher order mode having lowest loss among all the possible higher order modes of the fiber. It includes all higher order modes of core, all modes of resonant ring, mixed modes, and their polarizations. It was verified that for each resonant ring and trench thicknesses shown in figure 2.13(a), other possible higher order modes (excluding fundamental mode and least lossy higher order mode shown in figure 2.13(a)) in fiber have loss higher than 10dB/m.

Figure 2.13(b) shows their corresponding power fraction in core and figure 2.13(c) shows the effective area of the fundamental mode. Table 2.2 also shows the loss and power fraction of the fundamental mode and other higher order modes in more details. Table 2.2 shows that for 20 combinations (shown in red colour) out of 24 combinations of trench thicknesses t={6-13μm} and resonant ring thicknesses d={6-8μm}, the loss of the fundamental mode remains lower than 0.1dB/m and power fraction in core is higher than 80% while the loss of the higher order modes is higher than 10dB/m or they have atleast 30% lower power fraction in core compared to fundamental mode or both are fulfilled simultaneously. In this 40μm core fiber, power fraction in core for different modes of fiber remains same even in case of low index layer in place of PML layer as of 30μm core fiber. The effective area of the fundamental mode varies from 850μm^2 to 1120μm^2 for these 20 combinations (including bend induced distortions at 20cm bend radius). It

is worth noting that for these values of effective area, the MFD comes out to be ~33μm to ~38μm from a 40μm core bent at 20cm bend radius thanks to flattening of the fundamental mode due to resonant coupling between core and ring. In can be concluded that STF can offer ESM defined in term of "CBE" as criterion of loss as higher than 10dB/m for higher order modes and lower than 0.1dB/m for fundamental mode or criterion of power fraction in core as higher than 80% for fundamental mode and atleast 30% lower for higher order modes as compared to fundamental mode is being fulfilled at 20cm bend radius while achieving an effective area of $850\mu m^2$ to $1120\mu m^2$ at 1060nm wavelength depending on parameters of trench and resonant ring thicknesses. The higher order modes are presented in Table 2.2 in the order of their increasing loss. The suppression offered by STF here is extremely high, as the table contains many ring and mixed modes as well, which are very unlikely to be excited. Ring and mixed modes have low power fraction in core, although some of them may not have very high loss as of core higher order modes. For example, for d=7μm and t=10μm, the fundamental mode loss and power fraction in core are 0.024dB/m and ~90% respectively, on the other hand, higher order modes of core (having power fraction in core larger than 50%) have loss higher than 49dB/m. Here, ring modes having poor power fraction in core such as ~27% and ~11% can be ignored.

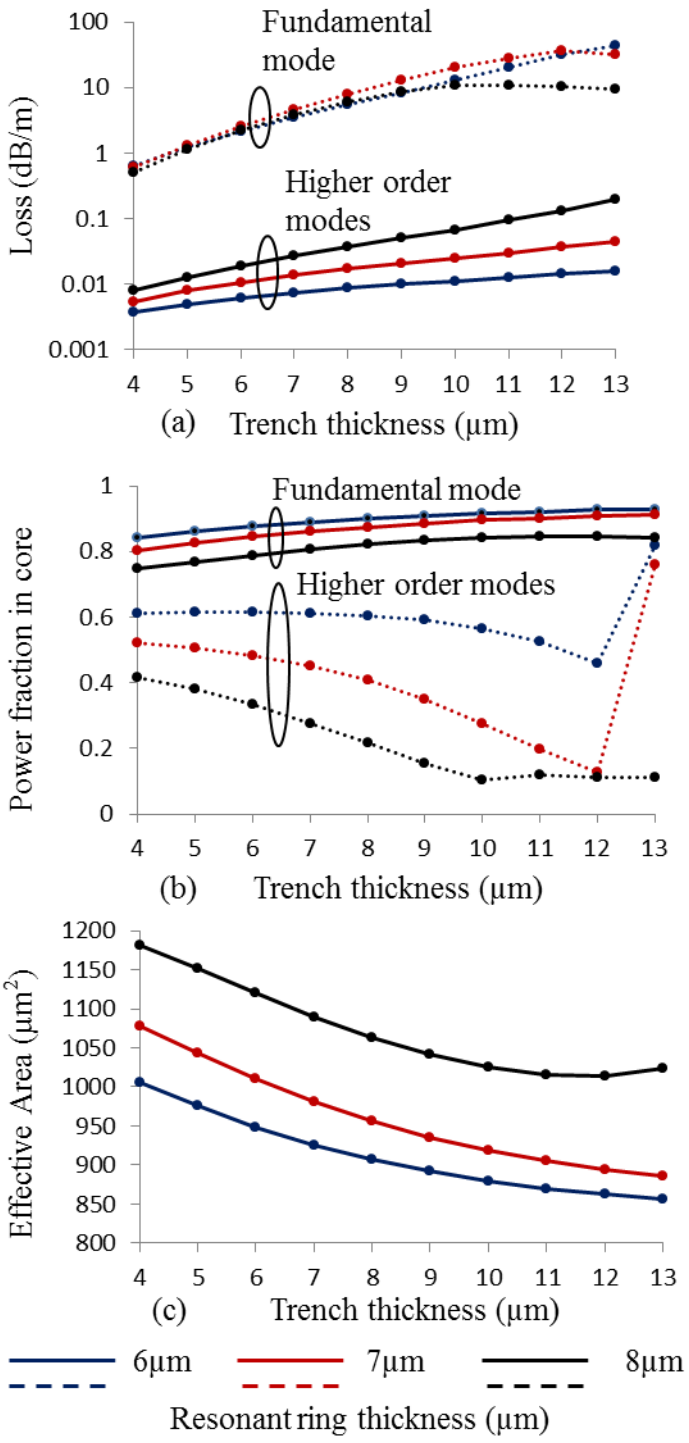

Figure 2.13(a) loss of the fundamental mode and the least lossy higher order mode of fiber, (b) Power fraction in core for fundamental mode and least lossy higher order mode of fiber, and (c) effective area of the fundamental mode of fiber for different resonant ring and trench thicknesses for 40μm core diameter STF with Δn=0.0005 at 20cm bend radius.

Table 2.2 showing loss and power fraction in core of fundamental mode and other higher order modes for different resonant ring thickness [d (μm)] and trench thickness [t (μm)].

Resonant ring thickness [d (μm)], trench thickness [t (μm)], (Effective area of fundamental mode μm^2)	**LP_{01} loss dB/m (power fraction in core)**	**Loss of other higher order modes dB/m (power fraction in core)**
6, 6 (948.72)	0.006 (0.88)	2.12(0.61), 27.08 (0.41), 68.69 (0.17), other modes>123(<47).
7, 6 (1010.71)	0.010 (0.84)	2.56 (0.48), 22.46 (0.31), 45.67(0.12), other modes>77(<62).
8, 6 (1120.07)	0.019(0.79)	2.21 (0.33), 11.29(0.28), 34.65 (0.120), other modes>45(<68).
6, 7 (925.83)	0.007(0.89)	3.46 (0.61), 38.45 (0.34), 89.24(0.12), other modes>144(<53).
7, 7 (981.26)	0.013 (0.86)	4.64 (0.45), 28.92 (0.24), 52.91 (0.08), other modes>75(<68).
8, 7 (1090.03)	0.027(0.81)	3.89 (0.28), 12.31 (0.23), 28.38 (0.08), other modes>43(<74).
6, 8 (907.02)	0.009(0.90)	5.42 (0.60), 52.38(0.27), 108.63(0.09), other modes>141(<60).
7, 8 (956.16)	0.017 (0.87)	7.94(0.41), 34.63(0.19), 59.00(0.06), other modes>72(<73).
8, 8 (1063.02)	0.037(0.82)	6.13(0.21), 12.55 (0.19), 15.69 (0.22), other modes>40(<61).
6, 9 (891.84)	0.010(0.91)	8.36(0.59), 68.34(0.21), 118.65 (0.65), other modes>124(<48).
7, 9 (935.39)	0.021(0.88)	12.95 (0.35), 38.73 (0.14), 61.10 (0.77), other modes>63(<57).
8, 9 (1041.92)	0.045 (0.83)	8.60 (0.15), 12.24 (0.16), 25.06 (0.74), other modes>35(<65).
6, 10 (879.75)	0.011(0.92)	12.91(0.57), 85.18 (0.15), 92.68 (0.71), other modes>134(<52).
7, 10 (918.54)	0.024(0.90)	19.92(0.27), 40.73 (0.11), 49.33(0.80), other modes>60(<62).
8, 10 (1025.00)	0.068 (0.84)	10.77 (0.10), 11.62 (0.13), 23.79 (0.81), other modes>30(<70).
6, 11 (870.15)	0.012(0.92)	20.19(0.52), 72.19 (0.76), 101.25 (0.11), other modes>130(<55).
7, 11 (905.084)	0.030(0.90)	28.23(0.20), 40.73 (0.08), 40.86 (0.82), other modes>51(<63).
8, 11 (1015.54)	0.093 (0.85)	10.89 (0.12), 12.24 (0.06), 20.39 (0.84), other modes>25(<74).
6, 12 (862.57)	0.014(0.93)	32.20(0.46), 56.32 (0.79), 114.60 (0.07), other modes>124(<58).
7, 12 (894.49)	0.036(0.91)	36.00(0.82), 36.05(0.13), 39.28 (0.06), other modes>40(<71).
8, 12 (1014.21)	0.13 (0.85)	10.17 (0.11), 12.93(0.04), 17.18 (0.85), other modes>21 (<77).
6, 13 (856.59)	0.01(0.93)	44.26(0.82), 51.59(0.36), 111.47 (0.44), other modes>123(<62).
7, 13 (886.34)	0.044(0.91)	31.28(0.76), 37.02 (0.05), 40.13(0.73), other modes>41(<58).
8, 13 (1024.47)	0.19(0.84)	9.52(0.11), 13.04 (0.02), 14.44 (0.86), other modes>18(<78).

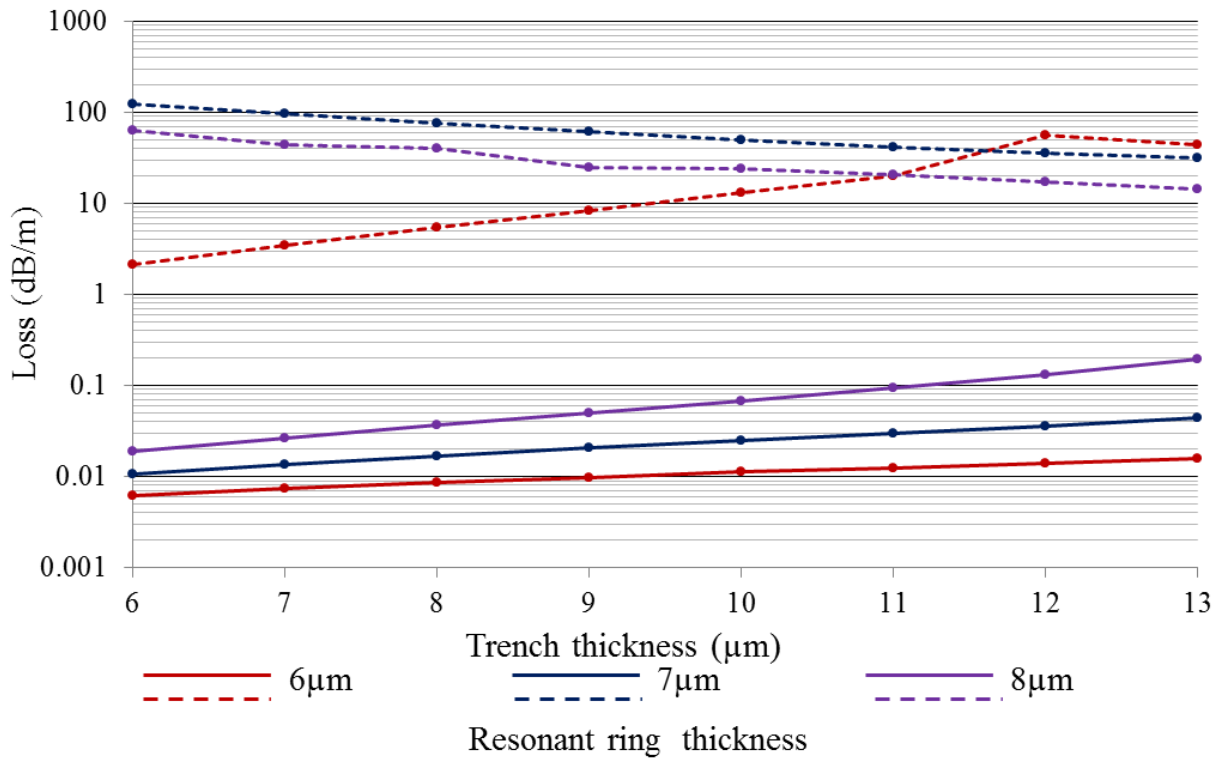

Figure 2.14 losses of the fundamental mode and the least lossy higher order mode of fiber. Here only higher order modes having power fraction more than 50% in core have been considered.

In order to further investigate the suppression of the higher order modes, any mode having power fraction in core lower than 50% shown in Table 2.2 has been ignored. Figure 2.14 depicts the loss of least lossy higher order mode (out of any possible mode in fiber having power fraction in core higher than 50%) and the loss of the fundamental mode for different trench and resonant ring thicknesses at 20cm bend radius. A ratio of 10^3 to 10^4 between least lossy higher order mode and fundamental mode can be achieved over a good range of trench and resonant ring thicknesses.

In order to further scale mode area, a STF of 50µm core diameter with $\Delta n=0.0005$ at 20cm bend radius for different ring and trench thickness was also investigated. Initial simulations show that an ESM can be ensured for an effective area between 1200µm^2 to 1500µm^2 depending on resonant ring and trench thicknesses.

2.5 Mode area scaling at longer wavelength using SIF

Fiber lasers around 1.55μm and 2μm are of prime importance due to their "eye-safe" nature and good atmospheric transmission. Fiber laser around these wavelengths are suitable for various applications such as atmospheric propagation of high-power laser beam for light detection and ranging (LIDAR) and directed-energy (DE) [1-2], medical surgery [3], gas-sensing and detection [4], pumping of mid-IR [3-5μm] optical parametric oscillators (OPO) [5], and material processing [6]. Er-doped fiber amplifier has been successfully used in data transmission applications. Afterwards, Er-doped fibers are being used for fiber lasers. However, still output power level has not been able to cross the kW barrier level. On the other hand, fiber lasers around 2μm have already achieved the kW output barrier level. Non-linear effects are also a severe challenge at these wavelengths like 1μm wavelength. However, threshold level of non-linear effect is directly proportional to wavelength of operation as shown here in equation 2.4:

$$P_{th} = \lambda . \frac{EA}{2\pi . n_2 . L} \tag{2.4}$$

Where, λ is the wavelength of operation, EA is the effective area of the fundamental mode, n_2 is the nonlinear-index coefficient, and L is the effective length of fiber.

So threshold of non-linear effects is higher for 1.55μm and 2μm wavelength operation compared to 1μm wavelength operation by a factor of 1.55 and 2 respectively. Moreover, mode area scaling for ESM at these wavelengths is relatively easier than 1μm as evident from following equation 2.5:

$$V = \frac{2.\pi.a.\sqrt{n_2^2 - n_1^2}}{\lambda} < 2.405 \tag{2.5}$$

Where, normalized frequency is inversely proportional to wavelength of operation. Figure 2.15 and figure 2.16 shows the maximum area scaling of SIF of core refractive index 0.0005 with respect to cladding at 1.55μm and 2μm respectively. The ESM is ensured following the criterion of loss of higher order modes to be larger than 10dB/m, while keeping the loss of fundamental mode to be lower than 0.1dB/m. A maximum effective area of ~1468μm^2 can be achieved from a 50.6μm core diameter SIF with Δn=0.0005 at ~44.5cm bend diameter for 1.55μm wavelength operation as shown in figure 2.15. On the other hand, a 50.8μm core diameter SIF is unable to fulfil the above mentioned criterion.

A maximum effective area of ~2264μm^2 can be achieved from a 60μm core diameter SIF with Δn=0.0005 at 63cm bend diameter for 2μm wavelength operation as shown in figure 2.16. On the other hand, a 61μm core diameter SIF is unable to fulfil the above mentioned criterion. However, a bend diameter of 63cm is large for a practical device size. In order to lower the bend diameter, core refractive index with respect to cladding can be increased. Figure 2.17 shows the maximum scalable effective area at 2μm for different core refractive index with respect to cladding. Figure 2.17 also shows the required bending diameter to induce enough loss. For core refractive index of 0.0006 with respect to cladding, an effective area of ~1962μm^2 can be achieved at a bending diameter of 46cm.

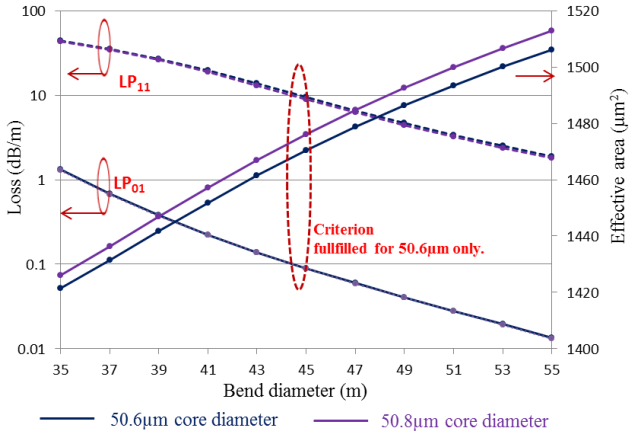

Figure 2.15 the loss of LP_{01} and LP_{11} modes and effective area of LP_{01} of SIF w.r.t. bending diameter for two different core diameters with a fixed core Δn of 0.0005 at 1.55µm.

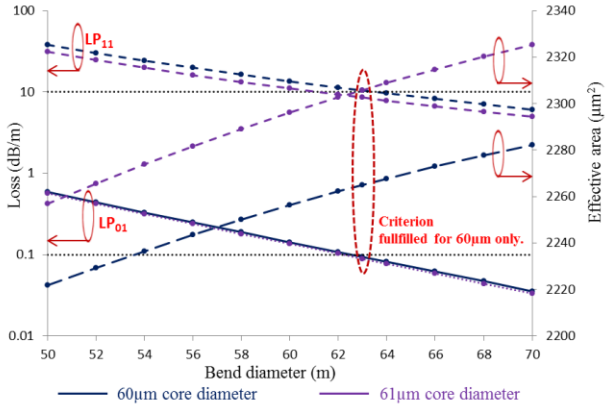

Figure 2.16 the loss of LP_{01} and LP_{11} modes and effective area of LP_{01} of SIF w.r.t. bending diameter for two different core diameters with a fixed core Δn of 0.0005 at 2µm.

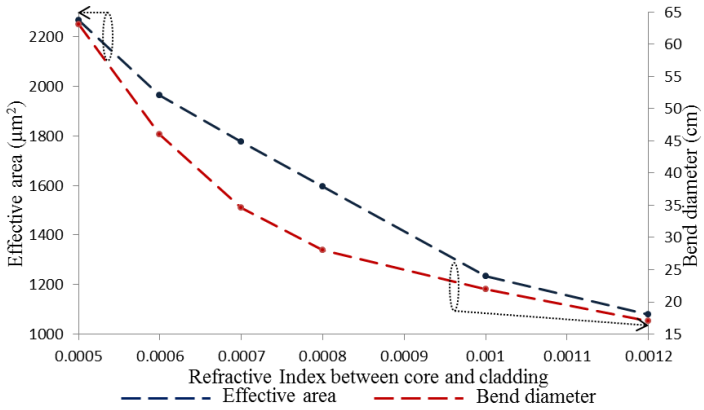

Figure 2.17 the maximum scalable effective area and required bend diameter for a different core and cladding refractive index difference for SIF at 2µm.

2.6 Mode area scaling at longer wavelength using STF

2.6.1 Mode area scaling for 1.55µm

In order to further scale the mode area at 1.55µm, it is worth using a single trench fiber at this wavelength. Figure 2.18 shows the numerical simulations for a 60µm core diameter STF at a wavelength of 1.55µm. The core refractive index with respect to cladding is assumed to be 0.0005 (corresponding to NA of ~0.038). The bend radius is fixed to 25cm. The varying parameters in simulations are trench thickness t={11-15µm}and resonant ring thickness d={6-8µm}. Other parameters such as core diameter, core refractive index with respect to cladding, bend radius, and operating wavelength are kept constant. Figure 2.18(a) shows the loss of the fundamental mode and the least lossy higher order mode. The loss of the other higher order modes are larger than 70dB/m and most of them have power fraction in core lower than 50%. Figure 2.18(b) shows the power fraction of the fundamental mode and least lossy mode. Figure 2.18(c) shows the calculated effective area of the fundamental mode.

From figure 2.18 it can be concluded that for t={13-15µm} and d={7-8µm}, the loss of the least lossy higher order mode is larger than 10dB/m and lower than 0.1dB/m for fundamental mode, on the other hand power fraction in core is lower than ~70% for higher order modes and more than 90% for the fundamental mode. The effective area of the fundamental mode varies from 1,840µm^2 to 1,940µm^2. In terms of "CBE" definition established in the beginning of this thesis, an ESM can be defined here as follow: A criterion of loss of the higher order modes larger than 10dB/m and the fundamental mode loss lower than 0.1dB/m at a bend diameter of ~50cm can be fulfilled for an effective area of ~1,840 to 1,940µm^2. Table 2.3 shows the comparative analysis of mode area scaling performance of SIF and STF. It is interesting to see that, the performance of STF is better from SIF by a factor of 1.25. Moreover, STF offers better delocalization of higher order modes compared to SIF. However, this is achieved at the cost of slightly large bend diameter to avoid any gain in effective area.

Table 2.3 comparative analysis of performance of mode area scaling of SIF and STF at 1.55µm, both has core NA to be ~0.038. The criterion of loss is 10dB/m for higher order modes and 0.1dB/m for the fundamental mode in both cases.

Fiber design	Core diameter (µm)	Power delocalization difference	Bend diameter (cm)	Effective area (µm^2)
SIF	50	~13%	~45.5	~1468
STF	60	~20 to 30%	~50	~1,840 to1,940

Numerical simulations show that it is possible to scale the mode area further but the bend diameter has to be increased to avoid bend-induced effective area reduction. The trade-off between effective area and device size (that depends on bend diameter) is a severe problem. Further scaling of effective area would require the use of straight fiber (also known as rod-type fiber), however this restricts the length of fiber to be used in a practical device size. Rod-type fiber lasers also suffer from modal-instability. Another important concern for 1.55µm high energy and high average power pulses generation is the requirement of Er-Yb doped Phospho-silicate host for efficient pump transfer from ytterbium to erbium and this is very difficult to

achieve in case of ultra-low-NA in STF as it is restricts high level of P_2O_5 [1]. Moreover, phosphorous is well-known to cause a refractive index dip which is detrimental for ESM. This problem is also applicable to other competitive fiber design such as PCF, LCF, 2D-ASPBGF. A solution in form multi-filament core (known as pixelated core) has been proposed, where core is constituted of several small diameter Er-Yb doped phospho-silicate elements and fluorine doped elements [2]. Similar approach can be implemented in STF, with enhanced delocalization of the higher order modes.

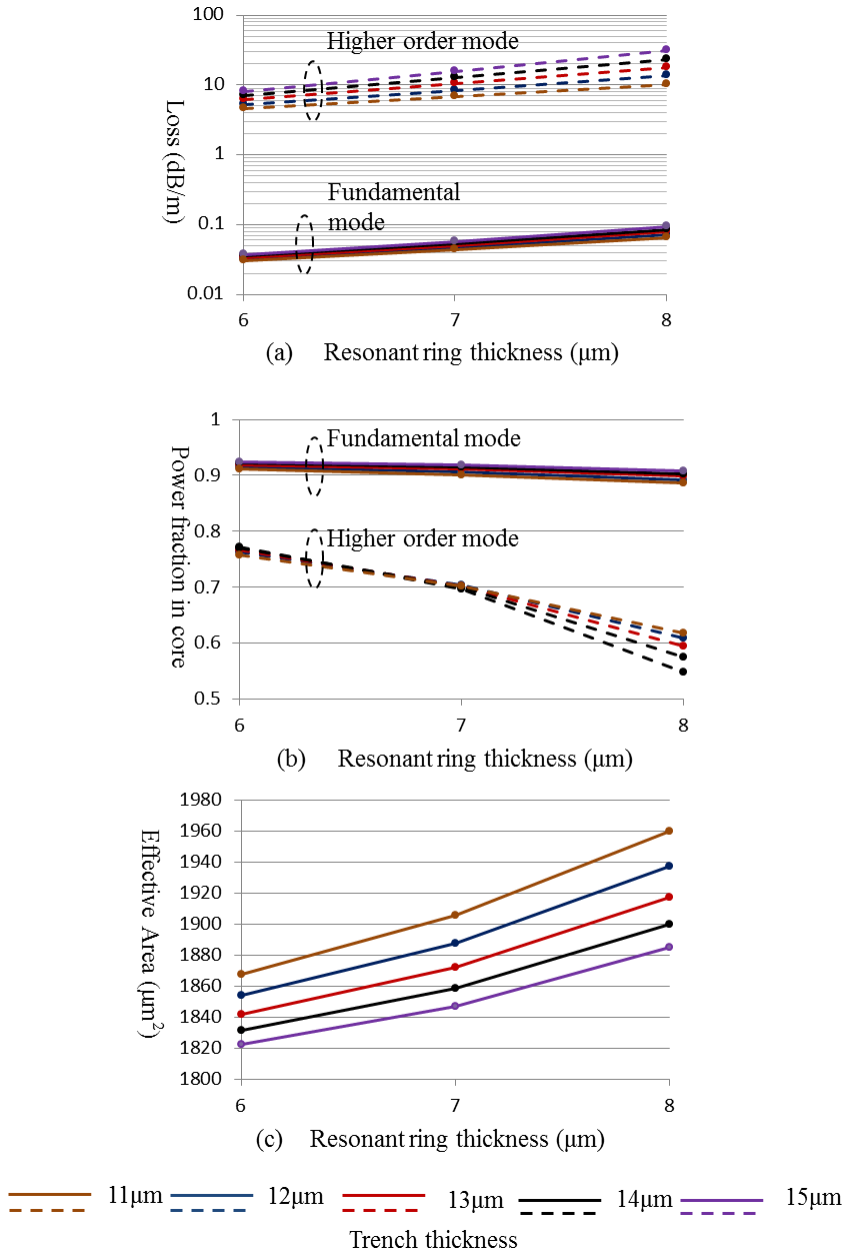

Figure 2.18(a) loss of the fundamental mode and the least lossy higher order mode of fiber, (b) power fraction in core for fundamental mode and least lossy higher order mode of fiber, and (c) effective area of the fundamental mode of fiber for different resonant ring and trench thicknesses for 60μm core diameter STF with Δn=0.0005 at 25cm bend radius for 1.55μm.

2.6.2 Mode area scaling for 2µm

Figure 2.19 shows the performance of STF with r_c=30µm and Δn=0.001 at 25cm bend radius for different thicknesses of trench t={5-7µm} and resonant ring d={11-15µm} at 2µm. Figure 2.19(a) shows the power fraction of the fundamental mode and the higher order mode having highest power fraction in core among all the possible higher order modes of fiber. However, there are few higher order modes which has high power fraction in core but their loss is larger than 20dB/m in core for different trench and resonant ring thicknesses, figure 2.19(b) shows the difference of these power fractions, and figure 2.19(c) shows the effective area of the fundamental mode for different thicknesses of trench and resonant ring.

It is interesting to note that for t={5-7µm} and d={11-15µm}, the power fraction difference remains larger than 20%. On the other hand, for t={5-7µm} and d={13-15µm} the power fraction difference remains larger than 30% else than for one case. The effective area is larger than 2,200µm^2 (~53µm MFD) for different thicknesses mentioned here. The effective area of the fundamental mode increases with increasing resonant ring thickness due to increasing coupling of the fundamental mode to ring. In terms of "CBE" following definition of ESM, for a Criterion (C) of 30% power fraction difference in core at a Bend (B) radius of 25cm, an Effective (E) area larger than 2,200µm^2 over a range of thicknesses of trench and resonant ring can be achieved.

Table 2.4 comparative analysis of performance of mode area scaling of SIF and STF at 2µm.

Fiber design	Core diameter (µm) and core NA	Criterion for ESM	Bend diameter (cm)	Effective area (µm^2)
SIF	60 and 0.038	10dB/m loss and 0.1dB/m loss for fundamental mode	~63	~2,264
STF	60 and 0.054	Power fraction difference of 30%	~50	>2,200

Table 2.4 shows the comparative analysis of SIF and STF. A maximum effective area of ~2264µm^2 can be achieved from a 60µm core diameter SIF with Δn=0.0005 at 63cm bend diameter as shown in figure 2.16. On the other hand, a 61µm core diameter SIF is unable to fulfil the above mentioned criterion. The maximum effective area of ~2,200µm^2 achieved here by 60µm SIF with core Δn of 0.0005 is same as of 60µm STF with core Δn of 0.001. However, it is interesting to note that a 63cm bend diameter is required in case of SIF, on the other hand a 50cm bend diameter is sufficient in case of STF. Moreover, STF can afford 0.001 refractive index of core with respect to cladding compared to SIF which can afford only ~0.0005 for this performance. The ESM operation is ensured by power delocalization in case of STF unlike SIF where bend-induced loss is the only mechanism to suppress higher order modes.

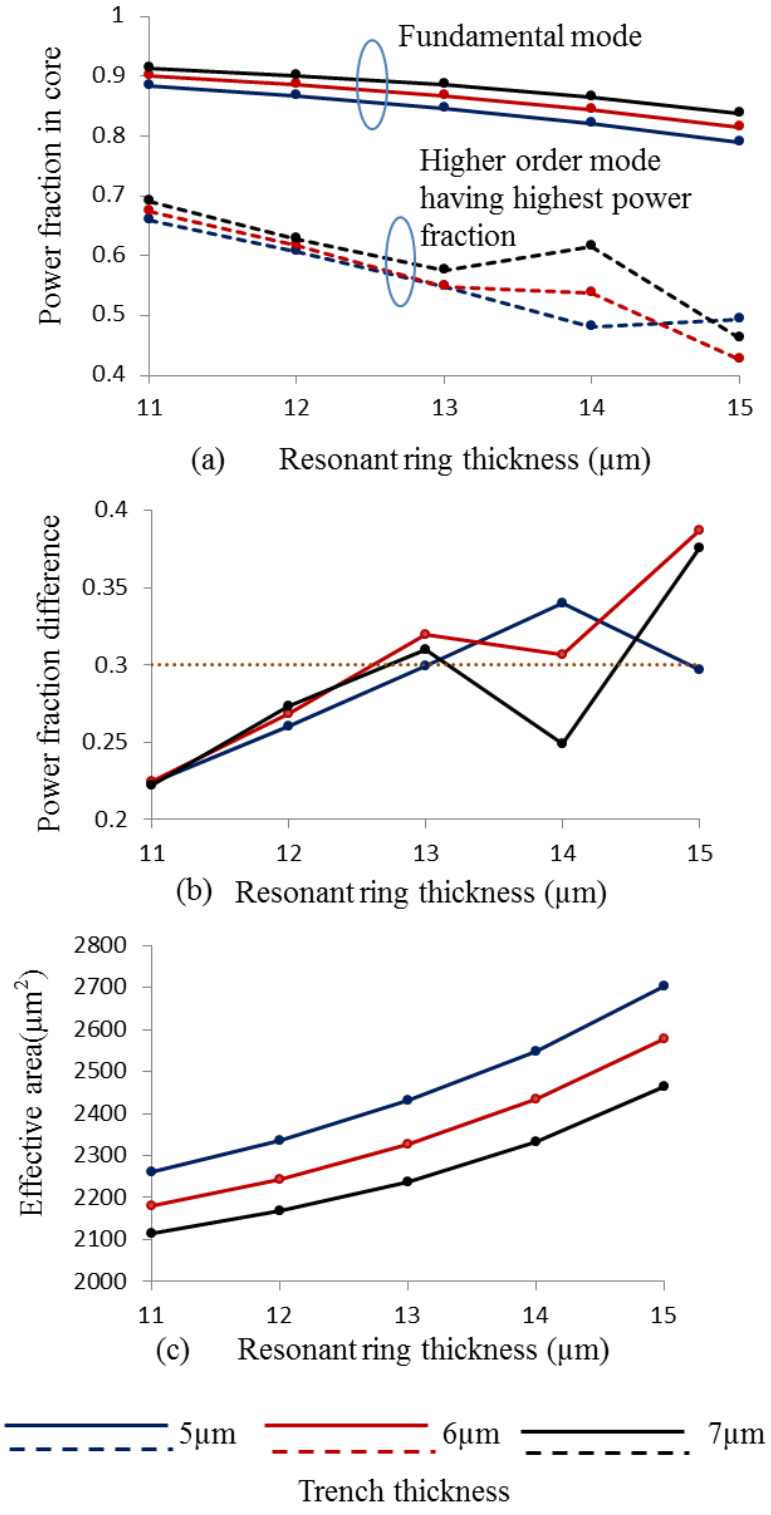

Figure 2.19(a) power fraction of the fundamental mode and the higher order mode (having highest power fraction in core among all possible higher order modes of core), (b) difference in power fraction of fundamental mode and higher order mode shown in figure 2.19(a), and (c) effective area of the fundamental mode of fiber for different resonant ring and trench thicknesses for 60μm core diameter STF with Δn=0.001 at 25cm bend radius.

In order to scale the effective area further, it is worth investigating 80μm core diameter STF with core Δn=0.0005 at two different bend radius namely 40cm and 30cm. Figure 2.20(a) shows the power fraction in core for fundamental mode and higher order mode having highest power fraction in core among all possible higher order modes (higher order modes having loss larger than 20dB/m has been ignored), figure 2.20(b) shows their corresponding loss, and figure 2.20(c) shows the effective area of the fundamental mode at 40cm bend radius. The difference in power fraction for fundamental and higher order mode (after ignoring higher order modes having loss larger than 10dB/m) is more than 30% for t={11-13μm} and d={14-15μm}, which ensures an ESM operation. The effective area varies between 3,615 μm^2 to 4,020μm^2, which corresponds to a modal filed diameter of ~68μm to ~71μm. Similarly, for 30cm bend radius case, figure 2.20(d) shows the power fraction in core for fundamental mode and higher order mode (having highest power fraction in core among all the possible higher order modes of fiber and other higher order modes have loss larger than 25dB/m), figure 2.20(e) shows their corresponding loss, and figure 2.20(f) shows the effective area of the fundamental mode. It is interesting to note that reduction of bend radius from 40cm to 30cm leads to a dramatic increase in effective area, on contrary to typical bend-induced detrimental effective area reduction. The effective area varies between ~3,895μm^2 to ~4,795μm^2, corresponding to ~70μm to ~78μm modal field diameter respectively. This dramatic increase can be attributed to bend-enhanced coupling between fundamental mode to resonant ring, which leads to flatter electric field. However, this increased effective area comes at the cost of reduced power content of the fundamental mode in core. The power content of fundamental mode varies from ~0.79 to ~0.66 in core, on the other hand the power of higher order mode having highest power fraction among other higher order modes varies from ~0.42 to ~0.20. The power difference fundamental and higher order mode is larger than ~35%, this ensures an ESM operation. However, reduced power content of the fundamental mode in core might influence fiber laser efficiency. Nevertheless, these 70μm and 80μm core STFs offer good performance of ESM for LMA applications.

On the other hand, comparing STF performance with current state of the art fiber such as rod-type PCF and large-pitch fiber (LPF), additional advantages offered by STF can be observed. These rod-type fibers are free from bend-induced effective area reduction and effective area in range of few thousand can be achieved, however they are limited by length of fiber (such as 1-2m) and also makes the device larger as they are not bendable [1]. Moreover, the refractive index matching of doped-core and undoped-cladding is a biggest challenge in case of LPF [2]. To avoid multi-mode behaviour in case of higher refractive index of core than cladding, typically an index depressed core with respect to cladding (~-0.0005) is used. However, this depressed core typically suffers from poor beam quality and lossy fundamental mode and requires enough heat to match the refractive index with cladding before lasing takes places. For example, a 81μm core LPF (the largest core diameter fiber demonstrated so far at 2μm to the best of my knowledge) requires a 115W threshold pump power in lasing configuration due to depressed index [3]. Moreover, with increasing output power level, core refractive index increases and this thermally induced gradient leads to decrease in effective area. For example, a 81μm core diameter LPF

provides a ~70µm modal field diameter at threshold power level and modal field diameter decreases to ~63µm at highest output power (merely ~52W), which is an early sign of modal-instability and further increase of pump power could lead to modal-instability [4].

STF unlike rod-type fiber is free from problem of refractive index mis-matching of core and cladding. STF is also bendable while maintaining a large effective area of the fundamental mode, so a longer length of fiber can dramatically reduce the heat load over the length of fiber in order to increase the threshold of modal-instability. Moreover, it is pertinent to mention that a large effective area in the range of 3,000µm^2-4,000µm^2 and 2,000µm^2-3,000µm^2 can be obtained at ~80cm and ~50cm bend diameter respectively. STF provides an option of achieving very large effective area in bend configuration, which can be useful in mitigating modal instability caused by thermo-optic effects. Bend configuration allows the use of a longer length of fiber unlike rod-type fibers to distribute heat over the length of fiber to avoid modal-instability. STF also offers the advantages of easy cleaving and splicing. In summary, STF shows the good potential at 2µm to address the challenges such as non-linear effects, modal instability, and tedious fabrication process due to complex fiber designs that are currently being faced by the fiber lasers.

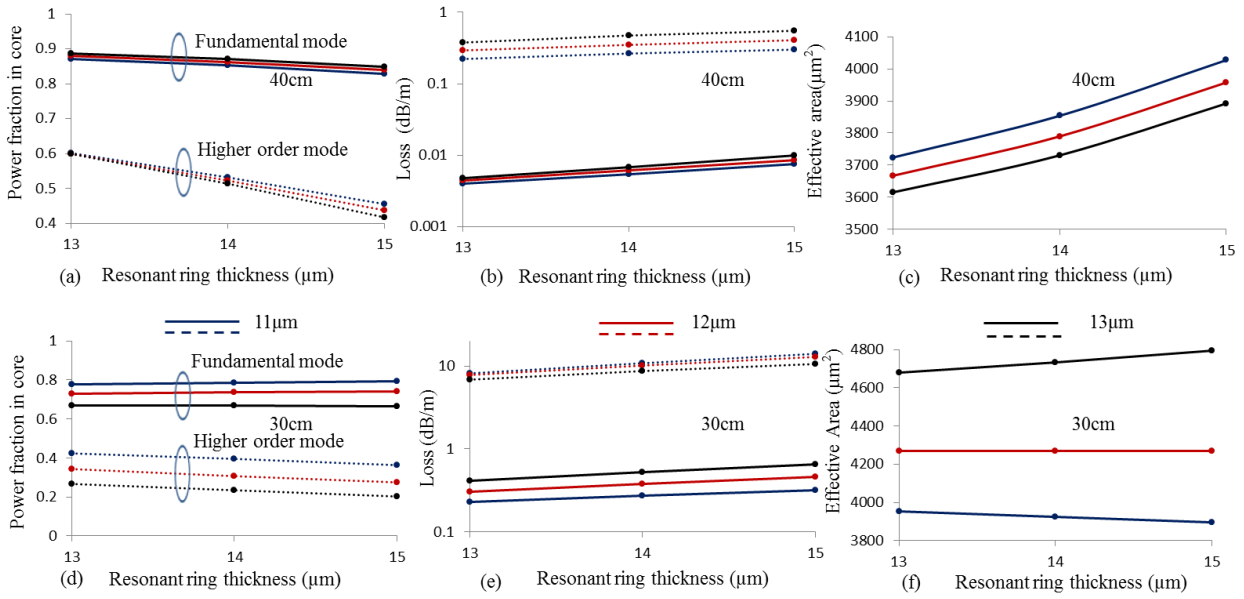

Figure 2.20(a) power fraction of the fundamental mode and the higher order mode (having highest power fraction in core among all possible higher order modes of core after ignoring higher order mode having loss larger 20dB/m) (b) loss of fundamental mode and higher order mode shown in figure 2.20(a), and (c) effective area of the fundamental mode of fiber for different resonant ring and trench thicknesses for 80µm core diameter STF with Δn=0.0005 at 40cm and 30cm bend radius.

2.7 Conclusion

In this chapter through detailed numerical study, it has been shown that an ultra-low NA of ~0.038 (corresponding to 0.0005 refractive index of core with respect to cladding) of rare-earth doped fiber can lead to dramatic increase in effective area. Following is the summary of ultra-low NA work achieved through this PhD study.

1. Ultra-low NA SIF: A SIF with ultra-low NA of ~0.038 can lead to ~700μm^2 effective area while following the criterion of loss of 10dB/m for higher order modes and 0.1dB/m for the fundamental mode at ~32cm bend diameter. This is the highest effective area ever reported for a SIF following a criterion for 10dB/m loss of higher order modes.

2. Single-trench fiber: the most impressive finding of the initial part of this PhD work is the invention of a *"simple design with great potential"* known as *Single-trench fiber*. Fiber design shows tremendous potential for an all-fiberized, ultra-low cost, LMA, and compact laser device with diffraction limited beam quality thanks to the all-solid design and simple design for fiber fabrication. Table 2.5 shows the summary of performance of STF for different core diameters, wavelengths, and NAs. Table 2.6 shows the comparison of various fiber designs discussed in chapter 1 along with improved performance of SIF and STF. It is pertinent to focus on the fact that STF offers best performance among different fiber designs as shown in table 2.6.

However, these two inclusions are based on the positive assumption of achieving ultra-low NA of 0.038 using solution doping technique. Next chapter will report realization of ultra-low NA rare-earth doped SIF and STF.

Table 2.5 summary of STFs results achieved in this chapter.

Wavelength of operation	**Core diameter and NA**	**Bend diameter**	**Maximum achievable effective area ensuring effective single mode** (take bend induced mode distortion)
1.06μm	20μm, 0.054	14cm	~290μm^2 to ~374μm^2
	30μm, 0.038	40cm	~618μm^2 to ~767μm^2
	40μm, 0.038	40cm	~1,000μm^2 to ~1,500μm^2
1.55μm	60μm, 0.038	50cm	~1,840 μm^2 to ~1,940μm^2
2μm	60μm, 0.054	60cm	~2,200μm^2 to ~2,800μm^2
	80μm, 0.038	60cm	~3,895μm^2 to ~4,795μm^2
	80μm, 0.038	80cm	~3,615 μm^2 to ~4,020μm^2

Table 2.6 comparison of different fiber designs. (Based on findings reported in this Chapter)

Fiber Design	**Maximum effective area** (Fundamental mode loss < 0.1dB/m & higher order mode loss >10dB/m)	**All-solid**	**Cylindrical symmetrical**	**Core index higher than cladding**
Low NA-SIF [1]	**~700μm^2**	Yes	Yes	Yes
LCF [2,3]	~900μm^2	Yes	No	No
2D-ASPBGF [4,5]	~1,000-1,400μm^2	Yes	No	No
Bragg Fiber [6]	~1,020μm^2	Yes	Yes	No
P-CCC [7]	Not provided	Yes	No	Yes
Bend compensated Parabolic fiber [8]	~1,000μm^2	Yes	Yes	Yes
Single trench fiber (this current work)	1,000μm^2-1,500μm^2	**Yes**	**Yes**	**Yes**

2.8 References:

[2.1 Introduction]

1. M.-J. Li, X. Chen, A. Liu, S. Gray, J. Wang, D. T. Walton, and L. A. Zenteno, "Limit of effective area for single-mode operation in step-index large mode area laser fibers," J. Lightwave Technol. **27**, 3010-3016 (2009).
2. Y. Jeong, J. K. Sahu, D. N. Payne, and J. Nilsson, "Ytterbium-doped large-core fiber laser with 1.36 kW continuous-wave output power," Opt. Express 12(25), 6088–6092 (2004).
3. V. Khitrov, J. D. Minelly, R. Tumminelli, V. Petit, and E. S. Pooler, "3kW single-mode direct diode-pumped fiber laser," in Fiber Lasers XI, Photonic West conference, San Francisco, Cali., 2014 Paper **8961.**
4. D. Marcuse, "Influence of curvature on the losses of doubly clad fibers," Appl. Opt. **21**, 4208-4213 (1982).
5. K. Nagano, S. Kawakani, and S. Nishida, "Change of the refractive index in an optical fiber due to external forces," Appl. Opt. **17**, 2080-2085 (1978).
6. D. A. Rockwell, V. V. Shkunov, and J. R. Marciante, "Semi-guiding high-aspect-ratio core (SHARC) fiber providing single-mode operation and an ultra-large core area in a compact coilable package," Opt. Express, 19(15), 14746-14762 (2011).
7. J. M. Fini, J. W. Nicholson, R. S. Windeler, E. M. Monberg, L. Meng, B. Mangan, A. DeSantolo, and F. V. DiMarcello, "Low-loss hollow-core fibers with improved single-modedness," Opt. Exp., 21(5), 6233-6242 (2013).
8. J. M. Fini, , J. W. Nicholson, B. Mangan, L. Meng, R. S. Windeler, E. M. Monberg, A. DeSantolo, F. V. DiMarcello, and K. Mukasa, "Polarization maintaining single-mode low-loss hollow-core fibres," Nat. Comm., Oct. (2014).
9. C. Baskiotis, A. M. Heidt, S.-U. Alam, D. J. Richardson, "LMA effectively single-mode thulium doped fire with normal dispersion at wavelengths around 2 microns" *CLEO-Europe/IQEC 2013* Munich 12-16 May 2013 CJ10_4.
10. X. Ma, C. Zhu, I-Ning Hu, A. Kaplan, and A. Galvanauskas, "Single-mode chirally-coupled-core fibers with larger than 50µm diameter cores," Opt. Exp. **22**, 9206-9219 (2014).
11. http://www.comsol.com/
12. Y. O. Agha, F. Zolla, A. Nicolet, and S. Guenneau, "On the use of PML for the computation of leaky modes: an application to microstructured optical fibers," COMPEL 27(1), 95–109 (2008).
13. A. W. Snyder and J. D. Love, *Optical Waveguide Theory* (Kluwer Academic Publishers, 1983).
14. J. M. Fini, R. T. Bise, M. F. Yan, A. D. Yablon, and P. W. Wisk, "Distributed fiber filter based on index-matched coupling between core and cladding," Opt. Exp. **13**, 10022-10033 (2005).
15. Z. Zhang, Y. Shi, B. Bian, and J. Lu, "Dependence of leaky mode coupling on loss in photonic crystal fiber with hybrid cladding," Opt. Exp. **16**, 1915-1922 (2008).

[2.5 Mode area scaling at 1.55µm and 2µm]

1. S. W. Henderson, P. J. M. Suni, C. P. Hale, S. M. Hannon, J. R. Magee, D. L. Bruns, and E. H. Yuen, "Coherent Laser Radar at 2µm Using Solid-State Lasers", IEEE Trans. On Geo. Sci. and Remote Sens., vol. 31, no. 1, pp. 4-15, Jan. 1993.
2. P. Sprangle, A. Ting, J. Penano, R. Fischer, and B. Hafizi, "Incoherent Combining and Atmospheric Propagation of High-Power Fiber Lasers for Directed-Energy Applications", IEEE J. of Quan. Elec., vol. 45, no. 2, pp. 138-148, Feb. 2009.
3. T. Bach, T. R. W. Herrmann, A. Haecker, M. S. Michel, and A. Gross, "Thulium: yttrium-aluminium-garnet laser prostatectomy in men with refractory urinary retention", British J. of Urology Int., vol. 104, no. 3, pp.361-364, Nov. 2008.
4. T. F. Morse, K. Oh., and L. J. Reinhart, "Carbon dioxide detection using a co-doped Tm-Ho optical fiber", Proc. SPIE, pp.158-164, 1995.
5. D. Creeden, P. A. Ketteridge, P. A. Budni, S. D. Setzler, Y. E. Young, J. C. McCarthy, K. Zawilski, P. G. Schunemann, T. M. Pollack, E.
6. P. Chicklis, and M. Jiang, " Mid-infrared $ZnGeP_2$ parametric oscillator directly pumped by a pulsed 2 µm Tm-doped fiber laser", Opt. Lett., vol. 33, no. 4, pp. 315-317, Feb., 2008.

[2.6.1 Mode area scaling for 1.55µm]

1. Y. Jeong, S. Yoo, C. A. Codemard, J. Nilsson, J. K. Sahu, D. N. Payne, R. Horley, P. W. Turner, L. Hickey, A. Harker, M. Lovelady, and A. Piper, "Erbium:Ytterbium Codoped Large-Core Fiber Laser With 297-W Continuous-Wave Output Power," IEEE JSTQE 13, 573-579 (2007).
2. G. Canat, S. Jetschke, S. Unger, L. Lombard, P. Bourdon, J. Kirchhof, V. Jolivet, A. Dolfi, and O. Vasseur, "Multifilament-core fibers for high energy pulse amplification at 1.5µm with excellent beam quality," Opt. Lett., 33 2701-2703 (2008).

[2.6.2 Mode area scaling for 2µm]

1. J. Limpert, F. Stutzki, F. Jansen, H. J. Otto, T. Eidam, C. Jauregui, and A. Tunnermann, "Yb-doped large-pitch fibers: effective single mode operation based on higher-order mode delocalization", Light: Sci. & App., vol. 1, pp. 1-5, March 2012.
2. F. Jansen, F. Stutzki, H. J. Otto, M. Baumgartl, C. Jauregui, J. Limpert, and A. Tünnermann, "The influence of index-depressions in core-pumped Yb-doped large pitch fibers," Opt. Exp., vol. 18, no. 26, pp. 26834–26842, Dec. 2010.
3. F. Jansen, F. Stutzki, C. Jauregui, J. Limpert, and A. Tünnermann, "High-power very large mode-area thulium-doped fiber laser," Opt. Lett., vol. 37, no. 21, pp. 4546-4548, Nov. 2012.
4. T. Eidam, C. Wirth, C. Jauregui, F. Stutzki, F. Jansen, H.-J. Otto, O. Schmidt, T. Schreiber, J. Limpert, and A. Tünnermann, "Experimental observations of the threshold-like onset of mode instabilities in high power fiber amplifiers," Opt. Exp., vol. 19, no. 14, pp. 13218–13224, Jun. 2011.

[2.7 Conclusion]

1. M.-J. Li, X. Chen, A. Liu, S. Gray, J. Wang, D. T. Walton, and L. A. Zenteno, "Limit of effective area for single-mode operation in step-index large mode area laser fibers," J. Lightwave Technol. **27**, 3010-3016 (2009).

2. G. Gu, F. Kong, T. W. Hawkins, P. Foy, K. Wei, B. Samson, and L. Dong, "Impact of fiber outer boundaries on leaky mode losses in leakage channel fibers," Opt. Exp. **21**, 24039-24048 (2013).

3. R. A. Barankov, K. Wei, B. Samson, and S. Ramachandran, "Resonant bend loss in leakage channel fibers," Opt. Lett. **37**, 3147-3149 (2012).

4. G. Gu, F. Kong, T. Hawkins, J. Parsons, M. Jones, C. Dunn, M. T. Kalichevsky-Dong, K. Saitoh, and L. Dong, "Ytterbium-doped large-mode-area all-solid photonic bandgap fiber lasers" Opt. Exp. **22**, 13962-13968 (2014).

5. S. Saitoh, K. Saitoh, M. Kashiwagi, S. Matsuo, and Liang Dong, "Design optimization of large-mode-area all-solid photonic bandgap fibers for high-power laser applications," J. Lightwave Technol. **32,** 440-449 (2014).

6. C. Baskiotis, Y. Quiquempois, M. Douay, and P. Sillard, "Extending the effective area of coiled all-solid silica single-mode Bragg fibers," in ECOC, Geneva, Switzerland, 2011, paper **We.10.P1.02**.

7. X. Ma, C. Zhu, I-Ning Hu, A. Kaplan, and A. Galvanauskas, "Single-mode chirally-coupled-core fibers with larger than 50μm diameter cores," Opt. Exp. **22**, 9206-9219 (2014).

8. J. M. Fini and J. W. Nicholson, "Bend compensated large-mode-area fibers: achieving robust single-modedness with transformation optics," Opt. Exp. **21**, 19173-19179 (2013).

Chapter 3 Fabrication of Ultra-low NA fiber

In this chapter, fabrication of STF and ultra-low NA SIF and their characterizations are being presented. Fabrications of STF and ultra-low NA SIF have been achieved by modified chemical vapour deposition process in conjunction with solution doping technique. The main challenges in fabrication process to achieve the desired refractive index profile have been discussed. Modal analysis of the output beam quality of fabricated fibers with respect to different input beam has been performed to ensure ESM operation. Afterwards, several laser operations have been demonstrated using these fibers to investigate their laser efficiency.

3.1 20µm core diameter STF

As demonstrated in chapter 2, a 20µm STF shows significant improvement over a SIF for mode area scaling. For example, for STF having r_c=10µm, t=1µm, Δn=0.001, and d=2µm the bending losses of the LP_{11} mode are larger than 18dB/m and for the fundamental mode it is lower than 0.012dB/m at 7cm bend radius. This ensures a loss ratio of the higher order modes to fundamental mode larger than 10^3 and the effective area of the fundamental mode is ~340µm^2. Moreover, power fraction ratio of the higher order modes to the fundamental mode in core maintains a good ratio of ~0.7 over a large range of bend radius. It is important to note that, in a double clad fiber where outermost coating is a low index coating, the real loss of the higher order mode may not be same as of calculated losses. A low power fraction of the higher order modes in core compared to the fundamental mode is an important factor to ensure ESM operation. Due to this low power fraction of the higher order modes compared to the fundamental mode in core, a single mode output can be ensured thanks to the delocalization of the LP_{11} mode.

Figure 3.1 shows the refractive index profile of RE doped preform for STF (targeting r_c=10µm, t=1µm, Δn=0.001, and d=2µm) fabricated by MCVD process in conjunction with solution doping technique. Here core is doped with Yb and Al, on the other hand, resonant ring surrounding core is doped with Ge only.

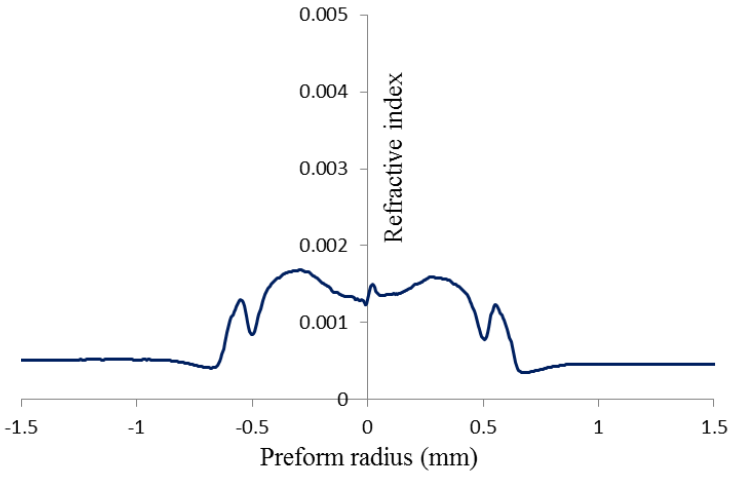

Figure 3.1 fabricated refractive index profile of Yb and Al doped preform for single trench fiber.

Table 3.1 recipe for fabrication of Yb and Al doped preform for STF.

Pass No.	$SiCl_4(O_2)$	$GeCl_4(O_2)$	O_2	Rotation	S(t)	T	Comments
1	----	----	600	30	150	1800	Warming
2	----	----	600	30	150	1950	Polish
3	----	----	600	30	150	2000	Polish
4	----	----	640	30	150	2025	Polish
5	100	40	600	30	150	2025	Resonant ring
6	30	----	600	30	150	2025	Trench
7	----	----	600	30	150	2000	Polish
8	100(Vent)	----	500	30	100	1515	Temp_Check
9	100	----	400	30	100	1515	Soot deposition

Where unit of gas flow is cm^3/minute, T is the temperature of burner in degree Celsius, and s(t) represents speed of burner (unit is mm/min).

Table 3.1 shows the various parameters used for different passes of recipe for preform fabrication. A F300 tube, an ultra-pure silica tube supplied by Heraeus [1], was used as a starting tube to deposit resonant ring, trench, and core inside it. F300 has same refractive index as of silica. Although due to presence of Cl_2 in F300 glass (which sets into the glass while removing OH contents), the refractive index of F300 is usually slightly higher than SiO_2 (such as 0.00035 to 0.0005). A F300 tube having 20mm (Outer diameter) X 16mm (Inner diameter) was used as a starting tube. Before deposition of resonant ring and trench, first four high temperature passes were executed to warm and polish the tube. These high temperature passes removed several impurities present inside the tube which were still present despite of organic cleaning of tube prior to being mounted on lathe. Afterwards, a resonant ring was deposited using flow of $SiCl_4$ and $GeCl_4$ to have higher refractive index than F300 tube. $GeCl_4$ was used to incorporate GeO_2 to increase refractive index of resonant ring with respect to F300 tube by 0.001. Further a layer corresponding to trench was deposited with only flow of $SiCl_4$. It is important to note that no $GeCl_4$ was given in this pass, despite of the fact that, refractive index of SiO_2 is slightly lower than F300. This step was taken based on the hypothesis that there will be some diffusion of GeO_2 from resonant ring to trench and this diffused GeO_2 will be enough to increase the refractive index of trench to F300 level. Flow rate of carrier gas of $SiCl_4$ for both resonant ring and trench and of $GeCl_4$ for resonant ring were chosen judiciously to achieve optimized thickness in optical fiber (such as 1μm and 2μm thickness for trench and resonant ring).

Afterwards, polishing of tube was done to completely consolidate the glass. In the next step, before depositing unconsolidated SiO_2 known as soot, a temp_check pass was executed. This pass includes optimization of temperature of burner while moving at a set step. In next step, silica soot was deposited at 1515^oC. A vertical solution doping process was used to soak the soot in tube with a solution of methanol having rare-earth chlorides. A 200ml methanol solution having 6gm $AlCl_3.6H_2O$ and 3gm $YbCl_3.6H_2O$ was used for soaking of soot. After proper drying of preform, soot was consolidated to glass. In further steps, preform was collapsed to a rod under optimized pressure conditions. The outer diameter of preform is

12mm. Figure 3.1 shows the measured refractive index profile of preform using PK2600 preform analyser. The refractive index profile of the fabricated preform is different from the proposed design. The refractive index profile of core is not flat and refractive index of ring is not high enough. On the other hand, the refractive index of trench is larger than F300 level and significant diffusion of GeO_2 can be observed in trench region. However with further optimizations of the preform fabrication process, it can be brought closer to the desired profile. In next sections, further progress towards flat core refractive index and matching of refractive index of resonant ring and core will be reported.
The preform was milled to the D-shape in order to improve the pump absorption efficiency in fiber, and subsequently drawn to 240µm diameter fiber. The fiber was coated with a low-index polymer which provided a nominal pump cladding NA of 0.48. A 20µm core diameter was obtained in the fabricated fiber.

3.1.1 Experimental characterization of 20µm STF

Figure 3.2 shows the absorption spectrum of the fabricated fiber. The absorption is 2.5dB/m at a wavelength of 976nm.

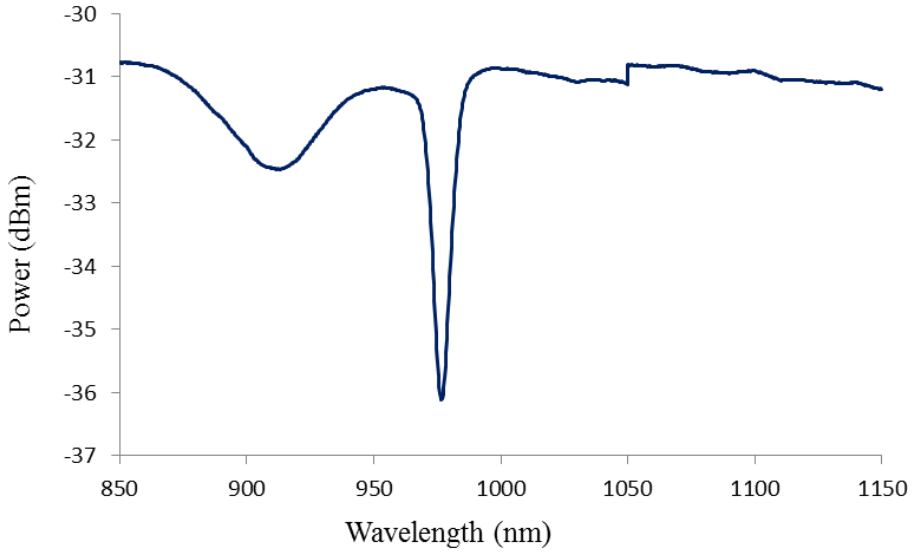

Figure 3.2 absorption spectrum of a 1.92m long Yb^{3+} and Al^{3+} doped STF.

Moreover, the fiber shows significant bend robustness. It did not show any considerable bend loss until a bend radius of 10cm. To verify the single-mode behaviour of the fiber, a *S*patial and *S*pectral (S^2) measurement of the output beam from the fiber was performed [2]. S^2 imaging can resolve the contents of different modes present in output beam, it relies on the group delay between different modes resulting in to spatial and spectral interference pattern between fundamental and higher order modes.

S^2 measurement was performed by Dr. Jaesun Kim at SPI Lasers, UK. Figure 3.3(a) shows the schematic of experimental set-up used for S^2 measurement. A tunable laser source (TLS) tuned from 1059nm to 1079nm with a step of 0.05nm was used for the measurement. The beam was launched into 20µm diameter core STF by splicing with 8µm diameter core Corning's HI1060 fiber. Fiber was coiled to 22cm bend diameter. During splicing, no efforts

were made to optimize the alignment of core of two different fibers and may have offset launching. A S^2 analysis was performed to analyse the modal quality. Figure 3.3(b) shows the measured multi-path interference (MPI) versus relative group delay. This measurement shows significant suppression of the higher order modes. LP_{11} and LP_{21} modes suffer high losses and their power level is 32dB lower than the fundamental mode power level. This S^2 measurement ensures an ESM operation.

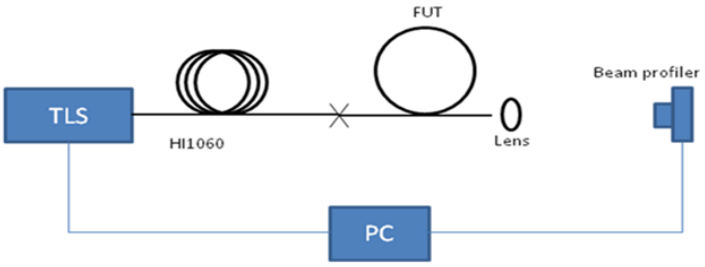

(a)

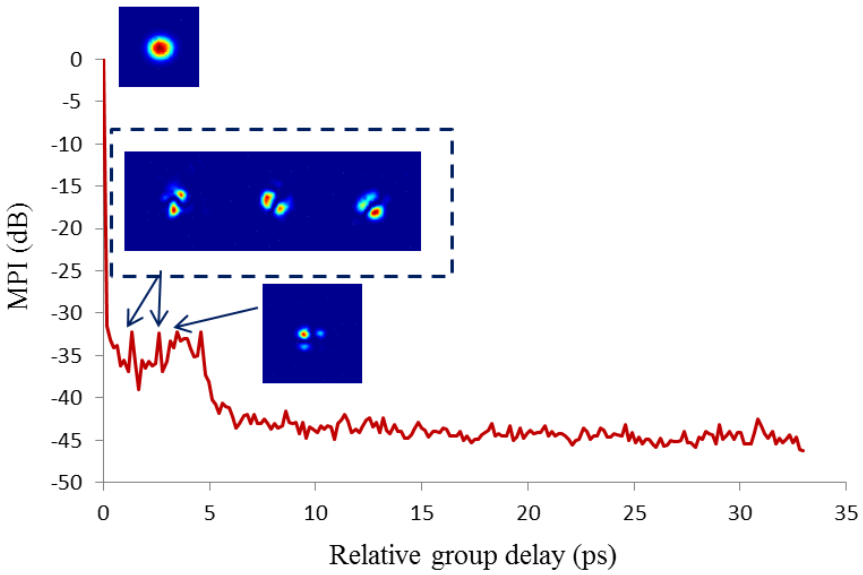

(b)

Figure 3.3(a) experimental set-up for S^2 measurement. TLS: tunable laser source, FUT: fiber under test, PC: computer (b) MPI (dB) versus relative group delay (ps). Inset images show the measured beam profiles of the modes obtained.

3.1.2 Laser efficiency of 20µm STF

The laser efficiency of the fabricated fiber was measured in a 4% - 4% laser cavity. Figure 3.4(a) shows the experimental set-up used for the laser efficiency measurement. A fiber coupled laser diode operating at a wavelength of 976nm was used as the pump source. The pump beam was launched into the fiber through an aspheric lens (focal length=8mm). Both ends of the fiber were cleaved perpendicularly to provide a Fresnel reflection for the laser cavity. In order to separate the signal and pump wavelengths, a dichroic mirror with high reflection at pump wavelength and high transmission at signal wavelength was used at the

pump launch end. At the pump exit end of the FUT, output beam was collimated and focused using aspheric lens (focal length=8mm) and a dichroic mirror with high transmission at pump wavelength and high reflection at signal wavelength was used to separate signal and pump wavelengths.

Figure 3.4(b) shows the output power versus launched pump power for 10.3m of the fiber. Fiber was coiled to ~30cm bend diameter. A slope efficiency of 85% with respect to the launched pump power was observed. The inset graph shows the output spectrum at the highest power and image shows the output beam profile captured by the CCD camera. The measured M^2 remains lower than 1.3. It is important to note that, even at a bend diameter of ~30cm, a reasonable M^2 was obtained inspite of the fact that, the losses of the higher order modes are low at ~30cm bend diameter thanks to the delocalization of the higher order modes. The spectral profile of the free running laser is shown in inset of figure 3.4(b) with the multiple peaks located at ~1080nm. No considerable change in slope efficiency was observed over the 6m to 10m length of the fiber. Moreover, even a tighter bending up to 15cm bend diameter did not change the slope efficiency.

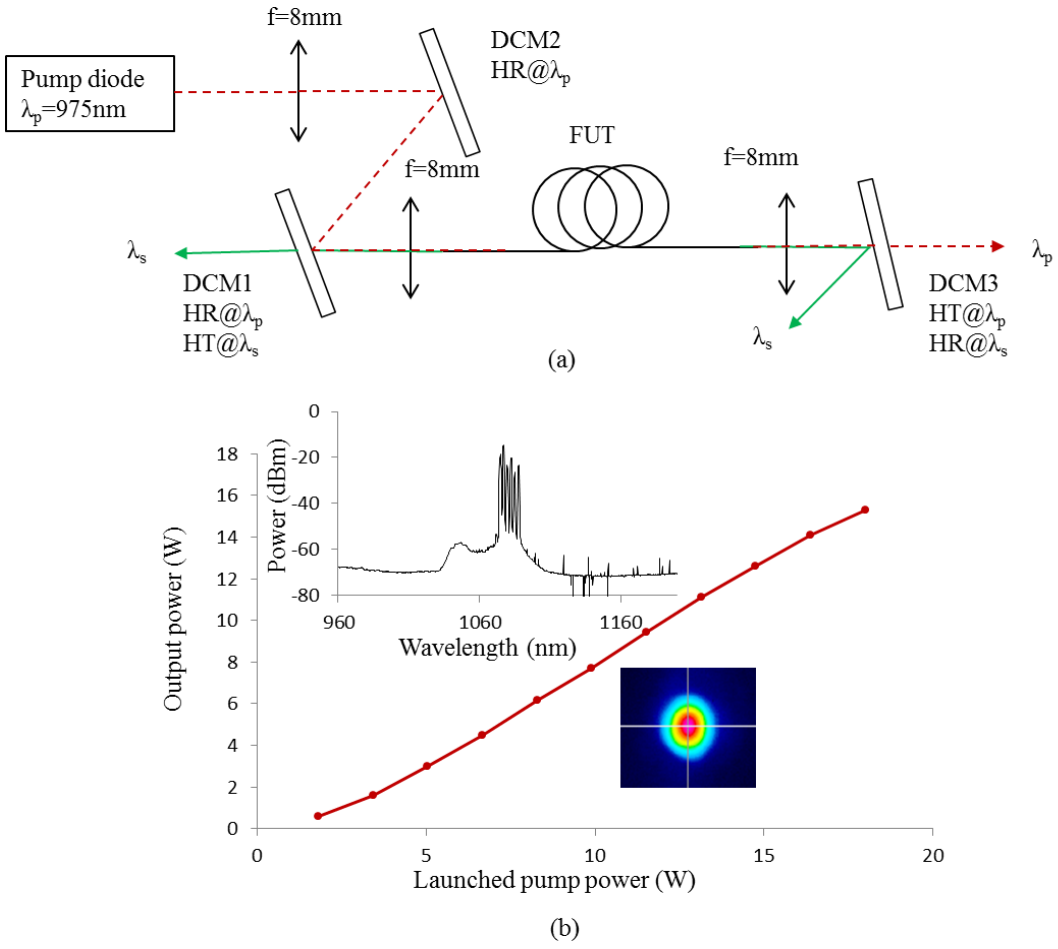

Figure 3.4(a) experimental setup for fiber laser efficiency measurement. DCM-Dichroic mirror, FUT-fiber under test, HR-High reflectivity, HT-High transmission, λ_p=pump wavelength, and λ_s=signal wavelength. (b) measured slope efficiency of the fabricated fiber. Inset image shows the output beam profile and inset graph shows the measured spectrum of the output beam.

3.2 30µm core diameter STF

In the first attempt of STF preform fabrication; there were two major discrepancies in refractive index profile with respect to desired profile of STF. First is a slight central dip in refractive index profile and second is the mis-match of refractive index of core and resonant ring. In order to get-rid of refractive index dip in preform profile, several preforms were fabricated at different soot temperatures. Few of them are shown here in figure 3.5.

In this process of preform fabrication (MCVD in conjunction with solution doping technique), quantity of dopants (both rare-earth and co-dopants) incorporation decides the core refractive index as these are the only index raising components in silica soot. Therefore, in order to control the core refractive index it is necessary to control the dopants incorporation. Dopants incorporation depends on several factors such as soot porosity, solution doping condition, solution draining speed, and soot oxidation temperature etc for a particular solution strength [3-5]. However, soot porosity is the most important factor as it not only decides the amount of the RE ion incorporation but also the uniformity of the profile. A non-uniform porosity can lead to a non-uniform transverse profile especially a central dip, which can be detrimental to preserve singe mode operation. Moreover, uniformity of profile becomes very crucial when the required core refractive index is on the order of 10^{-4} to maintain ESM operation. It is pertinent to mention here that it is possible to control the soot porosity by controlling soot deposition temperature. In order to control the soot porosity, several preform fabrications were done, using the same process parameters and solution strength but different soot deposition temperatures. During this investigation, it was observed that soot deposition temperature plays a very crucial role in determining core refractive index with respect to cladding and over all profile of the core.

Figure 3.5 shows the refractive index profile of three preforms, the changes in recipe for these three preforms are summarized in table 2, 3, and 4. It is interesting to note that, with optimization of soot deposition temperature it is possible to achieve a flat refractive index profile as achieved in case of preform shown in figure 3.5(c). Figure 3.5(c) shows the refractive index of core with respect to cladding with in the limit of +/- 0.0001. It is also important to note that, with change in slight parameters thickness and refractive index of trench and resonant ring can be controlled as well. In next section, a good control over thickness of trench and resonant ring has been achieved as well.

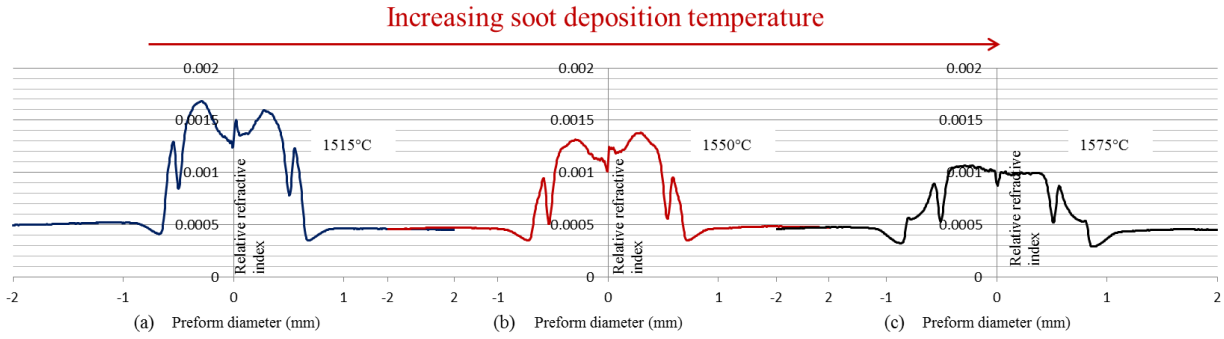

Figure 3.5 refractive index profiles for different soot deposition temperature (a) 1515°C (b) 1550°C (c) 1575°C.

Table 3.2 recipe for fabrication of Yb and Al doped preform A.

Pass No.	$SiCl_4(O_2)$	$GeCl_4(O_2)$	O_2	Rotation	S(t)	Temperature of burner	Comments
1	----	----	600	30	150	1800	Warming
2	----	----	600	30	150	1950	Polish
3	----	----	600	30	150	2000	Polish
4	----	----	640	30	150	2025	Polish
5	100	40	600	30	150	2025	Resonant ring
6	30	----	600	30	150	2025	Trench
7	----	----	600	30	150	2000	Polish
8	100(Vent)	----	500	30	100	1515	Temp_Check
9	100	----	400	30	100	1515	Soot deposition

Table 3.3 recipe for fabrication of Yb and Al doped preform B.

Pass No.	$SiCl_4(O_2)$	$GeCl_4(O_2)$	O_2	Rotation	S(t)	Temperature of burner	Comments
1	----	----	600	30	150	1800	Warming
2	----	----	600	30	150	1950	Polish
3	----	----	600	30	150	2000	Polish
4	----	----	640	30	150	2025	Polish
5	100	30	600	30	150	2025	Resonant ring
6	**40**	----	600	30	150	2025	Trench
7	----	----	600	30	150	2000	Polish
8	100(Vent)	----	500	30	100	**1550**	Temp_Check
9	100	----	400	30	100	1515	Soot deposition

Table 3.4 recipe for fabrication of Yb and Al doped preform C.

Pass No.	$SiCl_4(O_2)$	$GeCl_4(O_2)$	O_2	Rotation	S(t)	Temperature of burner	Comments
1	----	----	600	30	150	1800	Warming
2	----	----	600	30	150	1950	Polish
3	----	----	600	30	150	2000	Polish
4	----	----	640	30	150	2025	Polish
5	100	**32**	600	30	150	2025	Resonant ring
6	**40**	----	600	30	150	2025	Trench
7	----	----	600	30	150	2000	Polish
8	100(Vent)	----	500	30	100	**1575**	Temp_Check
9	100	----	400	30	100	1515	Soot deposition

Where unit of gas flow is cm^3/minute, temperature is degree Celsius, and s(t) represents speed of burner (unit is mm/min).

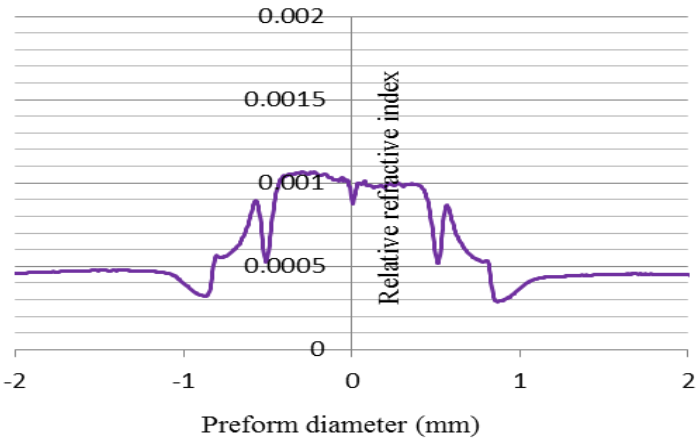

Figure 3.6 refractive index profile of Yb and Al doped preform fabricated by MCVD process in conjunction with solution doping process.

For a 30µm core STF, as shown in chapter 2, figure 12 for trench thickness t={4-5µm} and resonant ring thickness d={1-5µm}, the loss of the higher order modes remain larger than 8dB/m and power fraction in core is lower than ~0.70. On the other hand, loss of fundamental mode is lower than 0.03dB/m and power fraction in core is larger than ~0.80. The effective area of the fundamental mode varies from ~618µm^2 to ~767µm^2. The corresponding MFD is ~28µm to ~31.2µm. Here the intention was to fabricate STF with d={1-5µm}and t={4-5µm}.

Figure 3.6 shows the refractive index profile of fabricated Yb and Al doped STF preform. The preform diameter is ~12mm. The preform diameter was further reduced to 6mm by etching using HF acid. This was done in order to increase the ratio of core to cladding diameter, which can increase the pump absorption in a cladding pump configuration. The preform was milled to the D-shape in order to improve the pump absorption efficiency in fiber, and subsequently drawn to 185µm diameter fiber. The fiber was coated with a low-index polymer which provided a nominal pump cladding NA of 0.48. A 30µm core diameter was obtained in the fabricated fiber. The absorption is 13dB/m at a wavelength of 976nm.

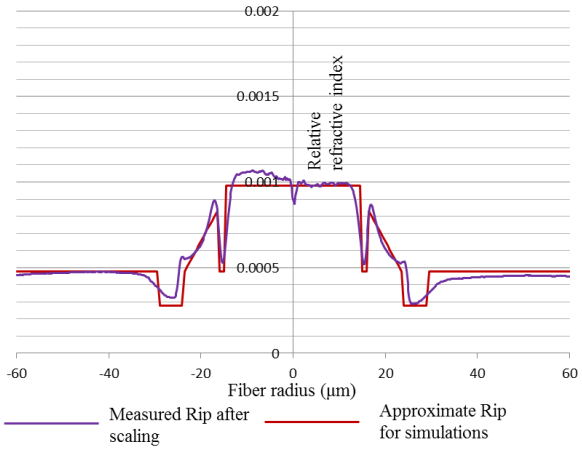

Figure 3.7 measured refractive index profile of preform after scaling down to a 30µm diameter STF and approximate refractive index profile of fiber used for simulations.

It is important to note that the refractive index profile of preform shown here is not ideal, so in order to study the impact of imperfections on performance of mode area scaling; it is necessary to investigate the achieved refractive index profile numerically. Figure 3.7 shows the preform refractive index profile scaled down to a fiber configuration of 30µm core diameter and approximated refractive index profile used for simulations. Figure 3.8(a) shows the calculated loss of LP_{01} and least lossy LP_{11} (mode having lowest loss among all possible higher order modes) and effective area of the fundamental mode. Figure 3.8(b) shows the power fraction in core for the fundamental mode and the least lossy LP_{11} mode. It is interesting to note that, there is a significant difference in loss and power fraction difference between LP_{01} and the higher order modes. This ensures an ESM operation. For example, at 20cm the bend radius, the loss of LP_{01} is lower than 0.01dB/m, on the other hand the loss of LP_{11} mode is higher than 8dB/m. This leads to loss ratio of higher order mode to fundamental mode larger than 800, which is larger than ideal case considered in simulations. Moreover, the power fraction difference is larger than 26% and the effective area is larger than 630µm^2. It is important to note that, the loss of the fundamental mode remains lower than 0.12dB/m till ~16cm bend diameter, without any considerable reduction in effective area of the fundamental mode. Infact, this fabricated fiber shows better performance than ideal one.

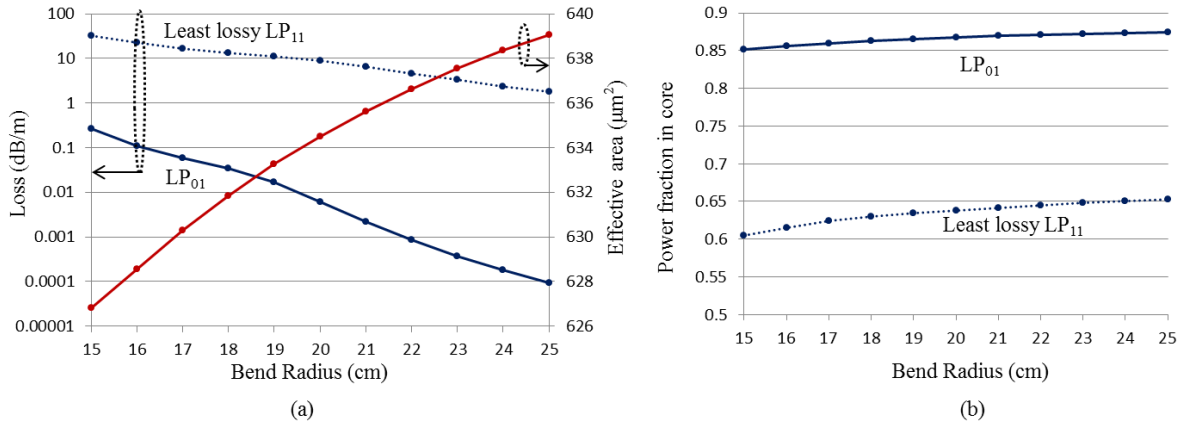

Figure 3.8 (a) calculated loss of the LP_{01} and least lossy LP_{11} mode and effective area of the fundamental mode (b) power fraction of the LP_{01} and least lossy LP_{11} in core. These calculations have been done using fabricated refractive index profile of preform after scaling down to fiber configuration.

3.2.1 Experimental characterization of 30µm STF

Figure 3.9 shows the experimental set-up used for verification of single mode behaviour of this STF. A 2.22m long fiber in a loosely coiled configuration (~40cm bend diameter) was used for characterization. In order to remove cladding modes, the low index polymer coating was stripped off and index matching oil was applied at both ends. In order to qualitatively analyse the behaviour of the output beam of fiber under test, the profile of the output beam was investigated with respect to different input beams. All experiments were done using a 1060nm laser source. Here single and multi-moded beam delivery fiber was used to deliver input beam for fiber under test. A binary phase plate was also used to launch LP_{11} mode into fiber by converting LP_{01} mode into LP_{11} mode. Offset launching of different input beams

were also used to excite the higher order modes and response of fiber with respect to these launchings.

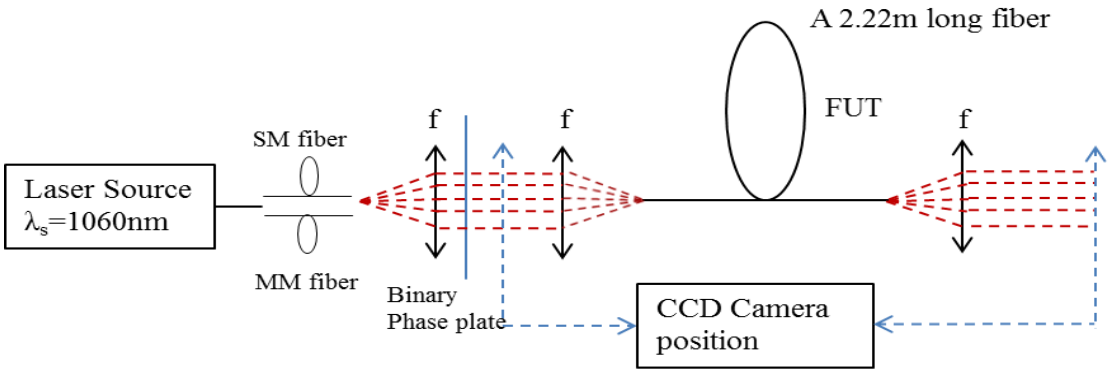

Figure 3.9 shows experimental set-up used for verification of single-mode behaviour of fiber.

Figure 3.10(a) shows the CCD image of output beam for different off-set launching of LP_{01} mode. It is interesting to note that, only the intensity of profile changes, with offset launching, which ensure absence of the higher order modes. Furthermore, different modes such as mixed mode (LP_{01} +LP_{11}) and pure LP_{11} modes were launched using multi-moded fiber and single mode fiber with binary phase-plate respectively (as shown in figure 3.10(b)). Profile of output beam ensures only a Gaussian beam w.r.t mixed mode and almost no light w.r.t pure LP_{11} mode (as shown in figure 3.10(c)). These experiments ensure a robust ESM operation.

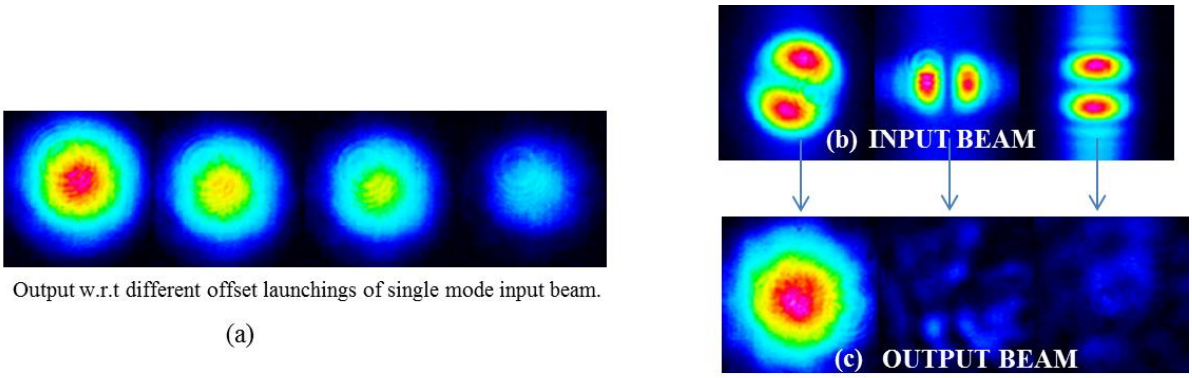

Output w.r.t different offset launchings of single mode input beam.

(a)

Figure 3.10(a) output beam profile w.r.t different input launching conditions (b) different higher order modes launched into the fiber and (c) output beam profile with respect to mixed (LP_{01}+LP_{11}) mode and pure LP_{11} mode input beam.

It is pertinent to mention that, these qualitative measurements do not eliminate the possibility of the presence of the contents of the higher order modes in output beam. However, these measurements definitely ensure that fiber offer significant discrimination to the higher order modes and capable of ensuring ESM operation. In order to quantify the contents of the higher order modes, a quantitative analysis such as S^2 can be performed, which is currently beyond the scope of this thesis. Moreover, it is not possible to measure qualitative and quantitative suppression of the higher order modes due to poor fraction in core as compared to the fundamental mode by different techniques discussed here. The feature of high power fraction

in core discrimination between fundamental mode and the higher order mode can be successfully exploited in a fiber laser configuration, as due to poor overlap with doped area of core higher order modes achieve less gain as compared to the fundamental mode. Several upcoming techniques based on real time monitoring of output beam of laser can be used to quantify the content of the higher order modes in fiber laser configuration [6-7]. However, these measurements are currently beyond the scope of this thesis.

3.2.2 Laser device using 30µm STF

In order to measure the performance of fiber in laser configuration, initially fiber was tested in a 4%-4% laser cavity. Further, fiber was investigated in pico-second and nano-second all-fiberized MOPA configurations.

(a) 4%-4% fiber laser cavity

The fiber laser efficiency was measured in a 4%-4% laser cavity using a 2.43m long STF. Figure 3.11(a) shows the experimental set-up used for the laser efficiency measurement. A fiber coupled laser diode operating at a wavelength of 976 nm was used as the pump source. The pump beam was launched in to the fiber through an aspheric lens (focal length=8mm). Both ends of the fiber were cleaved perpendicularly to provide a Fresnel reflection for the laser cavity. In order to separate the signal and pump wavelengths, a dichroic mirror with high reflection at pump wavelength and high transmission at signal wavelength was used at the pump launch end. At the pump exit end of the FUT, output beam was collimated and focused using aspheric lens (focal length=8mm) and a dichroic mirror with high transmission at pump wavelength and high reflection at signal wavelength was used to separate signal and pump wavelengths. Figure 3.11(b) shows the measured spectrum of output beam at different power level, showing laser output at ~1040nm. Figure 3.11(c) shows the measured slope efficiency with respect to launched power. A ~80% slope efficiency was obtained. Inset of figure 3.11(c) shows the profile of output beam captured by CCD.

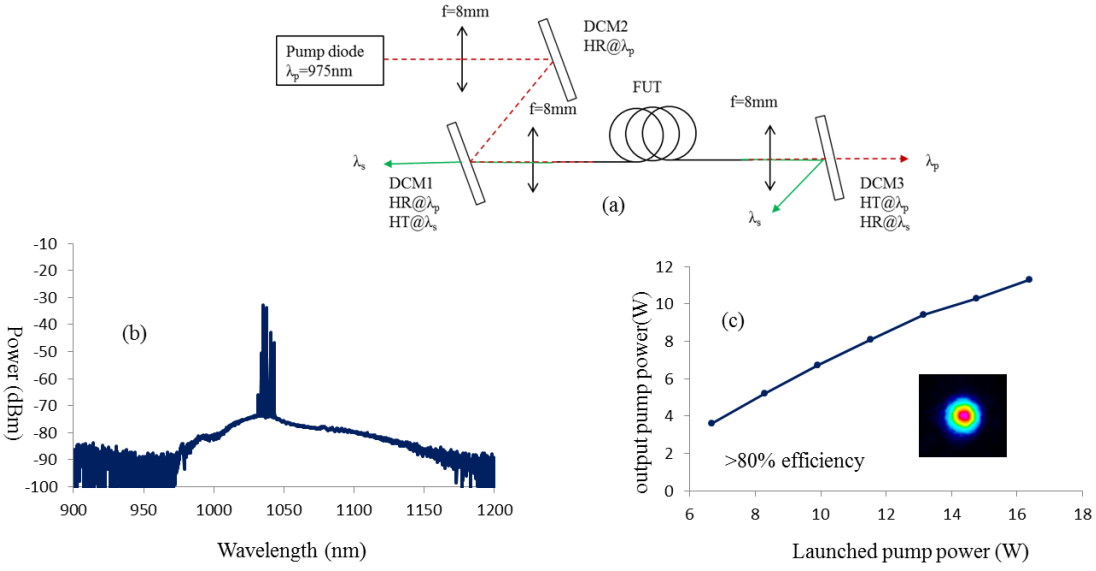

Figure 3.11(a) Experimental set-up used for fiber laser efficiency (b) measured spectrum of output beam at different power levels (c) slope efficiency of 2.43m long fiber. Inset shows the profile of output beam.

(b) MOPA configuration

Further, a 4-stage master oscillator power amplifier (MOPA) was built using this 30µm core diameter STF. A 2.7m long STF coiled at 32cm bend diameter was used in fourth stage of MOPA. The STF had 8dB/m cladding pump absorption at ~975nm. A 25ps gain-switched diode laser at 13.5MHz at 1040nm was used as a seed laser. The 30µm core diameter STF was spliced to 10µm core diameter fiber of third stage of the amplifier. In order to avoid the damage to output facet, a short endcap (~1.2mm) was spliced to the STF. Figure 3.12(a) shows the slope efficiency of launched pump power at ~975nm to average output signal power in final stage amplifier. The slope efficiency is ~76%. The maximum average signal power is limited only by available pump power. Figure 3.12(b) shows the measured spectrum at highest peak power. A simulated Raman scattering (SRS) peak can be clearly seen around ~1090nm, however it is lower in magnitude by 30dB from output signal, which states clear possibilities of further scaling of peak power level. The measured M^2 value is lower than 1.15. Figure 3.13(c) shows the measured temporal profile of output pulse at highest peak power. The full width half maximum (FWHM) of the output pulse is ~23.31ps. The output signal suffers from spectral broadening due to self-phase modulation (SPM) and measured 10dB linewidth at highest power is ~3nm. The highest peak power exceeds 160kW power level. The PER value is larger than 15dB at highest peak power. It is interesting to note that, a polarization maintaining 10µm active core diameter was used in third stage of MOPA, while current STF is not a polarization maintaining fiber. However still, output signal maintains single polarization, which is probably due to a reasonable bend diameter (~32cm) which does not cause bend-induced birefringence and maintains the polarization of input signal.

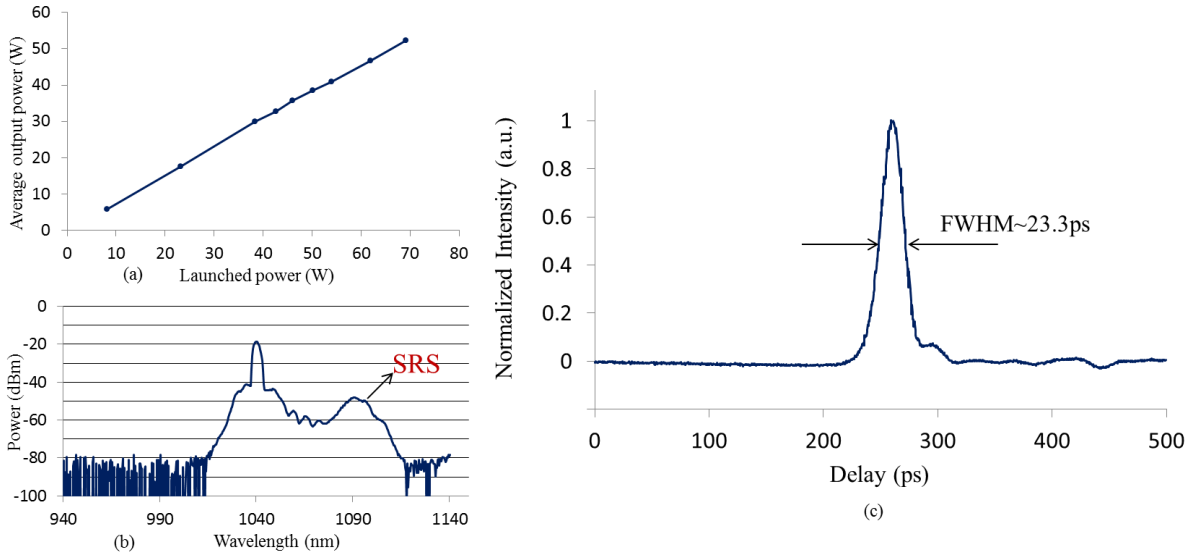

Figure 3.12 (a) average output signal power versus launched pump power of final amplifier (b) spectrum of output pulse at highest peak power and (c) measured temporal profile of output pulse at highest peak power.

(c) All fiberized device configuration

Fibers were provided to Prof. Tei at Tokai University, Japan for further experiments. Figure 3.13 (a) shows the experimental set-up used for nanosecond pulse generation. A single stage all fiberized amplifier was built consisting of a 4ns Q-switched Micro Chip Laser (MCL) at 100kHz as a seed source operating at 1064nm, multi-mode pump diodes at ~975nm, and a 2.3m long STF coiled at ~40cm bend diameter was used as an active fiber. An iris was used

at output end to remove the cladding light. Figure 3.13(b) shows the slope efficiency with respect to pump power in both situations with or without use of iris. A slope efficiency of ~63.5% and ~61.5% was achieved without and with iris respectively. Figure 3.13(c) shows the measured M^2 value at highest output power level, a value of 1.24 and 1.28 was achieved for the x and y-axis respectively. Figure 3.14 shows the splicing of STF with dissimilar fiber having different core and cladding diameters using conventional splicers, which shows the advantage of all-solid design of STF. Further work is being done by Prof. Tei to optimize the performance of amplifier.

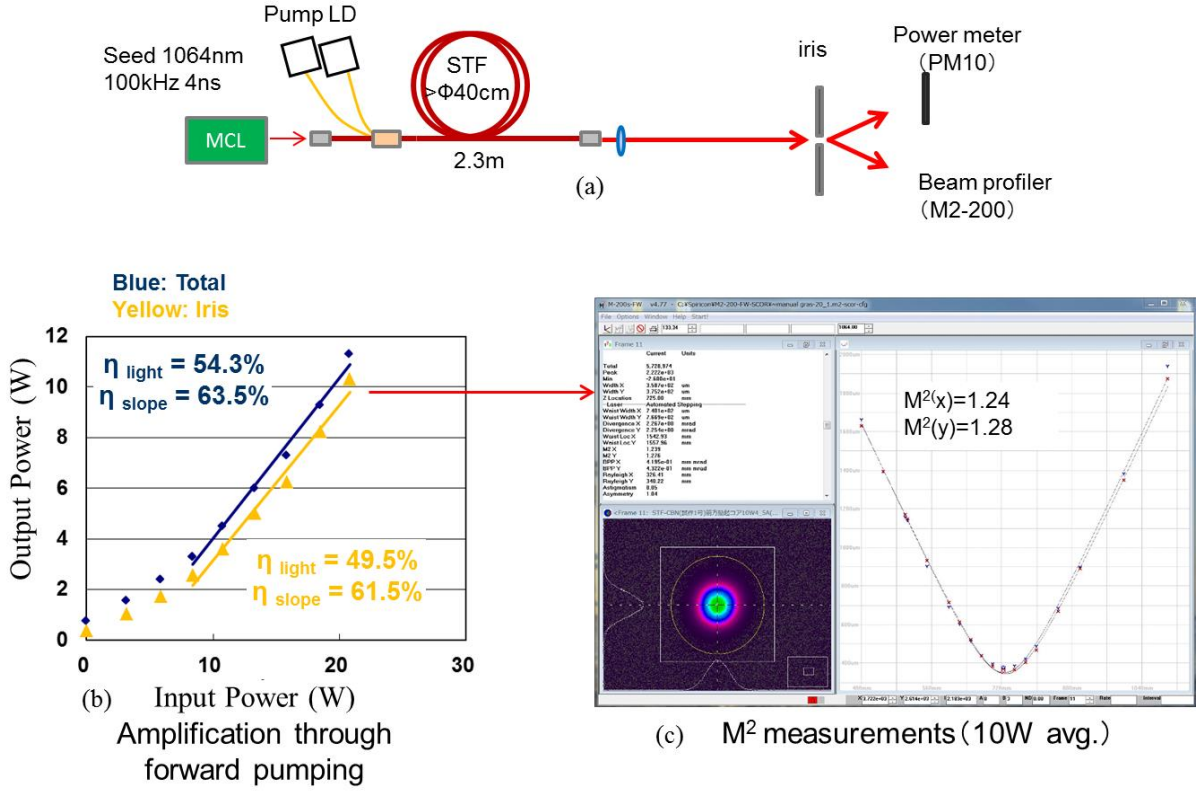

Figure 3.13 shows (a) experimental set-up (b) slope efficiency and (c) output Beam Quality. All of these measurements were done at Tokai University by Prof. Kazuyoku Tei and his team.

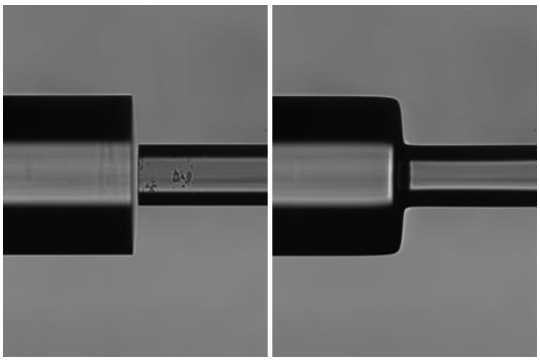

Figure 3.14 shows the splicing of STF (on right side) with dissimilar fiber using a conventional splicer demonstrating clear advantages of all solid design of doped fiber.

3.3 40µm core diameter STF

In order to further scale the mode area, an Yb doped preform was fabricated for 40µm core STF using MCVD process in conjunction with solution doping technique. As discussed in previous chapter, a 40µm core STF with ~0.038 NA for 20 different combinations (shown in red colour in table 2.2 in chapter 2) out of 24 combinations of trench thicknesses t={6-13µm} and resonant ring thicknesses d={6-8µm} can offer the loss of the fundamental mode lower than 0.1dB/m and power fraction in core is higher than 80% while the loss of the higher order modes is higher than 10dB/m or they have atleast 30% lower power fraction in core compared to fundamental mode or both are fulfilled simultaneously. In this 40µm core fiber, power fraction in core for different modes of fiber remains same even in case of low index layer in place of PML layer as of 30µm core fiber. The effective area of the fundamental mode varies from 850µm^2 to 1120µm^2 for these 20 combinations (including bend induced distortions at 20cm bend radius).

Table 3.5 shows the recipe used for fabrication of Yb and Al core doped preform for 40µm STF. The core of fiber is doped with Yb and Al and resonant ring is doped with Germanium as in previous preforms. In this preform same recipe was used as for the case of 30µm STF case as shown in table 3.3 and 3.4. However, the flow of $SiCl_4$ and $GeCl_4$ were changed to meet the demand of thickness of trench and resonant ring. The target was to achieve a STF having core diameter of ~ 40µm with 0.038NA, trench thickness (t) of ~9µm, and resonant ring thickness (d) of ~ 7µm. At these parameters, the loss of the fundamental mode is lower than 0.03dB/m and the loss of least lossy higher order modes is larger than 10dB/m. This will offer an effective area of the fundamental mode larger than 930µm^2.

Table 3.5 recipe for fabrication of Yb and Al doped preform for 40µm core diameter STF.

Pass No.	$SiCl_4(O_2)$	$GeCl_4(O_2)$	O_2	Rotation	S(t)	Temperature of burner	Comments
1	----	----	600	30	150	1800	Warming
2	----	----	600	30	150	1950	Polish
3	----	----	600	30	150	2000	Polish
4	----	----	640	30	150	2025	Polish
5	**200**	**70**	600	30	150	2025	Resonant ring
6	**160**	**10**	600	30	150	2025	Trench
7	----	----	600	30	150	2000	Polish
8	100(Vent)	----	500	30	100	**1575**	Temp_Check
9	100	----	400	30	100	1515	Soot deposition

Where unit of gas flow is cm^3/minute, T is the temperature of burner in degree Celsius, and s(t) represents speed of burner (unit is mm/min).

Figure 3.15(a) shows the refractive index profile of fabricated preform having a NA of ~0.038, the slight asymmetry in preform profile is a measurement artifact only. The refractive index profile of fiber is different from ideal SIF, however in further iterations of fabrication, the refractive index profile can be brought closer to ideal SIF. A flat refractive index profile was obtained for such a low NA using optimized process over 400mm length of preform. The process also ensures reproducibility of preform fabrication. The outer diameter of preform was 12mm, which was further etched down to 6mm using hydrofluoric acid. Etched preform was milled to have a D-shape and subsequently drawn into a fiber with cladding diameter of

~233µm. The fiber was coated with a low-index polymer which provided a nominal pump cladding NA of 0.48. Inset of figure 3.15(a) shows the microscope image of fiber cross-section. Core and resonant ring can be seen in microscope image of fiber. Figure 3.15(b) shows the white light absorption spectrum of ~1.55m long fiber and the absorption is 8dB/m at 976nm.

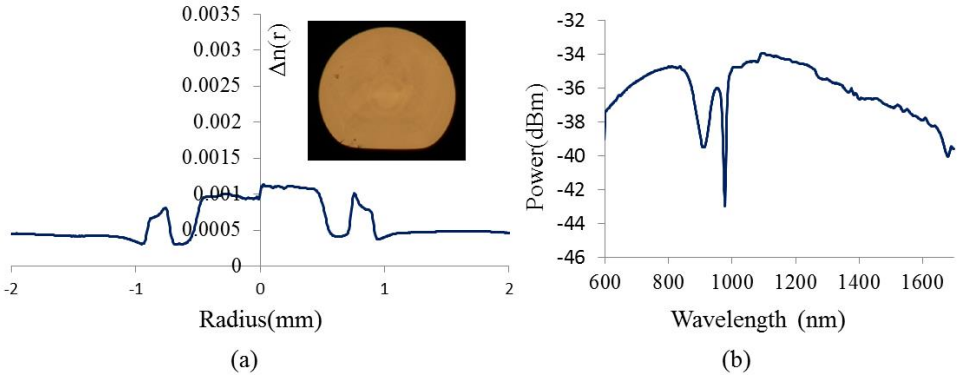

Figure 3.15 (a) refractive index profile of Yb and co-dopants doped preform. Inset shows the microscope image of fiber end (b) white light absorption spectrum of a 1.55m long fiber.

3.3.1 Experimental characterization of 40µm STF

Figure 3.16(a) shows the experiment set-up used for verification of single mode behaviour of the fiber. Here the output of STF was observed for different input launching conditions. The aim of different launching conditions is to increase the probability of the excitation of higher order modes. A ~1m long fabricated STF was used as fiber under test. The low-index polymer coating was stripped off at both ends and index matching oil was also applied at both ends to remove cladding modes.

In order to facilitate the higher order modes' excitation conditions by exploiting different modal field diameters (MFDs) and NAs of input beam and fiber under test, a single mode input at 1060nm wavelength was launched into fiber under test using a single mode fiber spliced to beam delivery fiber of laser source. Figure 3.16(b) shows the obtained output beam under two conditions of fiber under test namely loosely coiled and bent at 20cm bend radius condition, which ensures a Gaussian output beam.

In order to further enhance the multimode excitation, offset launching of input beam was used. Figure 3.16(c-d) shows the measured power of output beam with respect to misalignment of launching beam along x-axis and output beam profiles for various offset launchings of input beam respectively. The power level of output beam with respect to misalignment of launching beam along x-axis follows a nearly Gaussian curve, on the other hand the output beams ensure a Gaussian beam output irrespective of launching conditions. It is interesting to observe from figure 3.16(d) that, only the intensity of the output beam changes but it remains Gaussian, which ensures high loss for the higher order modes.

In order to further validate the single mode behaviour of fiber, a multimode input beam launch was ensured as shown in figure 3.17(a) by splicing the multimode optical fiber to the delivery fiber of 1060nm laser source, as shown in figure 3.17(a). Again a Gaussian beam output was observed as shown in figure 3.17(b), which ensures fairly robust single mode behaviour of the fiber. Few higher order modes such as LP_{11} and LP_{21} were generated using binary phase plate as shown in figure 3.17(c-d). Figure 3.17(e-f) shows the output profile with respect to pure LP_{11} input beam. The output profile ensures high suppression for LP_{11} mode as only residual light can be seen. Similarly, for LP_{21} launching there is no output as shown in figure 3.17(g).

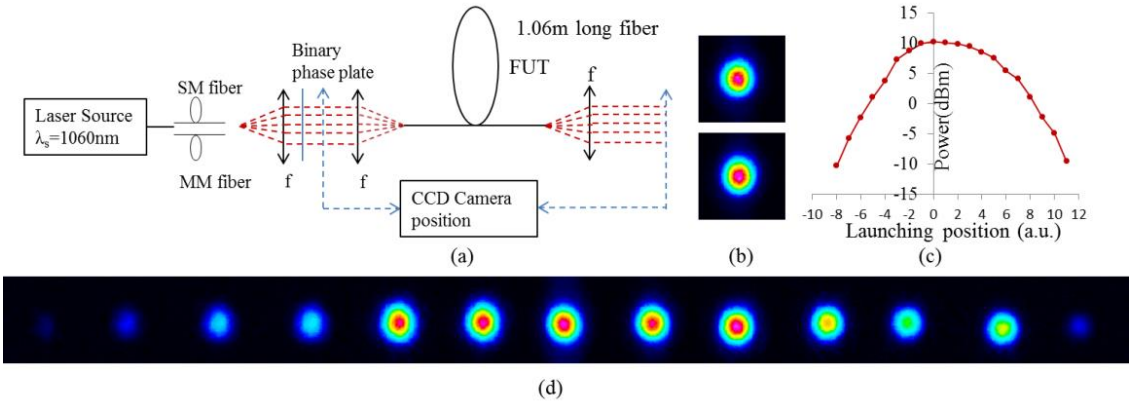

Figure 3.16 shows (a) experiment set-up used for single-mode characterization of STF (b) output with respect to optimum launching of single mode in loosely coiled and bent at 20cm conditions (c) output power with respect to offset launching of single mode input (d) output beam profile with respect to offset launching of single mode input.

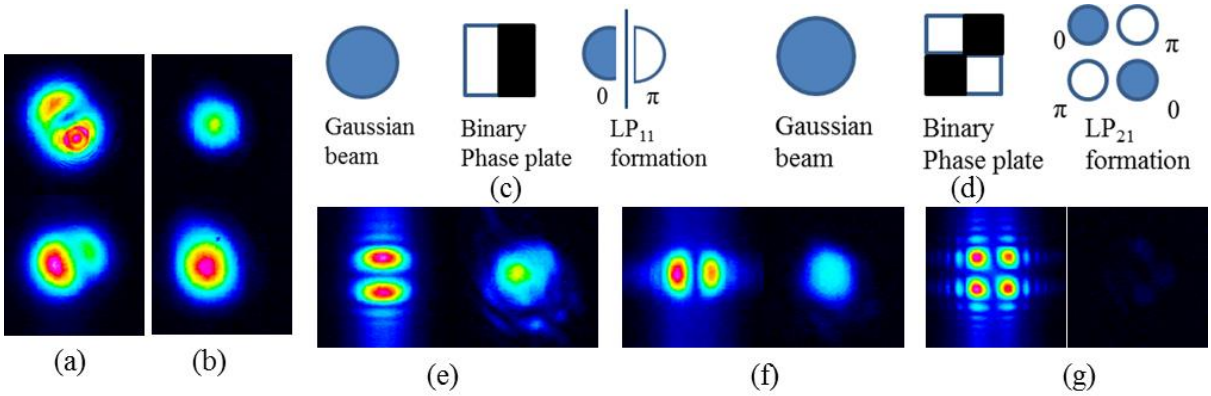

Figure 3.17 (a) profile of input multimode beam (b) output beam with respect to input beam (c) and (d) binary phase plate to generate pure LP_{11} and LP_{21} mode (c) and (f) shows the output profile with respect to pure LP_{11} mode (g) shows the output profile with respect to pure LP_{21} mode.

The bend loss of LP_{11} mode was measured using ~57cm long fiber. Only 57cm long fiber was used to estimate the LP_{11} loss, as the loss of LP_{11} is high and 1m long fiber does not show any output with respect to LP_{11} launching. Figure 3.18(a) shows the experiment set-up used for bend loss measurement. Again a binary phase plate was used for LP_{11} mode launching. The output power from 57cm long fiber was measured in unbent and different bend positions as shown in figure 3.18(a), during this movement the input end of fiber was fixed. Figure 3.18(b) shows the output power and output beam profiles of fiber placed along

different bend diameters shown in figure 3.18(a). Figure 3.18(b) also shows the profile of output beam in straight condition, which looks like LP_{11} mode. However, with changing bend diameter of fiber the output beam profile changes rapidly and at 40cm bend diameter only residual cladding modes were observed. Moreover, output power also decreases rapidly with decreasing bend diameter. The output suffers a decrement of 10.9dB power from unbent to bent case at 40cm bend diameter; on other hand for similar study of LP_{01} mode no considerable change in output power level was observed. The above mentioned results of qualitative experimental characterizations ensure a robust ESM operation of 40µm core diameter STF. It would be pertinent to note that merely 1m long length of fiber was used to verify single mode operation. Moreover, fiber has low index outer coating. In the light of these facts, it can be concluded fiber offers high suppression to the higher order modes and offers robust single-mode guidance for high power fiber laser application.

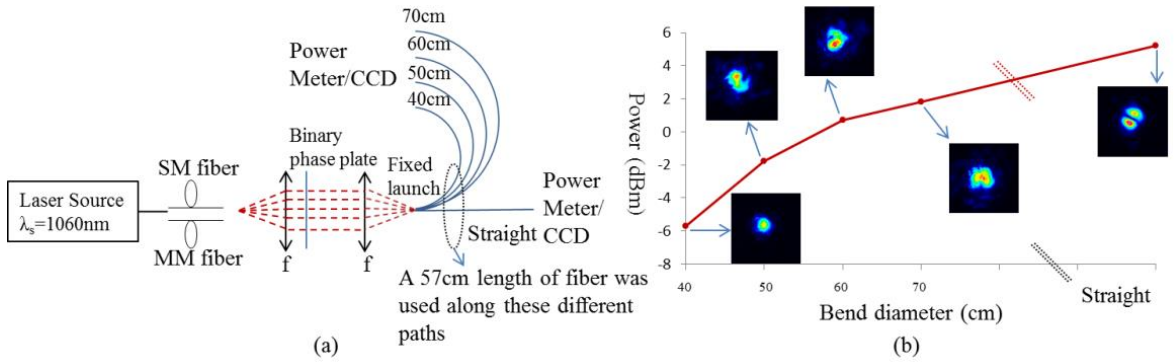

Figure 3.18 (a) experimental set-up used for calculating LP_{11} bend loss (b) output power of 57cm long fiber with respect to LP_{11} mode launch.

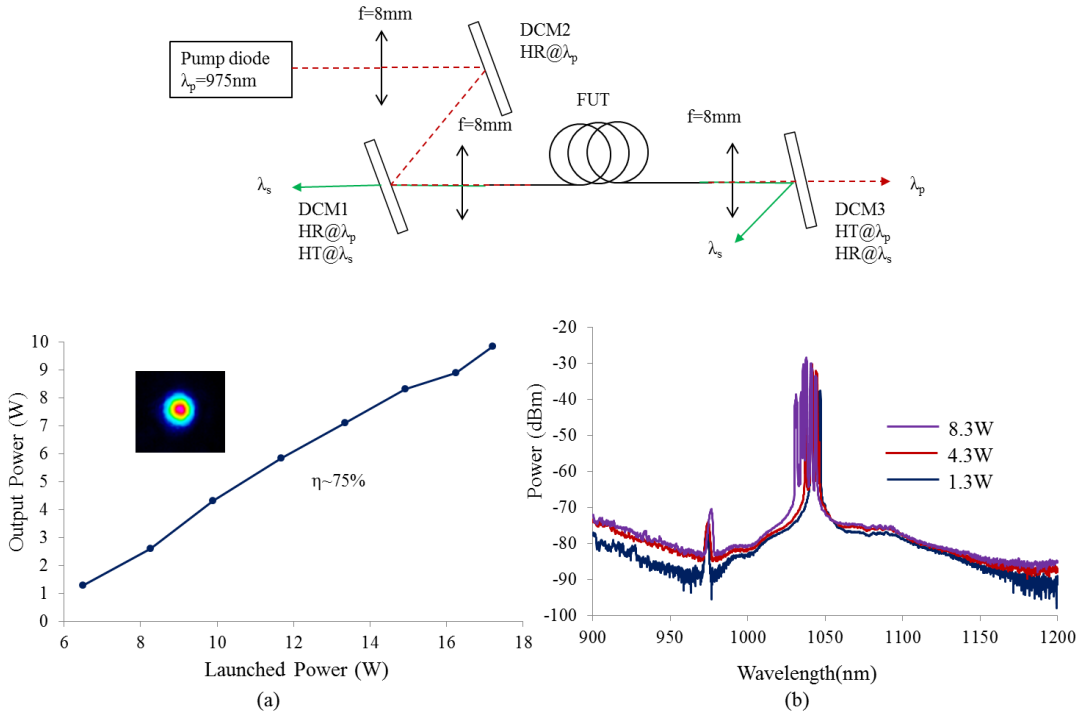

Figure 3.19 (a) experimental set-up used for fiber laser efficiency (b) slope efficiency of 3.3m long fiber. Inset shows the profile of output beam (c) measured spectrum of output beam at different power levels.

The fiber laser efficiency was measured in a 4%-4% fiber laser cavity using a 3.3m long STF. Figure 3.19(a) shows the experimental set-up used for the laser efficiency measurement. A fiber coupled laser diode operating at a wavelength of 976 nm was used as the pump source. The pump beam was launched in to the fiber through an aspheric lens (focal length=8mm). Both ends of the fiber were cleaved perpendicularly to provide a Fresnel reflection for the laser cavity. In order to separate the signal and pump wavelengths, a dichroic mirror with high reflection at pump wavelength and high transmission at signal wavelength was used at the pump launch end. At the pump exit end of the FUT, output beam was collimated and focused using aspheric lens (focal length=8mm) and a dichroic mirror with high transmission at pump wavelength and high reflection at signal wavelength was used to separate signal and pump wavelengths. Figure 3.19(b) shows the measured slope efficiency with respect to launched power, a ~75% slope efficiency was obtained. Inset show the obtained profile of output beam and a M^2 of ~1.15 was obtained for output beam. Figure 3.19(c) shows the measured spectrum of output beam at different power level, showing laser output at ~1040nm.

3.4 Ultra-low NA SIF

In this chapter, using MCVD process in conjunction with solution doping process, core NA of ~0.038 has been achieved. As discussed in previous chapter with such a low NA a 35µm core diameter SIF fiber can achieve ESM operation. An ESM operation can be achieved by ensuring the loss of the fundamental mode to be lower than 0.1dB/m, while the losses of the higher order modes are larger than 10dB/m at ~32cm bend diameter. The effective area of the fundamental mode is ~700µm^2. Table 3.6 shows the recipe used for fabrication of ultra-low NA SIF. There is very little change as compared to table 3.5. Here, there is no resonant ring; on the other hand little flow of $GeCl_4$ was allowed to match the refractive index of cladding with F300. Figure 3.20 shows the refractive index profile of the fabricated preform at different distance along the length of the preform namely at 100mm, 200mm, and 300mm of a 350mm long preform. Figure 3.20 also shows the preform profile at two different angular positions i.e. 0 and 90 degrees represented by blue and red colors respectively. The measured preform profiles ensure good uniformity along the length of the preform. Moreover, refractive index profile maintains a flat profile along the cross-section, while maintaining a very low refractive index with respect to cladding. It is important to note that, ~350mm long usable preform from a 400mm long starting F300 tube ensures a good yield of this optimized process. The preform outer diameter is 12mm, while the diameter of the deposited core is 1mm.

Table 3.6 recipe for fabrication of Yb and Al doped preform for Ultra-low NA SIF.

Pass No.	$SiCl_4(O_2)$	$GeCl_4(O_2)$	O_2	Rotation	S(t)	Temperature of burner	Comments
1	----	----	600	30	150	1800	Warming
2	----	----	600	30	150	1950	Polish
3	----	----	600	30	150	2000	Polish
4	----	----	640	30	150	2025	Polish
5	**160**	**18**	600	30	150	2025	Cladding 1
6	**160**	**18**	600	30	150	2025	Cladding 2
7	----	----	600	30	150	2000	Polish
8	100(Vent)	----	500	30	100	**1575**	Temp_Check
9	100	----	400	30	100	1515	Soot

Where unit of gas flow is cm^3/minute, T is the temperature of burner in degree Celsius, and s(t) represents speed of burner (unit is mm/min).

The observed peaks at the center of the profiles are merely the measurement artifact. The surrounding regions of the core suffer from slight index perturbations caused by the deposited cladding layers. Outside this, the starting F300 tube constitutes the cladding. Typically refractive index of F300 tube is slightly larger than deposited pure silica (e.g. ~0.00035 to 0.0005). In order to match the refractive indices of the deposited cladding and F300, a small quantity of Ge dopant is necessary. These index perturbations can be eliminated by avoiding cladding deposition altogether, so that F300 tube acts as a cladding region. Numerical simulations were performed to study the impact of the small index perturbations and observed slight reduction of losses for both fundamental mode and higher order mode. For example, at 32cm bend diameter the loss of the fundamental mode is estimated to be ~0.07dB/m whereas for the LP_{11} mode it is ~9.23dB/m. These reductions are small compared to the ideal SIF and can be ignored.

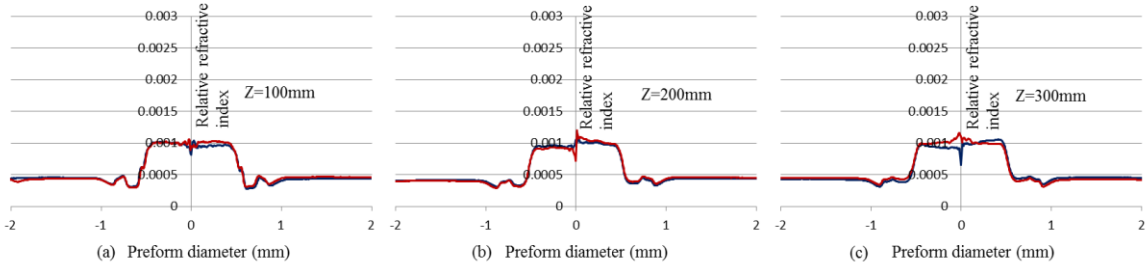

Figure 3.20 refractive index profiles at different positions along the length of the preform. Blue and Red colour corresponds to profiles at 0 degree and 90 degree angular positions respectively.

The preform was first milled to a D-shape to facilitate the cladding pumping by breaking the circular symmetry and subsequently drawn in to a fiber with an outer diameter of 420µm so as to have a 35µm core diameter. Fiber was coated with a low index polymer to allow pump light to be guided in the cladding. Figure 3.21(a) shows the CCD image of the cladding geometry of the fiber by launching a 1060nm laser into the cladding. The output profile shows cladding modes and a D-shape outer cladding. Figure 3.21(b) shows the white light transmission spectra for both unbent and bent conditions of a 1.26m long fiber. The absorption at ~975nm is 2dB/m for both straight and bent fibers.

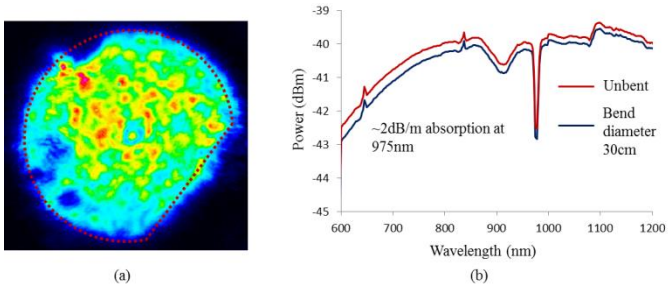

Figure 3.21 (a) output image of the fiber at 1064nm captured with a CCD camera (b) white light transmission spectra of 1.26m long fiber in bend and unbent configurations.

3.4.1 Experimental characterization of ultra-low NA SIF

In order to verify the ESM behaviour, the output beam profile was investigated for different lengths and bend diameters of the fiber. Figure 3.22(a) shows the experimental set-up used for the investigations. A 1060nm laser beam is coupled into the core using two lenses namely collimating and focusing lens. A binary phase plate was used to change the mode profile of the input beam, while a CCD camera is used to analyse the output beam profile. The low-index coating was removed at both ends of the fiber under test and index-matching oil was applied to strip-off the cladding modes. First a 1.55m long fiber was used in a straight condition with a slight bend as shown in the experimental set-up. A slight bend was required as there was not enough space on optical table. Figure 3.22(c) shows the output beam profile with respect to LP_{01} mode of launch beam. Here LP_{01} mode was the direct output from a single-mode laser source delivered by a conventional single mode fiber as shown in figure 3.22(a). Output beam profile (as shown in figure 3.22(c)) is clearly non-Gaussian and shows significant presence of the higher order modes. Moreover, fiber output as shown in figure 3.22(d) clearly shows the LP_{11} mode when a mixed mode (LP_{01} +LP_{11}) as shown in figure 3.22(b) was launched using binary phase plate. This ensures poor suppression of the higher order modes and this is in good agreement with simulation study presented in chapter 2, which also indicated a multi-mode behaviour under unbent condition.

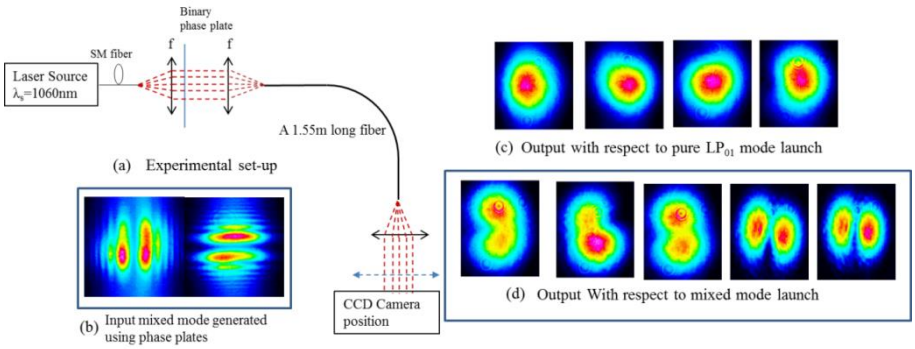

Figure 3.22 (a) experimental set-up for modal verification of the fiber, (b) input mixed modes (LP_{01} and LP_{11}) using phase plate, (c) output beam profiles for LP_{01} mode launch, and (d) output beam profiles for a mixed mode launch.

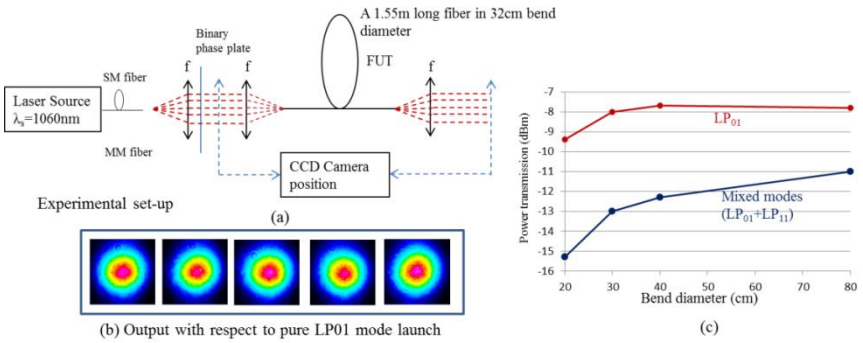

Figure 3.23 (a) experimental set-up for single mode verification, (b) profile of the output beam with respect to LP_{01} mode launch, and (c) profile of output beam with respect to mixed mode launch. A 3m long fiber coiled at ~32cm (+/- 0.5cm) bend diameter was used in this experiment.

Afterwards, fiber was bent to a diameter of ~32cm (+/- 0.5cm) as shown in figure 3.23(a) keeping rest of the experimental conditions same. A dramatic improvement was observed in the output beam profile. The output beam appears to be a near Gaussian profile as shown in figure 3.23(b) due to the bend induced loss of the higher order modes. The output power levels was observed, when LP_{01} and mixed modes were independently launched into the fiber for different bend diameters as shown in figure 3.23(c). This is a clear evident of a significant discrimination between LP_{01} and LP_{11} modes under bending. In order to improve the quality of the output beam profile, the length of the fiber was increased under test to ~3m to increase the aggregate loss for all the higher order modes. The profile of the output beam becomes almost Gaussian for the same bend diameter of ~32cm (+/- 0.5cm). The profile of output beam of fiber was observed with respect to multimode beam (dominating LP_{11} content as shown in the left hand column of figure 3.24(c)) into the fiber. The output beam maintains Gaussian profile as shown by the right hand columns in figure 3.24(c). These measurements verify that an ESM operation can be obtained from a low NA (~0.038) SIF by choosing an appropriate bend diameter.

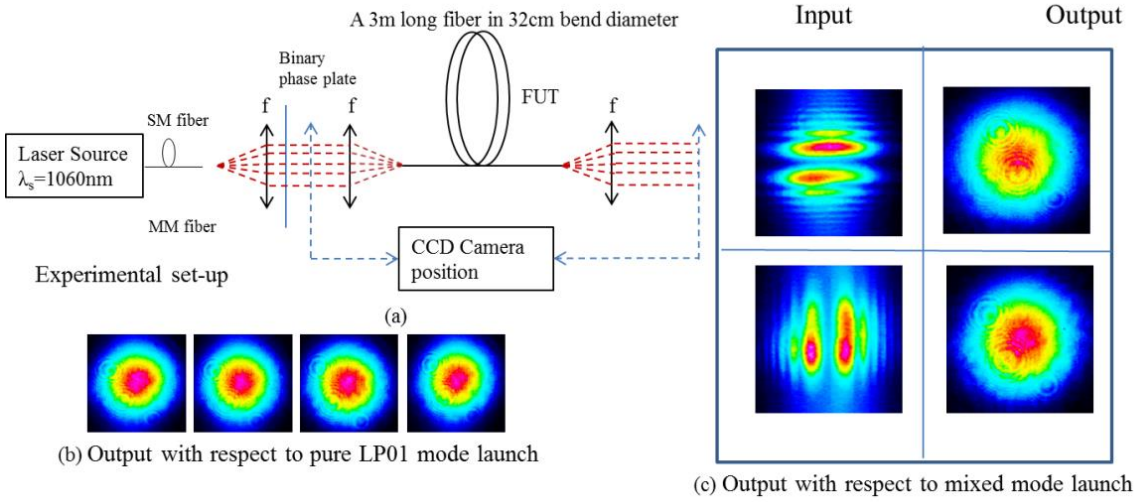

Figure 3.24 (a) experimental set-up for single mode verification, (b) profile of the output beam with respect to LP_{01} mode launch, and (c) profile of output beam with respect to mixed mode launch. A 3m long fiber coiled at ~32cm (+/- 0.5cm) bend diameter was used in this experiment.

The fiber laser efficiency was measured in a 4%-4% laser cavity using a 7m long fiber as shown in figure 3.25(a). A multimode diode laser operating at ~975nm was used as a pump source. Fiber under test was kept with a bend diameter of ~32cm (+/- 0.5cm). Figure 3.25(b) shows the measured slope efficiency with respect to absorbed pump power. A maximum output power of 50W was obtained at a launched pump power of ~72W that corresponds to a slope efficiency of ~81% with respect to absorbed pump power. Further power scaling was limited by the available pump power. Inset shows the output beam profile with a measured M^2 of ~1.07 in the x-direction and 1.09 in the y-direction. The spectral profile of the free running laser is shown in figure 3.25(c) with the multiple peaks located at ~1040nm.

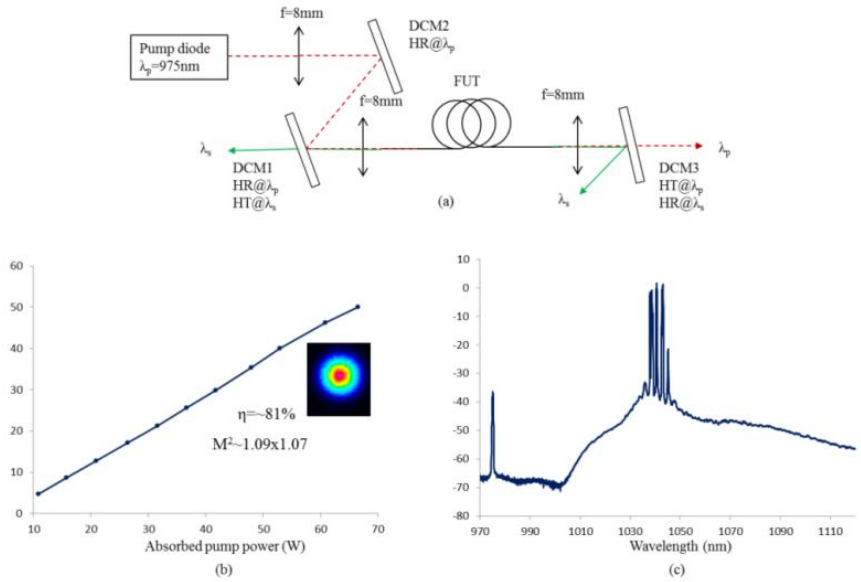

Figure 3.25 (a) experimental set-up used for laser efficiency measurement, (b) output power as a function of pump power of 4%-4% laser cavity. Inset shows the output beam profile, and (c) output spectrum taken with an OSA (ANDO (AQ6370B)) resolution of 0.2nm.

3.5 STF for eye safe wavelength

As discussed in previous chapter, significant mode area scaling can be achieved at 1550nm and 2000nm using STF. Figure 3.26 shows the refractive index profile of an Er and Al doped preform for STF, fabricated by modified chemical vapour deposition process in conjunction with solution doping process. In this fabrication process, same recipe as shown in table 3.5 was used, however during solution doping an aqueous solution of methanol having Er, La, and Al was used in place of Yb and Al. The total mass of Er and La was same as of Yb to achieve same NA of ~0.038. However, very little Er (1/3rd of toal rare earth) was used in solution to avoid quenching. The obtained preform has 1mm core diameter and 12mm outer diameter. Preform was milled to D-shape to increase the cladding pump absorption. Further, fiber was drawn to ~600µm outer diameter with low index polymer coating. This fiber has ~50µm core diameter, ~11µm trench thickness, and ~8µm resonant ring thickness.

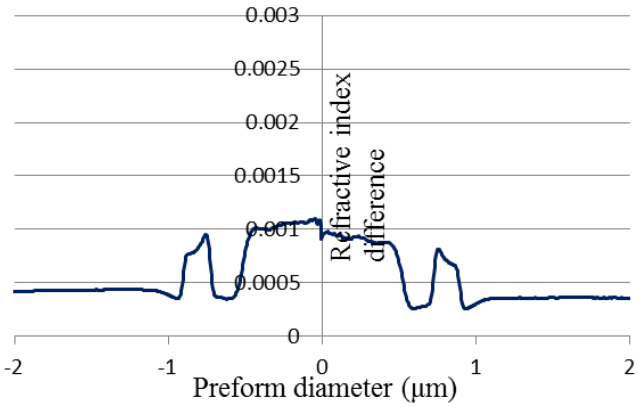

Figure 3.26 refractive index profile of Er and Al doped preform fabricated by MCVD process in conjunction with solution doping process.

3.5.1 Experimental characterization of ultra-low NA STF

In order to verify the ESM behaviour, the output beam profile was investigated for different input beams. Figure 3.27(a) shows the experimental set-up used for the investigations. A 1550nm laser beam is coupled into the core using two lenses namely collimating and focusing lens. A binary phase plate was used to change the mode profile of the input beam, while a CCD camera is used to analyse the output beam profile. The low-index coating was removed at both ends of the fiber under test and high index oil was applied at both ends to remove the cladding modes. Figure 3.27(b) shows the output of fiber with respect to offset launching. Similar to STF for 1µm, fiber ensures ESM operation. Output of fiber was also analysed with respect different higher order modes such as LP_{11}, LP_{21} etc as shown in figure 3.27(c). No output was observed with respect to these higher order modes as shown in figure 3.27(d).

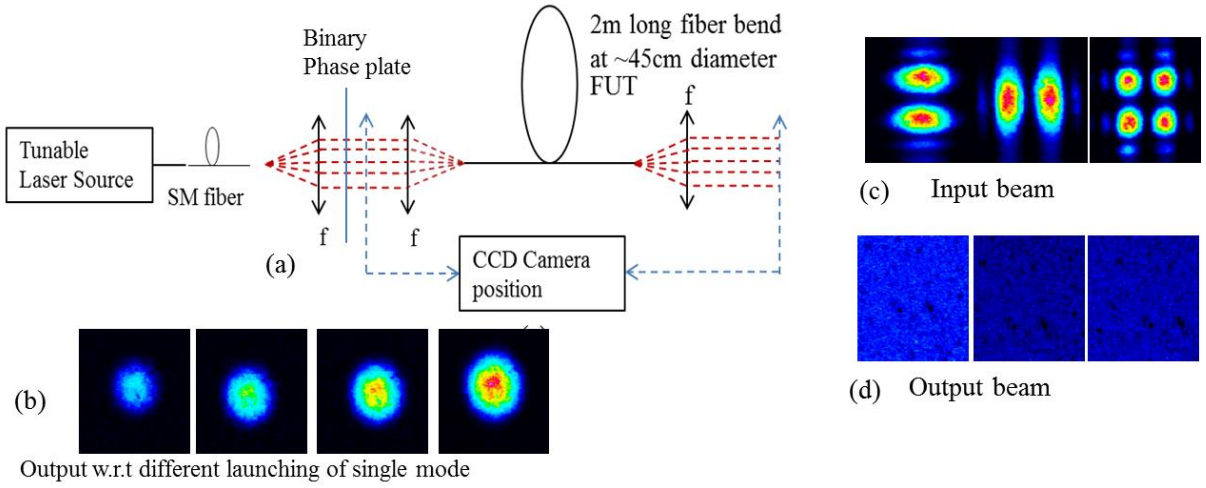

Figure 3.27 (a) experiment set-up used for single-mode characterization of STF, (b) output with respect to different offset launching of single mode, (c) different higher order modes launched into fiber, and (d) profiles of output beam profiles of fiber with respect to higher order modes.

Due to very low concentration of Er in this fiber, absorption at 980nm is very low. The initial hypothesis of using low Er in solution to avoid quenching was over implemented, while making this hypothesis the important fact of using high soot deposition temperature was ignored. As the use of high soot deposition temperature already reduced the incorporation of Er. The low incorporation of Er resulted in low absorption. Therefore, no fiber laser was built using this fiber. However in next iterations, only Er can be used in solution by avoiding La. So, the concentration of Er can be increased by 3 times without increasing the refractive index of core. Moreover, etching of preform can be done to increase core to cladding area ratio, which can increases the pump absorption. These steps can lead to high absorption and should be sufficient for a laser device. However, this can be intended as a future work.

3.6 Conclusion and Outlook

Two fiber designs STF and low NA SIF have been successfully fabricated for mode area scaling thanks to the optimized MCVD in conjunction with solution doping process. Fabrication process has been optimized to achieve ~0.038 NA for Yb and Al doped fiber. This ultra-low NA ~0.038 has brought SIF in close competitive to other LMA fibers without any compromise with quality. Further novel LMA fiber known as STF, which was proposed in previous chapter, has also been realized successfully. STF offers great potential of mode area scaling thanks to the ultra-low NA and resonance coupling feature of resonant ring present around the core. Fabrication reported in this chapter ensures the suitability of these designs for mass scale production. Further laser tests have been conducted using these fibers, which ensure high laser efficiency and good output beam quality. The majority of obtained results were published in conferences and peer-reviewed journals [8-15].

In future, fabrication process can be further optimized to reach to the ideal profiles as close as possible. Moreover, mode area can be scaled further by increasing core diameter to 50μm. In order to address photo-darkening, Ce doping can also be used to develop resistance for photo-darkening.

3.7 References

1. http://heraeus-quarzglas.com/en/home/Home.aspx
2. J. W. Nicholson, A. D. Yablon, J. M. Fini, M. D. Mermelstein, "Measuring the Modal Content of Large-Mode-Area Fibers," IEEE J. Sel. Top. Quantum Electron., vol. 15, no. 1, pp. 61-70, Feb. 2009.
3. V. Matejec, I. Kasik, D. Berkova, M. Hayer, M. Chomat, Z. Berka, and A. Langrova, "Properties of optical fiber performs prepared by inner coating of substrate tubes," Ceramics Silikaty **45** (2), 62-69 (2001).
4. Y. H. Kim, U. C. Paek, and W. T. Han, "Effect of soaking temperature on concentrations of rare-earth ions in optical fiber core in solution doping process," Rare-earth doped Materials and Devices, V. Shibin Jiang, eds., Proc. SPIE **4282**, 123 (2001).
5. A. Dhar, M. C. Paul, M. Pal, A. K. Mondal, S. Sen, H. S. Maiti, and R. Sen, "Characterization of Porous core layer for controlling rare earth incorporation in optical fiber," Opt. Exp. **14** (20), 9006-9015 (2006).
6. C. Schulze, A. Lorenz, D. Flamm, A. Hartung, S. Schröter, H. Bartelt, and M. Duparré, "Mode resolved bend loss in few-mode optical fibers," Opt. Express **21**(3), 3170–3181 (2013).
7. L. Huang, S. Guo, J. Leng, H. Lü, P. Zhou, and X. Cheng, "Real-time mode decomposition for few-mode fiber based on numerical method," Opt. Express **23**(4), 4620–4629 (2015).
8. D. Jain, C. Baskiotis, J. Kim, and J. K. Sahu, "First demonstration of single-trench fiber laser," CLEO, San Jose, USA, (Invited), SF1N.1, June 2014.
9. D. Jain, C. Baskiotis, T. C. May-Smith, J. Kim, and J. K. Sahu, "Large mode area multi-trench fiber with delocalization of higher order modes," IEEE Journal of Selected Topics in Quantum Electronics, Special issue on high power fiber lasers (INVITED), 20, 0902909 (2014).
10. D. Jain, Y. Jung, M. N. Velazquez, and J. K. Sahu, "Extending single mode performance of all-solid large-mode-area single trench fiber," Optics Express, 22, 31078 (2014).
11. D. Jain, Y. Jung, P. Barua, S. Alam, and J. K. Sahu, "Scaling the mode area of Rare-Earth doped step index fiber under current state of the art MCVD technology," CLEO-2015, San Jose, USA, SM2L.2, May 2015.
12. D. Jain, Y. Jung, P. Barua, S. Alam, and J. K. Sahu, "Demonstration of ultra-low step index fiber for high power fiber laser applications," 23, 7407, Optics Express, (2015).
13. D. Jain, P. Gorman, C. Codemard, Y. Jung, M. N. Zervas, and J. K. Sahu, "Picosecond Yb-doped single-trench-fiber amplifier with diffraction-limited output," Photonic West, San Francisco, USA, 9344-27, Feb. 2015.
14. D. Jain, C. Codemard, Y. Jung, S. Alam, M. N. Zervas, and J. K. Sahu, "High power, compact, picosecond MOPA based on single trench fiber with single polarized diffraction-limited output," Under preparation.
15. D. Jain and J. K. Sahu, "Performance of single-mode large-mode-area single-trench fiber for eye-safe wavelength," Under preparation.

Chapter 4 Multi-trench fibers

4.1 Multi trench fibers

This chapter discuss a novel fiber design, known as multi-trench fiber (MTF). In previous chapter, it was shown that STF can offer an effective area of around ~1,000μm^2 in 1μm wavelength region for ESM operation in a bend configuration that will offer a compact device. This area is suitable for few kW fiber laser in continuous wave regime and few hundreds of kW peak pulses but not suitable for ultra-high peak power pulses. These pulses require few thousands of effective area for the fundamental mode to overcome the non-linear effects in fiber. Due to bend induced detrimental effects the effective area of the fundamental mode cannot be scaled further sufficiently. One solution to avoid bend-induced reduction of effective area is to use fiber in rod-type configuration, where fiber is kept straight. Recently, rod-type large pitch fiber (LPF) and distributed modal filtering fiber (DMF) which are modified forms of PCF, have been successfully exploited for ultra-fast laser applications [1-2]. However, both of these designs involve complex fabrication steps due to their non-cylindrical design. Moreover, presence of air-holes causes considerable difficulties in post processing of fibers including cleaving and splicing. There is another approach of using higher order modes which can offer few thousands of effective area of the fundamental mode as discussed in chapter 1 [3]. Due to their natural-bend immunity they do not suffer from bend-induced mode distortions [3]. However, fiber lasers with high average output power have not been demonstrated using this approach.

MTF can offer effective area around 12,000μm^2 of the fundamental mode around 1μm wavelength in rod-type configuration. MTF also offer several other advantages such as easy fabrication suitable for mass scale production and all-solid cylindrical structure. Moreover, MTF of smaller core diameter (such as ~30μm core diameter) can also offer effective single mode operation over a wide range of bend radii, unlike STF and other LMA fiber which need a narrow range of bend radii to be effectively single moded. This property makes them suitable for beam delivery application. In latter part of this chapter, few approaches have been discussed to tailor dispersion and distributed spectral filtering in MTF.

4.1.1 Multi-trench fiber for rod-type applications

An optical fiber structure with a large core surrounded by a periodic cladding constituted of alternating low- and high-refractive index rings (as shown in figure 4.1) is being proposed here. The high-index rings and the outer infinite cladding present the same refractive index as the core. Consequently, the structure is formed by the inclusion of the low-index rings (trenches) only and given a name: Multi-Trench Fiber (MTF). Figure 4.1(b) presents the notations used here: r_c is the core radius, t is the thickness of the low-index rings, d is the thickness of high-index ring, n_c is the refractive index of the core, and Δn is the refractive index difference between the core and the low-index rings.

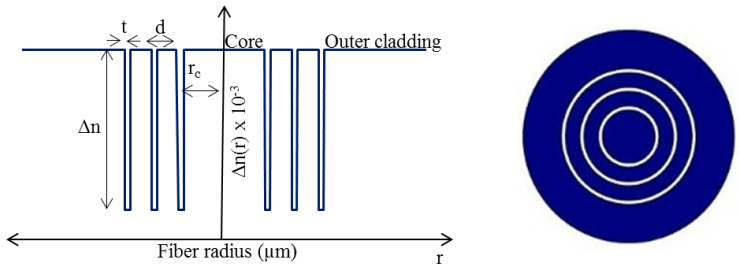

(a) (b)

Figure 4.1(a) refractive index profile of the proposed optical fiber, where r_c is the radius of the core, d is the thickness of the high-index rings (resonant rings), t is the thickness of the low-index rings (trenches), and Δn is the refractive-index difference between the resonant rings and the trenches (b) schematic cross-section of the proposed fiber structure. Blue and white colours represent high and low-refractive index regions respectively.

4.1.2 Prior art

It is important to discuss the relevant optical fiber designs proposed before MTF. Figure 4.2(a) and (b) shows two refractive index profiles reported by Kumar et. al. and Devautour et. al respectively [1-2]. It is evident that both of these designs are different from MTF. Moreover, both of these theoretical studies were restricted to 30μm core diameter fiber in unbent case only without a clear possibility of ESM.

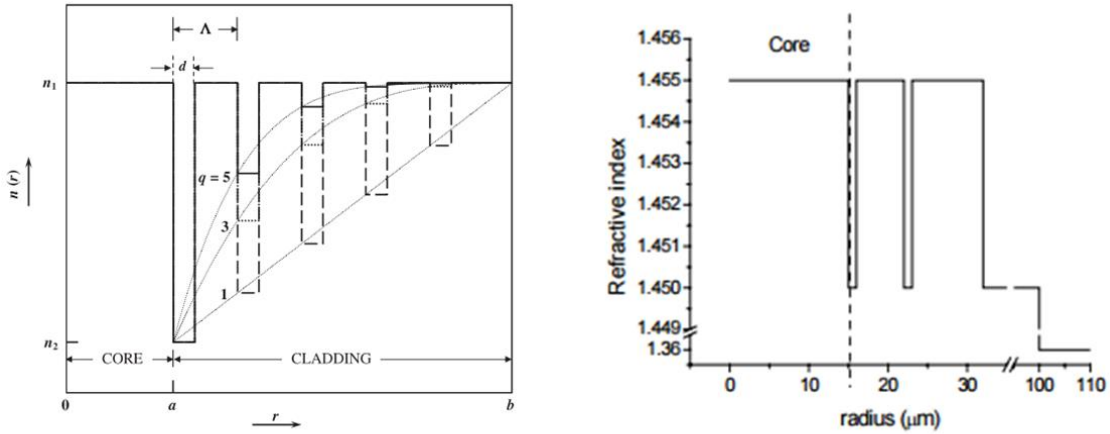

(a) (b)

Figure 4.2 refractive index profiles of the two different proposed optical fibers (a) and (b) proposed by Kumar et. al. and Devautour et. al. respectively. (Figure source: [1]; © 2008 OSA and [2]; © 2009 OSA).

4.1.3 Working principle

In a MTF, all core modes are leaky in nature, due to the fact that the refractive index of the core is equal to those of the outer cladding. For the analysis of the working principle of MTF, initially a fiber with single trench formed by the three first layers of the multi-trench fiber (as shown in figure 4.3(a)) was studied with structural parameters r_c=50μm, t=1.4μm, d=31μm, and Δn=0.001 at λ=1.06μm. In this case, the core modes present very high leakage loss as shown in figure 4.3(a). Moreover, the leakage loss ratio between the first higher order mode (LP_{11}) and the fundamental mode (LP_{01}) is small (<4 at 1.06μm).

The inclusion of additional trenches has two main effects (as shown in figure 4.3(b)). First of all, the leakage loss of the fundamental core mode is significantly decreased. This is due to the reduction of the tunneling of its power towards the infinite outer cladding. Secondly, the ratio between the loss of the first higher order mode and the fundamental mode is increased (>100 at 1.06µm) thanks to the resonant coupling between the first higher-order core mode of the core and the modes of the rings having same refractive index as the core (as shown in figure 4.3(c-d)). It is interesting to note that, for the specific case of figure 4.3(b) (three-trench fiber); three mode groups having the symmetry of a LP_{11} mode in the core coexist with a non-negligible amount of energy in the core and with a different level of leakage loss (cf. figure 4.3(b-c)). This is due to the coupling between the LP_{11} core mode of the single-trench fiber and the LP_{11} modes of each of the two rings of same refractive index as the core (resonant rings). This is also applicable for other higher order modes. In order to ensure an ESM operation, all the higher order modes were considered.

The intuitive mechanism of guidance of MTF can be seen as being guidance of the fundamental mode and non-guidance of the higher order modes by anti-resonance and resonance respectively. If the core mode finds no states in the cladding with which it is phase-matched, light cannot leak out but if sees a phase-matched cladding state, it can leak out. Here the thickness of the resonant ring can be optimized in such a way that the modes of ring are in resonance with the higher order modes of core, so that they suffer from leakage loss.

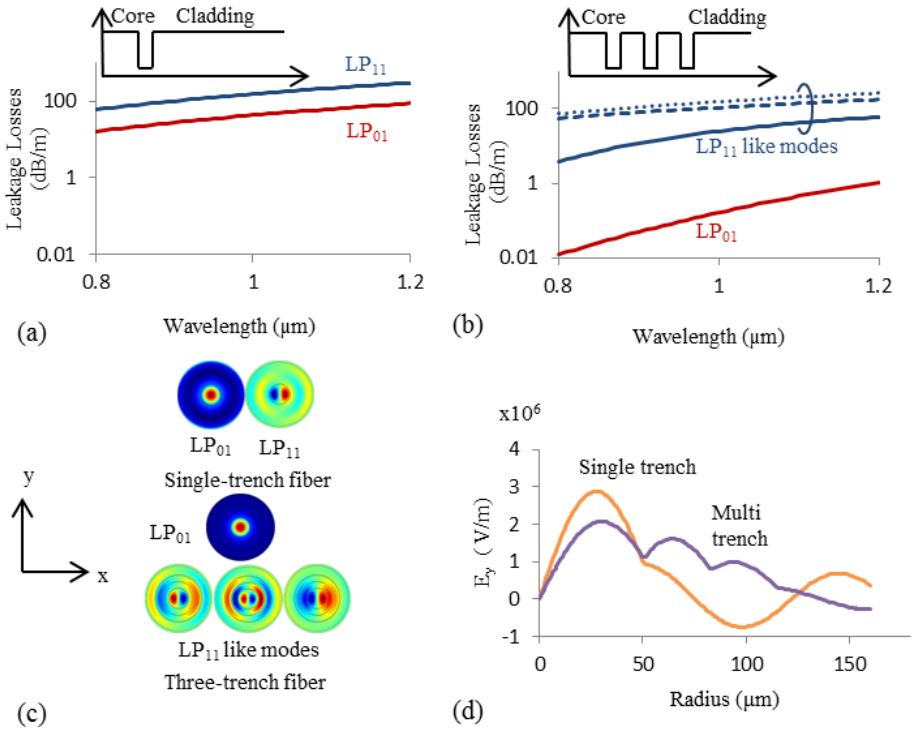

Figure 4.3 leakage loss spectrum of the fundamental core mode and the first higher order mode of: (a) a single trench fiber and (b) a fiber with three trenches (c) 2D profile of the transverse electric field component of the fundamental and the first higher order mode(s) of the single and three trench fiber (d) transverse electric field component along the x-axis of the first higher mode of both the fibers. The structural parameters are r_c=50µm, t=1.4µm, d=31µm, and Δn=0.001 at λ=1.06µm.

4.1.4 Comparison with Bragg fiber

Bragg fiber was proposed by Yeh et. al. in 1978[1]. The working principle of Bragg fiber has been discussed in chapter 1. Although one can achieve refractive index profile of MTF from profile of Bragg fiber by rotating it to 180^o, however it is interesting to note that this rotation of 180^o change the fiber properties significantly. Unlike Bragg fiber, MTF does not depend on anti-resonance guidance offered by high-index rings, as there is guidance due to total internal reflection offered by low-index rings. However, this guidance reduces with increasing wavelength, which is typical behavior of total internal reflection guidance. Moreover, depending on availability of phase-matched cladding state in resonant rings (that depends on the thickness of resonant ring and wavelength) resonance may take place, which can be used to suppress the higher order modes. On the other hand, in case of Bragg fiber, there is guidance and anti-guidance for all core modes offered by high–index rings at different wavelengths [2-4]. The wavelength of resonance is decided by the thickness and the refractive index of ring. Here, higher order modes can also be suppressed by phase-matched state present in resonant ring (low index ring) of Bragg fiber, which is similar to the case of MTF [2-4].

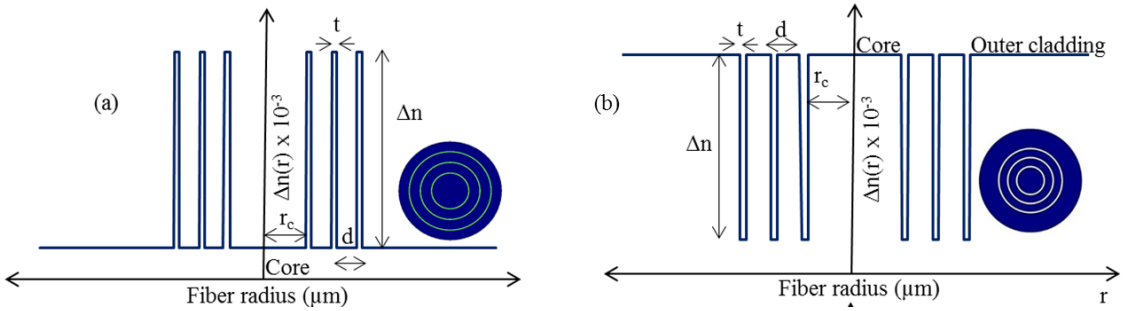

Figure 4.4(a) schematic of refractive index profile of the conventional Bragg fiber. Inset shows schematic of Bragg fiber (b) schematic of refractive index profile of the multi trench fiber. Inset shows schematic of multi trench fiber.

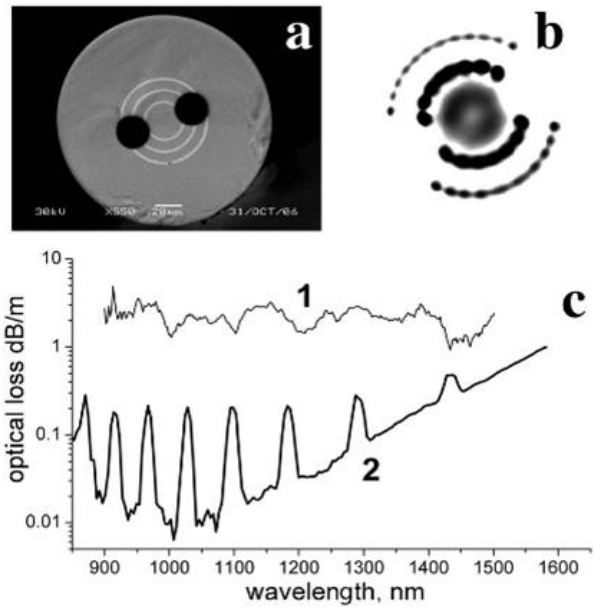

Figure 4.5(a) SEM image of the Bragg fiber with air holes; (b) photograph of the near-field intensity after 8m of the fiber bent with a radius of 20cm; (c) optical loss spectra, 1, in a structure with air holes and 2, in a circular symmetric structure [2]. Picture is from reference 4.

However, there is an issue with Bragg fiber of unwanted coupling between modes of core and high-index rings due to imperfections in circularity of resonant rings. This unwanted coupling has led to unwanted lossy peaks in transmission spectrum [5-6] as shown in graph 2 of figure 4.5 (c). Moreover, any disturbance to high index rings can lead to further coupling between modes of core and resonant rings as shown in case of polarization maintaining Bragg fiber. Figure 4.5(a) shows the SEM image of a polarization maintain fiber, where two holes were drilled to induce polarization. Figure 4.5(b) shows the near field intensity profile of fiber. Figure 4.5(c) shows the transmission spectrum of fiber before and after drilling holes, which shows the dramatic increase in loss level after drilling holes, which is due to unwanted coupling between core and high-index rings. However, MTF are free from such unwanted couplings due to absence of high index rings.

4.1.5 Design of a MTF with a core diameter of 100µm

The leakage loss of the higher order modes can be tuned by adjusting the thickness (d) of the resonant rings. Figure 4.6 illustrates this property for the case of a wavelength of 1.06µm and a 100µm-core diameter fiber having three trenches in which $\Delta n=1x10^{-3}$ and t=1.4µm. In this figure, only the mode presenting the lowest leakage loss in the core for a given symmetry has been plotted. From figure 4.6, a range of thickness d=28-38µm can be figured out for which the leakage loss of all the higher order modes having the symmetry of a LP_{11}, LP_{21} or LP_{02} mode are higher than 20dB/m, while the leakage loss of the fundamental mode are lower than 0.5dB/m. The loss of the higher order modes other than the above mentioned modes are also higher than 20dB/m for this range of thickness d. Therefore low-loss single-mode propagation for the fundamental mode can be ensured in this range. For an even stronger higher order modes filtering, it is interesting to note that, for d in the range 30-33µm, all the higher order modes have leakage loss higher than 30dB/m.

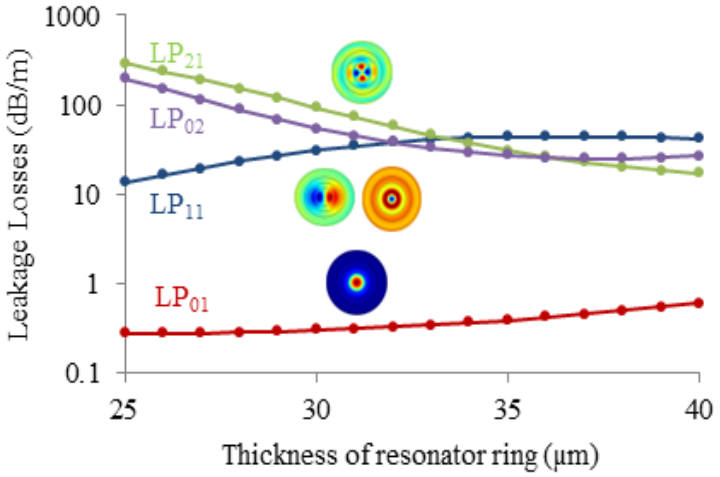

Figure 4.6 leakage loss of the fundamental mode and of higher order modes as a function of the resonant ring thickness (d) at a wavelength of 1.06µm for a fiber with $\Delta n=0.001$, rc=50µm, and t=1.4µm. Inset shows the 2D profile of the transverse component of the electric field for various modes at d=31µm.

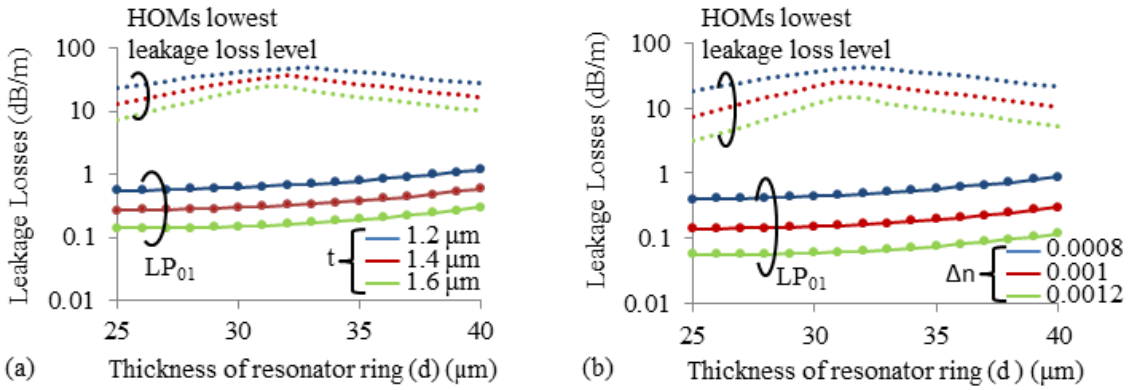

Figure 4.7 leakage loss of the fundamental mode and higher order mode (HOMs) that exhibit lowest leakage loss as a function of d for a 100µm core diameter fiber at 1.06µm wavelength (a) at Δn=0.001 for different t and (b) at t=1.4µm for different Δn.

From the perspective of practical realization, it is necessary to study the robustness of the single-mode operation of proposed 100µm-diameter core structure to small variations of the depth of the trench (Δn) and its thickness (t). Figure 4.7 shows the variation of the leakage loss of the fundamental mode and the higher order mode which has the lowest loss among all the possible higher order modes at 1.06µm for a 100µm diameter core as a function of d. Figure 4.7(a) and 4.7(b) show this variation for different t at constant Δn and for different Δn at constant t. For a fixed Δn of 0.001, a level of leakage loss higher than 20dB/m is obtained for all the higher order modes, for d in the range 30-33µm and t in the range 1.2-1.6µm. For a fixed t of 1.4µm, same level of higher order modes suppression is ensured for d in the range 30-33µm and Δn in the range 0.0008-0.001. The loss of the fundamental mode is maintained below 0.72dB/m for both of these cases. For these ranges of parameters, the effective area of the fundamental core mode LP_{01} is higher than 5000µm^2 at 1.06µm.

4.1.6 Mode area scaling

To further increase the effective area, while maintaining an ESM output for the fundamental mode, a higher core diameter (140µm) was chosen. Here the power delocalization for higher order modes filtering was taken into account. Figure 4.8(a) shows that, for the specifically chosen parameters of t=1µm, Δn=0.001, and for a d value between 42µm to 45µm, a leakage loss level higher than 20dB/m can be ensured for all the higher order modes except for the lowest loss mode having a symmetry of a LP_{11} mode that exhibits leakage loss higher than 15dB/m only. But, this mode is the result of couplings between core and ring modes and have a low percent of power in the core (<47%) (as shown in figure 4.8(b)). The overlap between this mode and the active core is thus small and a single-mode amplification of the fundamental mode that has leakage loss lower than 0.19dB/m and the percent of power in the core is higher than 93% is thus achievable.

Figure 4.9 shows two ranges of structural parameters d=42-45µm and t=0.8-1.0µm at Δn=0.001 and d=42-45µm and Δn=0.0008-0.001 at t=1.0µm in which the lowest loss LP_{11} has leakage loss higher than 15dB/m with a percent of power in the core lower than 47%. The other higher order modes have leakage loss higher than 20dB/m. In these ranges, the leakage

loss of the fundamental mode is lower than 0.5dB/m. Therefore low loss single-mode operation is ensured for the fundamental mode. For these ranges, the effective area of the fundamental mode ranges between 10,500µm^2 to 12,200µm^2.

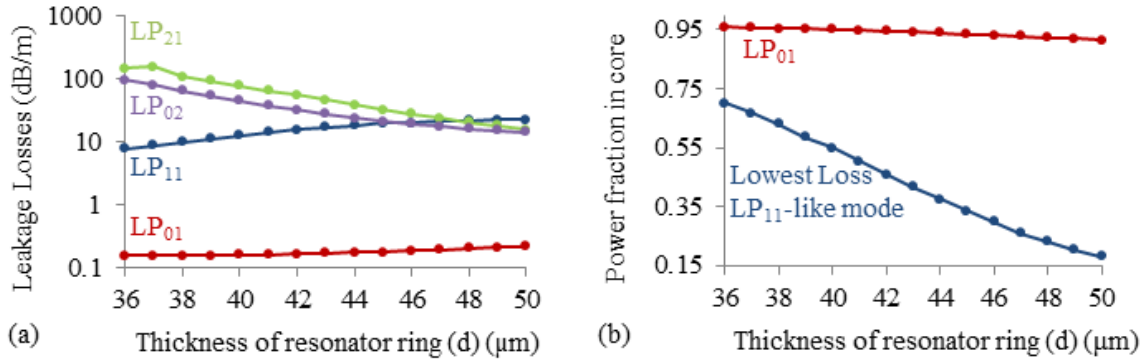

Figure 4.8(a) leakage loss of the fundamental mode and higher order modes as a function of d at λ=1.06µm for a fiber with of parameters Δn=0.001, rc=70µm, and t=1µm (b) fraction of power in the core for LP_{01} and LP_{11} modes as a function of d at λ=1.06µm of the same fiber.

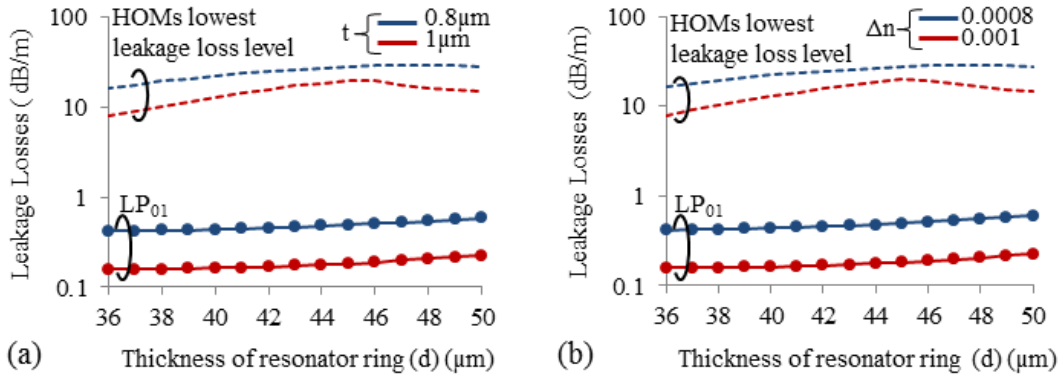

Figure 4.9 leakage loss, at λ=1.06µm, of the fundamental mode and lowest leakage loss level of the higher-order modes as a function of d for: (a) different t for a fixed Δn of 0.001 as well as for: (b) different Δn for a fixed t of 1µm for a 140µm-diameter core fiber.

4.1.7 Impact of small variations of the core refractive index

In the above study, perfect index-matching has been assumed between the rare-earth doped core and the surrounding undoped cladding material (formed by the rings and the infinite cladding), which is very challenging to achieve during the fabrication of the fiber.

For the above presented MTFs, if the core presents a refractive index slightly larger than those of the surrounding undoped material, several higher order modes are guided in the core with very low leakage loss. To avoid this configuration, it is possible to target a core refractive index that is lower than that of the surrounding undoped cladding material (i.e. a core refractive index depression Δn_c) [1].

Figure 4.10(a) shows the impact of a core-refractive index depression of $\Delta n_c = -1x10^{-4}$ for the case of a three-trench fiber with r_c=50µm, t=1.6µm and Δn=0.001. In the case of a perfect core-cladding index matching, this fiber presents an effective area of ~5000µm^2 at 1.06µm, a reasonable level of fundamental mode leakage loss and a good higher order mode filtering for d=30-33µm. In the case of a core refractive index depression of Δn_c=-1x10^{-4}, the leakage loss

of the fundamental mode are larger than 5dB/m for d=30-33µm, that is not acceptable for most of rod-type fiber laser applications. It is worth noting that the beam quality remains however good, the calculated M^2–parameter of the fundamental mode has been indeed evaluated to ~1.35. Moreover, the effective area remains larger than 4750µm^2.

To ensure low leakage loss for the fundamental mode, it is possible to adjust the MTF cladding for compensating the effects of the index depression in the core. For the above mentioned fiber, such adjustment can be done by increasing the thickness of the trenches (cf. figure 4.10(b)). For example for $\Delta n_c = -1x10^{-4}$, a low-loss single-mode operation can be ensured for d=37-39µm, t=2.4-2.8µm, and Δn=0.0008-0.001. Indeed, for appropriate combination of these parameters, the fundamental leakage loss remains lower than 2dB/m and the fundamental-mode power percent in the core is larger than 94%, and the higher order modes leakage loss are larger than 23dB/m (cf. figure 4.10(b)). In this range of structural parameters, the effective area is varying between 4850µm^2 and 5120µm^2. Moreover, thanks to the cylindrical symmetry of the structure, the beam-quality remains very good ($M^2 \leq 1.35$). Such MTF with adjusted cladding can be realized by fabricating separately the active core and the MTF cladding. Initial simulations suggest that, in depressed index core MTF, the effective area can be scaled further to a value of ~10,000µm^2, but it is intended for a future work.

It is worth noting that, in the case of depressed-core LPF, the fundamental mode M^2 parameter is rapidly increasing with increasing effective area [1]. Even a core index depression of $\Delta n_c = -0.2x10^{-4}$, leads to the deterioration of the M^2 to a value larger than 1.35, for effective area larger than 2500µm^2 [1]. Moreover, for a core index depression of $\Delta n_c = -1x10^{-4}$, the best M^2 values that can be achieved for an effective area of 2500µm^2 and 4000µm^2 are respectively of 1.7 and 2. The MTF presents therefore a dramatically better robustness to core-index depression than LPF in terms of beam quality preservation.

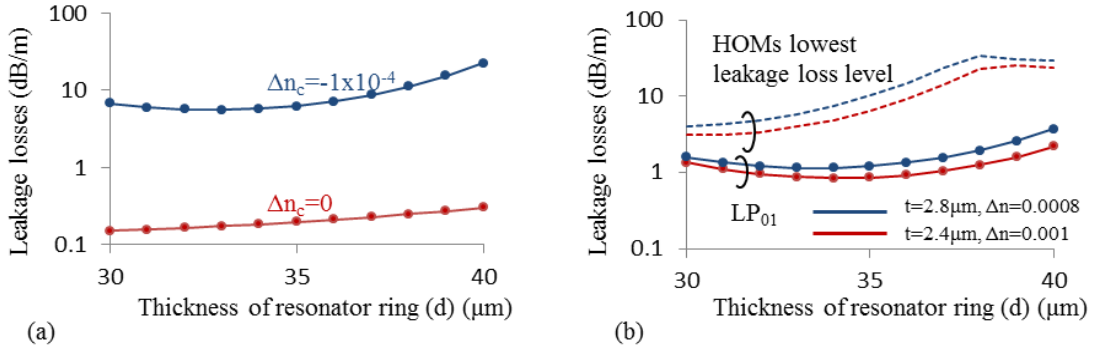

Figure 4.10 leakage loss, at λ=1.06µm and rc=50µm of (a) the fundamental mode at different Δn_c at t=1.6µm and Δn=0.001 of (b) the fundamental mode and higher order modes lowest leakage loss level for different t and Δn at $\Delta n_c = -1x10^{-4}$.

4.2 Bending behaviour of Multi Trench fiber

In order to verify the suitability for MTFs for beam delivery applications, it is necessary to achieve the ESM operation for different bend radii. This requirement of ensuring effective single mode over a wide range of bend radii is recommended, as beam delivery fiber need to be flexible unlike fibers for lasers. That is why; it is difficult to achieve LMA fibers for bam delivery as compared to laser applications.

This section shows the performance of MTF in bend configuration for different wavelengths region such as infrared, visible, and ultraviolet. Calculations show that MTF can be a suitable candidate for beam delivery applications.

4.2.1 Design of 30μm core MTF in straight and bent condition

The leakage loss of the fundamental mode and the first four higher order modes of a 30μm diameter core fiber, with t=2μm and Δn=0.006, as a function of thickness of the resonant ring (assuming both resonant rings thicknesses to be the same, i.e. first resonant ring (d_1) and second resonant ring (d_2)=d) are shown in figure 4.11(a). All the modes of the core are leaky due to their resonance coupling with the resonant rings modes. In order to ensure, an ESM operation of the core, high loss for the higher order modes of the core are required to be ensured by resonant couplings to the rings modes as compared to the fundamental modes. It is well known that for a complete resonant coupling to take place between two leaky modes, there are two basic conditions to satisfy. First one is the phase matching and second one is the loss matching of two leaky modes under coupling [1].

It is worth noting that the effective indices of the higher order modes of the core are different, so it is impossible to fulfill both of these conditions completely for all the relevant higher order modes of the core at a particular thickness of the resonant ring. However, the thickness of the resonant ring can be chosen in such a way that all the relevant higher order modes sustain sufficient leakage loss for ESM operation as shown in figure 4.11(a). The leakage loss of the fundamental mode are smaller than 0.0045dB/m for all the studied resonant ring thicknesses (5μm to 10μm) and the LP_{11} leakage loss remain larger than 1dB/m for resonant ring thickness from 8.5μm to 10.0μm. The leakage loss of other higher order modes of the core (all the possible higher order modes of the core have been considered here, although the loss of only few of them have been shown in figure 4.11(a)) are larger than 1.5dB/m for all the studied resonant ring thicknesses. The leakage loss of the higher order modes can be increased by decreasing the trench thickness (t), or the refractive index difference of trench (Δn) as observed in the design for 100μm and 140μm diameter core MTFs.

Bending loss of the MTF can be analyzed using standard conformal mapping [2] with additional stress perturbations [3] by following the standard equation 4.1:

$$n^2_{eq}(r,\varphi) = n^2(r) * \left(1 + \frac{2r}{\rho R}\cos\varphi\right), \qquad (4.1)$$

where n(r) is the index profile of the unbent fiber, R is the bend radius, φ is the azimuthal angle, and ρ (here fixed to 1.25) has been included to take account of the stress factor. Inset of figure 4.11(b) shows the obtained equivalent refractive index profile of the MTF shown in figure 4.11(a) for d=8µm, Δn=0.006, and t=2µm, at a bend radius of 15cm using the equation 4.1. It is clear from the equivalent profile of the fiber that, under the bent case the effective indices of the core and the ring modes change, and in turn the conditions of phase matching for resonance coupling also change. Figure 4.11(b) shows the bending loss of the LP_{01} and the LP_{11} modes (including both polarizations of the LP_{11} mode) of the core as a function of the resonant ring thickness. The loss in the bent case are large compared to the unbent case due to the bend-induced coupling with the resonant rings. Figure 4.11(b) shows the large loss for the LP_{11} mode (from 4dB/m to 14dB/m) for the resonant ring thickness from 8.0 to 8.5µm.

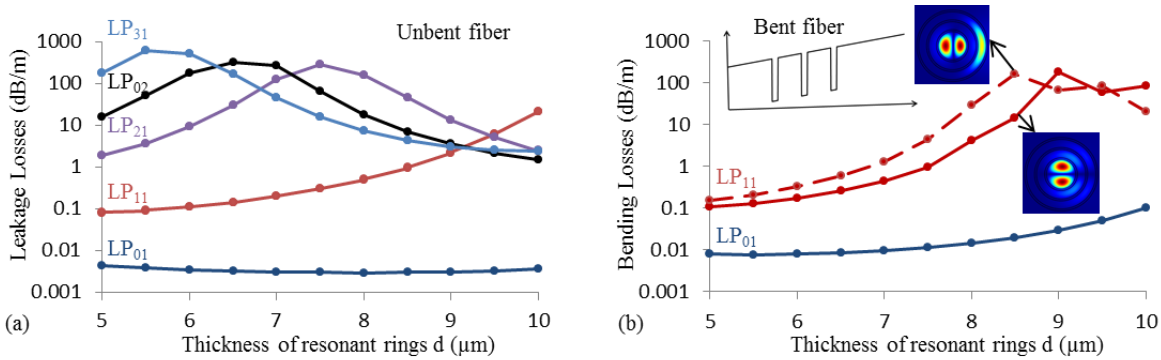

Figure 4.11 loss of the fundamental mode and higher order modes in (a) unbent (b) bent fiber at 15cm bend radius as a function of the resonant ring thickness of the fiber having r_c=15µm, t=2µm, and Δn=0.006.

From a perspective of fabrication, the ratio of lowest loss level of the higher order modes (expressed in dB/m) to the fundamental mode loss as a function of the resonant ring thickness was studied. The mismatch of both the resonant rings' thicknesses was considered since it is unlikely to obtain exactly the same thickness of both the resonant rings in a fabricated fiber. Figure 4.12(a) shows the ratio of lowest loss level of the higher order modes to the fundamental mode loss for different thicknesses of the resonant rings of a fiber with r_c=15µm, t=2µm, and Δn=0.006 at 15cm bend radius. X-axis shows the thickness of the first resonant ring (d_1). Y-axis shows the relative thickness of the second resonant ring (Y), whereas absolute thickness of the second resonant ring is d_2=2*Y-d_1. For example in figure 4.12(a), for a first resonant ring thickness (d_1) of 8µm, Y varies from 8µm to 8.5µm, so the absolute thickness of the second resonant ring (d_2) varies from 8µm to 9µm. Similarly for d_1=8.5µm, Y varies from 8µm to 8.5µm which corresponds to second ring thickness (d_2) from 8µm to 8.5µm. Figure 4.12(b) shows the loss ratio for the similar fiber as in figure 4.12(a) but for a different Δn=0.005. Figure 4.12(c) and 4.12(d) show the corresponding loss of the fundamental mode. It can be observed that for Δn=0.006, the fundamental mode loss vary from 0.014dB/m to 0.022dB/m, the loss ratio varies from 168 to 394, and the higher order modes lowest loss vary from 2.35dB/m to 7dB/m. Similarly for Δn=0.005, the fundamental mode loss vary from 0.06dB/m to 0.1dB/m, the loss ratio varies from 162 to 317, and the higher order modes lowest loss vary from 12dB/m to 22dB/m. From figure 4.12(c) and 4.12(d), it can be concluded that slight variations of the refractive-index have stronger impact

on the fundamental mode and the higher order modes loss than their loss ratio. This result is in good agreement with the study of the rod-type MTFs presented in previous section. Similarly, a slight increase and decrease of the trench thickness has stronger impact on the fundamental mode and the higher order modes loss than their loss ratio. The detailed study of impact of trench thickness on the loss of the core modes have been omitted here due to their similarity of the unbent case. It can be observed from these calculations that a good loss ratio between the higher order modes and the fundamental mode, which is an important property for the fiber lasers and for beam-delivery applications, can be obtained from a 30µm diameter core MTF. Moreover, this high ratio can be obtained for a wide range of bend radii, which is also a desired feature for beam delivery applications.

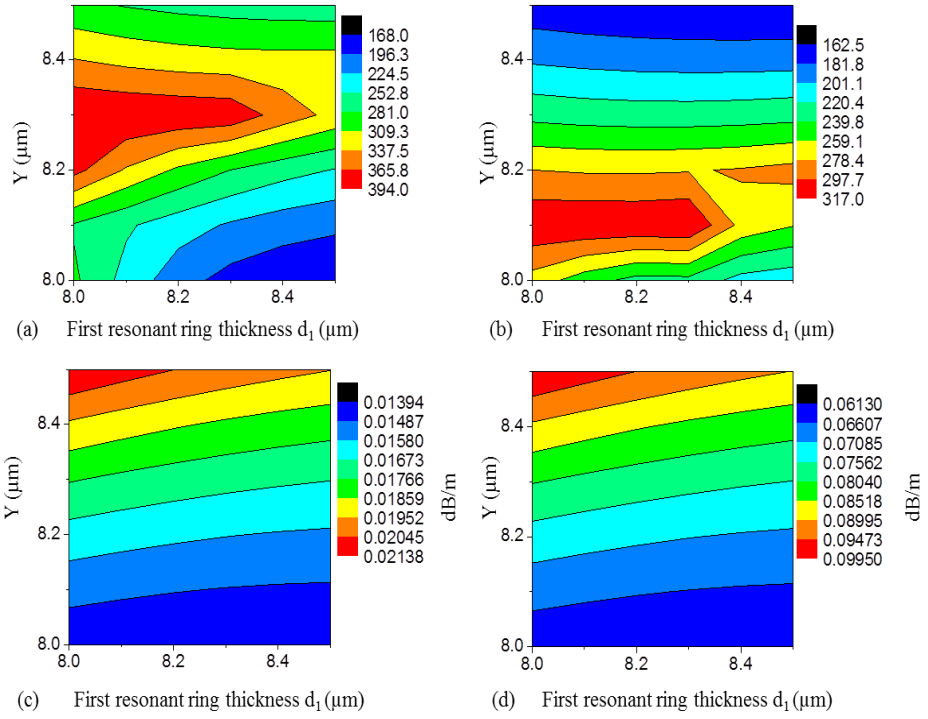

Figure 4.12 ratio of the higher order modes lowest loss level to the fundamental mode loss for different combinations of the first and the second resonant rings thicknesses for 30µm diameter core fiber with t=2µm (a) Δn=0.006 (b) Δn=0.005. (c) and (d) shows the respective fundamental mode loss for these fiber parameters. X-axis presents thickness of the first resonant ring (d_1) and Y-axis presents a parameter Y, where thickness of the second resonant ring is equal to d_2=2*Y-d_1. All figures have their individual colour scale.

Two sets of cladding parameters for the 30µm diameter core fiber were chosen (d=8.0µm, Δn=0.006 and d=8.5µm, Δn=0.005) at a fixed value of t=2µm, to further investigate the bend radii range for high loss ratio. These two sets of cladding parameters, present two extreme cases (lowest and highest) of the fundamental mode loss among d={8.0µm-8.5µm} and Δn={0.005-0.006} at a fixed t=2µm. The first case (d=8.0µm, Δn=0.006) presents lowest fundamental mode loss; we call it the best case and the second case (d=8.5µm, Δn=0.005) presents highest fundamental mode loss; we call it the worst case. Figure 4.13(a) shows the fundamental mode loss and the higher order modes lowest loss level for 8cm to 40cm bend radius for both the cases. Figure 4.13(b) shows the effective area of both the fibers over the bend radius range, which varies from 380µm^2 to 417µm^2. It is interesting to note that the

worst case offers a range of 15cm to 28cm, fulfilling the criterion of the fundamental mode loss smaller than 0.1dB/m and the higher order modes loss larger than 10dB/m, while the loss ratio varies from 162 to 440. It is worth noting that, this is a strongly recommended criterion for single mode operation for fiber laser applications. On the other hand, the best case offers a range of 18cm to 28cm bend radius, fulfilling the criterion of the fundamental mode loss smaller than 0.01dB/m and the higher order modes larger than 1dB/m, while the loss ratio varies from 200 to 320. It is important to note that this criterion would be sufficient for single-mode low-loss operation for several beam delivery applications (passive fibers). In unbent case, fundamental mode loss and higher order modes lowest loss are 0.012dB/m and 4.41dB/m respectively with fundamental mode effective area of 418.46μm^2 for worst case and fundamental mode loss and higher order mode lowest loss are 0.003dB/m and 0.5dB/m respectively with fundamental mode effective area of 406.56μm^2 for the best case.

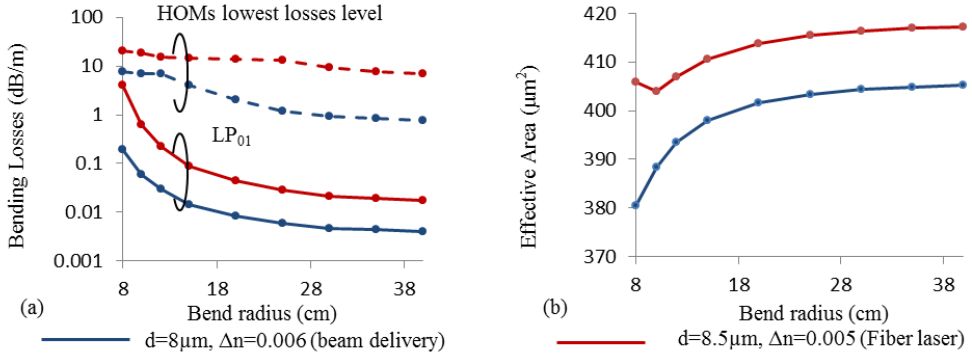

Figure 4.13(a) loss of the fundamental mode and the lowest loss level of the higher order modes as a function of the bend-radius (b) effective area of the fundamental core mode as a function of the bend radius.

4.2.2 Mode area scaling to 40μm and 46μm diameter core

To scale up the mode area further, we studied 40μm and 46μm diameter core MTFs with t=1.6μm and Δn=0.006 at 20cm bend radius. Figure 4.14(a) and 4.14(b) show the ratio of the higher order modes lowest loss level to the fundamental mode loss and the loss of the fundamental mode respectively, for different combinations of the first and second resonant ring thicknesses of 40μm diameter core fiber. For a large combinations of the resonant ring thicknesses shown in figure 4.14(a) and 4.14(b), the fundamental mode loss vary from 0.033dB/m to 0.099dB/m, while the loss ratio varies from 49 to 203. Figure 4.14(a) also shows a region covered by the dashed white line, which corresponds to the thicknesses of both the resonant rings varying from 10μm to 11μm. For these combinations of the thicknesses, the fundamental mode loss vary from 0.034dB/m to 0.075dB/m, while the loss ratio varies from 49 to 130, and the effective area is larger than 650μm^2. On the other hand, for certain combinations of ring thicknesses (shown in dark blue in figure 4.14(a)), the fundamental mode loss goes high up to 0.21dB/m and the loss ratio drops below 30. For these combinations, the second resonator thickness is large enough (from 12.5μm to 13μm) to induce the coupling between the fundamental mode and the second resonant ring modes, which in turn induces high loss to the fundamental mode. Figure 4.14(c) shows the ratio of the HOMs lowest loss level to the FM loss for 46μm diameter core. Again over a combinations of the resonant ring thicknesses, the FM loss remain smaller than 0.12dB/m (shown in figure 4.14(d)), while the loss ratio varies from 30 to 131, and the effective area exceeds 790μm^2. However, these calculations show that the performance of 40μm and 46μm

core diameter have poor performance than 30µm core diameter and may not be suitable for beam delivery application as 30µm core diameter fiber.

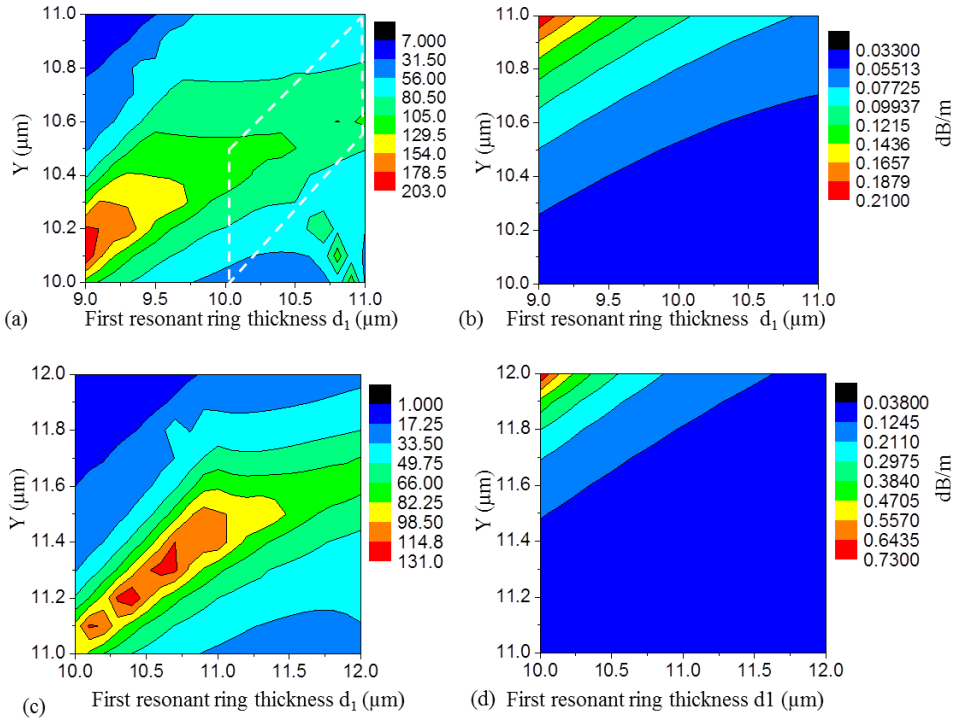

Figure 4.14(a) and (c) ratio of the HOMs lowest loss level to the FM loss for different combinations of the first and the second resonant rings thicknesses for 40µm and 46µm diameter core fibers respectively with t=1.6µm and Δn=0.006 at 20cm bend radius (b) and (d) shows the respective FM loss for these fiber parameters. X-axis presents the thickness of the first resonant ring (d_1) and Y-axis presents a parameter Y, where the thickness of the second resonant ring is equal to $d_2=2*Y-d_1$. All figures have their individual colour scale.

4.2.3 MTF for UV-VIS beam delivery

Beam delivery fibers are required for shorter wavelength as well. Moreover, at shorter wavelength it is more challenging to achieve single-mode operation compared to longer wavelength. For an example, for 0.005 core refractive index with respect to cladding, a 10µm core diameter can ensure single mode operation at 1550nm. On other hand, core diameter has to be ~4µm and ~2µm at λ=632nm and 300nm respectively for single mode operation. These small core diameter fibers pose severe challenges in terms of non-linear effects and launching light into fiber. That is why, there is a need for a LMA fiber for beam delivery at these visible and UV wavelengths for numerous applications.

At these shorter wavelengths, PCF and hollow core photonic bandgap fiber (HC-PBGF) have been proposed to address non-linear effects by offering large core diameter and air-core respectively [1-2]. It is worth mention that, solid-core silica fiber requires loading with hydrogen to achieve resistance against UV solarization, which includes solid-core PCF and MTF. This section investigates the performance of MTF as a beam delivery fiber at these short wavelengths. Figure 4.15(a) shows numerically computed bending loss of a 20µm core MTF with trench thickness (t)=1.34µm, refractive index difference between core and cladding (Δn)=0.005, and resonant ring thickness (d)=6µm at wavelength of 632nm. It is important to note that MTF ensures similar level of loss (as shown in figure 4.15 (a)) to the

higher order modes (>2dB/m) even in an unbent case thanks to the resonant coupling between modes of core and resonant ring. This ensures suitability for beam delivery applications. Figure 4.15(b) shows numerically computed bending loss of a 10µm core MTF with trench thickness (t)=0.67µm, refractive index difference between core and cladding (Δn)=0.005, and resonant ring thickness (d)=3µm at wavelength of 300nm. The loss of the higher order modes are higher than 1dB/m over a wide range of bend radii. The loss of the fundamental mode are lower than 0.01dB/m till 10cm bend radius and are lower than 0.1dB/m for 5cm bend radius.

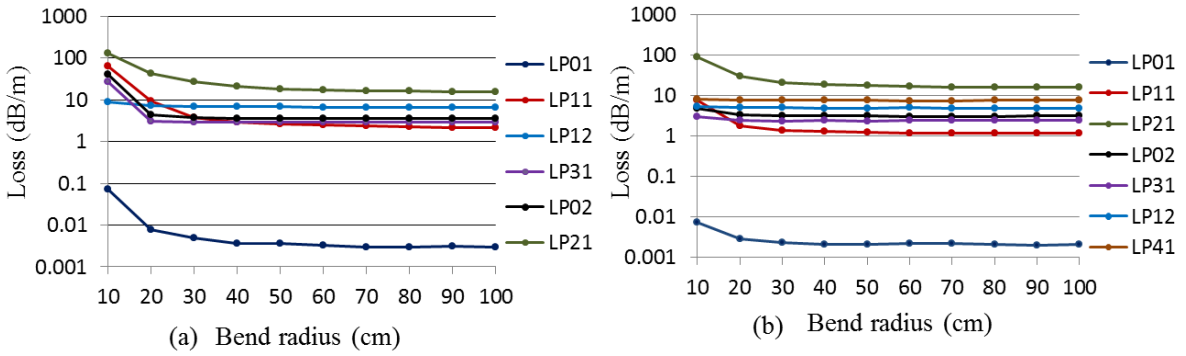

Figure 4.15(a) loss of the fundamental mode and the lowest loss level of the higher order modes as a function of the bend-radius (b) effective area of the fundamental core mode as a function of the bend radius.

Table 4.1 comparison of different fibers for UV transmission.

Fiber	Core diameter	Single mode	Fabrication	UV-solarization	handling
Photonic crystal fiber [1]	10µm	Intrinsically single mode	difficult	Need Hydrogen loading	difficult
Hollow core-Photonic bandgap fiber [2]	~20µm	Slightly multi-moded	difficult	Nothing required	difficult
Multi trench fiber	~10µm	Effective single mode	easy	Need Hydrogen loading	easy

Table 4.1 shows the comparison of different fibers suitable for UV beam delivery. It is pertinent to note that a PCF of ~10µm core diameter can be intrinsically single moded at ~300nm, on the other hand MTF can be effectively single moded only by offering high loss to the higher order modes. However, MTF offer other advantages of easy fabrication and all-solid design suitable for cleaving and splicing. On the other hand, a hollow core fiber does not require hydrogen loading to achieve resistance against UV solarization and furthermore, an air-core will be far superior to solid core to address non-linear effects as well. However,

HC-PBGF at ~300nm is slightly multi-moded and moreover they have high bend loss (~1dB/m) [2].

4.3 Hybrid Multi Trench Fiber (H-MTF)

This section deals with some modifications to MTF design in order to incorporate features such as spectral filtering of unwanted wavelengths and tailoring of dispersion. These additional features are required for several applications. For beam delivery applications, a LMA fiber is required with bending flexibility. It is clear from several calculations presented here that with increasing core diameter bending flexibility reduces. A fiber with a small core diameter with good bend robustness and filtering of Raman wavelength (~1.1μm) can be useful for high power transmission at ~1.06μm. Similarly, ASE outside the wavelength of interest can be filtered out to increase the laser efficiency. Furthermore, for generation of ultrashort pulses, a fiber with anomalous dispersion is required. Unfortunately, most of the fiber designs offering ESM operation for large effective area of the fundamental have normal dispersion around ~1μm. In order to compensate the dispersion within the laser cavity, a LMA fiber with anomalous dispersion can be used as a dispersion compensating element.

Several fiber designs with distributed spectral filtering have been proposed. A spectral filtering can be achieved by resonance coupling of core with high-index inclusions present in cladding. 2D-ASPBGFs have shown good potential for spectral filtering [1]. However, the cladding-pumping efficiency may be reduced in such fibers, due to the presence of the high index rods in their cladding, which confine a significant amount of the pump power. Hybrid Photonic Crystal Fiber (H-PCF), in which a line of air holes is replaced by the high index rods, introduced spectral filtering in PCF, thanks to resonant action of high-index rods [2-3]. A similar concept has also been applied to the SIFs [4]. These hybrid fibers have shown efficient spectral filtering but are limited in mode area scaling.

Several fiber designs with anomalous dispersion around 1μm have also been proposed to compensate the dispersion within the laser cavity, such as PCFs, HC-PBGFs, Bragg Fibers, fibers exploiting higher order modes, and 2D-ASPBGFs. PCFs offer high anomalous dispersion (~76 ps/nm.km) due to their strong confinement of light in the core but this can be achieved for small effective area of the fundamental mode which is less than $5\mu m^2$ [5]. Anomalous dispersion has also been demonstrated in Bragg fibers [6]. For example, recently a Bragg fiber with mode field diameter (MFD) ~7 μm at 1.064 μm with dispersion of 13 ps/(nm.km) and low loss of the FM (0.006 dB/m) has been demonstrated. However, both of these solutions provide low threshold of non-linear effects due to their limited effective area. Although, this problem of low threshold of non-linear effects can be solved by using HC-PBGFs, they also offer anomalous dispersion around 1μm but they are difficult to splice with standard solid core fibers [7]. Fibers exploiting higher order modes can provide anomalous dispersion at large effective area of the fundamental mode, but this technique requires long period gratings, which make the system cumbersome [8]. 2D-ASPBGFs show high anomalous dispersion at the long wavelength edge of Photonic Bandgap (PBG), for example a 2D-ASPBGFs, with FM loss ~0.07 dB/m and MFD ~9 μm at 1.04 μm, can achieve a dispersion of 90 ps/(nm.km) [9]. It is worth noting that anomalous dispersion in 2D-ASPBGFs is obtained at the long wavelength edge of the PBG which leads to high loss for the fundamental mode. The loss of the fundamental mode start increasing once the effective

area of the fundamental mode increases and it becomes difficult to obtain low loss for the fundamental mode at large effective area in the anomalous dispersion region. H-PCF and SIF with high index inclusions can offer anomalous dispersion [3-4]. These hybrid fibers can achieve anomalous dispersion at the long wavelength edge of bandgap due to the PBG action of the high index rods, while maintaining low loss due to presence of less number of rods compared to 2D-ASPBGFs. However, these fibers are limited to mode area scaling.

In order to add these features such as tailoring dispersion, filtering of Raman and ASE wavelengths in MTF, high index rods can be included in cladding along one axis of the fiber. Due to these additional high index rods in cladding, resonance and anti-resonance features can be achieved, that is why these fibers are known as Hybrid multi trench fiber (H-MTF). In next sections, a detailed study of H-MTF has been performed for spectral filtering and tailoring of dispersion.

4.3.1 H-MTF for spectral filtering

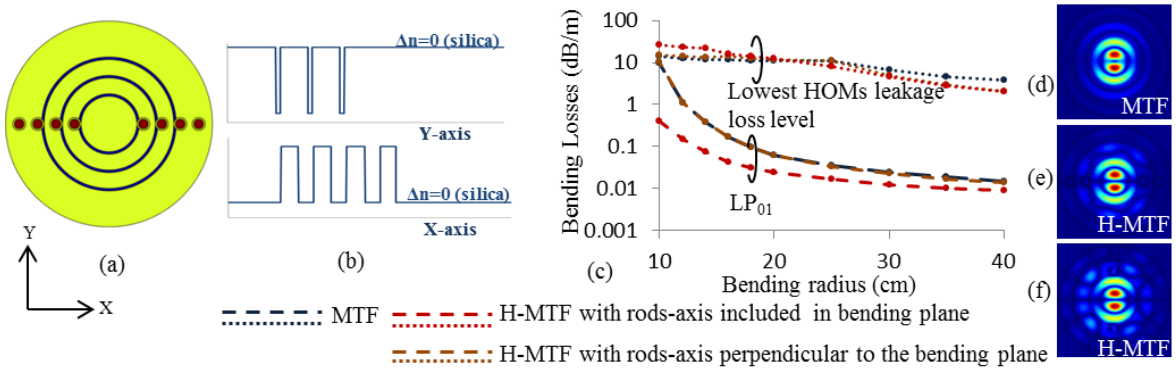

Figure 4.16(a) schematic cross-section of H-MTF. Blue, light green, and brown colours represent F-doped, undoped, and Ge-doped silica regions respectively. (b) refractive index profile of H-MTF along the X and Y axis (c) computed bending loss of the MTF and H-MTF for two orthogonal bend orientations (d) normalized electric field of the LP_{12} mode (which has lowest loss among HOMs at 20cm bend radius) for all three cases.

Figure 4.16(a) presents the H-MTF with the high-index rods (Ge-doped silica) positioned along the X-axis of the MTF with pitch Λ. The pitch (Λ) has been chosen in such a way that the high index rods lie on the trenches (F-doped silica) of the MTF. Figure 4.16(b) shows the refractive index profile of the fiber along X and Y axis. The structure parameters of MTF are, core radius(r_c)=17.5µm, trench thickness(t)=1.6µm, trench refractive-index w.r.t core index(Δn_-)=-0.006, and resonant-ring thickness(d)=10µm. The high-index rods have a step-index profile with core radius (r_{ch})=3.1µm, outer cladding radius(r_{oh})=4.1µm, pitch(Λ)=11.6µm, and refractive-index w.r.t pure-silica cladding(Δn_+)=0.035. Figure 4.16(c) shows the computed bending loss of the fundamental mode and the higher order mode having the lowest loss level, at a wavelength of 1060nm, for the MTF and H-MTF. For H-MTF two different bend orientations have been considered. Figure 4.16(d)-16(f) show the normalized electric field of the LP_{12} mode (which has lowest loss among all the higher order modes at 20cm bend radius) for all three cases. A single mode operation can be ensured in 18cm to 23cm bend radius range, where fundamental mode bend loss are lower than 0.1dB/m and all other higher order modes loss are larger than 10dB/m. The effective area remains larger than 520µm^2 for this bend radius range (including bend-induced effective area reduction). A configuration in which the rods are in the bending plane shows significantly lower bending

loss than other case due to additional reflections by rods. Figure 4.17(a) and 4.17(b) show the calculated wavelength spectra of the leakage loss and the power fraction in the core of the fundamental mode of the MTF and H-MTF, for the structure parameters of figure 4.16(c) in unbent case. H-MTF shows the filtering of the power from the core in 865nm-895nm, 975nm-980nm, and 1100-1145nm wavelength regions, corresponding to the cut-off of the LP_{03}-LP_{22}, LP_{41}, and LP_{12} modes of the high index rods respectively. The filtering of power from the core, by resonances with the modes of the high-index rods at 874nm, 892nm, 976nm, and 1119nm are shown in figure 4.17(c)-17(f). It is important to note that the bandgaps obtained here are different from the bandgaps obtained for a 2D-ASPBGF with the same structural parameters for the high-index rods. Indeed, here, a narrow transmission and wide forbidden bands for the high-index rods has been observed, which results in narrow forbidden and wide transmission bands for the core mode. This is due to the small number of the high-index rods, which limits the wavelengths extension of the super modes of the rods. Figure 4.18 shows the bend loss and power fraction wavelength spectra of the fundamental core mode, at bend radius of 20cm, for two different cases (namely rods axis included in the bending plane and orthogonal to it). This structure ensures a low loss single-mode operation at 1060nm along with the efficient filtering (>60dB/m) of the SRS at ~1116nm. Moreover, by tuning the parameters of high-index rods, other desired wavelengths (i.e. short and long wavelengths ASE) can be filtered out.

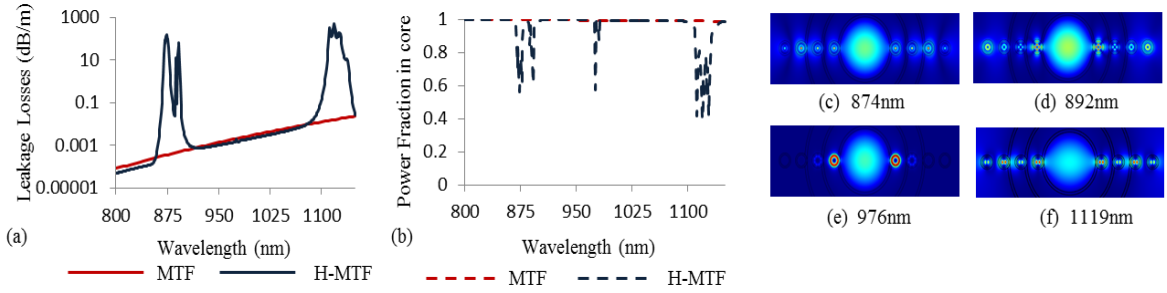

Figure 4.17(a-b) wavelength dependence of leakage loss (a) and power fraction in the core in the case of an unbent MTF and H-MTF of figure 4.16(c). 4.17(c)-(f) normalized electric field of the fundamental core mode at different wavelengths.

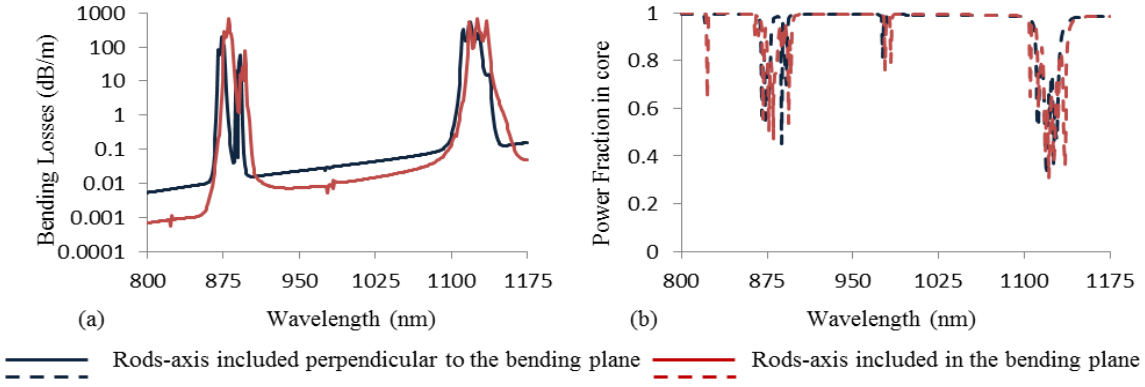

Figure 4.18 bend loss spectrum (a) and power fraction spectrum (b) of the fundamental core mode of the H-MTF for the same parameters used in figure 4.16(c) at a 20cm bend radius for two orthogonal bending orientations.

This study concludes that proposed Hybrid MTF (MTF with inclusion of high index rods along one axis of the fiber) ensures excellent suppression of the higher order modes by resonant ring surrounding the core. On the other hand, inclusion of the high-index rods ensures an efficient filtering of the unwanted wavelengths including SRS thanks to their resonant action.

4.3.2 H-MTF for tailoring dispersion

Figure 4.19(a) presents the H-MTF with only two high-index rods (Ge-doped silica) positioned along the X-axis of the MTF. Figure 4.19(b) shows the refractive index profile of the fiber along X and Y axis. The parameters of the MTF are: core radius(r_c)=15µm, trench thickness(t)=2.0µm, trench refractive-index w.r.t core index(Δn_-)=-0.006, and resonant-ring thickness(d)=8.5µm. The high-index rods have a step-index profile with core radius(r_{ch})=3.0 µm, outer cladding radius(r_{oh})=4.0µm, and refractive-index w.r.t pure-silica cladding(Δn_+)=0.035. Figure 4.19(c) shows the computed bending loss of the fundamental mode and the higher order mode having the lowest loss level, at a wavelength of 1064 nm, of the MTF and H- MTF, for two different bend orientations. A single mode operation can be ensured in the 14cm to 20cm bend radius range by keeping fundamental mode bend loss lower than 0.051dB/m and all other HOMs loss larger than 5dB/m. The effective area remains larger than 390µm^2 for this bend radius range (including the bend-induced effective area reduction).

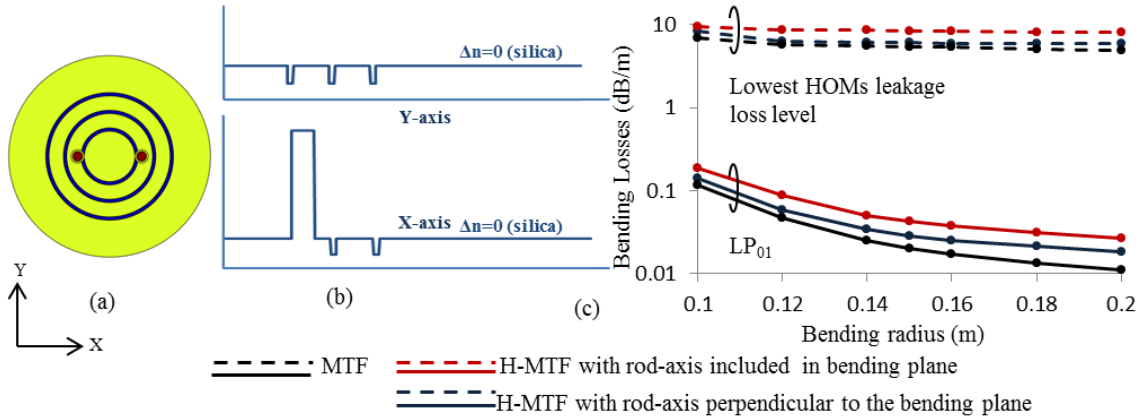

Figure 4.19(a) schematic cross-section of H-MTF. Blue, yellow-green, and brown colours represent F-doped, undoped, and Ge-doped silica regions respectively. (b) schematic of Refractive index profile of H-MTF along the X and Y axis (c) computed bending loss of the MTF and H-MTF with two orthogonal bend orientations.

Figure 4.20(a), 20(b) and 20(c) show the calculated wavelength spectra for the leakage loss, the dispersion, and the power fraction in the core respectively, of the fundamental mode for both MTF and H-MTF in unbent case, for the fiber parameters used in figure 4.19. Figure 4.20(c) also shows the normalized electric field of the fundamental mode at certain wavelengths. Additional high index rods in the MTF provide an additional guidance mechanism, which is clear from the spectrums of the H-MTF. H-MTF supports transmission of light in the core between the cut-off wavelengths of the high index rods' modes. Figure 4.20(c) shows the filtering of the power from the core in the 835-865 nm, 935-945 nm, 1075-1090 nm, and 1165-1175 nm wavelength regions, which correspond to the cut-off wavelengths of the LP_{03}-LP_{22}, LP_{41}, LP_{12}, and LP_{31} modes of the high index rods

respectively. Figure 4.20(b) shows the dispersion spectrum of MTF and H-MTF. In case of H-MTF, between the cut off wavelengths of two modes of high index rods, it shows normal dispersion (D<0) at short wavelength edge and anomalous dispersion (D>0) at long wavelength edge with a point of inflection (D=0) between them (which is similar to 2D-ASPBGFs). It is worth noting that the obtained spectrums for H-MTF are similar to that of a 2D-ASPBGF, although in the present case, the transmission region of the rods (forbidden region of the core) is quite narrow as compared to 2D-ASPBGFs (similar to the previous case). It is well known that in a 2D-ASPBGFs, the wavelength region over which anti-crossing between FM of core and high index rods' mode take place is broad due to formation of broadband supermode of high index rods' modes [10]. This broadband supermode formation took place due to mutual coupling between high index rods' modes. In the present case of H-MTF, limited number of high index rods avoids the formation of broadband supermode, which results in narrow forbidden region of core [10].

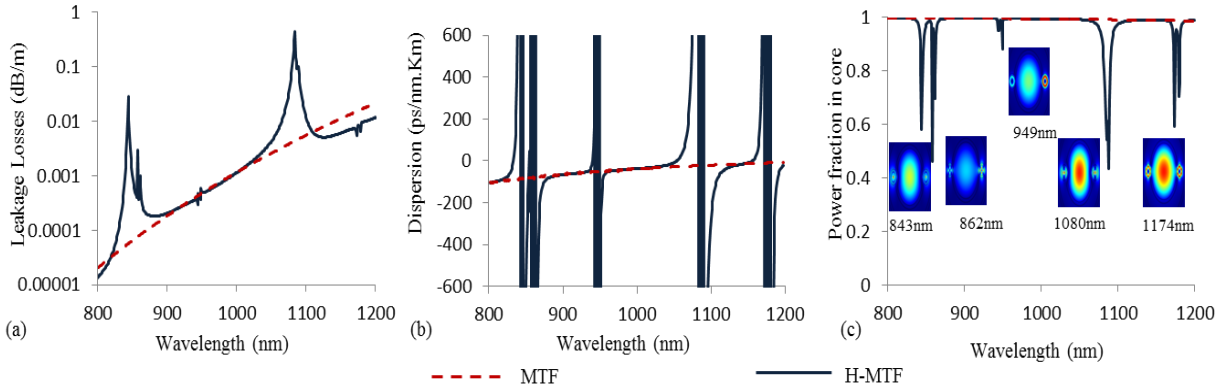

Figure 4.20(a), 4.20(b), and 4.20(c) calculated leakage loss, dispersion, and power fraction of the fundamental mode of MTF and H-MTF respectively in the case of an unbent configuration. Inset also shows normalized electric field of the fundamental core mode of H-MTF at certain wavelengths.

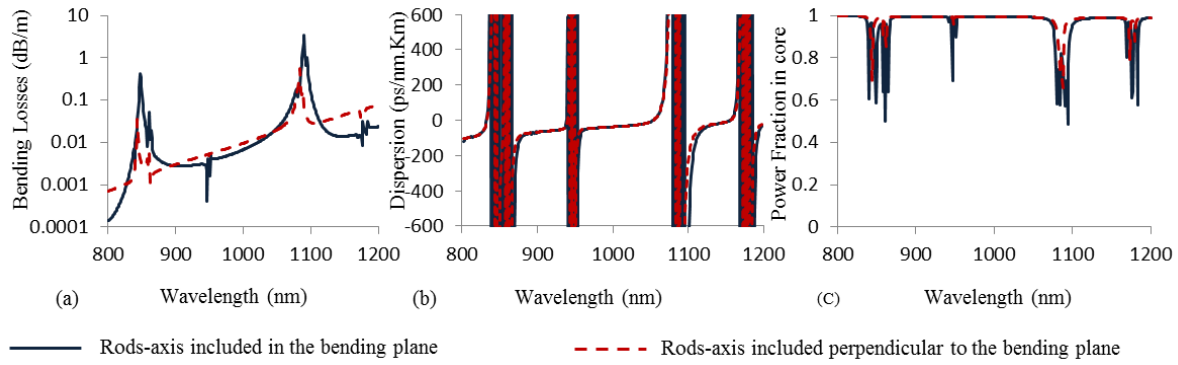

Figure 4.21 bend loss spectrum (a), power fraction spectrum (b) dispersion (c) of the fundamental core mode of the H-MTF of the figure 4.19(c) at a 15cm bend radius, for two orthogonal bending orientations.

Figure 4.21 shows the bend loss and power fraction dependence of wavelength of the fundamental mode, at a bend radius of 15 cm, for two different cases (namely rods axis included in the bending plane and orthogonal to it). An anomalous dispersion larger than 72ps/nm.km at a wavelength of 1064 nm with effective area larger than 390 μm^2 can be achieved here. The loss of the fundamental mode remains lower than 0.043 dB/m, while ensuring high loss to the higher order modes (>6 dB/m). Moreover, by tuning the parameters

(refractive index and core diameter) of the high-index rods, the zero dispersion wavelength (ZDW) can be shifted to other wavelengths in order to achieve anomalous dispersion at a desired wavelength. It is worth noting that in conventional 2D-ASPBGFs, a large anomalous dispersion at the long wavelength edge of a bandgap can be obtained but at the cost of large leakage loss of the fundamental mode [9]. Therefore, it is an interesting finding of this study that a large anomalous dispersion can be achieved at the long wavelength edge of the bandgap, which is similar to 2D-ASPBGFs. However, unlike 2D-ASPBGFs, this is achieved while ensuring low loss of the fundamental mode having a large effective area.

4.4 Conclusion

The simulations results presented in this chapter are encouraging for several important applications in lasers. Most of these results were published in peer reviewed journals and conferences. Table 4.2 summarizes the results achieved in this chapter:-

Table 4.2 different fiber designs and their applications.

Fiber	**Application**	**Properties**
MTF [1]	Rod-type lasers	ESM for large effective area on order of 10,000μm^2.
MTF [2]	High power beam delivery for infrared, visible and UV wavelengths	ESM for large effective area over wide range of bend radii.
H-MTF [3-4]	Raman and ASE filtering fiber and Dispersion compensating fiber	ESM for large effective area while filtering unwanted wavelengths or tailoring dispersion.

In next, chapter fabrication of passive MTFs and their characterization will be discussed.

4.5 References

[4.1 Introduction]

1. J. Limpert, F. Stutzki, F. Jansen, H.-J. Otto, T. Eidam, C. Jauregui and A. Tünnermann, "Yb-doped large-pitch fibres: effective single-mode operation based on higher-order mode delocalization," Light: Sci. & App., vol. 1, pp. 1-5, March (2012).
2. M. M. Jørgensen, S. R. Petersen, M. Laurila, J. Lægsgaard, and T. T. Alkeskjold, "Optimizing single mode robustness of the distributed modal filtering rod fiber amplifier," Opt. Express 20(7), 7263–7273 (2012).
3. S. Ramachandran, J. M. Fini, M. Mermelstein, J. W. Nicholson, S. Ghalmi, and M. F. Yan, "Ultra-large effective-area, higher-order mode fibers: a new strategy for high-power lasers," Lasers & Photon Rev., 2(6), 429-448 (2008).

[4.1.2 Prior art]

1. A. Kumar and V. Rastogi, "Design and analysis of a multilayer cladding large-mode-area optical fiber," J. Op. A: P. Appl. Opt. **10**, 1-6 (2008).
2. M. Devautour, P. Roy, and S. Fevrier, "3D Modeling of modal competition in fiber laser: application to HOM suppression in multi-layered fiber," Joint CLEO Poster Session II (JWA) (2009).

[4.1.4 Comparison with Bragg fiber]

1. P. Yeh, A. Yariv, and E. Marom, "Theory of Bragg fiber", JOSA B, vol. 68, no. 9, pp. 1196-1201, May 1978.
2. E. M. Dianov, M. E. Likhachev, and S. Fevrier, "Solid-core photonic bandgap fibers for high-power fiber lasers," IEEE J. Sel. Top. Quant. Electron. **15**, 20-29 (2009).
3. Baskiotis, D. Molin, G. Bouwmans, F. Gooijer, P. Sillard, Y. Quiquempois, and M Douay, "Bending behaviours of all-solid silica large mode area Bragg fibers," Proc. of SPIE **7195,** (2009).
4. Baskiotis, Y. Quiquempois, M. Douay, and P. Sillard, "Extending the effective area of coiled all-solid silica single-mode Bragg fibers," ECOC, Geneva, Switzerland, paper **We.10.P1.02**, (2011).
5. M. E. Likhachev, A. D. Pryamikov, D. A. Gaponov, M. M. Bubnov, M. Yu. Salganskii, V. F. Khopin, A. N. Guryanov, and S. Février, " Polarization-maintaining photonic bandgap Bragg fiber," Opt. Lett. 34, 1366-1369 (2009).
6. S. S. Aleshkina, M. E. Likhachev, A. D. Pryamikov, D. A. Gaponov, A. N. Denisov, M. M. Bubnov, M. Y. Salganskii, A. Y. Laptev, A. N. Guryanov, Y. A. Uspenskii, N. L. Popov, and S. Février, "Very-large-mode-area photonic bandgap Bragg fiber polarizing in a wide spectral range," Opt. Lett. **36**, 3566-3568 (2011).

[4.1.7 Impact of small variations of the core refractive index]

1. F. Jansen, F. Stutzki, H. J. Otto, M. Baumgartl, C. Jauregui, J. Limpert, and A. Tünnermann, "The influence of index-depressions in core-pumped Yb-doped large pitch fibers," Opt. Express 18(26), 26834–26842 (2010).

[4.2.1 Design of 30µm core MTF in straight and bent condition]

1. Z. Zhang, Y. Shi, B. Bian, and J. Lu, "Dependence of leaky mode coupling on loss in photonic crystal fiber with hybrid cladding," Opt. Exp **16**, 1915-1922 (2008).
2. D. Marcuse, "Influence of curvature on the loss of doubly clad fibers," Appl. Opt. **21**, 4208-4213 (1982).
3. K. Nagano, S. Kawakani, and S. Nishida, "Change of the refractive index in an optical fiber due to external forces," Appl. Opt. **17**, 2080-2085 (1978).

[4.2.3 MTF for UV-VIS beam delivery]

1. Y. Colombe, D. H. Slichter, A. C. Wilson, D. Leibfried, and D. J. Wineland, "Single-mode optical fiber for high-power, low-loss UV transmission," Opt. Exp., 22, 19783 (2014).
2. F. Gebert, M. H. Frosz, T. Weiss, Y. Wan, A. Ermolov, N. Y. Joly, P. O. Schmidt, and P. St. J. Russell, "Damage-free single-mode transmission of deepUV light in hollow-core PCF," Opt. Exp., 22, 15288 (2014).

[4.3 Hybrid Multi Trench Fiber (H-MTF)]

1. L. Bigot, V. Pureur, Y. Jaouen , Y. Quiquempois , and G. Bouwmans, "Ytterbium-doped 2D solid core photonic bandgap fiber for laser operation at 980nm," ECOC (2007).
2. A. Cerqueira S. Jr., F. Luan, C. M. B. Cordeiro, A. K. George, and J. C. Knight "Hybrid photonic crystal fibre," Opt. Express **14**, 926-931, (2006).
3. S. R. Petersen, Thomas T. Alkeskjold, Federica Poli, Enrico Coscelli, Mette M. Jørgensen, Marko Laurila, Jesper Lægsgaard, and Jes Broeng, "Hybrid Ytterbium-doped large-mode-area photonic crystal fiber amplifier for long wavelengths," Opt. Exp. **20**, 6010-6020 (2012).
4. R. Goto, S. D. Jackson, S. Fleming, B. T. Kuhlmey, B. J. Eggleton, and K. Himeno, "Birefringent all-solid hybrid microstructured fiber," Opt. Exp. **16**, 18752-18763 (2008).
5. H. Lim, F. Ö. Ilday, and F. W. Wise, "Femtosecond ytterbium fiber laser with photonic crystal fiber for dispersion control," Opt. Express **10**, 1497-1502 (2002).
6. S. S. Aleshkina, M. E. Likhachev, A. K. Senatorov, M. M. Bubnov, M. Y. Salaganskii, and A. N. Guryanov, "Low-loss hybrid fiber with zero dispersion wavelength shifted to 1 µm," Opt. Exp., **21**, 23838-23843 (2013).

7. H. Lim and F. W. Wise, “Control of dispersion in a femtosecond ytterbium laser by use of hollow-core photonic bandgap fiber,” Opt. Exp. **12,** 2231-2235 (2004).
8. S. Ramachandaran, S. Ghalmi, J. W. Nicholson, M. F. Yan, P. Wisk, E. Monberg, and F. V. Dimarcello, “Anomalous dispersion in a solid, silica-based fiber,” Opt. Letter **31**, 2532-2534 (2006).
9. Q. Fang, Z. Wang, L. Jin, J. Liu, Y. Yue, Y. Liu, G. Kai, S. Yuan, and X. Dong, “Dispersion design of all-solid photonic bandgap fiber,” JOSA B, **24**, 2899-2905, (2007).
10. J. Laegsgaard, “Gap formation and guided modes in photonic bandgap fibers with high-index rods,” J. Opt. A: P. App. Opt.**6** (2004).

[4.4 Conclusion]

1. D. Jain, C. Baskiotis, and J. K. Sahu, “Mode-area scaling with multi-trench rod type fiber,” Optics Express, 21, 1448 (2013).
2. D. Jain, C. Baskiotis, and J. K. Sahu, “Bending performance of large mode area multi-trench fibers,” Optics Express, 21, 26663 (2013).
3. D. Jain, C. Baskiotis, and J. K. Sahu, “Large mode area hybrid multi-trench fiber for spectral filtering,” FIO, Orlando, USA, FW2A.3, Oct 2013.
4. D. Jain, C. Baskiotis, and J. K. Sahu, “Large mode area hybrid multi-trench fiber for anomalous dispersion Large mode area hybrid multi-trench fiber for anomalous dispersion,” OFC, San Francisco, USA, Th2A.40, March 2014.

Chapter 5 Fabrication of Multi-trench fibers

This chapter reports the fabrication and characterization of passive MTF suitable for beam delivery and rod-type fiber laser applications. Fabrication process involves MCVD and rod-in-tube technique. Initially process has been optimized for 30μm and 20μm core diameter passive MTF for beam delivery. Afterwards, a 90μm core diameter passive MTF has been fabricated and characterized.

5.1 Fabrication and Characterization of 30μm MTF for 1060nm

5.1.1 Preform fabrication

Table 5.1 shows the various parameters used for different passes of recipe for preform fabrication. A F300 tube from Heraeus having 20mm (Outer diameter) X 16mm (Inner diameter) was used as a starting tube to deposit resonant rings, trenches, and core [1]. Before deposition of resonant rings and trenches, first three high temperature passes were executed to warm, etch, and fire polish the tube. During deposition of trenches, SiF_4 was used to reduce the refractive index, on the other hand for deposition of resonant ring and core only $SiCl_4$ was used.

Table 5.1 recipe A243.

Pass	$SiCl_4$	SiF_4	O_2	S(t) (mm/min)	Temp (^oC)
Trench_1	125	80	500	150	1850
Resonant Ring_1 (9 passes)	125	---	555	150	2025
Trench_2	125	80	500	150	1850
Resonant Ring_2 (5 passes)	125	---	555	150	2025
Trench_3	125	80	500	150	1850
Core (4 passes)	125	---	555	150	2025

Where unit of gas flow is cm^3/min, s(t) represents speed of burner, and tube is rotating at 30rpm.

Following this recipe, it was not easy to complete preform fabrication due to appearance of significant bubbles in the preform. In order to avoid the problem caused by bubbles, improvements were made to the recipe by having almost same deposition temperature for trenches (F-doped silica) and resonant rings (silica) layers. Changes made in new recipe (shown in table 5.2) are shown in red colour, following these changes, no bubbles were observed during fabrication. Figure 5.1 shows the obtained refractive index profile. The target parameters for this MTF was to achieve rc=30μm, t=1-3μm, d=7-9μm, and Δn=0.005. The refractive index profile shown in figure 5.1 is different from the target parameters. First, over all refractive index of core and resonant rings is lower than outer cladding by $5x10^{-4}$, as

outer cladding is constituted by F300 tube. F300 has slightly higher refractive index than silica (due to incorporated Cl_2). Second, there is a refractive index dip in core, which is probably due to evaporation of Cl_2 from innermost core layer. Third, the refractive indices of trenches with respect to silica are not equal to 0.005. Fourth, the thicknesses of the trenches and resonant ring are not with in the target limit.

Table 5.2 recipe B249.

Pass	$SiCl_4$	SiF_4	O_2	S(t) (mm/min)	Temp (^oC)
Trench_1	100	80	500	150	1850
Resonant Ring_1 (9 passes)	125	---	555	150	1865
Trench_2	100	80	500	150	1870
Resonant Ring_2 (5 passes)	125	---	555	150	1875
Trench_3	100	80	500	150	1880
Core (4 passes)	125	---	555	150	1900

Where unit of gas flow is cm^3/min, s(t) represents speed of burner, and tube is rotating at 30rpm. {Significant changes from previous iteration are shown in red colour}.

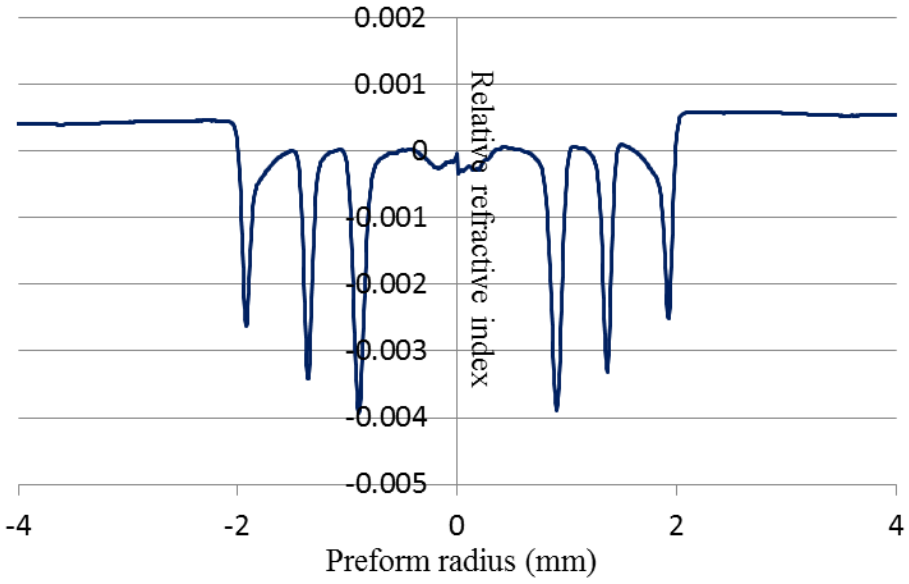

Figure 5.1 refractive index profile of fabricated MTF using recipe B249 shown in table 5.2.

In order to further optimize the thickness and index-depression of trenches, resonant rings, and core some modifications were made to recipe. Table 5.3 shows the modified recipe, where $GeCl_4$ was added in core and resonant ring passes to increase the refractive index (in order to match with the refractive index of outer cladding). The number of passes for second resonant rings was increased from 5 to 7 to increase the thickness. It is important to note that flow of SiF_4 was reduced from 80 to 65, in order to achieve reduced thickness of trenches. Few little changes were made to deposition temperatures, in order to achieve equal thickness and index of trenches and resonant rings. Figure 5.2 shows the obtained refractive index profile of preform. Core suffers from a central dip as shown in figure 5.2 due to evaporation

of GeO_2. Moreover, no significant changes in thickness were noticed, on the other hand trench index was reduced by 0.0005.

Table 5.3 recipe C256.

Pass	$SiCl_4$	SiF_4	$GeCl_4$	O_2	S(t) (mm/min)	Temp (^oC)
Trench_1	100	65	---	500	150	1825
Resonant Ring_1 (9 passes)	125	---	20	555	150	1865
Trench_2	100	65	---	500	150	1850
Resonant Ring_2 (7 passes)	125	---	20	555	150	1875
Trench_3	100	65	---	500	150	1870
Core (4 passes)	125	---	20	555	150	1900

Where unit of gas flow is cm^3/min, s(t) represents speed of burner, and tube is rotating at 30rpm. {Significant changes from previous iteration are shown in red colour}.

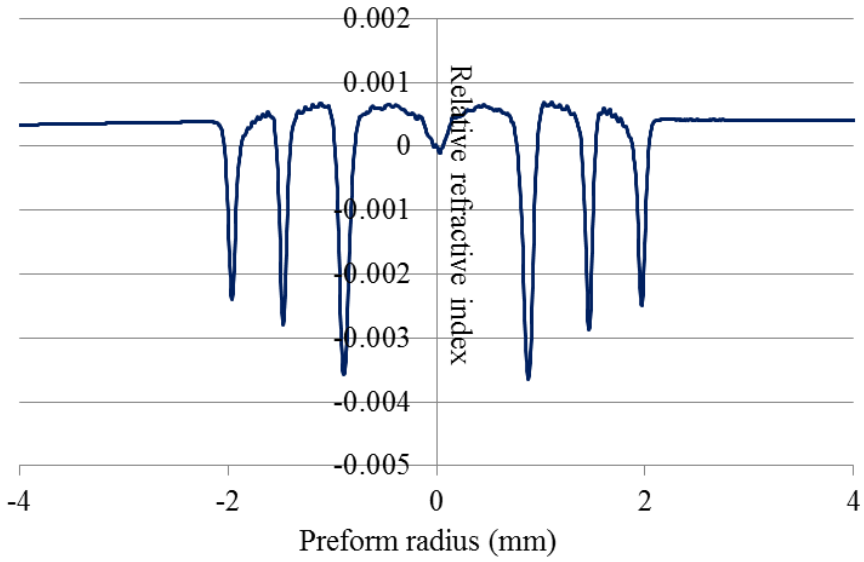

Figure 5.2 refractive index profile of fabricated MTF using recipe C256 shown in table 5.3.

In order to further optimize the fabrication process, few changes were made to the recipe as shown in table 5.4. Here, $GeCl_4$ was not used, as the intention was to optimize the thicknesses and indices of trenches and resonant rings. SiF_4 flow was increased to 100 in all three trenches deposition; on the other hand, flow of $SiCl_4$ was changed to 80 and 60 for trench_2 and trench_3 respectively. Figure 5.3 shows the refractive index profile of preform. It is interesting to note that, after comparing figure 5.1-5.3, a change of SiF_4 flow from 65 to 80 to 100 did not cause any considerable change in refractive index of trenches.

Table 5.4 recipe D266.

Pass	$SiCl_4$	SiF_4	$GeCl_4$	O_2	S(t) (mm/min)	Temp (^oC)
Trench_1	100	100	---	500	150	1825
Resonant Ring_1 (9 passes)	125	---	---	555	150	1865
Trench_2	80	100	---	500	150	1850
Resonant Ring_2 (7 passes)	125	---	---	555	150	1875
Trench_3	60	100	---	500	150	1870
Core (4 passes)	125	---	---	555	150	1900

Where unit of gas flow is cm^3/min, s(t) represents speed of burner, and tube is rotating at 30rpm. {Significant changes from previous iteration are shown in red colour}.

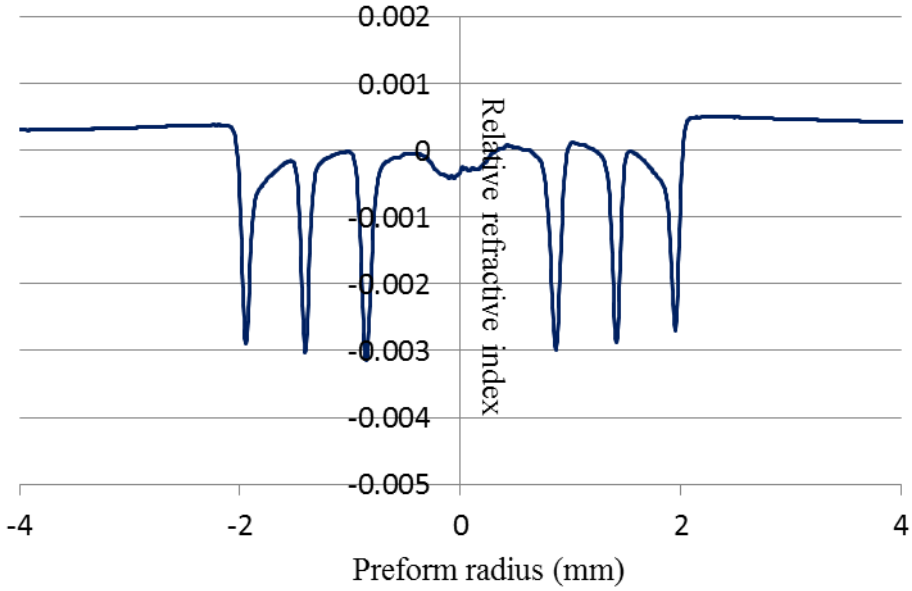

Figure 5.3 refractive index profile of fabricated MTF using recipe D266 shown in table 5.4.

Fluorine incorporation in silica is governed by following equation 5.1 [1]:-

$$3SiO_2(s) + SiF_4(g) = 4SiO_{1.5}F(s) \quad (5.1)$$

So that the concentration of F in the glass, X_F, depends on the partial pressure of SiF_4 as:-

$$X_F = a_{SiO2}^{3/4} P_{SiF4}^{1/4} \quad (5.2)$$

In order to increase the partial pressure, the flow of SiF_4 was increased to 320, 240, and 160 in layer 1, layer 2, and layer 3 respectively as shown in table 5.5. However the flow of $SiCl_4$ was decreased to 80, 60, and 40 in layer 1, layer 2, and layer 3 respectively in order to reduce the overall thickness of the trenches. The resultant refractive index profile of preform is shown in figure 5.4. The index profile does not show any considerable change with respect to

the profile shown in figure 5.3. This analysis shows that in order to incorporate a sufficient F in SiO_2, it is necessary to have a sufficiently thick SiO_2 layer. Here the intention was to deposit very thin layers of trenches having refractive index lower than 0.005 from silica. However it seems that it is difficult to achieve thin layers of silica doped high concentration of F. The alternative approach can be to optimize the F doping irrespective of thickness required. The final parameters can be achieved by increasing the thickness of core and resonant rings. Table 5.6 shows the modified recipe, where flow of $SiCl_4$ was increased to 200, 180, and 150 for three trenches and flow of SiF_4 was maintained to 150 in all three trenches.

Table 5.5 recipe E269.

Pass	$SiCl_4$	SiF_4	$GeCl_4$	O_2	S(t) (mm/min)	Temp (^oC)
Trench_1	80	320	---	500	150	1825
Resonant Ring_1 (10 passes)	125	---	---	555	150	1865
Trench_2	60	240	---	500	150	1850
Resonant Ring_2 (7 passes)	125	---	---	555	150	1875
Trench_3	40	160	---	500	150	1870
Core (4 passes)	125	---	---	555	150	1900

Where unit of gas flow is cm^3/min, s(t) represents speed of burner, and tube is rotating at 30rpm. {Significant changes from previous iteration are shown in red colour}.

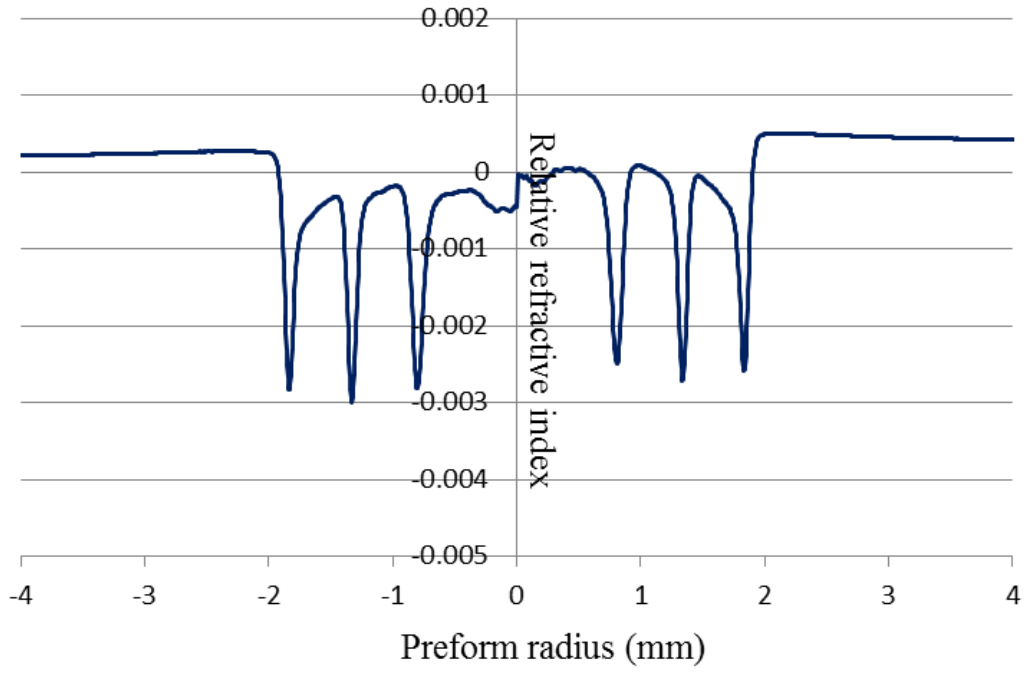

Figure 5.4 refractive index profile of fabricated MTF using recipe E269 shown in table 5.5.

Figure 5.5 shows the obtained refractive index profile using recipe shown in table 5.6. It is interesting to see that the refractive index of innermost and outermost trenches is more than -0.005. This proves the conclusion made in previous paragraph.

Table 5.6 recipe F320.

Pass	$SiCl_4$	SiF_4	$GeCl_4$	O_2	S(t) (mm/min)	Temp (^oC)
Trench_1	200	150	---	500	150	1825
Resonant Ring_1 (10 passes)	125	---	20	555	150	1865
Trench_2	180	150	---	500	150	1850
Resonant Ring_2 (7 passes)	125	---	20	555	150	1875
Trench_3	150	150	---	500	150	1870
Core (4 passes)	125	----	20	555	150	1900

Where unit of gas flow is cm^3/min, s(t) represents speed of burner, and tube is rotating at 30rpm. {Significant changes from previous iteration are shown in red colour}.

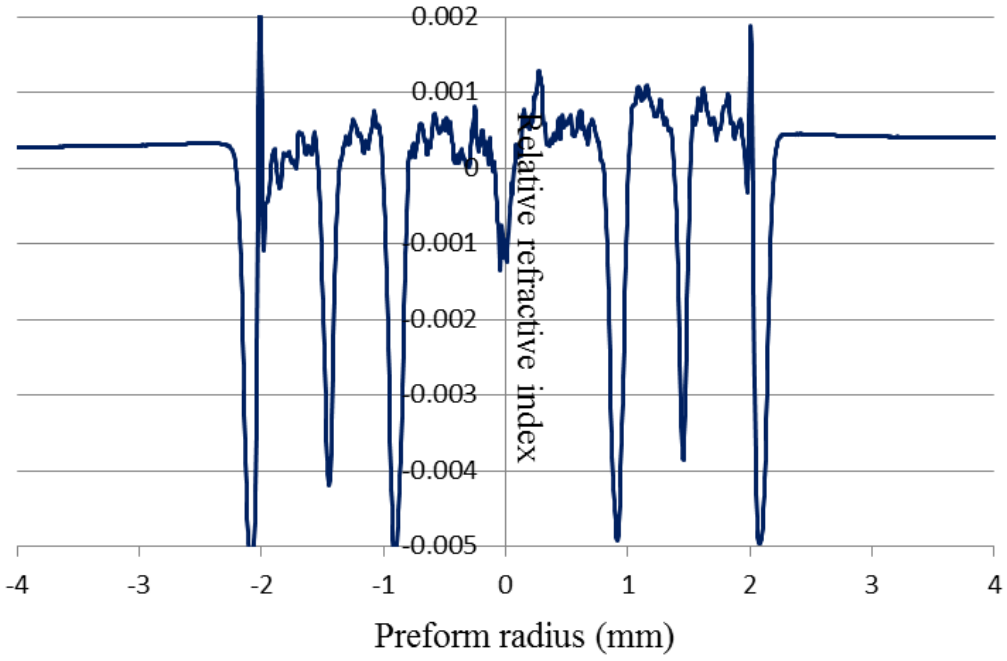

Figure 5.5 refractive index profile of fabricated MTF using recipe F320 shown in table 5.5.

In order to further enhance the incorporation of F, additions pass of SiF_4 soaking following the deposition of trench was added as shown in table 5.7. The resultant refractive index

profile is shown in figure 5.6. It is interesting to note that the, refractive index of trenches has decreased with respect to silica rather than increasing. Moreover, the thicknesses of the resonant rings and core have decreased, which suggest the etching action of SiF_4. Significant diffusion of F in silica layers can also be observed.

Table 5.7 recipe G324.

Pass	$SiCl_4$	SiF_4	$GeCl_4$	O_2	S(t) (mm/min)	Temp (^oC)
Trench_1	200	150	---	500	150	1825
F_doping	---	100		500	200	1825
Resonant Ring_1 (10 passes)	125	---	20	555	150	1865
Trench_2	180	150	---	500	150	1850
F_doping	---	40		500	200	1850
Resonant Ring_2 (7 passes)	125	---	20	555	150	1875
Trench_3	150	150	---	500	150	1870
F_doping	---	20		500	200	1870
Core (4 passes)	125	----	20	555	150	1900

Where unit of gas flow is cm^3/min, s(t) represents speed of burner, and tube is rotating at 30rpm. {Significant changes from previous iteration are shown in red colour}.

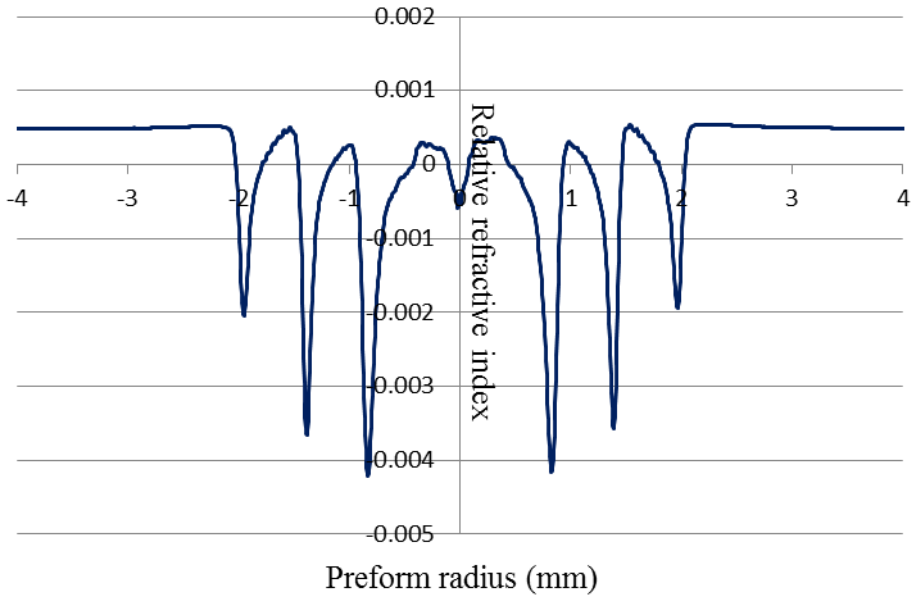

Figure 5.6 refractive index profile of fabricated MTF using recipe G324 shown in table 5.7.

Now, coming back to recipe shown in table 5.6, few changes were made to optimize the thickness of resonant rings and trenches as shown in table 5.8. The numbers of passes were

increased to 11 for first resonant ring. The flow of $GeCl_4$ was slowly decreased from 30 to 20 over 11 passes. On the other hand, for second resonant ring and core, only 20 $GeCl_4$ was used. The reason of using 30 to 20 over different passes for first resonant ring was to overcome reduction in refractive index due to F diffusion. The achieved refractive index profile is shown in figure 5.7 (using recipe shown in table 5.8) is not ideal, but a refractive index on the order of ~0.005 for trench with respect to silica has been achieved. Furthermore, the thicknesses of core, trenches, and resonant rings are sufficient to ensure single mode operation. However, there is a slight central dip (due to evaporation of Ge) which is undesirable.

Table 5.8 recipe H330.

Pass	$SiCl_4$	SiF_4	$GeCl_4$	O_2	S(t) (mm/min)	Temp (^oC)
Trench_1	200	150	---	500	150	1825
Resonant Ring_1 (11 passes)	125	---	30 to 20	555	150	1865
Trench_2	180	150	---	500	150	1850
Resonant Ring_2 (7 passes)	125	---	20	555	150	1875
Trench_3	150	150	---	500	150	1870
Core (4 passes)	125	----	20	555	150	1900

Where unit of gas flow is cm^3/min, s(t) represents speed of burner, and tube is rotating at 30rpm. {Significant changes from previous iteration are shown in red colour}.

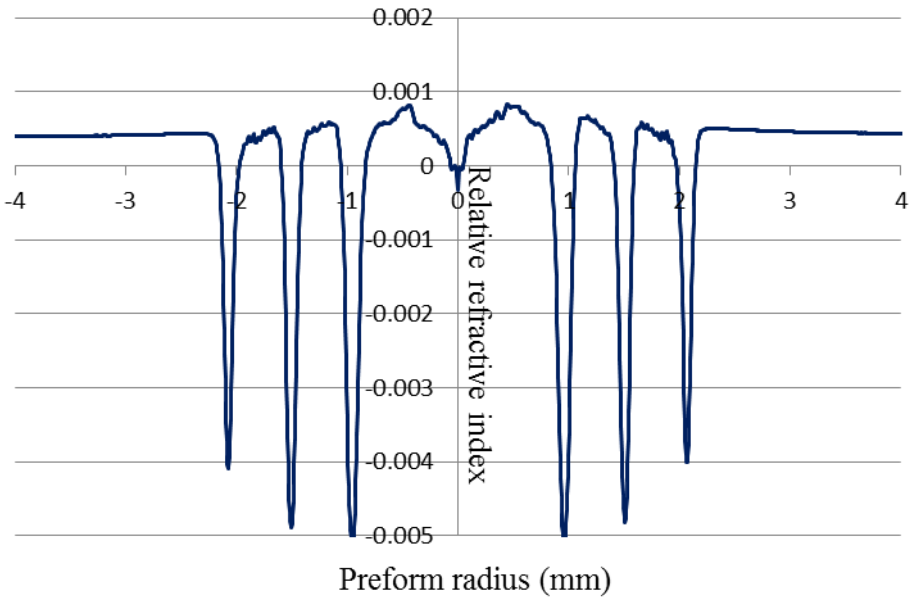

Figure 5.7 refractive index profile of fabricated MTF using recipe H330 shown in table 5.8.

In order to avoid the central-dip, rod-in-tube technique was implemented. In this case, all three trenches and two resonant rings were deposited using MCVD using recipe shown in

Table 5.9 similar to other preforms. All passes were executed to deposit resonant rings and trenches, however only one thin core layer was used to act as a barrier to prevent evaporation of F from trench 3 in subsequent collapse passes. Preform was further collapsed without deposition of core until the diameter of central hole reached around 2mm. Afterwards, a F300 cane of desired core diameter was drawn from commercially available F300 rod. F300 cane was then inserted into the unsealed preform and the two were combined in-situ while drawing into fiber. The outer diameter and core diameter of drawn fiber is 225µm and 30µm respectively. Fiber was drawn at a relatively low tension to minimize the stress-induced refractive index changes in the fiber [4]. Figure 5.8 shows the measured refractive index profile of fiber. Inset shows the microscope image of fiber end face. Fiber is free from any central dip unlike previous preforms, however the refractive index of core appears to be slightly lower than resonant ring. That is why, fiber appeared to be bend sensitive.

Table 5.9 Recipe I349.

Pass	$SiCl_4$	SiF_4	$GeCl_4$	O_2	S(t) (mm/min)	Temp (^oC)
Trench_1	200	170	---	500	150	1825
Resonant Ring_1 (11 passes)	125	---	30 to 20	555	150	1865
Trench_2	200	150	---	500	150	1850
Resonant Ring_2 (7 passes)	125	---	20	555	150	1875
Trench_3	150	135	---	500	150	1870
Core (1 passes)	40	----	20	555	150	1900

Where unit of gas flow is cm^3/min, s(t) represents speed of burner, and tube is rotating at 30rpm. {Significant changes from previous iteration are shown in red colour}.

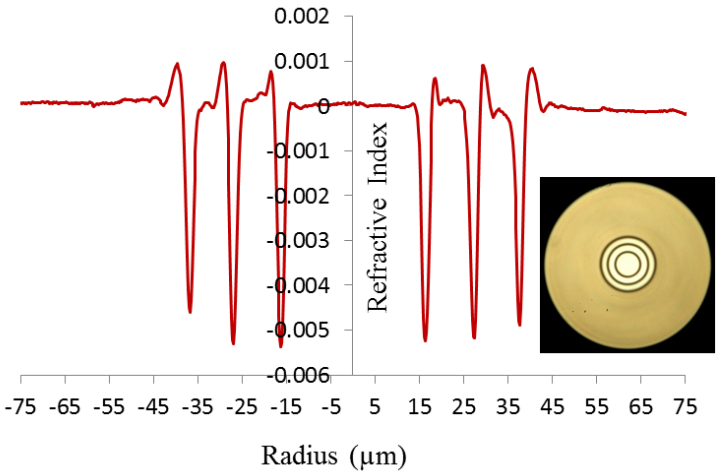

Figure 5.8 refractive index profile of fabricated MTF using recipe I349 shown in table 5.9 and rod-in-tube technique.

In order to further optimize the fabrication process, a F300 rod having same refractive index as of F300 tube was used. Preform was fabricated in a similar fashion to previous one with very little changes in recipe (as shown in table 5.10). However, preform was collapsed after inserting F300 silica rod on a glass working lathe rather than collapsing it during the fiber drawing. Figure 5.9 shows the measured refractive index profile of sealed preform. It is interesting to see that core is free from any central dip. Moreover, the refractive index of core is almost same as of resonant ring. There is a slight asymmetry in core, which is a measurement artifact only. Later on, this sealed preform was drawn into 203µm outer diameter fiber with high index polymer coating. Figure 5.10 shows the measured refractive index profile of fiber. Inset shows the microscope image of fiber. Next section discusses the detailed experimental characterization of this fiber.

Table 5.10 recipe J376

Pass	$SiCl_4$	SiF_4	$GeCl_4$	O_2	S(t) (mm/min)	Temp (^oC)
Trench_1	200	165	---	500	150	1825
Resonant Ring_1 (11 passes)	125	---	30 to 20	555	150	1865
Trench_2	200	155	---	500	150	1850
Resonant Ring_2 (8 passes)	125	---	20	555	150	1875
Trench_3	150	145	---	500	150	1870
Core (1passes)	40	----	20	555	150	1900

Where unit of gas flow is cm^3/min, s(t) represents speed of burner, and tube is rotating at 30rpm. {Significant changes from previous iteration are shown in red colour}.

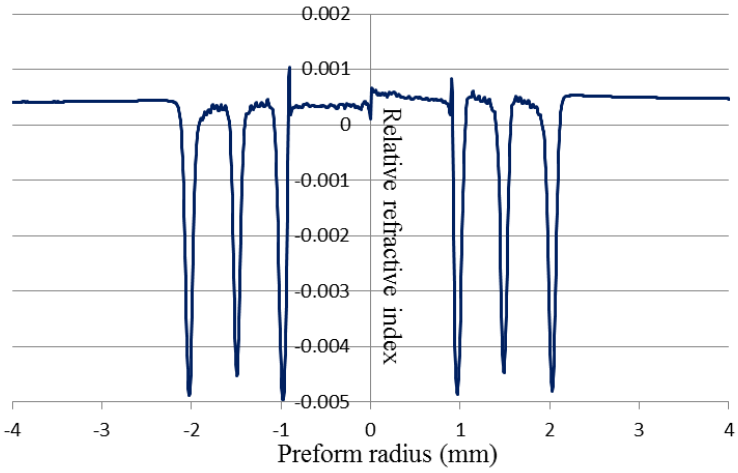

Figure 5.9 refractive index profile of fabricated MTF preform using recipe J376 shown in table 5.10 and rod-in-tube technique

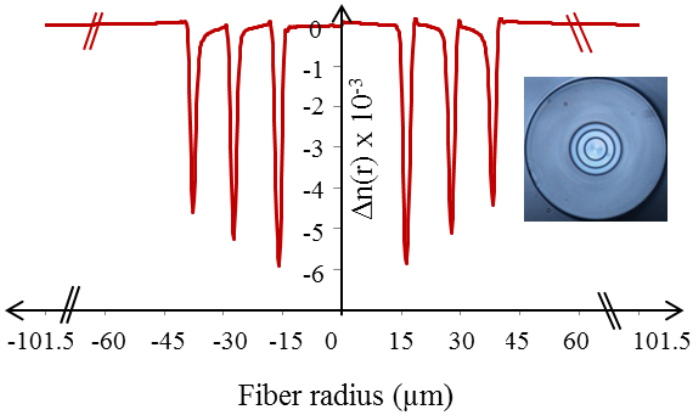

Figure 5.10 refractive index profile of fiber drawn from preform shown in figure 5.9.

5.1.2 Characterization of optimized 30μm MTF

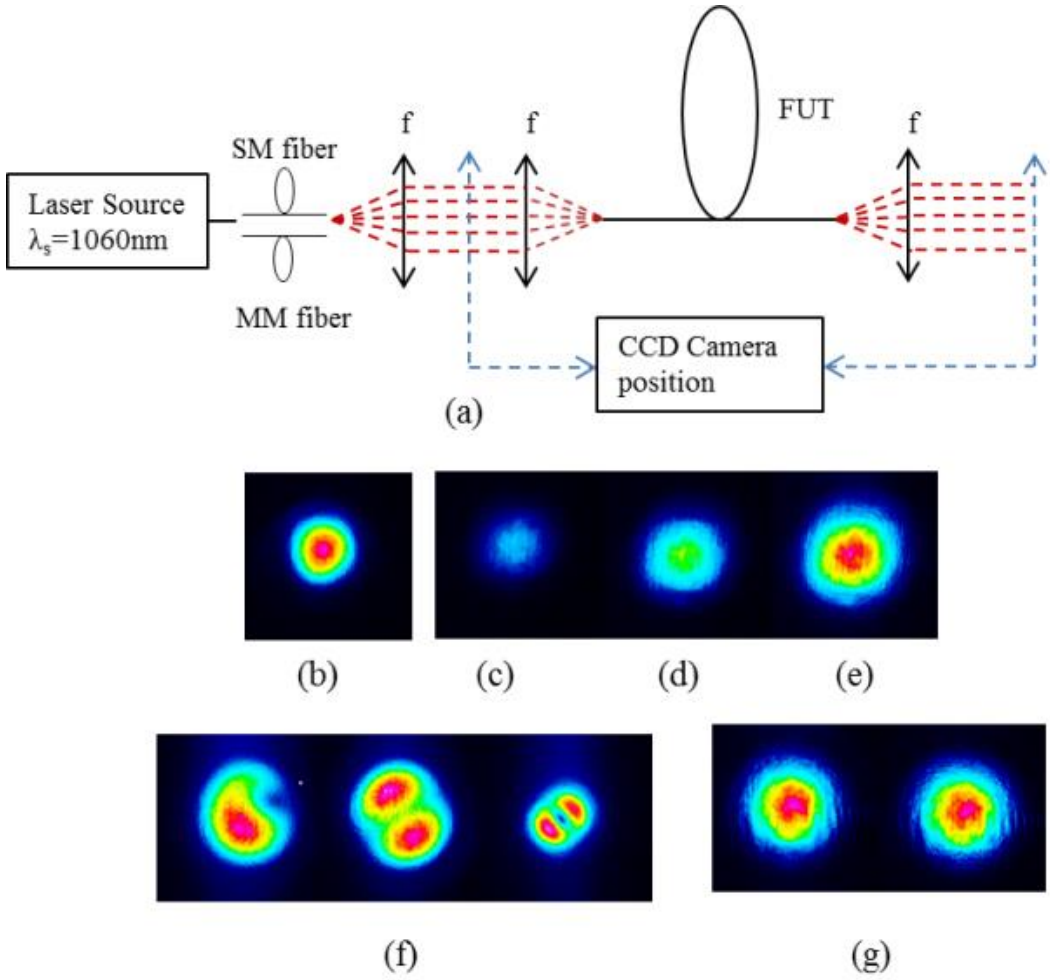

Figure 5.11(a) measurement set-up used for verification of single mode behaviour, (b) output beam profile with optimum single mode launching, (c), (d), (e) output beam profile under various launching conditions, (f) multimode input beam profile before launching into FUT, and (g) profile of output beam for different multimode input beam launch.

Figure 5.11(a) shows the experiment set-up used for verification of ESM behaviour of fiber (refractive index of profile of fiber is shown in figure 5.10). A 2m length of fiber in loosely coiled state (50cmx45cm) was used as FUT. A single mode laser at 1060nm wavelength was launched into FUT. Figure 5.11(b) and (c-e) shows the obtained output beam for optimum launching and for various offset launching conditions respectively, which ensure a Gaussian beam output irrespective of launching condition. It is interesting to note that, only the intensity of the output beam changes but it remains Gaussian in all cases, which ensures high loss for the higher order modes. In order to further validate the single mode behaviour of fiber, a multimode input launch was ensured by splicing the multimode optical fiber to the single mode delivery fiber of 1060nm laser source, as shown in figure 5.11(f). Again a Gaussian beam output was observed as shown in figure 5.11(g), which ensures fairly robust ESM behaviour of the fiber.

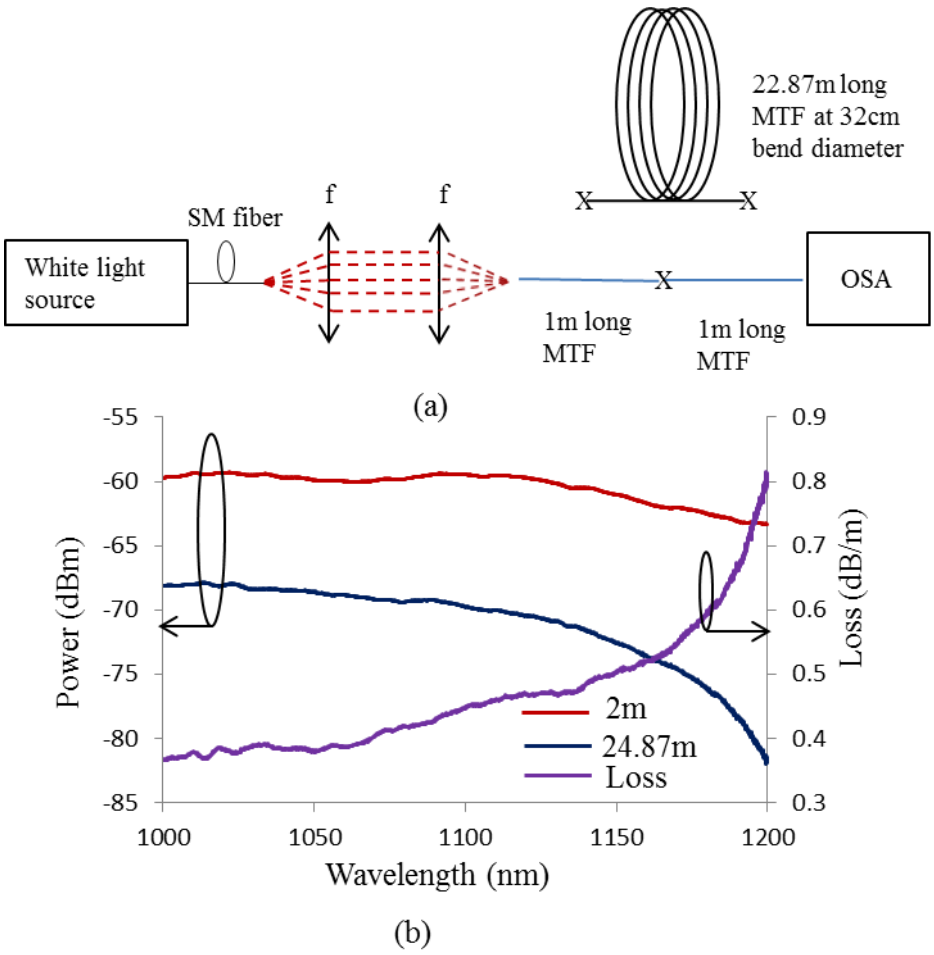

Figure 5.12(a) measurement setup used for transmission spectrum measurement (b) transmission spectra for two different length of fiber.

Figure 5.12(a) shows the experimental set-up used for transmission measurement. First, two 1m long MTFs were fixed both at input launching end and to the optical spectrum analyser (known as end connecting fibers), after that both ends of a 22.87m long MTF coiled on a bobbin of ~32cm diameter were spliced to connecting fibers and spectrum was measured as shown in figure 5.12(b). Thereafter, both connecting fibers were spliced and spectrum was measured as shown in figure 5.12(b). Figure 5.12(b) shows an overall loss of ~0.39dB/m at 1060nm, which is slightly larger than numerically computed value of lower than 0.1dB/m. However, it can be further improved by optimizing the fabrication process. It is important to note that, the bending loss here increases with wavelength, which is due to wavelength dependent resonant coupling. On the other hand, the fiber shows very high losses for the higher order modes, as shown in figure 5.13. To have a qualitative value of the higher order modes loss, cut back method was used. The higher order modes were excited into the fiber using a binary phase plate between two focal lenses in experimental setup as shown in figure 5.11(a). Figure 5.13(a) shows the profile of excited higher order mode in fiber. Here only 50cm length of fiber was used, as the higher order modes have high leakage loss. The higher order modes appears to be suffering from very high loss, even the slight bending of the fiber results in a significant loss of the higher order modes and only residual fundamental mode was observed, as shown in figure 5.13(a-b).

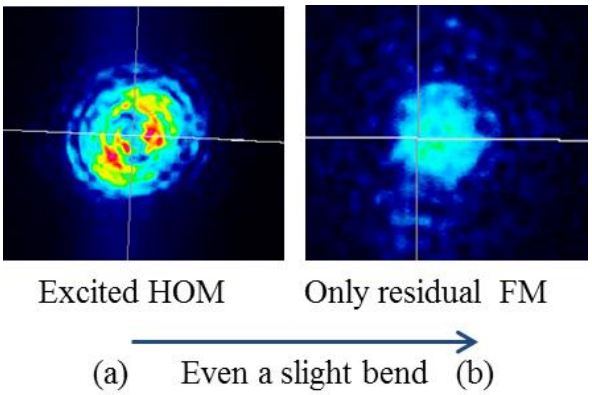

Figure 5.13(a) Output profile in unbent condition showing excited higher order mode (b) output profile in case of slightly bent case showing residual fundamental mode.

In order to study the impact of polymer coating, fiber with low index coating was drawn as well from the same preform shown in figure 5.9. Figure 5.14(a) shows the profile of output beam of the low index coated fiber, which shows several cladding modes. In order to strip off the cladding modes, index matching oil was applied after removing low index coating over a small length of fiber (~15cm) and afterwards, a Gaussian output profile was observed as shown in figure 5.14(b). In order to verify single mode behaviour, multimode laser beam (as shown in figure 5.14(c)) was launched. However, the output was again a Gaussian profile, as in the case of high index coated fiber (as shown in figure 5.14(d)), which ensures a single mode behaviour even in case of a low index coated fiber. Figure 5.14(e) shows the transmission spectra for two different lengths of fibers under ~32cm bend diameter. The fiber shows a loss of ~0.17dB/m at 1060nm, which is significantly lower than what was observed in case of high index coated fiber.

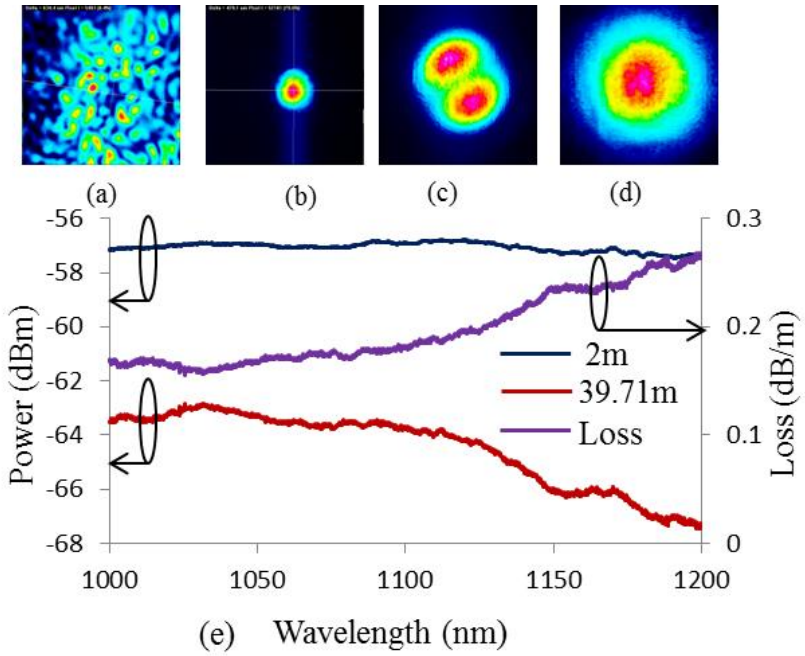

Figure 5.14(a) output beam profile of fiber having low index coating (b) output beam profile after stripping cladding modes (c) input multimode beam (d) output beam profile for input multimode beam (e) transmission spectra for two different length of the fiber at ~32cm bend diameter.

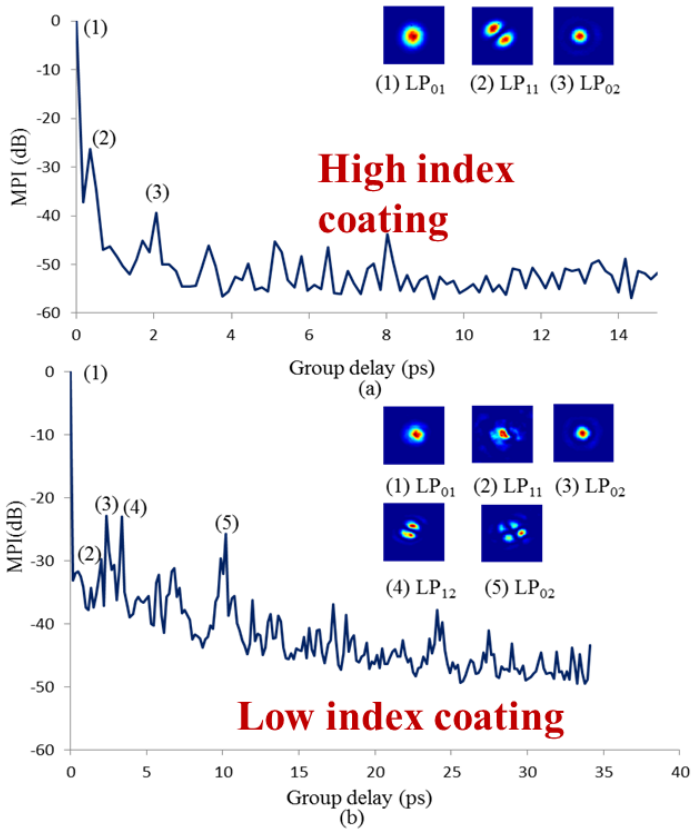

Figure 5.15 measured MPI (dB) versus group delay for two 30µm MTFs coated with (a) high and (b) low index coating respectively.

In order to quantify the higher order modes power content in the output profile, S^2 measurements were executed at SPI Lasers by Dr. Jaesun Kim using an experiment set-up as discussed in chapter 3, for both high index and low index coated fibers. A TLS tuned from 1041 to 1061nm with a step of 0.05nm was used for the measurement. The single mode beam was launched into 1m long MTF in a loosely coiled condition through butt coupling. Figure 5.15(a) and (b) shows the MPI versus group delay for both high index and low index coated fibers respectively. The measurement shows that the higher order modes contents are significantly lower than the fundamental mode for both fibers. It is worth mentioning here that, in this S^2 measurement just a 1m long fiber under loosely coiled condition (>1.2m bend diameter) was used. This ensures that these fibers do not require bending to filter out higher order modes. A comparative analysis of Figure 5.15(a) and (b) shows that, in the case of high index coating, higher order modes power content is 26dB lower than the fundamental mode. On the other hand, in the case of low index coating, higher order modes carry 22dB lower modal content than fundamental mode. However, it is interesting to note that, in case of low index coated fiber, other higher order modes such as LP_{02}, LP_{12}, and LP_{22} have higher modal content (~-22dB w.r.t fundamental mode) compared to lower modal content (~-39dB w.r.t fundamental mode) of LP_{02} shown by the high index coated fiber. On the top of this, few additional peaks are present, which are difficult to assign to a particular mode and might be due to cladding modes. Nevertheless, this measurement demonstrates that an ESM operation, even in a double clad MTF, while offering high suppression of the higher order modes can be ensured. In all of the above mentioned experiments, cleaving and splicing of MTF has been done using conventional cleaver and splicer thanks to the all-solid structure. In summary, a 30μm MTF can offer an ESM over a wide range of bend radii with easy fabrication and suitability for cleaving and splicing. However, further iterations of fabrication process are required to reduces the losses and bring refractive index profile more closer to ideal one.

5.2 Fabrication and Characterization of 20µm MTF for visible wavelengths

A 20µm core diameter MTF was drawn from the last perform (refractive index profile of preform is shown in figure 5.9). Figure 5.16(a) shows the measured refractive index profile and microscope image of fiber cross-section. Figure 5.16(b) shows the measured bending loss of fiber using white light source. The loss remains lower than 0.2dB/m and 0.5dB/m at ~30cm and ~15cm bend radius respectively at ~632nm. This loss can even be reduced down with further refinement in fabrication process.

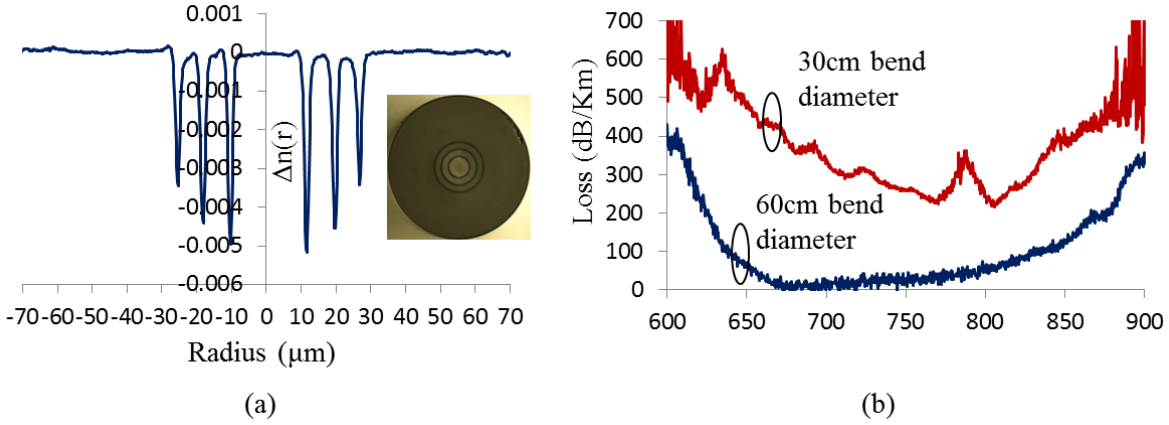

Figure 5.16(a) measured refractive index profile of the 20µm core diameter MTF. Inset shows the microscope image of fiber end. (b) Transmission spectra for different coil conditions.

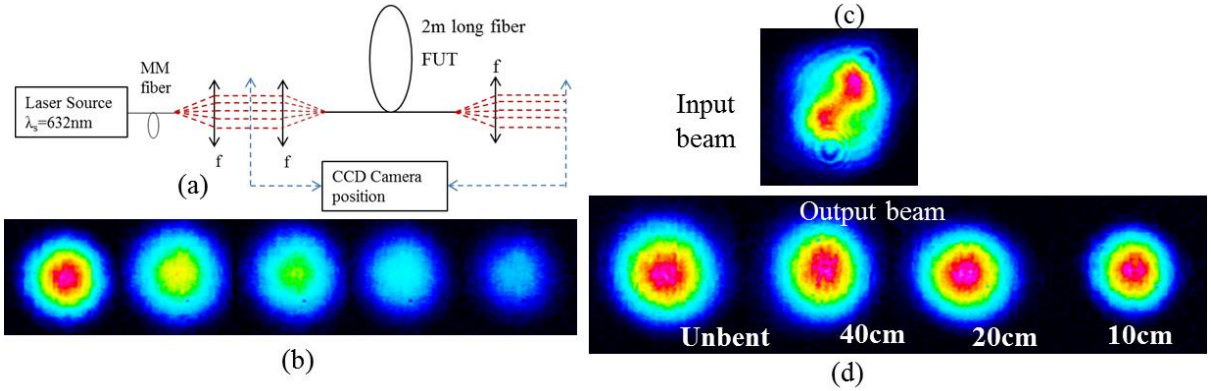

Figure 5.17(a) set-up used for verification of single mode behaviour, (b) output beam profile with different offset launching, (c) input launched beam, and (d) output beam with respect to input beam for different coiling diameters.

The output profile of a 2m long MTF was investigated using the experimental set-up shown in figure 5.17(a) with respect to different offset launching using laser source at ~632nm. Figure 5.17(b) shows the output of fiber for different offset launchings. On the other hand, figure 5.17(d) shows the output at different coil radii for launching of multi-moded input

beam shown in figure 5.17(c). This measurement ensures that fiber can be used as a beam delivery. Similarly, a 10μm core diameter MTF was drawn for beam delivery around ~300nm wavelength region. However, due to unavailability of laser source and CCD around ~300nm wavelength region, it is not possible to report the performance at 300nm wavelength. However, it can be intended as a future work.

5.3 Fabrication and Characterization of 90μm passive MTF rod-type fiber

In order to further scale the mode area, a 90μm core diameter passive MTF was fabricated with high index coating for rod type configuration. The fiber preform was fabricated by using conventional MCVD process in conjunction with rod-in-tube technique. However, the fabrication process of this 90μm MTF is different from previous 30μm MTF. In case of 30μm MTF, all trenches and resonant rings were deposited using MCVD, afterwards rod-in-tube was executed to desired core diameter. However, in the case of 90μm MTF, the ratio of trench thickness to resonant ring is small (<0.06), so it was difficult to achieve these small ratios by MCVD set up at ORC. So multiple rod-in-tube was executed to fabricate this 90μm MTF. Details of process are following:-

1. First step: A F300 tube was used to deposit a thin F_doped layer (third trench innermost trench layer) inside it, later on a F300 rod was inserted into tube (to act as a core) and preform was sealed. Further, in order to achieve desired thicknesses of trenches, resonant rings, and core, preform was stretched on a glass working lathe.

2. Second step: Again a F300 tube was used to deposit a thin F_doped layer (second trench) inside it, later on the preform made in first step was inserted into tube (to act as core, third trench, and third resonant ring) and the whole assembly was sealed. Now sealed preform has core, third trench, third resonant ring, second trench, and second ring.

2. Third step: Again a F300 tube was used to deposit a thin F_doped layer (first trench which is outermost trench layer) inside it, later on preform made in second step was inserted into tube (to act as core, third trench, third resonant ring, second trench, and second ring) and the whole assembly was sealed. Finally preform is ready, which consists of core, three trenches, three resonant rings, and outer cladding. Subsequently, preform was drawn into a fiber with 90μm core diameter and 370μm outer diameter.

Figure 5.18 shows the measured refractive index profile of the fiber and approximate refractive index profile used for numerical simulations. Inset also shows the microscope image of the fiber end. The obtained refractive index profile is different from the proposed fiber discussed in chapter 4. Due to stress-induced while stretching the preforms refractive indices of trenches differ. Moreover, diffusion of fluorine can also be observed. Numerical simulations over the approximate refractive index profile show the fundamental mode loss is lower than 0.05dB/m, LP_{11} mode loss is larger than 12dB/m, and other higher order modes loss are larger 35dB/m. On other hand, their power fractions in core are larger than 97% for

fundamental mode, lower than 60% for LP_{11}, and lower than 76% for other higher order modes. The effective area is larger than 3,100µm^2. It is important to note that, the higher order modes loss and power fraction can be much larger and lower respectively for optimized parameters, as shown in previous chapter. It is also worth noting that, the effective area for the fundamental mode could be much larger than 3,100µm^2 for a 90µm diameter core. However, it is not only the core diameter which decides the effective area of the fundamental mode, in fact it is the profile of the fundamental mode which decides the effective area. The profile of the fundamental mode also depends on cladding parameters. Normally, in case of poorly guiding waveguides (i.e. rod type fibers, which can afford high loss for the fundamental mode ~1dB/m), the electric field significantly penetrates in the cladding, thus results in a flatter field. The flat field yields larger effective area but lower power fraction in core and high loss for the fundamental mode.

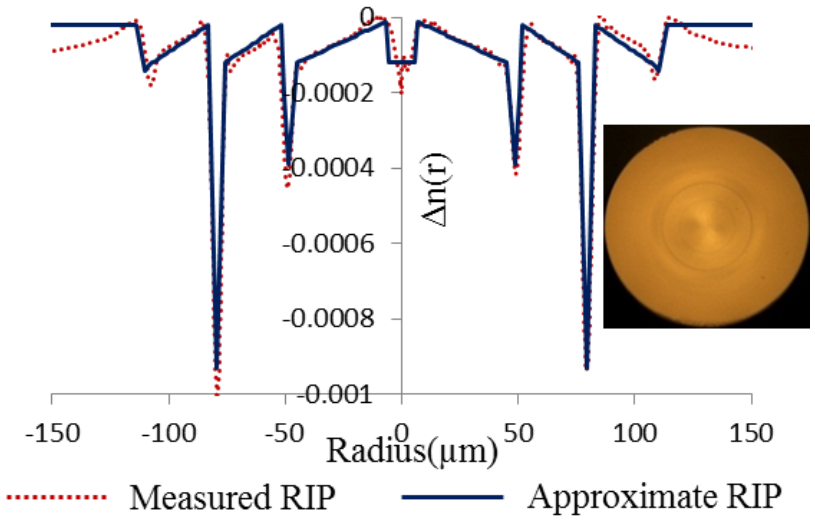

Figure 5.18 measured refractive index profile of the 90µm core diameter MTF and approximate refractive index profile of fiber used for simulations. Inset shows the microscope image of fiber end.

In the present fabricated fiber, gradient nature of refractive index profile in core results in a strongly confined fundamental mode, which is evident from low loss, high power fraction of the fundamental mode, and relatively low effective area compared to ideal refractive index profile of fiber. In order to exploit the flat field to achieve large effective area, cladding parameters can be optimized in further iterations. The qualitative analysis of output beam was executed using experimental set-up as shown in Figure 5.19. Figure 5.19 shows the output beam profile captured by the CCD camera. The output beam profile is nearly Gaussian although a few cladding modes can also be seen. This fiber shows significant microbend sensitivity as the outer diameter of the fiber is merely 370µm. To avoid any microbend sensitivity, the outer diameter of preform should have been ~1mm. This microbend sensitivity makes it significantly difficult to eliminate cladding and ring modes i.e. it is difficult to precisely calculate the fundamental mode loss.

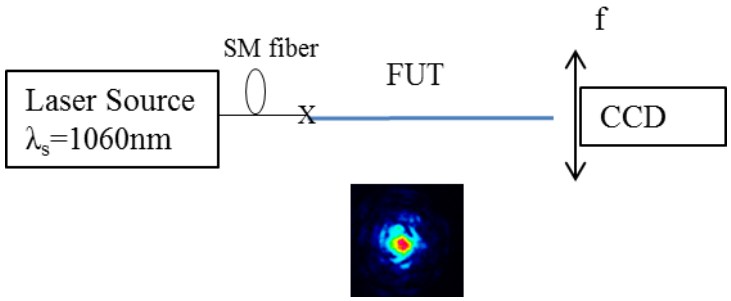

Figure 5.19 Experimental set-up and output image captured by CCD camera using set up shown here.

In summary, a process has been optimized to fabricate LMA MTF and initial results are encouraging. However, further refinement in fabrication process is required to achieve good performance.

5.4 Conclusion and Outlook

Results presented in this chapter show that MTF can be a potential candidate for beam delivery and rod-type fiber laser applications. Fiber fabrication can be simpler than stack and draw process required for other competitive designs. All solid fiber design ensures easy cleaving and splicing. A 90µm core diameter passive fiber has been fabricated in house using rod-in-tube technique in conjunction with MCVD process. Experiments ensure an ESM operation. Furthermore, fiber also shows the potential to be used for beam delivery applications with reduced core diameter thanks to ESM operation over a wide range of bend radii. A 30µm core diameter and 20µm core diameter has been successfully fabricated and ensures a robust single mode over a wide range of bend radii at 1060nm and 632nm respectively. Numerical simulations show the possibility of a 10µm fiber to be effectively single moded at 300nm.

However there is more refinement required in fabrication process to achieve impressive results. Further work is required to achieve rare-earth doped MTF, which is constituted of core having same refractive index as of cladding.

5.5 References:-

1. http://heraeus-quarzglas.com/en/home/Home.aspx

2. J. Kirchhof, S. Unger, B. Knappe, P. Kleinert, and A. Funke, “About the Fluorine Chemistry in MCVD: The Mechanism of Fluorine Incorporation into SiO2 Layers,” Cryst. Res. Technol., 22(4) 495-501 (1987).

3. D. J. Digiovanni, “Manufacture of optical fiber preforms using high pressure doping,” European Patent EP 1 431 254 A2 (2004).

4. V. A. Aksenov, G. A. Ivanov, V. A. Isaev, and M. E. Likhachev, “MCVD of Fluorosilicate Glass,” Inorganic Materials, 46(9) 994-997 (2010).

5. Y. Hibino, F. Hanawa, and M. Horiguchi, “Drawing-induced residual stress effects on optical characteristics in pure-silica-core single-mode fibers,” J. Appl. Phys., **65**, 30-34 (1989).

Chapter 6 Conclusion and Future scope

The motivation of this thesis work was to develop novel optical fibers for applications in fiber laser and beam delivery. This chapter concludes the work presented in this thesis and outlook is also being discussed.

6.1 Conclusion

This thesis ends with successful demonstrations of following novel fibers:-

(1) Ultra low-NA SIF: Optimized MCVD process in conjunction with solution doping process lead to achievement of an ultra-low-NA of ~0.038 (corresponding to core refractive index to be higher than cladding by 0.0005) Yb-Al doped SIF. This fiber can lead to an ESM by following the criterion of loss of higher order modes to be larger than 10dB/ and loss of the fundamental mode is lower than 0.1dB/m for an effective area of ~700μm^2 at 32cm bend diameter. Further, fiber shows a high laser efficiency of ~81% in a 4%-4% laser cavity with a M^2 less than 1.1. This brings SIF in close competition for mode area scaling to other fiber designs. Table 6.1 summarizes the gain in terms of mode area scaling due to ultra-low NA of core.

Table 6.1 comparative analysis of mode area scaling for different NA of core in case of SIF at 1060nm.

NA (corresponding to Δn)	**Core diameter (μm)**	**Required bend diameter in cm (for minimum 10dB/m loss for the higher order modes and less than 0.1dB/m for fundamental mode)**	**Achieved effective area in μm^2 (taking bend induced distortion into account)**
0.048 (0.0008)	~29	~15.5	~455
0.038 (0.0005)	~35	~32	~700

(2) STF: Further a new fiber design known as STF has been proposed by adding a Ge-doped ring around the core of a SIF. This fiber significantly enhances the suppression of the higher order modes by offering delocalization and loss of the higher order modes thanks to the resonant coupling of modes between core and resonant ring. This resonant coupling also leads to increased effective area of the fundamental mode by extending the field from core to ring. A 30μm core diameter STF has been successfully demonstrated with an ESM without need of a tight coil diameter. Numerical simulations over measured refractive index profile shows the loss of the fundamental mode is lower than 0.12dB/m and the loss of the least lossy higher order mode is larger than 22dB/m at 1060nm for a coil diameter of 32cm. The fundamental mode and least lossy higher order mode have ~0.85 and ~0.62 power fraction in respectively. The effective area of the fundamental mode is larger than 628μm^2 including bend induced distortion.

A MOPA was built using this fiber leading to generation of ~23.5ps pulses at 13.5MHz repetition rate carrying up to ~3.8μJ pulse energy corresponding to >160kW peak power and ~52.3W average power. The slope efficiency remains larger than ~76%. The output beam maintains a polarization extinction ratio of more than 15dB and a M^2 less than 1.15. Furthermore, a 40μm core diameter STF has also been successfully demonstrated offering a robust ESM. Fiber shows a high laser efficiency of ~75% in a 4%-4% laser cavity. STF also offers the advantages of easy fabrication and post-processing such as cleaving and splicing. Numerical simulations also show the possibilities of a ~50μm core diameter STF offering an effective area of 1,500μm^2, however it is intended as a future work.

A fair comparative analysis shows significant advantages over other competitive fiber designs. Comparative analysis includes the maximum achievable effective area at a maximum of bend radius ~20cm following the criterion of ESM as the loss of the higher order modes higher than 10dB/m and the loss of fundamental mode lower than 0.1dB/m. Further factors affecting manufacturing cost of fiber and easy post-processing of fiber such as cleaving and splicing have also been taken into account. Analysis clearly shows the substantial advantages of STF over other fiber designs. Table 6.2 summarizes the comparison of different fiber designs and also highlights the achievement of this thesis work.

Table 6.2 comparison of different fiber designs. (Based on findings reported in this thesis.)

Fiber Design	**Maximum effective area** (Fundamental mode loss < 0.1dB/m & higher order mode loss >10dB/m)	**All-solid**	**Cylindrical symmetrical**	**Core index higher than cladding**
Low NA-SIF [1]	**~700μm^2**	Yes	Yes	Yes
LCF [2,3]	~900μm^2	Yes	No	No
2D-ASPBGF [4,5]	~1,000-1,400μm^2	Yes	No	No
Bragg Fiber [6]	~1,020μm^2	Yes	Yes	No
P-CCC [7]	Not provided	Yes	No	Yes
Bend compensated Parabolic fiber [8]	~1,000μm^2	Yes	Yes	Yes
Single trench fiber (this current work)	1,000μm^2-1,500μm^2	**Yes**	**Yes**	**Yes**

Further table 6.3 shows the mode area scaling of STFs with different core diameter and NA at different wavelengths. It is clear that achievable mode area increases with increasing wavelengths. Obviously, this table ensures the suitability of STF for fiber laser operation at these wavelengths.

Table 6.3 summary of STFs results achieved in this thesis.

Wavelength of operation	**Core diameter and NA**	**Bend diameter**	**Maximum achievable effective area ensuring effective single mode** (take bend induced mode distortion)
1.06μm	20μm, 0.054	14cm	~290μm^2 to ~374μm^2
	30μm, 0.038	40cm	~618μm^2 to ~767μm^2
	40μm, 0.038	40cm	~1,000μm^2 to ~1,500μm^2
1.55μm	60μm, 0.038	50cm	~1,840 μm^2 to ~1,940μm^2
2μm	60μm, 0.054	60cm	~2,200μm^2 to ~2,800μm^2
	80μm, 0.038	60cm	~3,895μm^2 to ~4,795μm^2
	80μm, 0.038	80cm	~3,615 μm^2 to ~4,020μm^2

(3) MTF for beam delivery: A novel fiber design, known as MTF, has also been proposed and successfully demonstrated. MTF can achieve an ESM over a wide range of bend radii, thus suitable for beam delivery applications. Fiber has been fabricated using MCVD process in conjunction with rod-in-tube technique. Numerical simulations show that a 10μm, 20μm, and 30μm core diameter MTF can offer ESM in UV, VIS and near Infra-red region respectively. MTF having 30μm and 20μm core diameters have been experimentally demonstrated to show ESM over a wide range of bend radii at ~1060nm and ~632nm respectively, thus ensuring their suitability for beam delivery applications. Table 6.4 shows the comparison of MTF with different fibers for beam delivery applications for UV region.

Table 6.4 comparison of different fibers for UV region.

Fiber design	**Core diameter**	**Single mode**	**Fabrication and handling**	**UV-resistance**
PCF [9]	~10μm	Intrinsically single mode	difficult	Hydrogen loading
HCF [10]	~20μm	Slightly multi-moded	difficult	Nothing required
MTF	~10μm	Effective single mode	easy	Hydrogen loading

(4) MTF for rod-type laser applications: Further, MTF has been scaled to larger core diameters of 100μm and 140μm core diameter. Numerical simulations show the feasibility of ESM for effective area as large as ~10,000μm^2 at 1060nm wavelength in rod-type configuration. A 90μm core diameter passive MTF was successfully fabricated using rod-in-tube process in conjunction with MCVD process and experiment ensures an ESM operation.

Although MTF offers the advantages of easy fabrication, however the refractive index of RE-doped core and passive cladding has to be same like other competitive fibers. This has not been exploited in this thesis work. The full potential and advantages of rod-type MTF are yet to be proved.

6.2 Future Scope

(1) Demonstration of high power laser using ultra-low-NA SIF and STF

First, these ultra-low-NA SIF and STFs can be explored for their optimum power level in a MOPA configuration to analyze their full potential. Second, some work towards a 50μm core diameter STF can be done to further enhance the mode area scaling. Further, ultra-low NA SIF and STF can also be explored for high power lasers at other wavelengths such as 1.55μm and 2μm. Furthermore, STF in a pedestal configuration can be useful for higher doping levels of RE ions and co-dopant such as P_2O_5. High doping levels of RE-ions are required for short length fiber lasers to avoid non-linearity. Moreover, higher doping level of RE-ions also needs co-dopant such as P_2O_5 to avoid quenching and photo-darkening.

(2) Demonstration of ultrafast laser using RE doped rod-type MTF

A low cost method to fabricate RE doped ultra large core (100-140μm) MTF having same refractive index as of cladding can be developed. A lot of work will required to achieve appropriate RE composition and the issue of refractive index mis-match of core and cladding. The RE doped ultra large core diameter MTF can be used in ultrafast laser applications to achieve ultra-high peak power pulses.

6.3 References

1. M.-J. Li, X. Chen, A. Liu, S. Gray, J. Wang, D. T. Walton, and L. A. Zenteno, "Limit of effective area for single-mode operation in step-index large mode area laser fibers," J. Lightwave Technol. **27**, 3010-3016 (2009).

2. G. Gu, F. Kong, T. W. Hawkins, P. Foy, K. Wei, B. Samson, and L. Dong, "Impact of fiber outer boundaries on leaky mode losses in leakage channel fibers," Opt. Exp. **21**, 24039-24048 (2013).

3. R. A. Barankov, K. Wei, B. Samson, and S. Ramachandran, "Resonant bend loss in leakage channel fibers," Opt. Lett. **37**, 3147-3149 (2012).

4. G. Gu, F. Kong, T. Hawkins, J. Parsons, M. Jones, C. Dunn, M. T. Kalichevsky-Dong, K. Saitoh, and L. Dong, "Ytterbium-doped large-mode-area all-solid photonic bandgap fiber lasers" Opt. Exp. **22**, 13962-13968 (2014).

5. S. Saitoh, K. Saitoh, M. Kashiwagi, S. Matsuo, and Liang Dong, "Design optimization of large-mode-area all-solid photonic bandgap fibers for high-power laser applications," J. Lightwave Technol. **32,** 440-449 (2014).

6. C. Baskiotis, Y. Quiquempois, M. Douay, and P. Sillard, "Extending the effective area of coiled all-solid silica single-mode Bragg fibers," in ECOC, Geneva, Switzerland, 2011, paper **We.10.P1.02**.

7. X. Ma, C. Zhu, I-Ning Hu, A. Kaplan, and A. Galvanauskas, "Single-mode chirally-coupled-core fibers with larger than 50μm diameter cores," Opt. Exp. **22**, 9206-9219 (2014).

8. J. M. Fini and J. W. Nicholson, "Bend compensated large-mode-area fibers: achieving robust single-modedness with transformation optics," Opt. Exp. **21**, 19173-19179 (2013).

9. Y. Colombe, D. H. Slichter, A. C. Wilson, D. Leibfried, and D. J. Wineland, Opt. Exp., **22**(16) 19783-19793 (2014).

10. S. Février, F. Gérôme, A. Labruyère, B. Beaudou, G. Humbert, and J.-L. Auguste, Opt. Lett., **34**(19) 2888-2890 (2009).